New Insights in
the Working Principles
of Europium-Based Methane
Oxychlorination Catalysts

Bas Johan Pieter Terlingen

New Insights in the Working Principles of
Europium-Based Methane Oxychlorination Catalysts

Bas Johan Pieter Terlingen

New Insights in the Working Principles of Europium-Based Methane Oxychlorination Catalysts

Nieuwe Inzichten in de Werking van Europium-Gebaseerde Katalysatoren voor de Oxidatieve Chlorering van Methaan

(met een samenvatting in het Nederlands)

Proefschrift

ter verkrijging van de graad van doctor aan de

Universiteit Utrecht

op gezag van de

rector magnificus, prof. dr. H.R.B.M. Kummeling,

ingevolge het besluit van het college voor promoties

in het openbaar te verdedigen op

maandag 16 januari 2023 des middags te 2.15 uur

door

Bas Johan Pieter Terlingen

Geboren op 14 augustus 1994

Te Hengelo (o)

Promotor:

Prof. dr. B.M. Weckhuysen

Copromotor:

Dr. E.M. Hutter

Beoordelingscommissie:

Prof. dr. E.T.C. Vogt

Prof. dr. A. Meijerink
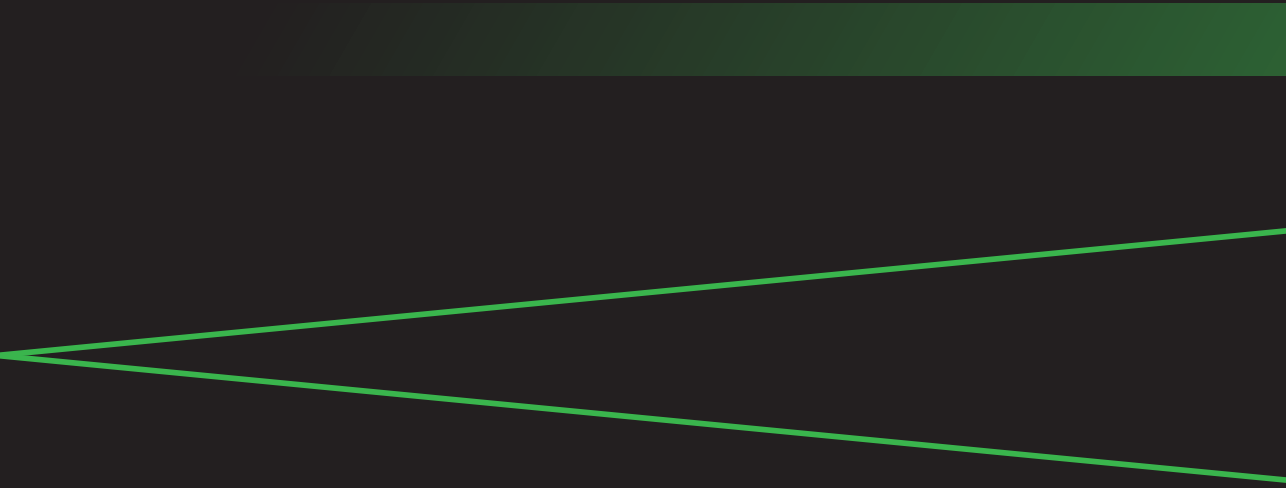
Prof. dr. P.C.A. Bruijnincx

Prof. dr. J. Pérez-Ramirez

Dr. C. van Lare

Table of Contents

1

Introduction

Abstract

This PhD thesis focusses on development of new catalyst materials for the methane (CH_4) oxychlorination (MOC) reaction with the aim to selectively produce methyl chloride (CH_3Cl) from CH_4. Being able to efficiently use of CH_4 as feedstock via direct conversion routes is crucial for the transition from fossil-based to renewable feedstocks as CH_4 can, for instance, be produced from via anaerobic digestion of agricultural and municipal waste, which is better known as bio-CH_4. However, these one-step conversions of CH_4 to valuable chemical building blocks are notoriously difficult and the currently developed processes do not meet economic and environmental standards. Of the direct conversion routes, the MOC reaction has one of the highest potentials to see commercialization, with the proviso that more active and selective catalysts will be developed and the re-lated issues for safe chemical operation can be maintained. The status quo is that the development of MOC catalysts is still in its infancy, even though the first catalytic system was developed a century ago. Hence, the technology readiness level is low and its full potential is not yet fully explored.

The aim of this chapter is to put the research presented in this thesis into context and explain several concepts that are crucial for the development of new MOC catalyst mate-rials. First, the potential of the MOC reaction will be discussed to see whether there is a role for this relatively unknown reaction in the future. Subsequently, challenges that the scientific community and industry face with catalyst development and the overall pro-cess are introduced by going through the history of the MOC reaction. Then, the design criteria for the development of new catalyst materials are set and the current benchmark MOC catalysts are discussed. In the last section, the use of lanthanide-based materials as MOC catalysts is discussed and how these catalysts can be studied under reaction conditions with light, i.e., by using the operando spectroscopy methodology. The working principles of the applied analytical techniques will be explained as well as how this infor-mation may contribute to the development of improved catalyst materials.

1.1 DIFFERENT SOURCES OF METHANE

Methane, or CH_4, would be a great source of carbon for the production of chemicals and fuels, now and in the future, as CH_4 will be readily available. However, up to this day, CH_4 has been a problem for our society as CH_4 emissions contributed significantly to climate change. Up till the year of 2021, CH_4 was responsible for 30% of the global temperature rise, either as greenhouse gas or in the combusted form of CO_2.[1–3] It therefore goes without saying that preventing CH_4 emissions is key to mitigate global warming. The biggest contributor of CH_4 emissions is the energy sector. Roughly 45% of the CH_4 emissions today could have been prevented by implementing facile preventive measures. Addressing equipment leaks and repairs, banning non-emergency flaring and setting minimal technological requirements could contribute to a rapid reduction in emissions. Policy makers must force similar measures upon oil and gas companies, as there is no financial incentive for these companies to either directly or indirectly utilize CH_4. Other human-induced CH_4 emission sources that contribute to climate change substantially are agriculture (24%) and waste treatment (11%).[4] However, reducing CH_4 emissions from these two sectors is less cost-effective.

The effective utilization of CH_4 is a double faceted problem for the oil and gas industry. First of all, CH_4 is a gas with a low energy density. This, combined with the fact that CH_4 is often found at remote locations, make it that transportation is very costly. Shipping is up to three orders more costly compared to oil, and transportation via pipelines requires an enormous capital investment.[5] The alternative would be to convert it on-site to a liquefied and/or an added-value compound. The liquefied natural gas (LNG) process and the commercial Fischer-Tropsch synthesis (FTS) face the same problem; so far these solutions only become economically attractive at very large scale. Hence, viable alternatives need to be developed for smaller scale on-site production of CH_4-derived liquids, providing an alternative to the unsustainable flaring and leaking. An important remark is that we should phase out the use of fossil-based resources and replace it by circular alternatives as soon as possible. Hence, the utilization of CH_4 from mining operations should be regarded as a temporary solution to mitigate emission issues that we face at present.

With the phasing out of fossil-based resources, alternative renewable carbon-containing sources for the future must be developed. Due to the enormous scale at which this substitution needs to take place, bio-CH_4 may offer the only real viable option at this point.[6] The technical potential in the European Union of bio-CH_4 was estimated at 151 - 246 billion normal m^3 (Nm^3) from anaerobic digestion (AD) and gasification.[7] This implies that up to 50% of the total consumption of the EU (361 billion Nm^3 in 2019)[8] could be produced renewably, while the biogas production in 2015 contributed only ~ 3% (18,4 billion Nm^3). Biogas can be produced via the AD of waste and residues from agriculture, industry, municipal organic waste, sewage, sludge and manure.[9] Critical is that the biomass source does not compete with food crops and prevent indirect land use changes.[7] Biogas production from waste and residues has no side effects that affect the food supply chain and it provides the highest greenhouse gas emission reduction among many bioenergy
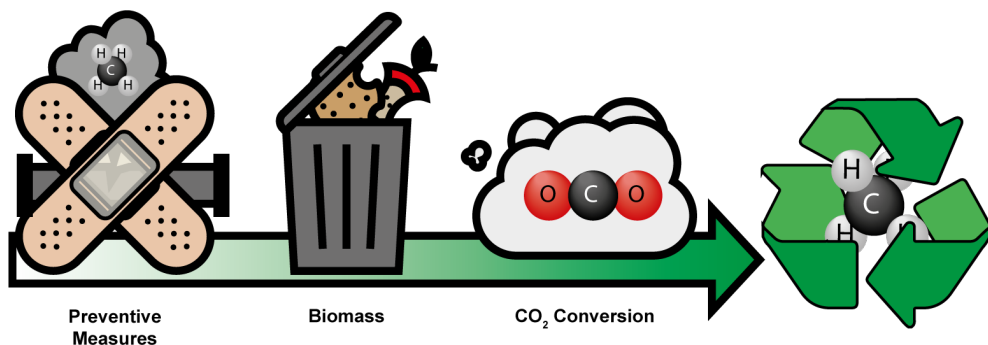
Figure 1.1. CH_4 from preventive measures, anaerobic digestion of biomass and CO_2 conversion is available now and in the future for the renewable production of fuels and chemicals.

supply chains.[7] The obtained biogas can be readily purified to yield high purity CH_4, with low concentrations of H_2S, H_2O and CO_2. By using the existing gas network, storage and transportation of this bio-CH_4 is cheap and allows for use at the place of need.

To get a feel of the operation of scale to replace fossil-based CH_4 by bio-CH_4: to realize the desired process in this PhD thesis, roughly 50 kton/year of CH_4 is required. This implies that similar facilities as the largest bio-CH_4 plant in the world, i.e., the Nature Energy Korskro in Denmark, capable of producing 75 Nm^3/year CH_4 and consuming 1 million ton of manure and agricultural waste when fully expanded, are needed.[10,11]

To permanently mitigate human-induced climate change and work towards a circular economy, we must utilize CO_2 as the carbon source for our (partial) carbon-based economy. The Technology Readiness Level (TRL) of integrated processes that collect solar energy, H_2O and CO_2 for the production of chemicals and fuels will take years to decades before becoming economical competitive, but clearly hold the future.[5] However, the CO_2 methanation process is already commercialized[12], and is expected to become economically more attractive in the future[13], especially when the cost of renewable hydrogen can be suppressed.[14] Hence, CH_4 will most probably be readily available as a chemical building block for carbon containing chemicals in the future (Figure 1.1).

A global transition is occurring in which sectors that were very reliant on hydrocarbon fuels are being replaced by electric or non-carbon containing feedstock alternatives, as is the case for light duty transportation. Hence, the need for hydrocarbon-based fuels and chemicals will most probably decline in those sectors. However, not all sectors can be properly electrified or will make use of non-hydrocarbon containing sources. Many energy carriers are not as energy dense per unit volume as hydrocarbons. If the same total energy as a diesel fuel storage system is required, a liquid hydrogen storage system would be roughly six times heavier and eight times larger.[15] Hence, long-distance travelling is hampered in the case that shipping and aviation would run on non-carbon containing fuels. Furthermore, many chemicals used nowadays are still carbon-based, and just the feedstock ought to be replaced by a renewable feedstock. For the production of fuels and carbon-containing chemicals, CH_4 would be a suitable feedstock if efficient

conversion processes would be developed. Key is that products and waste streams will be recycled to close the carbon cycle, thereby preventing pollution and emissions.

1.2. METHANE OXYCHLORINATION REACTION AS DIRECT CONVERSION ROUTE

Direct conversions of CH_4 to valuable compounds are conceptually more interesting than multi-step routes, but lack the TRL for commercial application.[5,16–21] Single-step conversions produce less waste, and require less energy and smaller capital investments than the multi-step approaches. Furthermore, endothermic CH_4 reforming needed in multi-step approaches can be circumvented, opening up the possibility to convert CH_4 at smaller scales.[5]

There are several direct conversion routes, all having their advantages and disadvantages. The non-oxidative CH_4 dehydroaromatization (MDA) reaction converts CH_4 into aromatics and H_2. The valuable products can be made with a benzene selectivity of ~ 80%. However, high temperatures are needed, extensive coke is formed, the reaction is thermodynamically limited and relatively low conversions are achieved (10 - 15%).[17] In the CH_4-to-methanol (MTM) conversion, the partial oxidation of CH_4 is performed. This reaction holds great promise for the future and is regarded as the dream reaction by many scientists.[21] The process is economically friendly, as it can be operated at temperatures of ~ 200 °C. However, the reaction is severely limited by the activity-selectivity trade-off, with the selectivity dropping fast at conversion levels above 1%. Extensive research is needed to overcome the reaction limitations.[21] Via the oxidative coupling of CH_4 (OCM) reaction, C_2H_4 can be synthesized with a good activity/selectivity relation. A conversion level of 20-30% with C_2H_4 selectivity of 60 - 80% can be achieved, but the reaction is thermodynamically limited. Furthermore, a high reaction temperature is needed which poses catalyst stability issues and the formation of CO_x is substantial.[21] Even though extensive research has been put in these three direct conversions, none of the direct CH_4 conversion processes has seen commercialization.[22,23]

The (oxy)halogenation of CH_4 is less well studied, but has great potential. In this reaction, CH_4 is converted to produce methyl halide, a chemical building block, by the reaction with either HCl or HBr and O_2. The advantage of performing these type of chemical reactions is that already a good activity/selectivity relation can be achieved under moderate reaction conditions, even though the related catalyst research is still in an early stage.[24] The oxyhalogenation reactions are described as promising[18,21,24] and commercially the most interesting[25], but more research needs to be conducted to explore the full potential of the reaction. Issues that need to be solved are related to the production of polyhalogenated C_1, for which there is little use, and CO_x. Lastly, an everlasting concern with halogenation reactions is use/formation of toxic and corrosive compounds, posing process and environmental issues.[18] Pivotal is the design of a closed chlorine loop in order for the chlorine to be recycled and not end up in the environment.
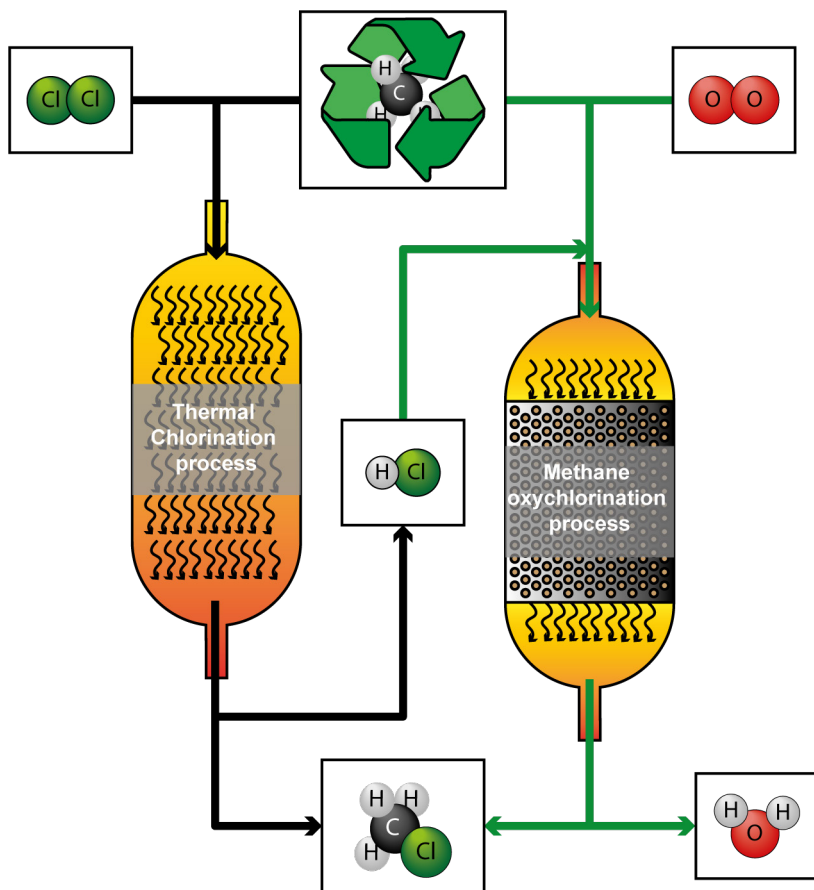
1

Figure 1.2. Integrated process of the thermal chlorination of CH_4 (black arrows) and the CH_4 oxychlorination (MOC) reaction (green arrows). The realization of the MOC process would mean that the by-product HCl could be recycled, thereby producing CH_3Cl and H_2O.

In this PhD thesis, the CH_4 oxychlorination (MOC) reaction is studied in detail. The MOC reaction can be operated at moderate temperatures (350 - 600 °C) and achieve high conversion levels (X_{CH4} > 30%) and high selectivity towards CH_3Cl (> 70%). The reaction with HCl has the additional advantage over the thermal chlorination with Cl_2 that the use of expensive Cl_2 can be substituted with the by-product HCl obtained from chlorination reactions. Hence, the Cl is converted with a 100% atom efficiency. The realisation of the MOC reaction would mean that it could be incorporated into existing technology for the production of CH_3Cl, as the same products are made during the thermal chlorination and the oxychlorination (Figure 1.2). Furthermore, the desired product, CH_3Cl, is the chemical analogue of CH_3OH. Hence, similar chemistry as for CH_3OH can be performed with CH_3Cl, such as the methyl chloride to hydrocarbons reaction, making CH_3Cl a valuable product.[26]

1.3. BRIEF HISTORY OF THE METHANE OXYCHLORINA-TION REACTION

Since the invention of the first MOC catalyst in 1922, roughly 30 articles and 40 patents have been published on the topic, ranging from new catalyst compositions to complete process designs. In those years, the MOC reaction has undergone some major changes since the invention of the first catalytic system. Influenced by inventions in related fields, regulatory adjustments and societal issues, the focus of research has shifted throughout the years. By following the history of the MOC reaction, the development of MOC catalyst materials will be discussed and some key scientific and technological challenges will be highlighted.

1.3.1. 1922 - 1945 The Discovery of the Benchmark Cu Catalyst.

The field of MOC was discovered in the early 1920's when the first Cu-based catalyst was patented by Tizard, Chapman and Taylor.[27] A well-known deacon catalyst of that time, $CuCl_2$/pumice (volcanic rock), was found capable of directly chlorinating CH_4. Before that time, phosphorus pentachloride (PCl_5), sulfuryl chloride (SO_2Cl_2) or antimony chloride ($SbCl_3$) were also found capable of chlorinating CH_4, but were single-use bulk reagents. With the invention of $CuCl_2$/pumice, a regeneration step enabled a swing mode operation, hence forming a catalytic cycle. Not only Cu^{2+} was tried as MOC catalyst in that era, but also reports on the use of Ce^{4+} and Fe^{3+} can be found.[27–30] However, the catalytic performance of Ce^{4+} and Fe^{3+} could not compete with the performance of the Cu^{2+}-based system.

The thermal chlorination of CH_4 was already commercial at that time, but it suffered from two major drawbacks. The first drawback was that Cl_2 prices fluctuated heavily and large quantities of HCl by-product were produced, for which there was no market.[30] The realization of the MOC reaction would mitigate these problems, as both Cl-atoms from Cl_2 ended up reacting with the C_1 molecule. In a typical process described in the patent literature, Cl_2 would be fed with CH_4 and react to CH_3Cl and HCl. The HCl could be converted back to Cl_2 gas with O_2, which could again react with a hydrocarbon.[28] The second issue is that the thermal chlorination of CH_4 is highly exothermic and the product selectivity thermally driven. This problem was not resolved with the invention of the oxychlorination reaction since the addition of O_2 in the chemical process also causes overoxidation of CH_4, which is still the largest hurdle to overcome nowadays.

Unlike today, the desired products at that time were $CHCl_3$ and CCl_4, mainly due to the discovery of chlorofluorocarbons (CFC's or Freon). The discovery was made in 1928 by Thomas Midgley, later called the "one-man environmental disaster" for also inventing leaded gasoline.[31–33] At the time, there was a very high need for efficient, non-toxic and non-flammable refrigerants. Before the general use of CFC's, the toxic CH_3Cl, NH_4OH and SO_2 were used as refrigerants for consumer applications.[34] Fatal accidents happened with domestic refrigerators where CH_3Cl was used as refrigerant. Thomas Midgley, so convinced that CFC compounds were non-toxic and non-flammable, inhaled the vapor of

one of his CFC compounds and extinguished a burning candle by exhaling softly.[35] The use of CFC's soon found its way as refrigerant in everyday life, thereby increasing the demand for CFC precursors.[34] With the discovery of CFC's, the safety requirements were met, but it was unknown at these days that CFC's would have such a huge impact on the environment as would turn out later.[36,37]

1.3.2. Post WW II - 1970 Improving the Cu^{2+}-based Catalyst

Research in the field of MOC intensified after WW II. The market of CFC's was in a rise and the only viable route for making polychlorinated C_1 ($CHCl_3$ and CCl_4) was still via the expensive thermal chlorination route.[38] New catalyst compositions were reported as the incentive to commercialize the MOC process increased. The Cu-based catalyst system was still the focal point and the a reaction mechanism, as outlined in Figure 1.3, was proposed.[39,40] The active $CuCl_2$ phase is operated in a molten state, resulting in an enhancement of Cl_2 evolution.[39,41] However, the dechlorination of $CuCl_2$ to $CuCl$ induces not only a chemical, but also physical change. A solid $CuCl$ phase forms on top of this molten state, blocking the active sites. The re-oxidation of $CuCl$ to Cu_2OCl_2 was identified as rate determining, thus the formation of this passivating layer was a key issue to address. A far more serious problem was the fact that $CuCl_x$ exhibit a significant vapor pressure at reaction conditions. Not only did this result in both catalyst and activity loss, equipment corrosion was also accelerated.[42] Soon after WW II, the activity and stability of the Cu^{2+}-based catalyst was improved by adding promotors.[43] The addition of alkali promotors, more specifically K^+, accelerated the rate determining re-oxidation step and kept the catalyst in the molten state.[44] Heavy metals, such as Pb, Zn, Ag or Th, and alkali metals were added to lower the vapor pressure, which enhanced the life-time of the catalyst.[43] The stability of the Cu-based catalyst system was still poor and many attempts were tried over the years to increase the stability by altering catalyst composition, i.e., promotors, additives, supports[42,45–47], operating conditions[42,48,49] and reactor design[43,50]. Next to the fixed bed reactor, the fluidized bed reactor was proposed as a promising design in 1966.[51] Heat spots that occur in the fixed bed are prevented due to the fluidic nature of the catalyst bed, enhancing the heat exchange and preventing overoxidation of CH_4 by combustion. As turned out, the stability of Cu-based catalysts operated in fluidized bed was even lower than in fixed bed reactors, resulting in shorter catalyst lifetimes.[46]

1.3.3. 1970 - 2002 Safety, Oil Crisis and Regulations

With the production of polychlorinated C_1 peaking in the 1970's and 1980's, environmental and health hazards became apparent.[38] The ban of CCl_4 in consumer goods in 1970, the ban of CFC's in aerosols in 1978 and the carcinogenicity of CH_2Cl_2 proven in mice in 1985, caused a rapid decrease in the demand of polychlorinated C_1.[38] In 1987, the Montreal protocol was signed by 197 parties worldwide to phase out the use of ozone depleting substances (ODS).[52] The treaty was of great importance since the production of CFC's peaked in the 1970's and 1980's and, due to the volatile nature, ended up in the stratosphere.[38] Here it reacted with ozone, depleting the UV-protective layer around earth. The treaty went in effect from the first of January 1989. A major focus shift of oxychlorination
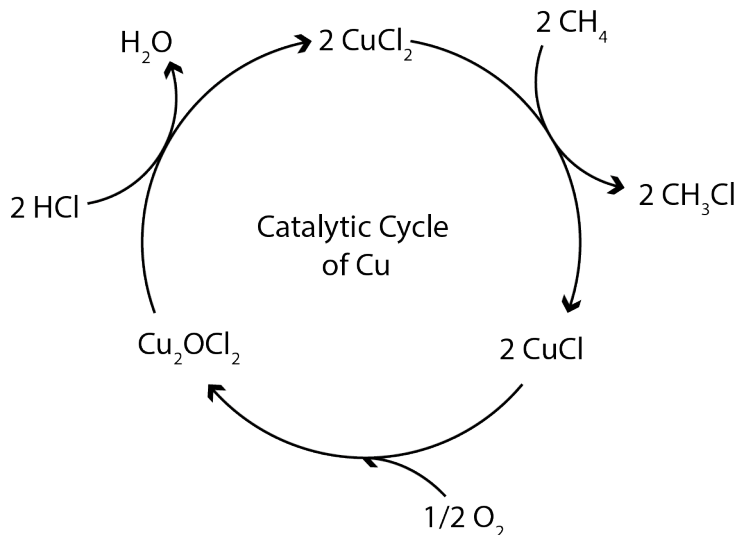
Figure 1.3. Catalytic cycle of the CH_4 oxychlorination (MOC) reaction over Cu^{2+}-based catalysts where Cu^{2+} is reduced to Cu^+ during the chlorination of CH_4. The re-oxidation of Cu^+ to Cu^{2+} is the rate determining step.

research was triggered by the oil crisis in 1973 and 1979 when the price of oil-based resources and energy sky-rocketed. After the oil crisis in 1979, the realization came that the world was too dependent on oil-based feedstock for fuels and chemicals.[53] Olefins, such as ethylene and propylene, are key building blocks for plastics and other chemicals, but were solely obtained from oil.[53] CH_4 and coal were identified as potential carbon-based feedstocks, but the conversion thereof to fuels and chemicals was not heavily investigated. An approach already known in the literature was the syngas-to-methanol (STM) route and the subsequent condensation to olefins.[53] However, the production of syngas is energy intensive and requires high pressures and temperatures for reasonable conversion levels.[26] A patent from the fuel company BP in 1987 describes the use of CH_3Cl as a replacement for methanol to produce hydrocarbons in the gasoline boiling range.[54] CH_3Cl, obtained from the direct chlorination of CH_4 at moderate reaction conditions, is converted into olefins without the additional energy penalty of O^{2-} removal.[55] The development of the methyl chloride-to-olefins (MCTO) on one hand, and the Montreal protocol & toxicology reports on the other hand, shifted the focus of the research from polychlorinated C_1 in the 1970's and early 1980's[40,56–60] to the selective production of CH_3Cl in the late 1980's[61,62]. However, the Cu-based catalyst system still suffered from leaching and overoxidation of the feedstock. In the late 1960's till early 1970's, the use of lanthanides as a promotor was established to boost catalytic activity of the Cu/K-based catalyst, which turned out to be an important finding.[45,47,56,63] Lanthanide chloride ($LnCl_3$) salts have a high boiling point, which lowers the vapor pressure of $CuCl_2$ and prevent melt segregation between Cu and K, thereby improving the stability and preserving the activity.[41,44] The support material of choice was not very clear over the years. Both SiO_2 and Al_2O_3 seemed promising candidates, but the Al_2O_3 support induces a higher stability of the Cu phase

and is less pronounced to deactivation.[58,64] The Cu/K/La/Al$_2$O$_3$ catalyst is considered a benchmark catalyst due to the vast amount of research conducted and due the fact that it is a commercial ethylene oxychlorination catalyst, but chances were found to be slim that it will make it into a commercial MOC catalyst.[65,66]

1.3.4. 2002 - 2006 The Post Copper Era

While La was often used as an additive, it was never regarded as an active metal in the oxychlorination reaction due to its inability to change oxidation state. It was therefore very surprising when Dow Global Technologies filed a patent in which bulk catalysts solely based on rare-earth metals was reported for the MOC reaction.[55] The use of La in particular was preferred since it could achieve a high selectivity towards CH$_3$Cl (> 70%) at reasonable conversion levels (~ 10%) and low CO$_x$ selectivity (< 20%). A process is described to go from CH$_4$ to olefins via an HCl-assisted route. The same catalyst was used for the oxychlorination of C$_2$ hydrocarbons and for the integrated oxychlorination of C$_1$ and C$_2$ hydrocarbons, both for the production of vinyl chloride monomer (VCM).[67,68] Even though the La-based catalyst is stable for weeks, the activity was still too low for industrial application. The low conversion of CH$_4$ and HCl caused large recycle streams and the costly separation of the HCl/H$_2$O azeotrope.[69] At temperatures where reasonable conversion levels are obtained, the selectivity towards the unwanted polychlorinated C$_1$ is increased. Very few publications in the patent literature are reported from that moment on. However, the topic of MOC regained interest after 2006 in the academic literature, with the publication of 23 articles between 2006 and 2022. The current state-of-the-art is discussed in section 1.4.3 of this chapter.

1.4. DESIGN OF METHANE OXYCHLORINATION CATALYSTS

Evident from the MOC history is that the stability and activity/selectivity relation are crucial design features to make the entire process feasible. Hence, in this section, those two design criteria will be discussed, and an overview of the current benchmark catalysts is presented.

1.4.1. Stability and Chlorination Behavior

The stability of the catalyst is a critical design feature as replacing the catalyst is costly in terms of raw material and process downtime. The elements applied as active site, support and/or promotor must be resistant to the harsh reaction conditions, i.e., chlorinating and oxidative environment at ~ 500 °C.[70] Catalyst leaching, caused by chlorination of the metal which exhibits a high vapor pressure at reaction conditions, was the main concern when operating the CuCl$_2$-based catalyst. The stability of a suitable MOC catalyst can be ensured in two scenarios. The first scenario is when the material does not chlorinate at all under reaction conditions, even though the metal chloride counterpart would possess a very low boiling point, e.g., Al$_2$O$_3$ or SiO$_2$. The second scenario is when the material readily chlorinates, but has a very low vapor pressure under reaction temperatures, e.g.,

LaCl$_3$. Hammes et al. reported a comprehensive overview on the stability of numerous elements for application in HCl environments at various temperature.[70] Apparent is that the playing field for the design of new MOC catalyst materials is more restricted than in other fields, irrespective of the elements' catalytic performance (Figure 1.4). Depending on the application of the element, i.e., active metal, support or promotor, the resistance to chlorination may vary. Chlorination of the metal is favoured in the case of a Mars-van Krevelen-type of mechanism, where the adsorption of one molecule occurs on top of another adsorbed molecule, as bulk chlorine can participate in the reaction mechanism.[71] However, bulk chlorination is unwanted for support materials and in the case of a Langmuir-Hinshelwood-type of mechanism, where adsorption and dissociation of two or more molecules on the catalyst surface must occur before reacting, as bulk chlorination can impose unwanted changes in morphology and surface area.[71] These selection rules should act as the basis for the design of new MOC catalysts.

1.4.2. The Activity-Selectivity Relation

Achieving a high activity, while maintaining a high selectivity towards the desired product is the holy grail in any direct CH$_4$ conversion reaction. High conversion levels are needed to reduce separation cost of the recycle stream, while a high selectivity is required to make efficient use of the feedstock. Both are crucial to reduce the operation cost and environmental impact. A general trend observed for the MOC is that the selectivity towards polychlorinated C$_1$ and CO$_x$ increases with increasing conversion levels. This prob-

Figure 1.4. Stability of the pure metal oxides against chlorination with HCl adapted from reference 70 with permission from Elsevier. Literature data on bulk chlorination of the metal oxides is combined with melting/sublimation points of the metal oxides/chlorides. Furthermore, the temperature at which the metal halide pressure attains a value of 10^{-4} atm is also included to account for metal halide leaching.

Table 1.1. Charge calculations on C, H and Cl of CH_4, CH_3Cl, CH_2Cl_2, $CHCl_3$ and CCl_4. Polarization increases with increasing Cl functionalization. Charge calculations were performed with Chem3D Pro 12.0.

Charge (extended huckel)	CH_4	CH_3Cl	CH_2Cl_2	$CHCl_3$	CCl_4
C	-0.20	-0.03	0.14	0.30	0.47
H	0.05	0.03	0.01	0	-
Cl	-	-0.07	-0.08	-0.10	-0.12

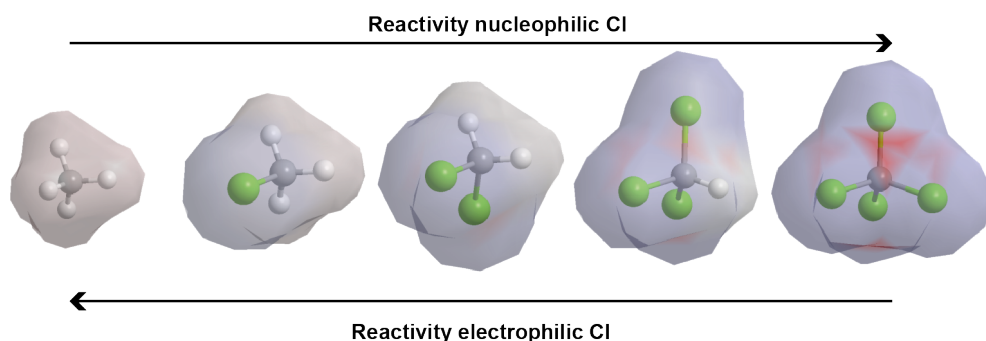**Reactivity nucleophilic Cl**

Reactivity electrophilic Cl

Figure 1.5. The reactivity of the C_1 increases with the reaction of a nucleophilic Cl and decreases with the reaction of an electrophilic Cl, going from CH_4 to CCl_4. The C_1 molecule becomes more polarized with every Cl functionalization. The colour of the cloud indicates the polarization with blue, grey and red being a negative, neutral and positive charge. Molecules were drawn with Chem3D Pro 12.0.

lem is twofold and self-amplifying. The first issue is that with every chlorination step, the C_1 molecule becomes more reactive to over-functionalization and over-oxidation. CH_4 has a tetrahedral geometry with four equivalent weakly polarized C-H sp^3 bonds (Figure 1.5). This makes CH_4 the least reactive alkane, with a bond dissociation energy of 439 kJ/mol.[72] Functionalization of the C_1 molecule with a nucleophilic Cl atom polarizes the molecule, and makes the C more reactive to nucleophilic attacks by Cl or O (Table 1.1). Simultaneously, the C-H bond dissociation energy decreases with increasing polarization of the molecule.[73] Hence, the reactivity of the C_1 molecule increases with every chlorination step.

The second issue is that, for Mars-van Krevelen type of reaction mechanisms, the higher activity generates terminal surface lattice O^{2-} where chlorinated C_1 can be broken down on.[74] With the increasing reactivity of the C_1 molecule with every chlorination step, also the likelihood to be the catalytically destructed to CO_x increases. Thus, the reactivity of C_1 for the catalytic destruction over basic oxides increases in the following order: CH_3Cl < CH_2Cl_2 < $CHCl_3$ < CCl_4.[75] Basic oxides, such as lanthanide (La, Ce, Pr and Nd) and alkali-earth metals (Mg, Ca, Sr and Ba), are potent catalytic materials for the catalytic destruction of polychlorinated C_1.[74–81]

Crucial in optimizing the activity-selectivity performance is the fundamental understanding of the reaction mechanism at play. Olah et al. found that an inserting an electrophilic
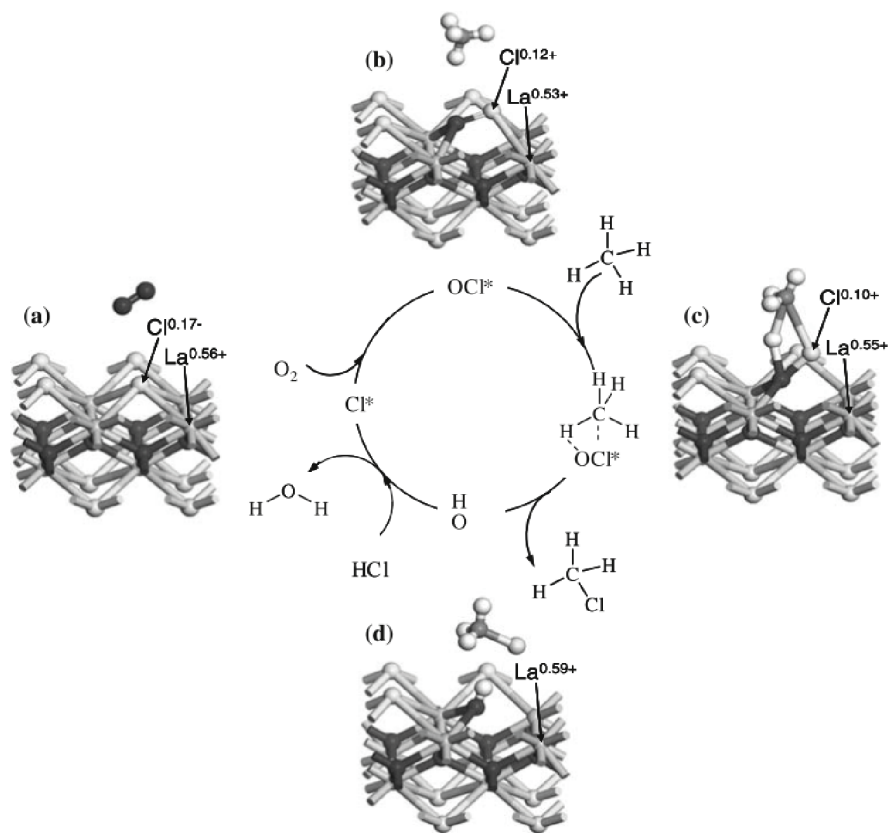
Figure 1.6. The catalytic cycle of the CH_4 oxychlorination reaction over LaOCl adapted from reference 83. By performing density functional theory (DFT) calculations, a reaction mechanism was constructed where an electrophilic Cl atom was inserted in the C_1 molecule and where the irreducible La^{3+} did not change oxidation state. Reprinted by permission from Springer Nature Customer Service Centre GmbH.

Cl catalytically over solid (super)acids could reverse this over-functionalization effect and obtained a great activity/selectivity relation towards CH_3Cl for chlorination with Cl_2 which was previously thermally driven.[82] The principle of inserting an electrophilic Cl was reproduced by Lercher et al. for the MOC reaction.[83,84] A density functional theory (DFT) study was performed to elucidate the reaction mechanism over LaOCl (Figure 1.6). The activation of surface Cl by the dissociative adsorption of O_2 results in a surface OCl^- bridge, where the formal oxidation state of Cl changes from -1 to +1. CH_4 coordinates to this OCl^-, and an atom exchange occurs, leaving a OH^- group on the surface and the chlorinated C_1. This surface OH^- is regenerated by reaction with HCl. At moderate conversions levels (X_{CH4} = 10%), a high CH_3Cl selectivity (S_{CH3Cl} ~ 80%) was obtained with minor by-products of CH_2Cl (12%) and CO (8%), essentially free of CO_2, $CHCl_3$ and CCl_4. These examples illustrate the importance of catalysis to fight the troublesome activity-selectivity relation in reactions with CH_4. Concluding, identification of the reaction mechanism and control over the surface composition is crucial for optimization of the activity/selectivity relation.

1.4.3. Current Benchmark Catalyst Materials

An overview of the reported MOC catalyst compositions from 2006 until 2022 onwards in the academic literature reveals the use of noble metals, transition metals and lanthanides (Figure 1.7A). The wide variety in chemical composition brings a wide variety in catalytic performance along. For several catalyst compositions, a CH_3Cl selectivity (S_{CH3Cl}) > 70% at a conversion level of 10% or higher are reported. However, the temperature at which this performance could be achieved and the normalized reaction rate differ drastically. The best performing catalyst compositions are based on the redox active $Fe^{26,85}$, Ru^{86}, Pd^{87} and Ce^{26} elements, with the exception of the irreducible La^{71}.

A redox active couple therefore seems pivotal for great catalytic activity. This phenomenon can be explained by the fact that for reducible elements, both surface-driven chlorination as well as thermal chlorination contribute to the overall performance. Catalysts based on Ru and Ce are known Deacon catalysts, i.e., the oxidation of HCl and O_2 to produce Cl_2, and exhibit significant Deacon activity under MOC reaction conditions.[95,96] The formed Cl_2 is readily reacted by a free radical mechanism, yielding a product mix that is thermally driven.[97] The exception here is the irreducible La^{3+}-based catalyst material for which a reaction mechanism is proposed in which La^{3+} does not change oxidation state. The CH_4 conversion rate of the non-redox active La^{3+} is significantly lower than for redox active elements. However, non-redox active catalyst compositions must not be written off due to the fact that the reaction is purely surface driven. The reaction mechanism allows for the selective production of CH_3Cl, while for redox-active elements also the production of CO_x and polychlorinated contributes significantly. Of the reported catalyst compositions, the stability of the benchmark catalysts is not always reported or application is not suited for long-term applicability (Table 1.2). The catalyst materials for which chemical, structural and/or catalytic stability is reported are summarized in Figure 1.7B. By applying this selection rule, only a limited number of catalytic materials would potentially be suited for long-term application applications, but none of these catalysts

Figure 1.7. (A) The selectivity plotted versus the temperature at which 10% CH_4 conversion is reached for the catalyst systems of Table 1.2. The colour of the symbol represents the reaction rate, normalized to the catalyst weight ($g_{catalyst}$)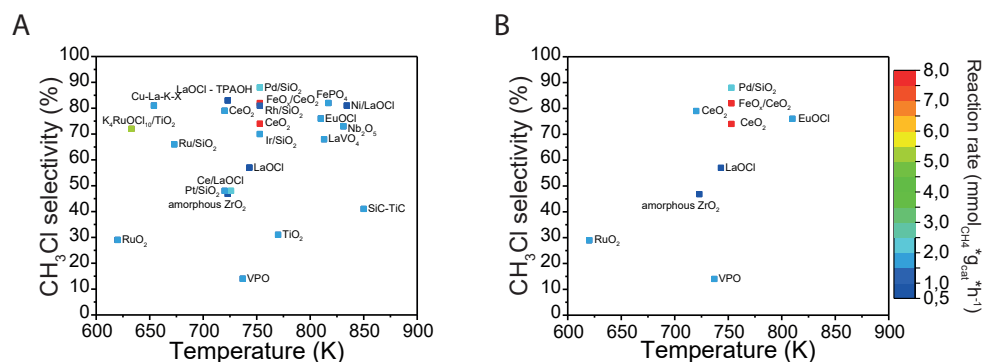. (B) The selectivity plotted versus the temperature at which 10% CH_4 conversion is reached for the catalytic systems of Table 1.2 where stable (chemical, structural and/or catalytic) performance is reported.

can fulfil the stringent activity/selectivity requirements.

1.5. LANTHANIDES AS CATALYST MATERIALS

1.5.1. Tunable Lanthanide-based Catalyst Materials

The lanthanide series, commonly referred to as the rare-earth elements, ranges from La to Lu with the electronic configuration $[Xe]6s^24f^x5d^1$ where x = 0 - 14. The key feature of these elements is that they are chemically very similar, with a common stable oxidation state of 3+ for all lanthanides.[98] The 4f orbitals are shielded from bonding as the 4f orbitals are attracted to the nucleus. A total of three electrons can be drawn from the s and d orbital, which leads to the common 3+ oxidation state. The 4f electrons are held tightly by the nucleus and do not hold any directional preference. Therefore, when comparing two

Table 1.2. Catalytic systems reported in the academic literature. Temperature, CH_3Cl selectivity (S_{CH3Cl}), CO selectivity (S_{CO}) and reaction rate are given at 10% CH_4 conversion. The catalytic systems are graphically depicted in Figure 1.7A. Subsequently, the reported stability (chemical, structural and/or catalytic) is tabulated. Only the catalytic systems for which no stability issues were reported are graphically depicted in Figure 1.7B.

Catalytic System	Temp. (K)	S_{CH3Cl} (%)	S_{CO} (%)	Reaction Rate $(mmol_{CH4}*g_{cat}^{-1}*h^{-1})$	Reaction Rate $(mmol_{CH4} *cm^3_{bed}*h^{-1})$	Remark on stability	Ref
LaOCl	743	57	35	0.99	-	Stable	83,88
LaOCl - TPAOH	723	83	8.4	0.99	-	Not reported	71
Ni/LaOCl	834	81	12	0.99	-	Dopant loss	88
Ce/LaOCl	723	48	48	0.99	-	dopant loss	88
CeO_2	753	74	-	7.88	-	Stable	26
FeO_x-CeO_2	753	82	-	7.88	-	Stable	26
K_4RuOCl_{10}/TiO_2	633	72	13	5.11	-	Not reported	86
RuO_2	620	29	67	1.59	0.88	Known stability [89]	90
CeO_2	720	79	11	1.59	0.88	Known stability [26]	90
$LaVO_4$	813	68	31	1.59	0.88	Not reported	90
Nb_2O_5	831	73	26	1.59	0.88	Not reported	90
TiO_2	770	31	68	1.59	0.88	Not reported	90
VPO	737	14	84	1.59	0.88	Stable	90
EuOCl	810	76	12	1.59	0.88	Known stability [91]	92
Cu-La-K-X	654	81	9	1.59	0.88	Not stable	85
$FePO_4$	817	82	18	1.59	0.88	Not reported	85
SiC-TiC	850	41	55	1.59	0.88	Not reported	93
amorphous ZrO_2	723	48	32	2.46	-	Stable	94
Ru/SiO_2	673	66	27	1.98	0.99	RuSix formation	87
Pt/SiO_2	723	48	48	1.59	0.79	PtO_2 formation	87
Ir/SiO_2	753	70	20	1.74	0.87	Ir and IrSi formation	87
Rh/SiO_2	753	81	11	1.27	0.63	Rh formation	87
Pd/SiO_2	753	88	6	2.38	1.19	Stable	87

lanthanides, the only significant difference is the decrease of ionic radius with increasing atom charge going from La to Lu, commonly referred to as the lanthanide contraction. However, stable oxidation states besides the common 3+ can be observed when the 4f orbitals can be empty, half-filled or completely filled, which is for instance the case in the well-known Ce^{3+}/Ce^{4+} ($4f^1/4f^0$) or in the case of the Eu^{2+}/Eu^{3+} ($4f^7/4f^6$) redox couples.

The tuneable character of the material properties, e.g., electronic and redox, combined with the unexplored potential as catalyst material, make the lanthanide series an interesting case study for the MOC reaction as the chemical and thermodynamic properties can be changed accordingly. This can be achieved by changing the lanthanide element, or making solid solutions of different lanthanides. Lanthanides as catalytic material for the MOC are particularly interesting due to their high stability in corrosive environments.[55,83] The lanthanide series as catalytic materials is not completely unknown, as a number of lanthanide elements were tested for reactions involving Cl, such as the catalytic destruction of chlorinated C_1[75] and the ethylene oxychlorination.[99] The chemical resemblance of the lanthanide series also resulted in comparable catalytic performance for the catalytic destruction reaction. The redox-active site does not seem beneficial as the La^{3+} was more potent than Ce^{4+} for the reaction. However, outliers to the general trends were noticed for the ethylene oxychlorination. A redox couple seems pivotal for obtaining great activity, as the most active elements was Ce^{4+}, followed by Eu^{3+}. Depending on the reaction mechanism at play, acid/base, redox and/or geometric properties must be optimized for enhanced catalysis.

Considering the MOC process, a handful of publications report on the use of La,[71,83,84,88] Ce,[26,95,100] and Eu[101] as catalytic center. The rest of the lanthanide series remains so far largely unexplored. The only study where the entire lanthanide-series is reported for the MOC is in a patent from Dow Global Technologies,[55] but any detailed information on the catalytic performance of different lanthanide elements is lacking. Hence, in this PhD thesis, lanthanide-based MOC catalysts will be synthesized, characterized and tested for their catalytic performance to elucidate the trends in the lanthanide series and couple it to pivotal catalyst design features.

1.5.2. Operando Spectroscopy on Lanthanide-based Catalyst Materials

In order to improve the catalyst design of the lanthanide-based MOC catalyst, information on the structural and chemical properties is required, preferably under varying reaction conditions. Typically, ex-situ (non-reactive conditions) or in-situ (conditions that approach real conditions) characterization of the catalyst material is performed, providing information that might not be representative to the catalyst under real working conditions. Moreover, by performing ex-situ measurements, information on reaction dynamics is lost as the materials is characterized in a static, non-reactive environment. With operando spectroscopy, the catalyst material is studied under working conditions by applying light. This is done by bringing the analytical equipment to the set-up, enabling the coupling of the catalytic performance to the observations made with the analytical technique (Figure 1.8). The presence or absence of the probed changes provides information on reaction
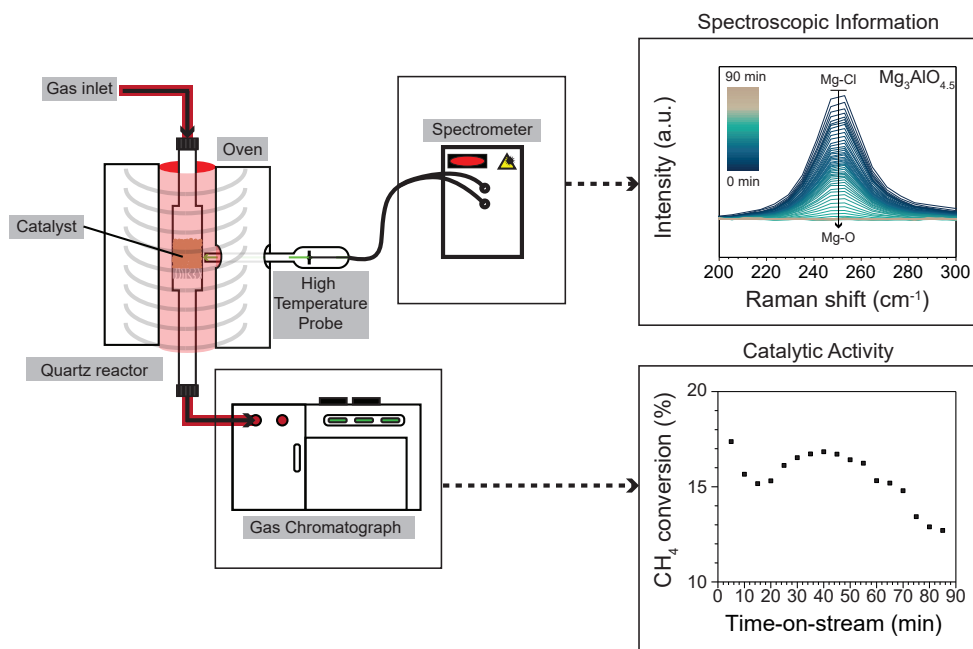
Figure 1.8. Schematic of the operando spectroscopy set-up where the spectrometer is used to obtain chemical information from the catalyst, while the gas chromatograph is used to analyse the catalytic performance of the material under study in the CH_4 oxychlorination (MOC) reaction.

dynamics and material properties. An additional advantage of applying operando spectroscopy is that the analytical equipment is protected from any corrosion issues, as the reactor wall is transparent for light, but it is still a barrier for the reaction mixture.

The two operando techniques applied in this PhD thesis are Raman spectroscopy and luminescence spectroscopy, providing chemical and thermometric information. In both cases, a monochromatic laser is used, but the physical principles and the obtained information is different. With Raman spectroscopy, a laser beam hits the sample and transfer of energy occurs between the material and the incident photons. The absorption of a photon excites the material from a ground state to a virtual excited state. Subsequent re-emission causes the material relaxes back to a different ground state. A photon is emitted which either lost (stokes) or gained (anti-stokes) in energy, thereby mapping vibrational transitions. This process is called inelastic scattering, or Raman scattering. Raman scattering is only allowed if the polarizability of the states is different, hence not all material vibrations can be observed. Plotting the energy difference between the incident photon and the scattered photon versus the intensity yields the Raman spectrum. For solid inorganic materials, the interaction of light mostly occurs with lattice phonons, providing information on bond strength, crystal structure, oxidation state, etc.[102] For the bulk lanthanide-based materials under study in this PhD thesis, chlorination/dechlorination of the catalyst material can occur, causing a change in phonon energy vibration and intensity. By performing operando Raman spectroscopy, the changes in the bulk of the

catalyst can be correlated with the applied reaction conditions, providing mechanistic insights. When performing luminescence spectroscopy, electrons are excited from the ground state to an excited state by absorbing the energy of an incoming photon or other external stimulus.[103] The excited electron relaxes back to the ground state, thereby emitting a photon. The energy of the emitted photon is the energy difference between the excited state and the ground state. Lanthanides have very narrow spectral luminescence features, as there is only weak coupling of the 4f orbitals with molecular vibrations of ligands.[98] The weak interaction with the ligands also causes the spectral features to be largely independent of the chemical environment and coordination number. All but La (4f[0]) and Lu (4f[14]) show luminescence. The emission is strong for all lanthanides as there are a large number of excited states, enabling intersystem crossing. Furthermore, the weak interaction with the environment results in long non-radiative lifetimes, with Eu^{3+} and Tb^{3+} having particularly strong luminescence. The luminescence of the lanthanide elements as characterization is mostly applied to deduct thermometric information [104–107], in this PhD thesis performed in chapter 4. Here, band shape luminescence is applied where the ratio of two thermally coupled excited states is determined. Less well-known is that the luminescence signal can be applied to study the chemical environment of the lanthanide atom[108], applied in chapters 2, 3, 4 and 5.

1.6. SCOPE AND OUTLINE OF THE PHD THESIS

In this PhD thesis, a deeper dive is taken into the field of CH_4 oxychlorination (MOC) catalysis. New catalyst materials are developed for this commercially important reaction and studied in detail with operando spectroscopy. The deducted information on the working principles is applied to improve the catalyst design, and move towards an commercially interesting MOC catalyst material.

The work on designing an improved catalyst material for the MOC reactions starts in chapter 2 where a screening of the materials on the entire lanthanide series is performed. The catalytic materials based on La^{3+}, Pr^{3+}, Nd^{3+}, Sm^{3+}, Eu^{3+}, Tb^{3+}, Dy^{3+}, Ho^{3+}, Er^{3+} and Yb^{3+} in the form of the lanthanide oxide chloride phase are synthesized with comparable physicochemical properties, allowing for a fair comparison of the catalytic performance. Even though all the lanthanide elements exhibited activity in the MOC reaction, Eu^{3+} performed significantly better than the other lanthanides analysed in this screening. Mechanistic insights in the working principles of EuOCl were obtained by performing operando Raman spectroscopy measurements. For EuOCl, the chlorination of the catalyst surface is rate limiting, hence increasing the HCl concentration improves the catalytic performance. The CO selectivity could be suppressed from 30% to 15%, while the CH_4 conversion more than doubled from 11% to 24%, solely by increasing the HCl concentration from 10% to 60% at 450°C.

In chapter 3 the catalyst design of EuOCl for the MOC reaction is improved by the addition of La^{3+} to form solid solutions. The properties of Eu^{3+} and La^{3+} appeared complementary; Eu^{3+} was highly active but the chlorination step of the catalyst surface was rate

limiting and La^{3+} was readily chlorinated, but not very active in the MOC reaction. The La$_{0.50}$Eu$_{0.50}$OCl catalyst revealed synergistic effect, which was reflected in the fact that it was significantly more active than the linear combination of LaOCl and EuOCl. Actually, the CH$_4$ conversion rate of La$_{0.50}$Eu$_{0.50}$OCl was almost as high as EuOCl even though LaOCl did not show any significant activity under the tested condition. Moreover, the activity-selectivity relation was significantly improved, allowing for a more efficient process. Operando luminescence spectroscopy evidenced the faster chlorination of Eu^{3+} by the addition of La^{3+}, facilitating the rate determining step.

In chapter 4 the bifunctionality of Eu^{3+}, i.e., activity in the MOC reaction and luminescence properties, was exploited to correlate the observed activity to the catalyst temperature. By varying the reaction temperature and the gas feed conditions, the dynamic response on the catalyst temperature could be analysed. The catalyst temperature was positively correlated to the CH$_4$ conversion rate, while the gas hourly space velocity (GHSV) did not show a good correlation. A maximum temperature increase of 16 °C compared to the oven temperature was observed. Heat transfer calculations and experimental data evidence that heat dissipation by means of radiation is the predominant heat loss mechanism, resulting in a uniform catalyst bed temperature.

In chapter 5 more insights are obtained into the role of the redox properties and synergistic effects for MOC catalysis. Here it is shown that a catalyst material based on irreducible, synergistic elements can be very active by the design of Mg^{2+}-Al^{3+} mixed-metal oxide (MMO) catalysts. Even though the reference materials MgO and γ-Al$_2$O$_3$ did not show any significant activity in the MOC reaction, the Mg^{2+}-Al^{3+} MMO's were highly active. Synergy between Mg^{2+} and Al^{3+} was only present when intimate contact between these two elements was achieved. Operando Raman spectroscopy revealed that Mg^{2+} is readily chlorinated and can act as a Cl$^-$ buffer. The Al^{3+} present in the catalytic material is able to activate the Cl$^-$ and chlorinate CH$_4$. Hence, the functionalities of Mg^{2+} and Al^{3+} are complementary. The addition of the redox active Eu^{3+} to the irreducible Mg^{2+}-Al^{3+} catalyst enabled tuning of the activity-selectivity relation and made EuMg$_3$Al one of the most active catalyst materials reported. The MMO matrix allowed for facile substitution of atoms, hence the properties of the catalyst material could be altered easily. These results indicate that both redox activity as well as synergistic effects are required to obtaining benchmark performance.

Chapter 6 provides a summary of the PhD thesis in addition to some concluding remarks and future perspectives.

1.7. REFERENCES

(1)   Rodhe, H. A Comparison of the Contribution of Various Gases to the Greenhouse Effect. Science. 1990, 248, 1217–1219.

(2)   Weiland, P. Biogas Production: Current State and Perspectives. Appl. Microbiol. Biotechnol. 2010, 85, 849–860. https://doi.org/10.1007/s00253-009-2246-7.

(3)   International Energy Agency. World Energy Outlook 2021; Paris, 2021.

(4)   International Energy Agency. Methane Tracker 2020 https://www.iea.org/reports/methane-tracker-2020 (accessed Mar 27, 2022).

(5)   Zichittella, G.; Pérez-Ramírez, J. Status and Prospects of the Decentralised Valorisation of Natural Gas into Energy and Energy Carriers. Chem. Soc. Rev. 2021, 50, 2984–3012. https://doi.org/10.1039/D0CS01506G.

(6)   Dincer, I.; Acar, C. Review and Evaluation of Hydrogen Production Methods for Better Sustainability. Int. J. Hydrogen Energy 2014, 40, 11094–11111. https://doi.org/10.1016/j.ijhydene.2014.12.035.

(7)   Scarlat, N.; Dallemand, J.-F.; Fahl, F. Biogas: Developments and Perspectives in Europe. Renew. Energy 2018, 129, 457–472. https://doi.org/10.1016/j.renene.2018.03.006.

(8)   International Energy Agency. IEA Natural Gas Information https://www.iea.org/data-and-statistics/data-product/natural-gas-information (accessed Jun 23, 2022).

(9)   Bui, M.; Adjiman, C. S.; Bardow, A.; Anthony, E. J.; Boston, A.; Brown, S.; Fennell, P. S.; Fuss, S.; Galindo, A.; Hackett, L. A.; Hallett, J. P.; Herzog, H. J.; Jackson, G.; Kemper, J.; Krevor, S.; Maitland, G. C.; Matuszewski, M.; Metcalfe, I. S.; Petit, C.; Puxty, G.; Reimer, J.; Reiner, D. M.; Rubin, E. S.; Scott, S. A.; Shah, N.; Smit, B.; Trusler, J. P. M.; Webley, P.; Wilcox, J.; Mac Dowell, N. Carbon Capture and Storage (CCS): The Way Forward. Energy Environ. Sci. 2018, 11, 1062–1176. https://doi.org/10.1039/c7ee02342a.

(10)   European Biogas Association. Denmark: Countries largest biogas plant under construction https://www.europeanbiogas.eu/denmark-countries-largest-biogas-plant-under-construction/ (accessed July 14, 2022).

(11)   Bioenergy International. Nature Energy inaugurate Korskro biogas plant https://bioenergyinternational.com/nature-energy-inaugurate-korskro-biogas-plant/ (accessed July 14, 2022).

(12)   Otten, R. The first industrial PtG plant – Audi e-gas as driver for the energy turnaround http://www.cedec.com/files/default/8-2014-05-27-cedec-gas-day-reinhard-otten-audi-ag.pdf (accessed June 14, 2022).

(13)   Hepburn, C.; Adlen, E.; Beddington, J.; Carter, E. A.; Fuss, S.; Mac Dowell, N.; Minx, J. C.; Smith, P.; Williams, C. K. The Technological and Economic Prospects for CO_2 Utilization and Removal. Nature 2019, 575, 87–97. https://doi.org/10.1038/s41586-019-1681-6.

(14)   Jarvis, S. M.; Samsatli, S. Technologies and Infrastructures Underpinning Future CO_2 Value Chains: A Comprehensive Review and Comparative Analysis. Renew. Sustain. Energy Rev. 2018, 85, 46–68. https://doi.org/10.1016/j.rser.2018.01.007.

(15)   Davis, S. J.; Lewis, N. S.; Shaner, M.; Aggarwal, S.; Arent, D.; Azevedo, I. L.; Benson, S. M.; Bradley, T.; Brouwer, J.; Chiang, Y.-M.; Clack, C. T. M.; Cohen, A.; Doig, S.; Edmonds, J.; Fennell, P.; Field, C. B.; Hannegan, B.; Hodge, B.-M.; Hoffert, M. I.; Ingersoll, E.; Jaramillo, P.; Lackner, K. S.; Mach, K. J.; Mastrandrea, M.; Ogden, J.; Peterson, P. F.; Sanchez, D. L.; Sperling, D.; Stagner, J.; Trancik, J. E.; Yang, C.-J.; Caldeira, K. Net-Zero Emissions Energy Systems. Science. 2018, 360. https://doi.org/10.1126/science.aas9793.

(16)   Guo, X.; Fang, G.; Li, G.; Ma, H.; Fan, H.; Yu, L.; Ma, C.; Wu, X.; Deng, D.; Wei, M.; Tan, D.; Si, R.; Zhang, S.; Li, J.; Sun, L.; Tang, Z.; Pan, X.; Bao, X. Direct, Nonoxidative Conversion of Methane to Ethylene, Aromatics, and Hydrogen. Science. 2014, 344, 616–619. https://doi.org/10.1126/science.1253150.

(17)   Taifan, W.; Baltrusaitis, J. CH_4 Conversion to Value Added Products: Potential, Limitations and Extensions of a Single Step Heterogeneous Catalysis. Appl. Catal. B Environ. 2016, 198, 525–547. https://doi.org/10.1016/j.apcatb.2016.05.081.

(18)   Olivos-Suarez, A. I.; Szécsényi, À.; Hensen, E. J. M.; Ruiz-Martinez, J.; Pidko, E. A.; Gascon, J. Strategies for the Direct Catalytic Valorization of Methane Using Heterogeneous Catalysis: Challenges and Opportunities. ACS Catal. 2016, 6, 2965–2981. https://doi.org/10.1021/acscatal.6b00428.

(19)   Wang, B.; Albarracín-Suazo, S.; Pagán-Torres, Y.; Nikolla, E. Advances in Methane Conversion Processes. Catal. Today 2017, 285, 147–158. https://doi.org/10.1016/J.CATTOD.2017.01.023.

(20)   Ravi, M.; Ranocchiari, M.; van Bokhoven, J. A. The Direct Catalytic Oxidation of Methane to Methanol—A Critical Assessment. Angew. Chem. Int. Ed. 2017, 56, 16464–16483. https://doi.org/10.1002/anie.201702550.

(21)   Sun, L.; Wang, Y.; Guan, N.; Li, L. Methane Activation and Utilization: Current Status and Future Challenges. Energy Technol. 2020, 8, 1900826. https://doi.org/10.1002/ente.201900826.

(22)   Arinaga, A. M.; Ziegelski, M. C.; Marks, T. J. Alternative Oxidants for the Catalytic Oxidative Coupling of Methane. Angew. Chem. Int. Ed. 2021, 60, 10502–10515. https://doi.org/10.1002/anie.202012862.

(23)   Schwach, P.; Pan, X.; Bao, X. Direct Conver-

sion of Methane to Value-Added Chemicals over Heterogeneous Catalysts: Challenges and Prospects. Chem. Rev. 2017, 117, 8497–8520. https://doi.org/10.1021/acs.chemrev.6b00715.

(24)   Lange, J. P.; De Jong, K. P.; Ansorge, J.; Tijm, P. J. A. Keys to Methane Conversion Technologies. Stud. Surf. Sci. Catal. 1997, 107, 81–86. https://doi.org/10.1016/S0167-2991(97)80320-5.

(25)   Lange, J. P.; Tijm, P. J. A. Processes for Converting Methane to Liquid Fuels: Economic Screening through Energy Management. Chem. Eng. Sci. 1996, 51, 2379–2387. https://doi.org/10.1016/0009-2509(96)00094-2.

(26)   He, J.; Xu, T.; Wang, Z.; Zhang, Q.; Deng, W.; Wang, Y. Transformation of Methane to Propylene: A Two-Step Reaction Route Catalyzed by Modified CeO_2 Nanocrystals and Zeolites. Angew. Chem. Int. Ed. 2012, 51, 2438–2442. https://doi.org/10.1002/anie.201104071.

(27)   Tizard, H. T.; Chapman, D. L.; Taylor, R. Improvements in and Relating to the Halogenation of Hydrocarbons and Their Derivatives. Great Britain Patent 214,293A, 1922.

(28)   Riblett, E. W. Production of Alkyl Halides. United States Patent 2,334,003, 1943.

(29)   Krause, E. Process for the Chlorination of Methane. United States Patent 1,677,831, 1928.

(30)   Lin, R.; Amrute, A. P.; Pérez-Ramírez, J. Halogen-Mediated Conversion of Hydrocarbons to Commodities. Chem. Rev. 2017, 117, 4182–4247. https://doi.org/10.1021/acs.chemrev.6b00551.

(31)   Pierce, F. Inventor hero was a one-man environmental disaster https://www.newscientist.com/article/mg23431290-800-inventor-hero-was-a-oneman-environmental-disaster/ (accessed June 9, 2022).

(32)   Midgley, T. J. Process of Making Organic Lead Compounds. United States Patent 1,622,228, 1927.

(33)   Midgley, T. J.; Henne, A. L.; McNary, R. R. Manufacture of Aliphatic Fluoro Compounds. United States Patent 1,930,129, 1933.

(34)   Barach, A. L. Dangers of Methyl Chloride as a Substitute for Freon. J. Am. Med. Assoc. 1944, 124, 94. https://doi.org/10.1001/jama.1944.62850020002008.

(35)   Kettering, C. F. Biographical Memoir of Thomas Midgeley Jr. (1889-1944). Natl. Acad. Sci. 1947, 14, 370.

(36)   Elkins, J. W.; Thompson, T. M.; Swanson, T. H.; Butler, J. H.; Hall, B. D.; Cummings, S. O.; Fishers, D. A.; Raffo, A. G. Decrease in the Growth Rates of Atmospheric Chlorofluorocarbons 11 and 12. Nature 1993, 364, 780–783. https://doi.org/10.1038/364780a0.

(37)   Wallington, T. J.; Schneider, W. F.; Worsnop, D. R.; Nielsen, O. J.; Sehested, J.; Debruyn, W. J.; Shorter, J. A. The Environmental Impact of CFC Replacements HFCs and HCFCs. Environ. Sci. Technol. 1994, 28, 320A-326A. https://doi.org/10.1021/es00056a714.

(38)   Morrison, R. D.; Murphy, B. L. Chlorinated Solvents. In Environmental Forensics; Elsevier, Amsterdam, 2005; pp 260–273. https://doi.org/10.1016/B978-0-12-507751-4.X5021-6.

(39)   Gorin, E.; Fontana, C. M.; Kidder, G. A. Chlorination of Methane with Copper Chloride Melts Rate of Chlorination. Ind. Eng. Chem. 1948, 40, 2128–2134. https://doi.org/10.1021/ie50467a025.

(40)   Ohtsuka, Y.; Tamai, Y. Oxychlorination of Methane in the Presence of Molten Metallic Chlorides. J. Catal. 1978, 51, 169–172. https://doi.org/10.1016/0021-9517(78)90290-7.

(41)   García, C. L.; Resasco, D. E. High-Temperature Oxychlorination Catalysts: Role of $LaCl_3$ as an Inhibitor of the Segregation of Active Species during Heating/Cooling Cycles. J. Catal. 1990, 122, 151–165. https://doi.org/10.1016/0021-9517(90)90267-N.

(42)   Makris, W. E.; Milam, J. E. Process for the Production of Chlorinated Hydrocarbons. Great Britain Patent 894,137, 1962.

(43)   Gorin, E. Manufacture of Halogenated Hydrocarbons. United States Patent 2,498,546, 1950.

(44)   Garcia, C. L.; Resasco, D. E. Effects of the Support and the Addition of a Second Promoter on Potassium Chloride-Copper(II) Chloride Catalysts Used in the Oxychlorination of Methane. Appl. Catal. 1989, 46, 251–267. https://doi.org/10.1016/S0166-9834(00)81121-5.

(45)   Caprara, G.; Giordano, N.; Montorsi, G. Improvements in or Relating to the Catalytic Conversion of Hydrogen Chloride to Chlorine and the Catalytic Chlorination of Hydrocarbons. Great Britain Patent 1,016,495, 1966.

(46)   Li, T. P. Cupric Chloride-Alumina Catalyst. United States Patent 3,461,084, 1969.

(47)   Rectenwald, C. E.; Keller, G. E. Oxychlorination of Hydrocarbons and a Catalyst Therefor. United States Patent 3,427,359, 1969.

(48)   Improvements in or Relating to Catalytic Oxychlorination Processes. Great Britain Patent 993,939, 1965.

(49)   Piester, L. W.; Vancamp, R. M. Control of Oxychlorination Reactions. United States Patent 3,345,422, 1967.

(50)   Carroll, R. T.; de Witt, E. J. Oxychlorination of Lower Alkanes. United States Patent 3,173,962, 1965.

(51)   Bellis, H. E. Supported Copper Chloride Catalyst and Its Preparation. United States Patent 3,232,889, 1966.

(52)   OxyChem. Chlorinated Organics Handbook; 2014.

(53)   Torres Galvis, H. M.; De Jong, K. P. Catalysts for Production of Lower Olefins from Synthesis Gas: A Review. ACS Catal. 2013, 3, 2130–2149. https://doi.org/10.1021/cs4003436.

(54)   Brophy, J. H.; Font-Freide, J. J. H. M.; Tomkin-

son, J. D. Process for the Production of Hydrocarbons from Hetero-Substituted Methanes. United States Patent 4,652,688, 1987.

(55)		Schweizer, A. E.; Jones, M. E.; Hickman, D. A. Oxidative Halogenation of C1 Hydrocarbons to Halogenated C1 Hydrocarbons and Integrated Processes Related Thereto. United States Patent 6,452,058 B1, 2002.

(56)		Berkowitz, S. Oxychlorination of Mixed Hydrocarbons. United States Patent 3,496,242, 1970.

(57)		Stauffer Chemical Company. Process for Methane Oxychlorination. Great Britain Patent 1,281,406, 1972.

(58)		Pieters, W. J. M.; Carlson, E. J.; Gates, W. E.; Conner, W. C. Pyrogenic Silica or Titania or Alpha-Alumina Cuprous Chloride Catalyst of Hydrogen Chloride/Oxygen Reaction. United States Patent 4,123,389, 1978.

(59)		Tretyakov, V. P.; Zimtseva, G. P.; Rudakov, E. S.; Osetskii, A. N. Low-Temperature Oxidative Chlorination of Methane over Supported Platinum Chloride Catalyst. React. Kinet. Catal. Lett. 1979, 12, 543–546. https://doi.org/10.1007/BF02061769.

(60)		Riegel, H.; Schindler, H. D.; Sze, M. C. Oxychlorination of Methane. United States Patent 4,207,268, 1980.

(61)		Bromhead, J.; Font-Freide, J. J. H. M.; Westlake, D. J. Process for the Production of Methyl Chloride or Ethyl Mono-Chloride or Bromide. European Patent 0,117,731, 1984.

(62)		Noceti, R. P.; Taylor, C. E. Process for Converting Light Alkanes to Higher Hydrocarbons. United States Patent 4,769,504, 1988.

(63)		Blake, R. J.; Roy, G. W. Oxychlorination of Saturated and Unsaturated Hydrocarbons in the Presence of a Fluidized Catalyst Containing Lanthanum and Didymium. United States Patent 3,657,367, 1972.

(64)		Fortini, E. M.; García, C. L.; Resasco, D. E. Stabilization of the Active Phase by Interaction with the Support in CuCl$_2$ Oxychlorination Catalysts. J. Catal. 1986, 99, 12–18. https://doi.org/10.1016/0021-9517(86)90193-4.

(65)		Blake, R. J.; Roy, G. W. Catalyst Regeneration. United States Patent 4,284,833, 1981.

(66)		Ma, H.; Wang, Y.; Qi, Y.; Rout, K. R.; Chen, D. Critical Review of Catalysis for Ethylene Oxychlorination. ACS Catal. 2020, 10, 9299–9319. https://doi.org/10.1021/acscatal.0c01698.

(67)		Gulotty, R. J.; Jones, M. E.; Hickman, D. A. Oxyhalogenation Process Using Catalyst Having Porous Rare Earth Halide Support. United States Patent 6,680,415 B1, 2004.

(68)		Clarke, W. D.; Haymon, T. D.; Henley, J. P.; Hickman, D. A.; Jones, M. E.; Miller, M. C.; Morris, T. E.; Reed, D. J.; Samson, L. J.; Schweizer, A. E.; Smith, S. A. Production of Vinyl Halide from Single Carbon Feedstocks. United States Patent 2005/0,027,084 A1, 2005.

(69)		Podkolzin, S. G.; Stangland, E. E.; Schweiz-er, A. E.; Jones, M. E. Oxidative Halogenation of C1 Hydrocarbons to Halogenated C1 Hydrocarbons. United States Patent 2008/0,275,279 A1, 2008.

(70)		Hammes, M.; Valtchev, M.; Roth, M. B.; Stöwe, K.; Maier, W. F. A Search for Alternative Deacon Catalysts. Appl. Catal. B Environ. 2013, 132–133, 389–400. https://doi.org/10.1016/j.apcatb.2012.11.034.

(71)		Peringer, E.; Tejuja, C.; Salzinger, M.; Lemonidou, A. A.; Lercher, J. A. On the Synthesis of LaCl$_3$ Catalysts for Oxidative Chlorination of Methane. Appl. Catal. A Gen. 2008, 350, 178–185. https://doi.org/10.1016/j.apcata.2008.08.009.

(72)		Luo, Y.-R. Comprehensive Handbook of Chemical Bond Energies, 1st ed.; CRC Press: Boca Raton, 2007. https://doi.org/10.1201/9781420007282.

(73)		Tschuikow-Roux, E.; Paddison, S. Bond Dissociation Energies and Radical Heats of Formation in CH$_3$Cl, CH$_2$Cl$_2$, CH$_3$Br, CH$_2$Br$_2$, CH$_2$FCl, and CHFCl$_2$. Int. J. Chem. Kinet. 1987, 19, 15–24. https://doi.org/10.1002/kin.550190103.

(74)		Van der Avert, P.; Podkolzin, S. G.; Manoilova, O.; de Winne, H.; Weckhuysen, B. M. Low-Temperature Destruction of Carbon Tetrachloride over Lanthanide Oxide-Based Catalysts: From Destructive Adsorption to a Catalytic Reaction Cycle. Chem. Eur. J. 2004, 10, 1637–1646. https://doi.org/10.1002/chem.200305442.

(75)		Van der Avert, P.; Weckhuysen, B. M. Low-Temperature Catalytic Destruction of CCl$_4$, CHCl$_3$ and CH$_2$Cl$_2$ over Basic Oxides. Phys. Chem. Chem. Phys. 2004, 6, 5256–5262. https://doi.org/10.1039/b413876g.

(76)		Van der Avert, P.; Weckhuysen, B. M. Low-Temperature Destruction of Chlorinated Hydrocarbons over Lanthanide Oxide Based Catalysts. Angew. Chem. Int. Ed. 2002, 41, 4730–4732. https://doi.org/10.1002/anie.200290030.

(77)		Weckhuysen, B. M.; Mestl, G.; Rosynek, M. P.; Krawietz, T. R.; Haw, J. F.; Lunsford, J. H. Destructive Adsorption of Carbon Tetrachloride on Alkaline Earth Metal Oxides. J. Phys. Chem. B 1998, 102, 3773–3778. https://doi.org/10.1021/jp980185k.

(78)		van der Heijden, A. W. A. M.; Garcia Ramos, M.; Weckhuysen, B. M. Intermediates in the Destruction of Chlorinated C1 Hydrocarbons on La-Based Materials: Mechanistic Implications. Chem. Eur. J. 2007, 13, 9561–9571. https://doi.org/10.1002/chem.200700901.

(79)		Weckhuysen, B. M.; Rosynek, M. P.; Lunsford, J. H. Destructive Adsorption of Carbon Tetrachloride on Lanthanum and Cerium Oxides. Phys. Chem. Chem. Phys. 1999, 1, 3157–3162. https://doi.org/10.1039/a901847f.

(80)		Podkolzin, S. G.; Manoilova, O. V.; Weckhuysen, B. M. Relative Activity of La$_2$O$_3$, LaOCl, and LaCl$_3$ in Reaction with CCl$_4$ Studied with Infrared Spectroscopy and Density Functional Theory Calculations. J. Phys. Chem. B 2005, 109, 11634–11642. https://doi.org/10.1021/jp050680y.

(81)   Van Der Heijden, A. W. A. M.; Bellière, V.; Alonso, L. E.; Daturi, M.; Manoilova, O. V.; Weckhuysen, B. M. Destructive Adsorption of CCl_4 over Lanthanum-Based Solids: Linking Activity to Acid-Base Properties. J. Phys. Chem. B 2005, 109, 23993–24001. https://doi.org/10.1021/jp054689b.

(82)   Olah, G. A.; Gupta, B.; Felberg, J. D.; Ip, W. M.; Husain, A.; Karpeles, R.; Lammertsma, K.; Melhotra, A. K.; Trivedi, N. J. Electrophilic Reactions at Single Bonds. 20. Selective Monohalogenation of Methane over Supported Acidic or Platinum Metal Catalysts and Hydrolysis of Methyl Halides over Gamma-Alumina-Supported Metal Oxide/Hydroxide Catalysts. A Feasible Path for the O. J. Am. Chem. Soc. 1985, 107, 7097–7105. https://doi.org/10.1021/ja00310a057.

(83)   Peringer, E.; Podkolzin, S. G.; Jones, M. E.; Olindo, R.; Lercher, J. A. $LaCl_3$-Based Catalysts for Oxidative Chlorination of CH_4. Top. Catal. 2006, 38, 211–220. https://doi.org/10.1007/s11244-006-0085-7.

(84)   Podkolzin, S. G.; Stangland, E. E.; Jones, M. E.; Peringer, E.; Lercher, J. A. Methyl Chloride Production from Methane over Lanthanum-Based Catalysts. J. Am. Chem. Soc. 2007, 129, 2569–2576. https://doi.org/10.1021/ja066913w.

(85)   Zichittella, G.; Paunović, V.; Amrute, A. P.; Pérez-Ramírez, J. Catalytic Oxychlorination versus Oxybromination for Methane Functionalization. ACS Catal. 2017, 7, 1805–1817. https://doi.org/10.1021/acscatal.6b03600.

(86)   Shalygin, A.; Paukshtis, E.; Kovalyov, E.; Bal'zhinimaev, B. Light Olefins Synthesis from C1-C2 Paraffins via Oxychlorination Processes. Front. Chem. Sci. Eng. 2013, 7, 279–288. https://doi.org/10.1007/s11705-013-1338-1.

(87)   Paunović, V.; Zichittella, G.; Hemberger, P.; Bodi, A.; Pérez-Ramírez, J. Selective Methane Functionalization via Oxyhalogenation over Supported Noble Metal Nanoparticles. ACS Catal. 2019, 9, 1710–1725. https://doi.org/10.1021/acscatal.8b04375.

(88)   Peringer, E.; Salzinger, M.; Hutt, M.; Lemonidou, A. A.; Lercher, J. A. Modified Lanthanum Catalysts for Oxidative Chlorination of Methane. Top. Catal. 2009, 52, 1220–1231. https://doi.org/10.1007/s11244-009-9265-6.

(89)   Over, H. Atomic-Scale Understanding of the HCl Oxidation over RuO_2, a Novel Deacon Process. J. Phys. Chem. C 2012, 116, 6779–6792. https://doi.org/10.1021/jp212108b.

(90)   Paunović, V.; Zichittella, G.; Verel, R.; Amrute, A. P.; Pérez-Ramírez, J. Selective Production of Carbon Monoxide via Methane Oxychlorination over Vanadyl Pyrophosphate. Angew. Chem. Int. Ed. 2016, 55, 15619–15623. https://doi.org/10.1002/anie.201608165.

(91)   Terlingen, B.; Oord, R.; Ahr, M.; Hutter, E.; van Lare, C.; Weckhuysen, B. M. Mechanistic Insights into the Lanthanide-Catalyzed Oxychlorination of Methane as Revealed by Operando Spectroscopy. ACS Catal. 2021, 11, 10574–10588. https://doi.org/10.1021/acscatal.1c00393.

(92)   Zichittella, G.; Aellen, N.; Paunović, V.; Amrute, A. P.; Pérez-Ramírez, J. Olefins from Natural Gas by Oxychlorination. Angew. Chem. Int. Ed. 2017, 56, 13670–13674. https://doi.org/10.1002/anie.201706624.

(93)   Zichittella, G.; Puértolas, B.; Siol, S.; Paunović, V.; Mitchell, S.; Pérez-Ramírez, J. An Activated TiC-SiC Composite for Natural Gas Upgrading via Catalytic Oxyhalogenation. ChemCatChem 2018, 10, 1282–1290. https://doi.org/10.1002/cctc.201701632.

(94)   Huang, J.; Wang, W.; Li, D.; Xu, S.; Liu, Q.; Chen, X.; Fei, Z.; Zhang, Z.; Cui, M.; Tang, J.; Qiao, X. Facile Construction of Non-Crystalline ZrO_2 as an Active yet Durable Catalyst for Methane Oxychlorination. J. Sol-Gel Sci. Technol. 2019, 92, 163–172. https://doi.org/10.1007/s10971-019-05089-x.

(95)   Scharfe, M.; Zichittella, G.; Paunović, V.; Pérez-Ramírez, J. Ceria in Halogen Chemistry. Chinese J. Catal. 2020, 41, 915–927. https://doi.org/10.1016/S1872-2067(19)63528-X.

(96)   Liu, Y.; Li, S.; Lu, X.; Ma, R.; Fu, Y.; Wang, S.; Zhou, L.; Zhu, W. Insights into the Sintering Resistance of RuO_2/TiO_2-SiO_2 in the Deacon Process: Role of SiO_2. Catal. Sci. Technol. 2021, 11, 5460–5466. https://doi.org/10.1039/d1cy01023a.

(97)   Olah, G. A. Electrophilic Methane Conversion. Acc. Chem. Res. 1987, 20, 422–428. https://doi.org/10.1021/ar00143a006.

(98)   Shriver and Atkins' Inorganic Chemistry, 5th Ed.; Oxford University Press: New York, 2010.

(99)   Scharfe, M.; Lira-Parada, P. A.; Amrute, A. P.; Mitchell, S.; Pérez-Ramírez, J. Lanthanide Compounds as Catalysts for the One-Step Synthesis of Vinyl Chloride from Ethylene. J. Catal. 2016, 344, 524–534. https://doi.org/10.1016/j.jcat.2016.10.026.

(100)   Kim, J.; Ryou, Y.; Hwang, G.; Bang, J.; Jung, J.; Bang, Y.; Kim, D. H. Oxychlorination of Methane over FeO_x/CeO_2 Catalysts. Korean J. Chem. Eng. 2018, 35, 2185–2190. https://doi.org/10.1007/s11814-018-0135-4.

(101)   Zichittella, G.; Aellen, N.; Paunović, V.; Amrute, A. P.; Pérez-Ramírez, J. Olefins from Natural Gas by Oxychlorination. Angew. Chem. Int. Ed. 2017, 56, 13670–13674. https://doi.org/10.1002/anie.201706624.

(102)   Cong, X.; Liu, X. L.; Lin, M. L.; Tan, P. H. Application of Raman Spectroscopy to Probe Fundamental Properties of Two-Dimensional Materials. 2D Mater. Appl. 2020, 4, 13. https://doi.org/10.1038/s41699-020-0140-4.

(103)   Tanner, P. A. Lanthanide Luminescence; Hänninen, P., Härmä, H., Eds.; Springer Series on Fluorescence; Springer Berlin, 2011; Vol. 7. https://doi.org/10.1007/978-3-642-21023-5.

1

(104)   Geitenbeek, R. G.; Vollenbroek, J. C.; Weijgertze, H. M. H.; Tregouet, C. B. M.; Nieuwelink, A. E.; Kennedy, C. L.; Weckhuysen, B. M.; Lohse, D.; Van Blaaderen, A.; Van Den Berg, A.; Odijk, M.; Meijerink, A. Luminescence Thermometry for: In Situ Temperature Measurements in Microfluidic Devices. Lab Chip 2019, 19, 1236–1246. https://doi.org/10.1039/c8lc01292j.

(105)   Brites, C. D. S.; Balabhadra, S.; Carlos, L. D. Lanthanide-Based Thermometers: At the Cutting-Edge of Luminescence Thermometry. Adv. Opt. Mater. 2019, 7, 1801239. https://doi.org/10.1002/adom.201801239.

(106)   Geitenbeek, R. G.; de Wijn, H. W.; Meijerink, A. Non-Boltzmann Luminescence in NaYF$_4$:Eu^{3+}: Implications for Luminescence Thermometry. Phys. Rev. Appl. 2018, 10, 064006. https://doi.org/10.1103/PhysRevApplied.10.064006.

(107)   Geitenbeek, R. G.; Nieuwelink, A.-E.; Jacobs, T. S.; Salzmann, B. B. V.; Goetze, J.; Meijerink, A.; Weckhuysen, B. M. In Situ Luminescence Thermometry To Locally Measure Temperature Gradients during Catalytic Reactions. ACS Catal. 2018, 8, 2397–2401. https://doi.org/10.1021/acscatal.7b04154.

(108)   Zhao, Y.; Li, J. G.; Fang, F.; Chu, N.; Ma, H.; Yang, X. Structure and Luminescence Behaviour of As-Synthesized, Calcined, and Restored MgAlEu-LDH with High Crystallinity. Dalt. Trans. 2012, 41, 12175–12184. https://doi.org/10.1039/c2dt31249b.
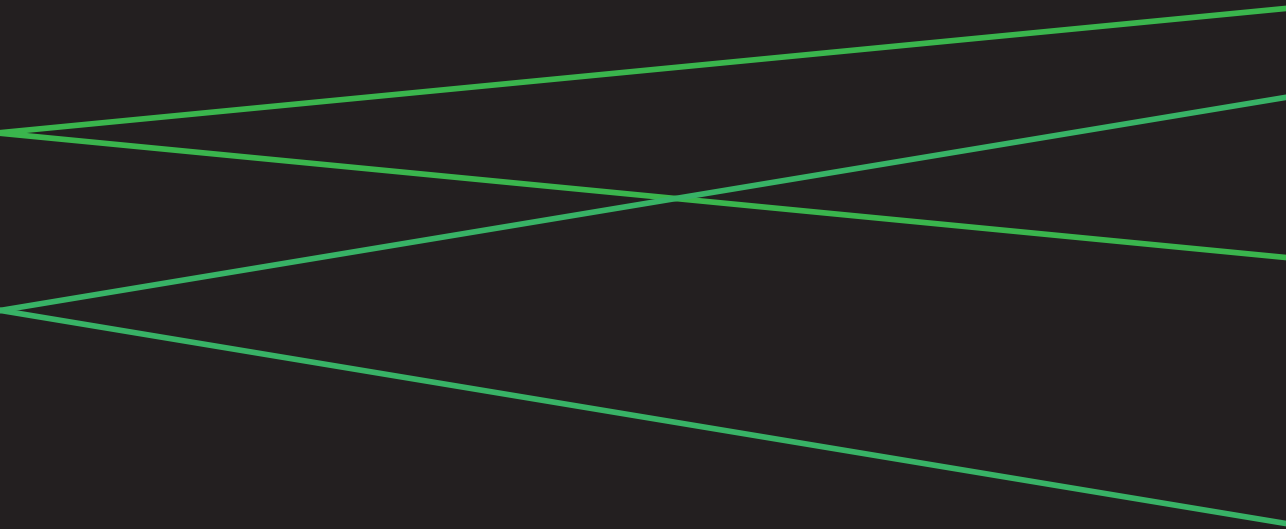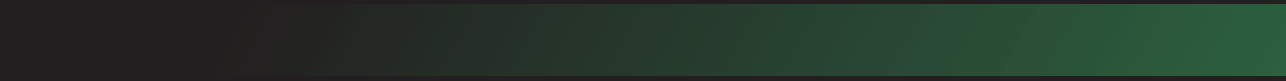
2

Mechanistic Insights in the Lanthanide-Catalyzed Oxychlorination of Methane as Revealed by *Operando* Spectroscopy

Abstract

Commercialization of CH_4 valorization processes is currently hampered by the lack of suitable catalysts, which should be active, selective and stable. CH_4 oxychlorination is one of the promising conversion routes to directly functionalize CH_4. Lanthanide-based catalysts show great potential for facilitating this chemical reaction, although relatively little is known about their functioning. In this chapter, a set of lanthanide oxychlorides (i.e., LnOCl with Ln = La, Pr, Nd, Sm, Eu, Gd, Tb, Dy, Ho) as well as Er- and Yb-based catalysts were synthesized, characterized and tested. All lanthanide-based catalyst materials were able to convert CH_4 into chloromethanes, but their catalytic properties differed significantly. EuOCl possessed the most promising catalytic activity and selectivity as very high conversion levels (> 30%) and CH_3Cl selectivity values (> 50%) could be reached at moderate reaction temperatures (~ 425 °C). Operando Raman spectroscopy revealed that the chlorination of the surface of the EuOCl catalyst material was rate limiting, hence increasing the HCl concentration improved the overall catalytic performance. The CO selectivity could be suppressed from 30% to 15%, while the CH_4 conversion more than doubled from 11% to 24%, solely by increasing the HCl concentration from 10% to 60% at 450°C. Even though more solid catalysts, reported in this chapter as well as in the literature, show a negative correlation between the S_{CO} and HCl concentration, this effect was never as substantial as observed for EuOCl. Hence, EuOCl has promising properties to bring the oxychlorination one step closer to an economically viable CH_4 valorisation process.

2.1. INTRODUCTION

The use of CH_4 from natural gas in chemical industry is expected to grow in the coming years, especially in view of its lower CO_2 footprint relative to other fossil-based resources, such as coal and crude oil.[1] CH_4 is used in the synthesis of chemical building blocks, such as ammonia, methanol, and acetic acid.[2,3] Central in the synthesis of these molecules is the partial oxidation of CH_4 to CO and H_2 via reforming reactions, followed by one or more synthesis steps to obtain the desired reaction product.[4] A major drawback of this approach is the energy-intensive, multistep process to obtain the desired bulk chemicals. Direct conversion routes of CH_4 into chemical building blocks could possible reduce the energy needed for CH_4 upgrading. To this date, however, direct conversion routes have not been commercialized since high selectivities are often only achieved at low CH_4 conversion levels, while high CH_4 conversion levels lead to the formation of e.g., CO_2.[2,5]

The direct conversion of CH_4 into mono-halogenated C_1, such as CH_3Cl and CH_3Br, via e.g., CH_4 oxychlorination (MOC)[6–11] and CH_4 oxybromination (MOB)[8,12–15] are promising routes for efficient hydrocarbon utilization.[16] Compared to other direct conversion routes of CH_4, high selectivities to the desired product and relatively high conversions can be achieved, while being operated under moderate reaction conditions (i.e., in the 400 - 600 °C temperature range and with p = ~ 1 bar).[14] Chlorinated methanes (CM's) are commodity chemicals and CH_3Cl is especially of great interest due to the chemical analogy between CH_3Cl and CH_3OH.[9,17] It can serve as a building block for the production of valuable commodity chemicals, such as ethylene, propylene and acetic acid.[5,18] Therefore, a high selectivity to the desired CH_3Cl is of great interest in the open literature[8–11,14,19–22], as well as in the patent literature.[18,23–28] However, the selective conversion of CH_4 into CH_3Cl remains very challenging. The polarized bonds in the functionalized molecule are often more reactive than the inert C-H bonds present in CH_4, resulting in undesired by-product formation.[2,5] For MOC, other chlorinated products, such as CH_2Cl_2, are thus also obtained. In the upgrading of CH_3Cl into olefins, even small amounts of CH_2Cl_2 cause rapid zeolite deactivation and thus CH_2Cl_2 needs to be removed from the feedstock.[20] This increases the cost to separate CH_3Cl and requires the development of, for instance, the hydro-dechlorination process to convert polychlorinated C_1 into CH_3Cl.[29]

Olah et al. found that inserting an electrophilic Cl atom catalytically over solid (super) acids could reverse CH_4 over-functionalization and obtain high yields towards CH_3Cl for direct chlorination.[30] However, the chlorination of CH_4 via the oxychlorination reaction is preferred since it utilizes HCl, produced as a by-product in chlorination reactions, with a 100% Cl atom efficiency. In comparison, the Cl atom efficiency of thermal chlorination reactions is only 50%.[30] This concept of an electrophilic Cl atom was successfully adapted by Podkolzin, Lercher et al. and applied in the MOC reaction over LaOCl.[10] Interestingly, a reaction mechanism was proposed where La^{3+} catalyzes the reaction without changing oxidation state.[22] The activation of terminal surface lattice Cl by the dissociative adsorption of O_2 results in a surface hypochlorite (ClO^-), where the formal oxidation state of Cl changes from -1 to +1. CH_4 coordinates to this ClO^-, and an atom exchange occurs, leaving

a hydroxyl (OH^-) group on the surface and the CM. This surface OH^- group reacts with HCl to regenerate the chlorinated surface and producing water. Bulk LaOCl catalysts with S_{BET} of around 20 m^2/g were activated with HCl and were able to chlorinate CH_4.[10] At moderate conversions levels (X_{CH4} = 10%), S_{CH3Cl} ~ 80% was obtained with minor by-products of CH_2Cl_2 (12%) and CO (8%), essentially free of CO_2, $CHCl_3$ and CCl_4.

However, these high selectivities were only obtained at low CH_4 conversion levels (X_{CH4} = < 10%). As the conversion of CH_4 was increased (X_{CH4} = ~ 18%), the CO yield would surpass the CH_3Cl yield.[11] Overoxidation of CH_4 into CO_x at high conversion levels is the biggest challenge in the catalyst and process development for the MOC reaction.[8,32] Controlling the degree of surface chlorination of the solid catalysts, while maintaining a high conversion level is crucial for an economically viable process. For La-based catalysts, it is known that the CH_4 chlorination step leaves a terminal surface lattice O^{2-}, while the exact same site is also responsible for the catalytic destruction of polychlorinated hydrocarbons.[33] Balancing the chlorination rate with HCl and dechlorination rate by the reaction with CH_4 and O_2 is crucial for controlling the catalyst selectivity.

While a handful of scientific publications report on the use of La[10,11,21,22], Ce[7,9,19] and Eu[6], the rest of the lanthanide series remains so far largely unexplored. Lanthanides are interesting due to their high stability in corrosive environments, tunable redox properties and are thought to exhibit comparable chemistry in the oxychlorination reaction.[18] Eu-based catalyst materials were previously reported as promising ethylene/propylene oxychlorination and CH_4 oxybromination catalysts.[6,13] The well-tailored redox properties of EuOX (with X = Cl or Br) were crucial in developing an active and selective catalysts.[6] Less successful was the use of EuOCl in MOC where overoxidation seemed to be a large issue. For example, a S_{CO} value of ~ 20% was observed at similar CH_4 conversion levels, which is too high for industrial application.[6]

In this chapter, a comprehensive study on the CH_4 oxychlorination over a series of lanthanide-based catalysts with the general formula LnOCl, where Ln = La, Pr, Nd, Sm, Eu, Gd, Tb, Dy, Ho, is performed. Two other lanthanide catalyst materials, namely Er- and Yb-based catalysts, were also synthesized with the same synthesis technique, which did not yield the LnOCl phase. Although not all lanthanide-based catalysts showed equally high activity, the results in this chapter revealed that they can be used to directly activate CH_4 into CM's. Moreover, we show that a EuOCl catalyst possesses unique characteristics that make it possible to develop solid catalysts with high conversions and low selectivities towards CO_x as unwanted by-products. Central in this study is the possibility to operate a EuOCl catalyst in HCl-rich environments. The CO selectivity could be suppressed, while the CH_4 conversion more than doubled, solely by increasing the HCl concentration. Even though more reported catalyst materials show this behavior (e.g., CeO_2 when HCl% 6% -> 15 %, X_{CH4} ~ 31% -> ~ 34% and S_{CO} ~ 17% -> ~ 15%),[14] this effect was never as substantial as observed for EuOCl. Furthermore, new mechanistic insights in the working principles of this superior EuOCl catalyst material was obtained by using operando spectroscopy.

2.2. RESULTS AND DISCUSSION

2.2.1. Physicochemical Properties of the Lanthanide Oxychlorides

All lanthanide oxychloride (LnOCl) materials under investigation, which have been made by precipitating $LnCl_3 \cdot xH_2O$ with ammonium hydroxide, were characterized in detail with a range of analytical methods. The result is a set of solid catalysts with surface areas, crystal phase and particle morphology in the same order of magnitude. This enabled us to study the role of the lanthanide ion within the LnOCl structure and its effect on MOC performances. As an example, Figure 2.1A shows the x-ray diffraction (XRD) patterns of the as-synthesized catalysts. All LnOCl materials have the exact same crystal structure as LaOCl (ICDD 00-00800477). The general trend is that the peak positions (e.g., the [101] diffraction peak) are shifting towards higher angles with increasing atom number, as can be concluded from Figure 2.1B. This reveals a contraction of the lattice parameters, which is caused by the lanthanide contraction effect.[34] Significant contributions of Ho_2O_3 (COD 1537840) and Ho_3O_4Cl[35] were observed in the case of HoOCl, but the dominating phase is LnOCl. Unfortunately, for Er and Yb we were not able to obtain a similar crystal phase, as indicated by the absence of the typical XRD pattern for LnOCl materials. In addition, the broadness of the XRD peaks suggests relatively small crystalline domains. For simplicity, we have labeled the Er and Yb catalyst materials as ErOCl and YbOCl, respectively, although this is formally incorrect.

An overview of the physicochemical properties of the different as-synthesized catalysts synthesized is given in Table 2.1. It can be noted that Brunauer Emmett Teller (BET) sur-
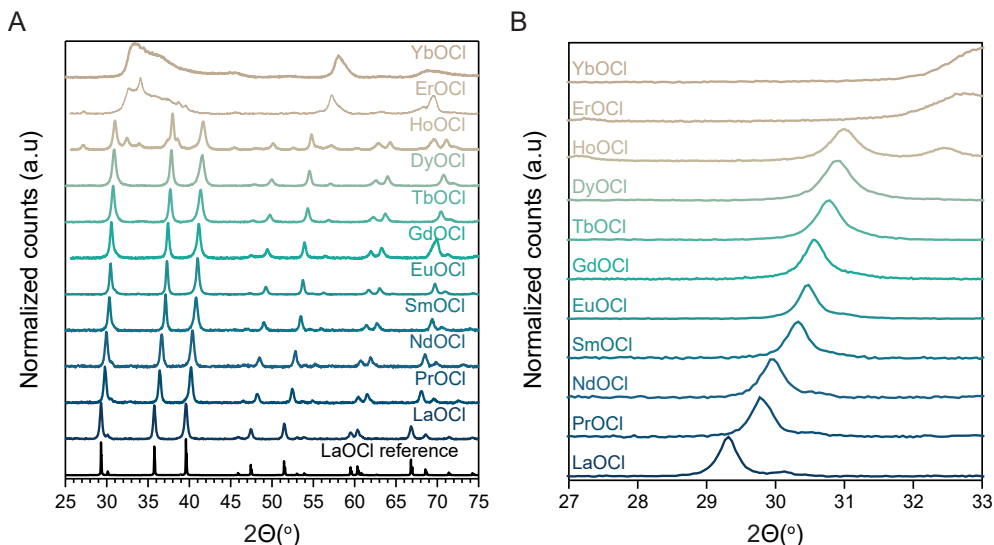
Figure 2.1. (A) X-ray Diffraction (XRD) patterns of the catalyst materials under study, including LaOCl, PrOCl, NdOCl, SmOCl, EuOCl, GdOCl, TbOCl, DyOCl, HoOCl, ErOCl and YbOCl. Each of these materials was obtained in the LnOCl phase, except for ErOCl and YbOCl; and (B) Zoom-in of the XRD patterns, revealing lanthanide contraction in the LnOCl materials, as indicated by the shift of the [101] diffraction in the 27 - 33° region.

Table 2.1. S_{BET} and V_{pore} of as-synthesized Lanthanide Oxychloride (LnOCl) catalyst materials (where Ln = La, Pr, Nd, Sm, Eu, Gd, Tb, Dy, Ho, Er or Yb).

	S_{BET} (m²/g)	V_{pore} (cm³/g)
LaOCl	24.4	0.06
PrOCl	43.2	0.05
NdOCl	47.9	0.06
SmOCl	50.2	0.11
EuOCl	37.4	0.23
GdOCl	30.7	0.10
TbOCl	24.9	0.13
DyOCl	18.1	0.14
HoOCl	20.5	0.10
ErOCl	29.8	0.11
YbOCl	15.5	0.10
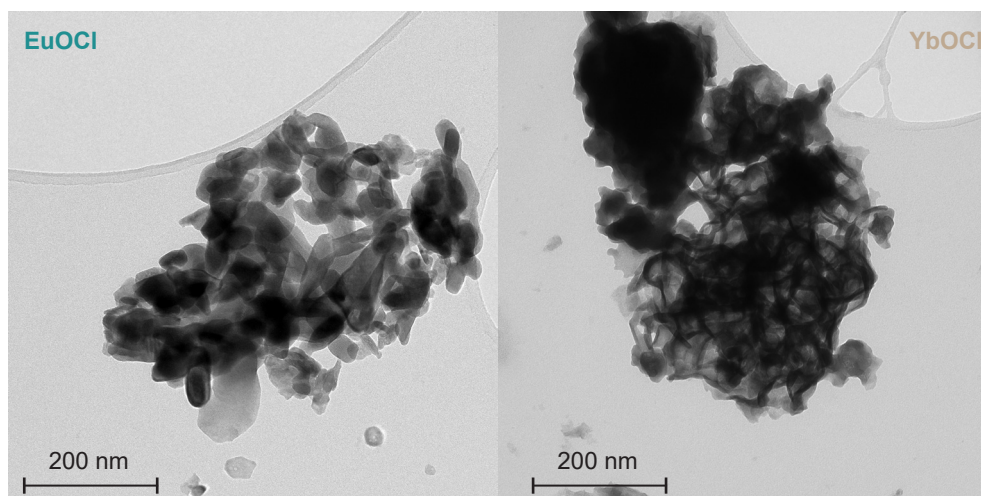
Figure 2.2. Transmission electron microscopy (TEM) image of as-synthesized EuOCl (left) and YbOCl (right) where ill-defined catalyst particles with varying particle sizes are observed.

face areas (S_{BET}) within the same order are obtained, albeit we observed some variations, ranging from 15.5 m²/g (YbOCl) to 50.2 m²/g (SmOCl). Similarly, the determined pore volume (V_{pore}) ranged from 0.05 cm³/g (PrOCl) to 0.23 cm³/g (EuOCl). All the other S_{BET} and V_{pore} values fell within this range and correspond well to the S_{BET} reported for the same synthesis of LaOCl materials by a base precipitation method.[10,17,21,22] As the solid catalysts under study are bulk materials and made with base precipitation, ill-defined particles with a particle size ranging from a few nanometers to hundreds of nanometers are obtained. A representative transmission electron microscopy (TEM) image of EuOCl and

YbOCl are given in Figure 2.2. Especially for YbOCl, only larger irregularly shaped particles were observed. The fact that the S_{BET} values (Table 2.1) were in the same range (15.5 - 50.2 m^2/g) and that the catalyst materials were synthesized with the same crystal structure, allowed us to fairly compare the set of synthesized catalyst materials and study the unique role of the lanthanide element on the activity and selectivity observed in the MOC reaction. HoOCl, ErOCl and YbOCl do not fully comply to these criteria, but since interesting catalytic behavior was observed, and a complete overview of the lanthanide series could be presented, these catalyst materials are also included in this chapter.

2.2.2 Catalytic Performances

The catalytic activity of the as-synthesized lanthanide-based catalyst materials were compared by performing temperature ramp experiments under standard oxychlorination conditions for the production of CH_3Cl. The methane conversion (X_{CH4}) and selectivity to x (S_x) are plotted versus the temperature in Figure 2.3 for every catalyst material individually. The selectivity is plotted when both CH_3Cl and CO were above the detection limit of the Gas Chromatography (GC) and the onset temperature at which the catalyst become active is determined as the temperature at which $X_{CH4} > 2\%$. All catalyst materials tested in this chapter show activity in the MOC reaction. Furthermore, the catalyst materials follow the same trend that the X_{CH4}, S_{CO} and S_{CH2Cl2} increase with increasing temperature, while the S_{CH3Cl} decreases. Nevertheless, some unique catalytic behavior can be observed when comparing the catalyst materials, and large differences in activity and selectivity were observed. Hence, the catalytic materials are now discussed one by one.

LaOCl, known for its high S_{CH3Cl},[10,22] became active at 480 °C and reaches a maximum X_{CH4} of 21% at 550 °C. With increasing reaction temperature, the S_{CH3Cl} decreased from 66% to 32% and the S_{CO} increased from 25% to 45%. It is important to note that substantial amounts of CH_2Cl_2 were formed at 550 °C ($S_{CH2Cl2} = 18\%$), while no CCl_4 nor CO_2 was detected.

PrOCl also became active at 480 °C and reached a maximum X_{CH4} of 20%. However, the selectivity differed drastically compared to the selectivity obtained with LaOCl. Much of the CH_4 is converted to CO, which is the dominant product at temperatures > 495 °C. All four CM's can be observed at temperatures > 535 °C, albeit in very low concentrations in the case of CCl_4 ($S_{CCl4} < 2\%$).

For NdOCl, the same onset temperature as for LaOCl and PrOCl was found, namely 480 °C. However, the X_{CH4} showed a sharp increase in activity up from 495 °C up till 520 °C (X_{CH4}: 5% → 16%) after which the activity reached a maximum till 535 °C. During this sharp increase of the X_{CH4}, the selectivity is also impacted quite drastically as the S_{CH3Cl} decreased from 64% to 38% and the S_{CO} is increased from 24% to 38%. Subsequently, the X_{CH4} increased further and reached a maximum X_{CH4} of 22%. The S_{CH3Cl} decreased further to 28%, while the S_{CO} increased to 46%. The S_{CH2Cl2} increased gradually from 10% to 19%, while $CHCl_3$ was only detected in minor amounts ($S_{CH3Cl} < 6\%$).

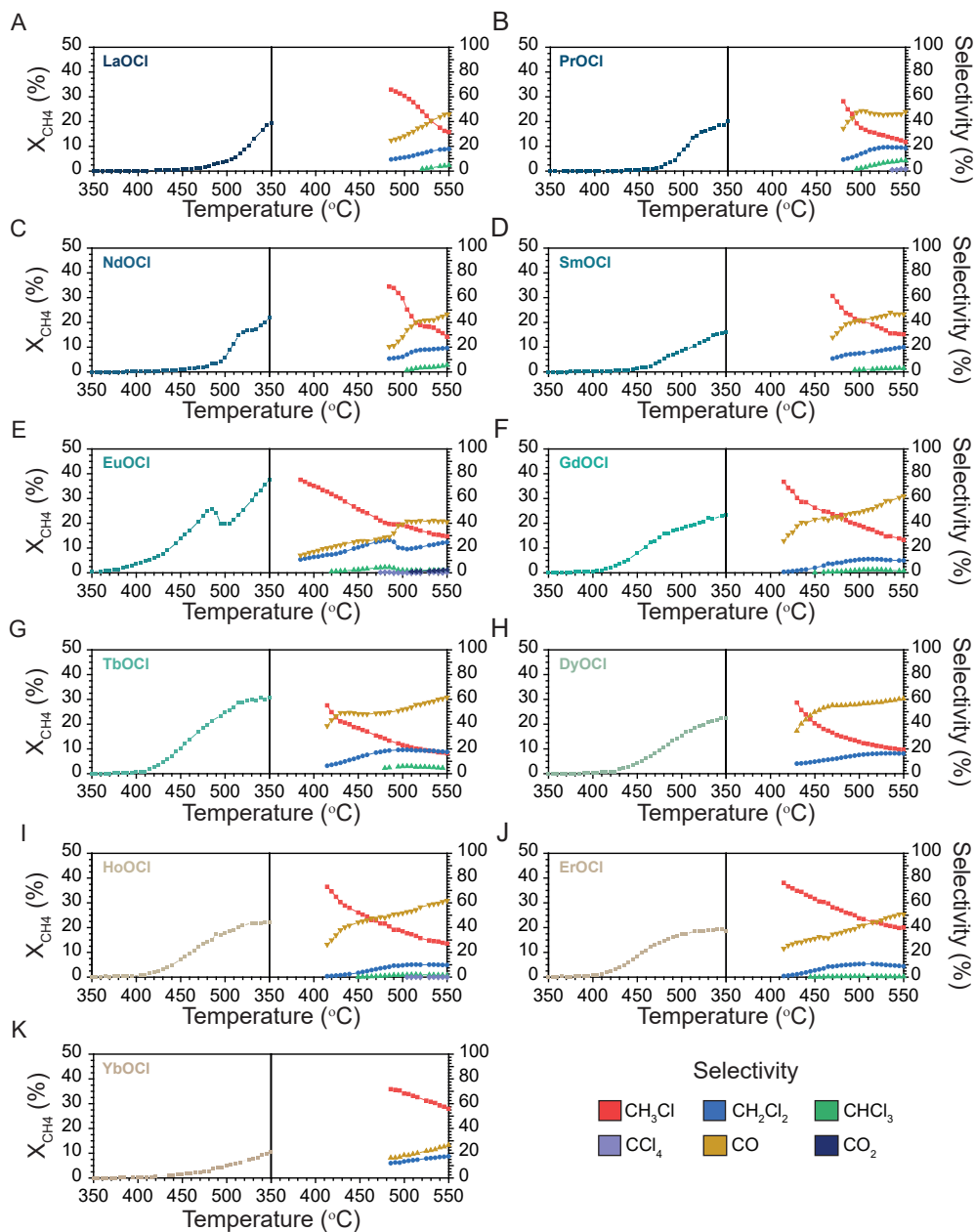SmOCl showed higher activity at lower temperatures as $X_{CH4} > 2\%$ is reached at 465 °C. A

Figure 2.3. The CH_4 conversion (X_{CH4}) and corresponding selectivity plotted versus the temperature for LnOCl where Ln = (A) La, (B) Pr, (C) Nd, (D) Sm, (E) Eu, (F) Gd, (G) Tb, (H) Dy, (I) Ho, (J) Er and (K) Yb. Conditions: CH_4:HCl:O_2:N_2:He of 2:2:1:1:14 (in ml/min) from 350 - 550 °C with a ramp rate of 1 °C/min. Selectivity is given when CH_3Cl and CO were above the detection limit of the Gas Chromatograph (GC).

gradual increase in the activity was observed up to 550 °C where it reached a final X_{CH4} of 16%. The S_{CH3Cl} decreased from 61% to 30%, while the S_{CO} increased from 28% to 46%. The

S_{CH2Cl2} increased with the same trend as the S_{CO} from 11% to 20%. $CHCl_3$ was detected in minor amounts ($S_{CH3Cl} < 3\%$).

The catalytic behavior of EuOCl is unique in a number of aspects. EuOCl showed activity already at low temperatures as $X_{CH4} > 2\%$ is reached at 385 °C. A maximum X_{CH4} of 26% is reached at 485 °C, after which the X_{CH4} drops to 19% at 500 °C. Once the temperature further increased, the X_{CH4} steadily increases to the maximum X_{CH4} of 38%, which is the highest value for all lanthanide-based catalysts tested here under standard oxychlorination conditions. The nature of this drop in X_{CH4} is discussed in section 2.2.4 of this chapter. The unique performance is also reflected in the selectivity plot, where EuOCl started with a maximum S_{CH3Cl} of 75%, which gradually decreased to 29% with increasing reaction temperature. The S_{CO} and S_{CH2Cl2} both increased as a function of temperature, up till the onset of the activity drop at 485 °C. The S_{CO} further increased, while the S_{CH2Cl2} decreased simultaneously up till the end of the drop at 505 °C. From 505 °C to 550 °C, the S_{CO} reached a maximum at 42%, while the S_{CH2Cl2} slightly increased to 24%. $CHCl_3$, CCl_4 and CO_2 were all detected, albeit in very low amounts (i.e., $S_{CHCl3} < 5\%$, $S_{CCl4} < 1\%$, $S_{CO2} < 2\%$).

GdOCl, TbOCl, DyOCl, HoOCl and ErOCl qualitatively show the same trends in activity and selectivity. These catalyst materials became active at reaction temperatures between 420 – 430 °C, after which the X_{CH4} increased very gradual up to 500 °C. Finally, the X_{CH4} increase slightly leveled off and reached the maximum X_{CH4} at 550 °C. For GdOCl, TbOCl, DyOCl, HoOCl and ErOCl, the maximum X_{CH4} was 23%, 30%, 26%, 22% and 19%, respectively. Furthermore, these catalyst materials showed similar selectivity profiles. The S_{CH3Cl} steadily decreased over the tested temperature range, with the best performance for ErOCl (S_{CH3Cl} 76% → 40%) and the worst performance for DyOCl (S_{CH3Cl} 55% → 16%). The S_{CO} first sharply increased up till ~ 440 °C and then gradually increased to a value for S_{CO} of 51% - 62% with the best performance again for ErOCl. The S_{CH2Cl2} increased up till ~ 500 °C after which it leveled off/slightly decreased and reached a final S_{CH2Cl2} of 10% - 20%. $CHCl_3$ was only detected in reasonable amounts for TbOCl and did not increase above 6% over the tested temperature range. CCl_4 and CO_2 were not detected.

Lastly, YbOCl showed relatively low overall activity as $X_{CH4} > 2\%$ is reached at 465 °C and climbing to a maximum X_{CH4} of 11%. The S_{CH3Cl} decreased from 72% to 56%, and the S_{CO} increased from 16% to 26%. Furthermore, only CH_2Cl_2 is detected, which grows from 12% to 18%. No higher CM's were observed and no CO_2 was detected.

The CH_4 conversion rate and the corresponding selectivity for every catalyst material, which are tested at a reaction temperature of 480 °C, are plotted in Figures 2.4A and 2.4B, respectively. This comparative plot clearly shows that, even though the catalysts are chemically and physically comparable, large differences in both the activity and selectivity are induced by the lanthanide element. The highest CH_4 conversion rate of 2.43 mmol $CH_4 \cdot h^{-1} \cdot g^{-1}_{cat}$ was observed for EuOCl, ~ 13x times higher than for LaOCl. Based on the CH_4 conversion rate, the following activity ranking was found: Eu > Tb > Gd ~ Ho ~ Er > Dy > Sm > Pr ≈ Nd ≈ La ≈ Yb with a maximum X_{CH4} of 24% for EuOCl and a minimum X_{CH4} of 2% for LaOCl (Figure 2.3). A similar ranking was constructed based on the S_{CO} (Eu > Pr
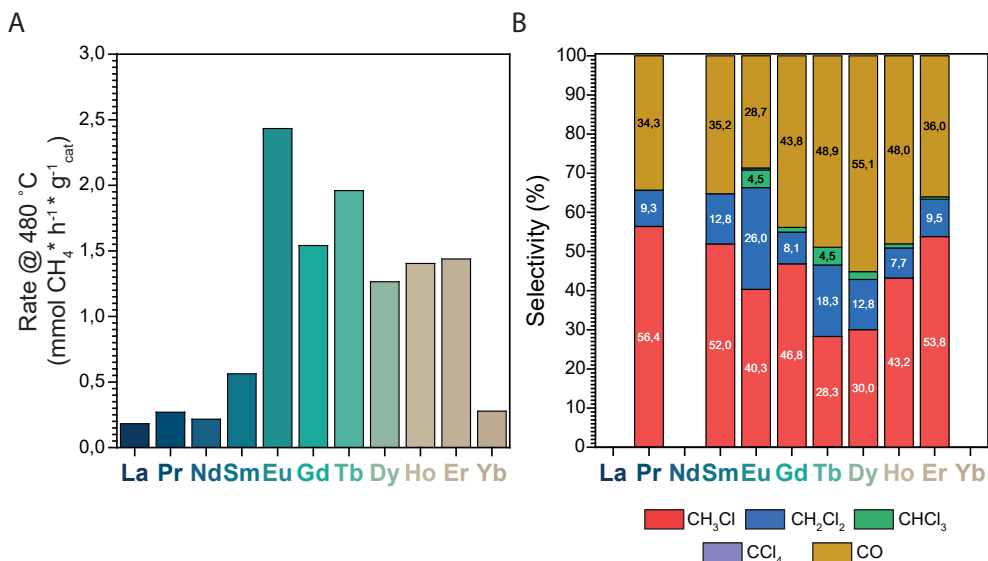
A

B

Figure 2.4. (A) CH_4 conversion rate and (B) selectivity towards CH_3Cl, CH_2Cl_2, $CHCl_3$, CCl_4 and CO for LnOCl (with Ln = La, Pr, Nd, Sm, Eu, Gd, Tb, Dy, Ho, Er or Yb) at a reaction temperature of 480 °C. Note that for LaOCl, NdOCl and YbOCl, the CO yield was below the detection limit, and therefore the selectivity is not displayed. For all catalysts, the CO_2 levels were below the detection limit of the Gas Chromatograph (GC).

~ Sm ~ Er > Gd > Ho ~ Tb > Dy) and $S_{CH3Cl + CH2Cl2}$ (Eu ~ Pr ~ Sm ~ Er > Gd > Ho ~ Tb > Dy) at 480 °C. La, Nd and Yb are not considered with the selectivity ranking as the CO yield was below the detection level.

Based on the activity and selectivity performance, EuOCl possessed the most promising catalytic behaviour as the highest X_{CH4} and the best selectivity at reasonable conversion levels is found. Interestingly, LaOCl was reported for its high S_{CH3Cl} at reasonable conversion levels, but compared to the other lanthanide catalysts tested, its catalytic performance is mediocre under the reaction conditions applied here.[10,11,22]

Based on the above experimental findings, it is important to understand how to tune the reaction selectivity. Four key processes occurring during the MOC reaction for LnOCl materials are schematically depicted in Figure 2.5. These four processes, namely the oxychlorination of C_1 (arrows 1 - 4),[21] a possible pathway for the catalytic destruction of CR_2Cl_2 (arrows 5 - 8),[33,36] chlorination of terminal lattice O^{2-} (arrow 9), and bulk diffusion of O/Cl (arrow 10) are connected as they transition over the same surface compositions. The premise is to skip the catalytic destruction cycle, and accelerate the oxychlorination cycle. In the catalytic chlorination of CH_4, surface chlorination via HCl plays a crucial role. Surface OH^- groups react with HCl to form surface Cl^- and H_2O (arrows 1 - 2). The surface OH^- groups are regenerated as a C_1 and O_2 react over the surface Cl^- (arrows 3 - 4). However, the oxychlorination cycle can be skipped once terminal lattice O^{2-} is formed via condensation via the hydrolysis of surface OH^- groups (arrow 5).[37] The catalytic destruc-
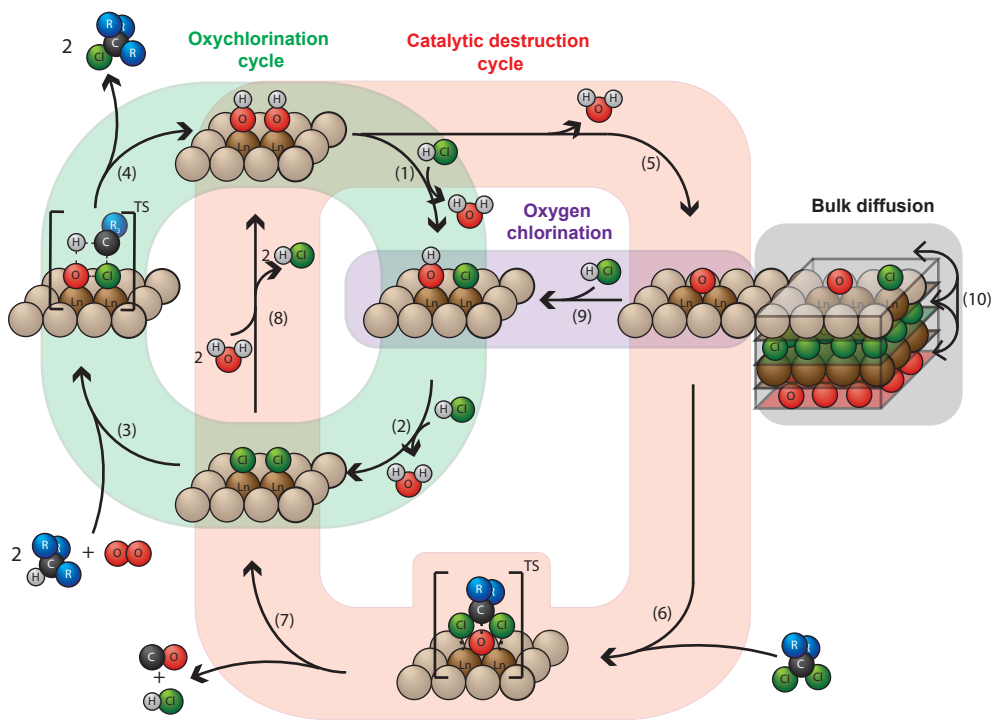
Figure 2.5. Schematic representation of relevant processes occurring during the CH_4 oxychlorination reaction over LnOCl materials. The oxychlorination cycle (green, arrows 1 - 4) and catalytic destruction cycle (red, arrows 5 - 8) are in competition with one another. The chlorination of terminal lattice O^{2-} (purple, arrow 9) is an important step since terminal lattice O^{2-} is held responsible for the catalytic destruction of higher chloromethanes. The surface composition is not only determined by the reactants, but also by bulk diffusion of ions (grey, arrow 10).

tion of CM's over terminal lattice O^{2-} of La is well described[38] and it is hypothesized that a similar mechanism plays a role for the lanthanide-based catalysts tested in the work described in this chapter. When the CM catalytically destructs (arrows 6 - 7), surface chlorination is again obtained, where it crosses paths with the oxychlorination cycle again. H_2O formed during the oxychlorination reaction and surface condensation can react with the formed surface Cl^-, regenerating the surface OH^- groups (arrow 8). Important to note is that terminal lattice O^{2-}, over which catalytic destruction of CM's can occur, can either be chlorinated with HCl (arrow 9) or exchanged with mobile bulk Cl^- (arrow 10). In the case of non-steady state behavior of the catalyst composition, bulk diffusion of ions is partly accountable for changing catalyst surface compositions.[38] Pivotal in the envisaged reaction cycles is the regeneration of the surface Cl^- on which MOC can occur and the catalytic destruction of CM's is prevented.

A direct way to influence the degree of surface chlorination is by altering the HCl concentration under isothermal conditions. To investigate this effect, the catalysts were brought to $X_{CH4} \approx 10\%$ and the concentration of HCl in the feed was increased. The X_{CH4}, S_{CH3Cl}, S_{CO} as well as the S_{CH2Cl2} are summarized in Figure 2.6, while the S_{CHCl3} and S_{CCl4} can be found in
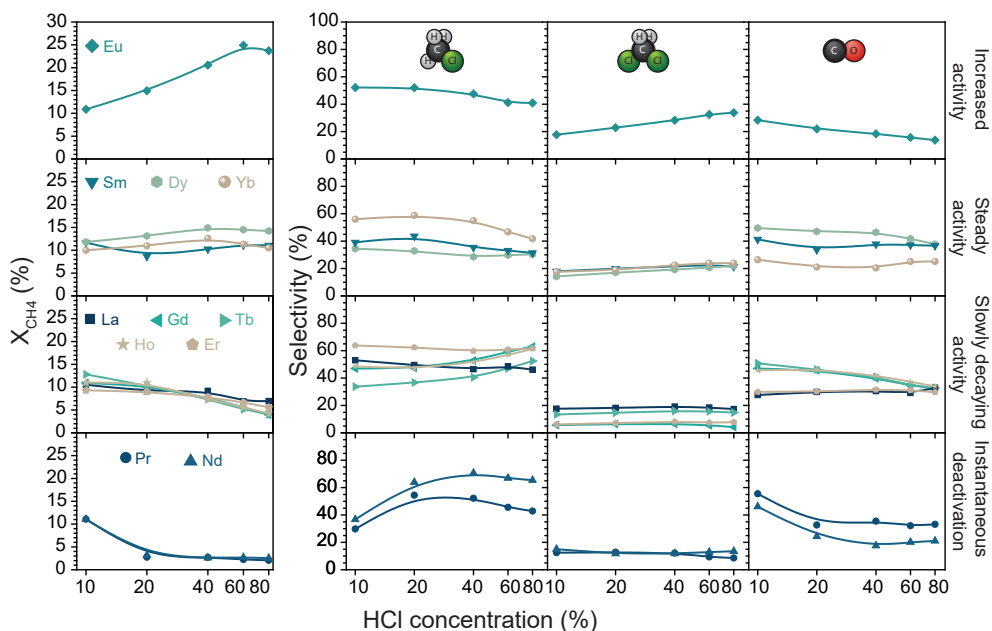
Figure 2.6. The CH_4 conversion (X_{CH4}) and the selectivity towards CH_3Cl (S_{CH3Cl}), CH_2Cl_2 (S_{CH2Cl2}) and CO (S_{CO}) over LnOCl materials (with Ln = La, Pr, Nd, Sm, Eu, Gd, Tb, Dy, Ho, Er or Yb) plotted versus the HCl concentration for the four different categories of catalytic behavior under study. The elements with their corresponding symbol are displayed in the X_{CH4} – HCl concentration plot.

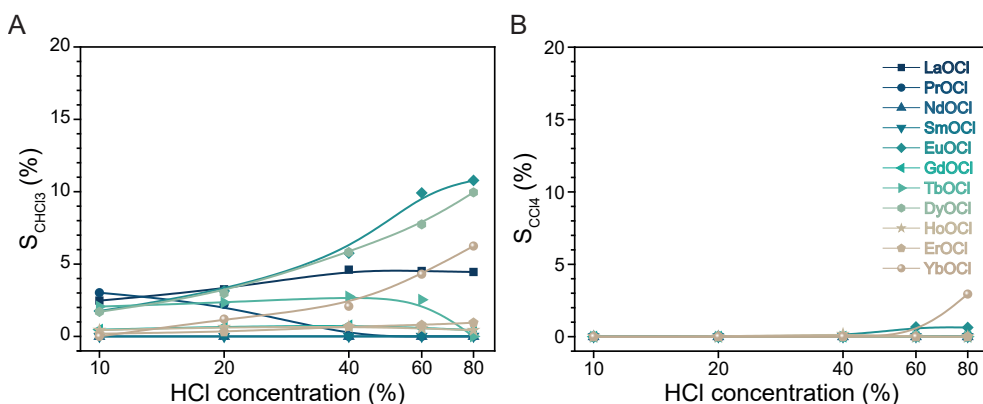Figure 2.7. The (A) selectivity towards $CHCl_3$ (S_{CHCl3}) and (B) CCl_4 (S_{CCl4}) over LnOCl materials (with Ln = La, Pr, Nd, Sm, Eu, Gd, Tb, Dy, Ho, Er or Yb) plotted versus the HCl concentration in the feed. With increasing HCl concentration in the feed, the S_{CHCl3} increases for LaOCl, EuOCl, DyOCl and YbOCl. The S_{CCl4} was not significantly affected by the increment in HCl concentration, except for YbOCl where the S_{CCl4} increased to 3%.

Figure 2.7. Generally, four types of responses can be identified for the different catalyst materials tested on the basis of their measured X_{CH4} values: 1) increased activity (Figure 2.6, first row), 2) steady activity (Figure 2.6, second row), 3) slowly decaying activity (Figure 2.6, third row) and 4) instantaneous deactivation (Figure 2.6, bottom row).

EuOCl is ascribed to the first category; increased activity with increasing HCl concentration. The X_{CH4} is increased from 11% to 25% going from 10 to 60% HCl in the gas feed. Thereafter, the activity reached a maximum of 80% HCl. The increase in HCl concentration did not only boost the activity, but also suppressed the S_{CO} from 28% to 14%. Furthermore, the S_{CH3Cl} is decreasing slightly, while the S_{CH2Cl2} and S_{CHCl3} are increasing with increasing HCl concentration. The formation of CO was largely caused by the catalytic destruction of CH_2Cl_2 and $CHCl_3$ as the S_{CO} and S_{CH2Cl2}/S_{CHCl3} are negatively correlated. The prevention of the catalytic destruction of higher CM's is evidenced by the observed S_{CCl4} for EuOCl. The increase in HCl concentration thus has a double-sided effect: 1) less surface O^{2-} where higher CM's can be catalytically destructed on and 2) the generation of more active sites where chlorination of the C_1 can occur. Carefully choosing the CH_4:HCl:O_2 ratio is thus of great importance for optimal catalytic activity.

SmOCl, DyOCl and YbOCl showed similar activity response with increasing HCl concentration, although the exact values differed significantly. Their X_{CH4} is rather insensitive to the HCl concentration in the feed and only increased slightly. The S_{CH3Cl} and S_{CO} slightly decreased or remained constant, which is in line with the X_{CH4}. The S_{CHCl3} seemed inversely proportional to S_{CO} and S_{CH3Cl} for DyOCl and YbOCl since it shows an upward trend with increasing HCl concentration (Figure 2.7A). For SmOCl, no formation of $CHCl_3$ was observed, indicating that no $CHCl_3$ was formed or that all formed $CHCl_3$ was destructed. For these catalyst materials, the S_{CO} could not be suppressed as dramatically as for EuOCl (for DyOCl 49% → 37% vs. for EuOCl 29% → 14%). A higher degree of surface chlorination mainly resulted in preventing the catalytic destruction of higher CM's for DyOCl and YbOCl and, to a lesser extent, the generation of more active sites for all three catalysts. The generation of more active sites did not result in a higher X_{CH4} but in a higher overall degree of chlorination of CH_4. The reactivity of C_1 increases with increasing Cl content[21] and it appears that CH_4 and the other CM's are in competition over the same active site(s).

LaOCl, GdOCl, TbOCl, HoOCl and ErOCl all revealed a decaying activity profile with increasing HCl concentration in the feed. The activity drops from the most for TbOCl (X_{CH4} 12% → 4%) and the least for LaOCl (X_{CH4} 10% → 7%). When further comparing these five catalysts based on their selectivity, LaOCl and ErOCl show very similar behavior, and GdOCl, TbOCl and HoOCl show very similar behavior. While the X_{CH4} of LaOCl and ErOCl decrease gradually, the S_{CH3Cl}, S_{CO} and S_{CH2Cl2} are not significantly affected. The largest difference in selectivity of these two catalysts can be observed for LaOCl where the S_{CH3Cl} is reduced by 7%. The higher HCl concentration caused the CH_3Cl to be further chlorinated to CH_2Cl_2. The additional CH_2Cl_2 was catalytically destructed, either directly or indirectly via the formation of $CHCl_3$. For GdOCl, TbOCl, and HoOCl, however, larger differences in selectivity were observed, as the S_{CO} decreased from 51% to 33% for TbOCl, while the S_{CH3Cl} simultaneously increased from 33% to 52%. GdOCl, TbOCl, and HoOCl were the only catalysts that showed an increase in the S_{CH3Cl} with increasing HCl concentration. The lower X_{CH4} caused less $CHCl_3$ to form (Figure 2.7A) preventing the destruction to CO. The lower activity also affected the degree of CH_4 chlorination, and thus lowered the quantity of higher CM's present in the system that can be destructed.[33,36]

PrOCl and NdOCl fall within the last category having a catalytic activity that is almost completely lost with increasing HCl concentration. As the activity is correlated to the selectivity observed in the reaction, the S_{CH3Cl} drastically increased with increasing HCl concentration. However, X_{CH4} (< 5%) is too low for commercial use and therefore the selectivity observed is irrelevant. The nature of this rapid X_{CH4} decrease is not investigated in this study, but it is hypothesized that a completely chlorinated surface inhibits the activation of O_2 and/or CH_4 by a change in material acidity/basicity.

Unlike the other catalyst materials tested in this chapter, the catalytic performance of EuOCl can be steered by tuning two key parameters, namely reaction temperature and HCl concentration. To further demonstrate the remarkable tuneability of EuOCl upon increasing the HCl concentration and temperature, the X_{CH4} is plotted versus the reaction temperature for all catalyst materials at a HCl concentration of 10% and 80% in Figures 2.8A and 2.8C, respectively. Except for EuOCl, the X_{CH4} of all catalysts was negatively influenced by the increase in HCl concentration over the entire temperature range. The maximum X_{CH4} of all catalysts dropped significantly, e.g., from 31% to 19% for TbOCl. This coincided with the results presented in Figure 2.6, where EuOCl was the only catalyst that saw an increase in X_{CH4} when increasing the HCl concentration. Under 10% HCl, the maximum X_{CH4} of 38% is reached at 550 °C for EuOCl. The increase in HCl concentration simultaneously lowered the temperature at which the maximum X_{CH4} is reached to 505 °C and increases the max X_{CH4} to 42%. Furthermore, the observed activity drop is delayed by 20 °C; the nature of this drop will be discussed in section 2.2.4 of this chapter. When further comparing the temperature dependent performance of EuOCl at 10% and 80% HCl concentration, large selectivity differences are observed (Figures 2.8B and 2.8D). The S_{CO} is suppressed below 15% at 80% HCl, even at very high conversion levels (X_{CH4} = ~ 40%). To our best knowledge, such low CO selectivities at high conversion levels are yet unreported and make EuOCl in this chapter a potential catalyst material for practical applications. The result of the lower CO selectivity is an increase in selectivity towards higher CM's. At 80% HCl concentration and 475 °C, all four CM's are produced. One major drawback from operating the EuOCl system at such high conversion levels is that the selectivity towards CH_3Cl drastically decreased. The generation of more active sites by the fast chlorination due to the excess of HCl, caused the formed CH_3Cl to react further to higher CM's. In that regard, the HCl concentration did not have a significant effect on the CH_3Cl selectivity when comparing the two different ratios. At 10% conversion, both ratios had S_{CH3Cl} = ~ 60% at X_{CH4} = 10%. CO_2 was only detected at high temperatures (> 500 °C) and the selectivity was very low (< 1.2%).

With such large formations of CH_2Cl_2 and $CHCl_3$ and noticeable amounts of CCl_4 observed at high conversion levels at 80% HCl, thermal chlorination might be a viable route instead of the surface catalyzed reaction. This is supported by the fact that a discrepancy in the product selectivity was observed when comparing the 10% and 80% HCl in the feed (Figures 2.8B and 2.8D). Previous work by Pérez-Ramírez et al. already investigated the HCl oxidation over EuOCl.[6] Based on these findings, the thermal chlorination of CH_4 with Cl_2 seemed to only have a minor contribution to the total chlorination of CH_4 at the
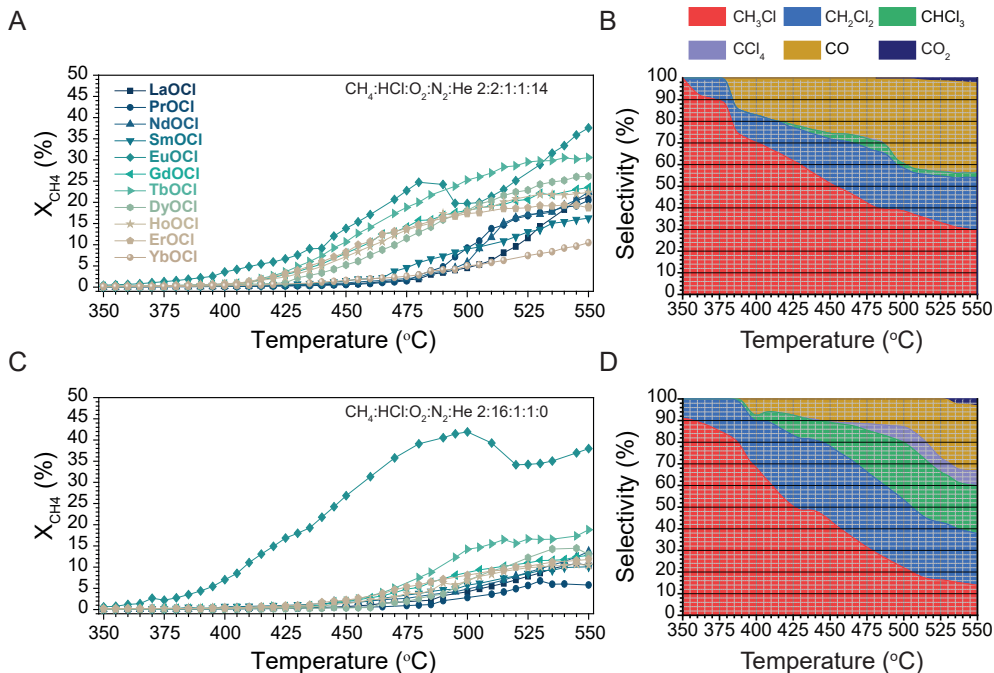
A

B

C

D

Figure 2.8. The CH_4 conversion (X_{CH4}) plotted versus the temperature for LnOCl (where Ln = La, Pr, Nd, Sm, Eu, Gd, Tb, Dy, Ho, Er or Yb) under (A) 10% HCl and (C) 80% HCl. The increment in HCl concentration enhanced the activity of EuOCl while for all the other catalysts, the activity was decreased. Selectivity towards CH_3Cl, CH_2Cl_2, $CHCl_3$, CCl_4, CO and CO_2 plotted versus the temperature for EuOCl tested in (B) 10% HCl and (D) 80% HCl.

A

B
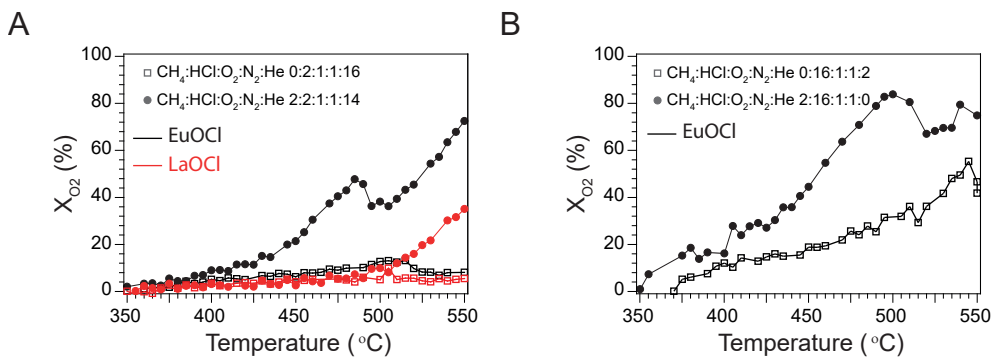
Figure 2.9. Temperature ramp experiments where oxygen conversion (X_{O2}) is plotted versus the temperature for HCl oxidation reaction (square) and CH oxychlorination (circle) for (A) LaOCl (red) and EuOCl (black) with 10% HCl (open) in the feed, (B) EuOCl with 80% HCl (filled) in the feed.

used temperature range in this study. However, the reaction mechanism proposed for LaOCl does not explain how such high selectivity towards e.g., $CHCl_3$ can be formed as observed for EuOCl. Previous work by our group already proposed a mechanism where La is shortly reduced by accepting a H from CH_2Cl_2.[33] The proven presence of the redox couple Eu^{2+}/Eu^{3+}, could participate in the reaction via a similar role and a mechanism can

be proposed for EuOCl where Eu changes oxidation state during the reaction.[39] Furthermore, the presence of substantial amounts of Eu^{2+} was proven under oxychlorination conditions at T > 753K. To investigate what the contribution of the gas-phase chlorination of CH_4 is to the total catalytic performance of LaOCl and EuOCl, the oxygen conversion (X_{O2}) was determined in a reaction mixture with and without CH_4 present. The HCl oxidation results are compared to the oxychlorination reaction with the same $HCl:O_2$ feed ratio. For LaOCl (Figure 2.9A), the X_{O2} was below 5% over the entire tested temperature range. For the oxychlorination reaction over LaOCl, a sharp increase in the X_{O2} is observed from 500 °C to 550 °C where the X_{O2} reaches a final value of 35%. As expected from the literature, no Cl_2 seems to evolve, and thus the gas-phase chlorination of CH_4 does not contribute to the overall activity of LaOCl.[10] HCl oxidation over EuOCl was tested at 10% and 80% HCl in the feed (Figures 2.9A and 2.9B, respectively) as large differences in activity and selectivity were observed when the HCl concentration was varied. At 10% HCl in the feed, the X_{O2} for the oxychlorination reaction was significantly higher than for the HCl oxidation over the entire temperature range. However, some consumption of O_2 was visible for the HCl oxidation with a maximum X_{O2} of 13%, thus contributing to the overall performance although the activity and selectivity are predominantly governed by the surface catalyzed reaction. The discrepancy between the X_{O2} of the HCl oxidation and MOC reaction is reduced when the HCl concentration is increased to 80%. The X_{O2} of both reactions increased, and the relative difference is decreased. Solely by increasing the HCl concentration, the maximum X_{O2} is enhanced from 13% to 55% for the HCl oxidation reaction. The HCl oxidation reaction is accelerated by the large excess of Cl^- present on/in the catalyst, and HCl oxidation played a major role in the overall performance of the catalyst. The large difference in HCl oxidation potency at 10% and 80% HCl also partly explains why the degree of CH_4 chlorination is enhanced when a high HCl concentration is used. The total product selectivity here is partly governed by the free radical reaction which offers very limited control over the selectivity.[16,40] Further research is needed to investigate if the reducibility of Eu^{3+} is enhanced by the excess of HCl.

Up till this point, the excellent performance of EuOCl is demonstrated and compared to the other catalyst materials reported in this chapter. However, the reducible CeO_2 is arguably the best performing catalyst in MOC with a combined yield of CH_3Cl and CH_2Cl_2 of ~ 27%.[14] For EuOCl, a remarkable maximum combined yield of 24% is obtained at 485 °C at 80% HCl. We hypothesize, that by altering the reducibility,[41] enhance the surface area of the active phase,[22,42] and/or increasing the rate of chlorination by adding additives, the benchmark performance of CeO_2 can be matched and potentially exceeded.

Lastly, the response to the change in HCl concentration in the MOC reaction differs quite drastically from lanthanide material to lanthanide material. For catalysts that have the same chemical composition (e.g., supported catalysts with different particle sizes), the S_{BET} of the active phase is often correlated to an increase in activity.[43,44] However, in this study the element is varied, while the physical properties of the materials are kept within the same order. To evaluate whether the activity is correlated to the S_{BET}, the as-synthesized S_{BET} was taken and correlated to the temperature where the $X_{CH4} = 10\%$ at 10% HCl

flow. The calculated R^2 was negative (results not shown), indicating that there is no correlation between the activity of the various lanthanide materials and the S_{BET}. Thus, the difference in catalytic performance is due to the unique properties of the lanthanide element. Correlating the activity to physical properties of lanthanide-based catalyst materials was attempted in the literature for oxychlorination[22] and C_1 catalytic destruction[33,38,42], but this did not yield conclusive results. Due to the fact that the oxychlorination reaction is comprised of two non-catalytic reactions coupled in a catalytic cycle, we must also study the catalyst condition since a more complex mechanism is most probably present that determines the catalyst performance.

2.2.3 Operando Raman Spectroscopy

In the next stage of our study, operando Raman spectroscopy was performed to investigate the occurring phase changes during the chlorination, dechlorination and oxychlorination reactions of LaOCl and EuOCl. The chlorination and dechlorination steps are studied separately as both steps occur simultaneously, and form the catalytic cycle of the MOC reaction. LaOCl and EuOCl were selected as EuOCl possessed the most promising catalytic performance of the catalysts tested in this chapter and LaOCl is often reported for its high S_{CH3Cl} at reasonable conversion levels.[10,11,22] Moreover, both catalysts react differently to a changing HCl concentration in the feed and hence detailed characterization studies could provide further insights in the differences between both systems. The results of the operando Raman study are presented in Figure 2.10. The band assignments are summarized in Table 2.2.

The spectral data of LaOCl is visualized as a contour plot in Figure 2.10A and individual spectra are plotted in Figure 2.10B. Above the contour plot, the intensity plot of three characteristic vibrations, i.e., 217 cm^{-1} ($2E_{2g} + A_g$ of LaCl$_3$), 341 cm^{-1} (A_{1g}, B_{2g} of LaOCl) and 440 cm^{-1} (E_g of LaOCl) are plotted versus the time-on-stream. During the 0-120 min time window, the catalyst is chlorinated (CH$_4$:HCl:O$_2$:N$_2$:He 0:20:0:1:19 in ml/min) at 450 ˚C. The fresh LaOCl is rapidly converted into LaCl$_3$ since the A_{1g}/B_{2g} and E_g of LaOCl disappears within several minutes, while the $2E_{2g} + A_g$ of LaCl$_3$ showed the opposite trend. The intensity of the vibrational modes corresponding to LaOCl did not change significantly after 10 min and disappeared in the background. Simultaneous with the intensity decrease of the LaOCl vibrational modes is the growth of the LaCl$_3$ vibrational mode at 217 cm^{-1}. A rapid increase in peak intensity is observed within the first 10 min after which the Raman vibration intensity growth levels off, as can be seen in the intensity plot. This indicates that the LaOCl is almost fully converted into LaCl$_3$ within 15 min of chlorination. For the 120-210 min time period, the catalyst was first heated to 500 °C and a dechlorination step (CH$_4$:HCl:O$_2$:N$_2$:He 2:0:1:1:16) was performed. The dechlorination of the catalyst material was complete after 155 min since the A_{1g}/B_{2g} and E_g of LaOCl reach their final value and the $2E_{2g} + A_g$ of LaCl$_3$ disappears in the background. No Raman vibration at 408 cm^{-1}, corresponding to La$_2$O$_3$, was observed.[42,46] From the 210-330 min time period, a typical oxychlorination reaction mixture (CH$_4$:HCl:O$_2$:N$_2$:He 2:2:1:1:14) was fed into the reactor at 500 °C. No observable spectral changes occurred for the 210-245 min time period, which

Table 2.2. Overview of the Raman shifts (cm^{-1}) of Raman vibrational modes observable for LaOCl, EuOCl, LaCl$_3$ and EuCl$_3$.

	E_g	A_{1g}	E_g	$A_{1g'}$ B_{2g}	E_g	Ref
LaOCl	125	189	215	336	441	45,46
EuOCl	120	182	235	357	489	47,48
	E_{2g}	A_g	E_{1g}	$2E_{2g} + A_g$		Ref
LaCl$_3$	110	179	185	208 & 213		46,49
EuCl$_3$	95	184	198	228		49
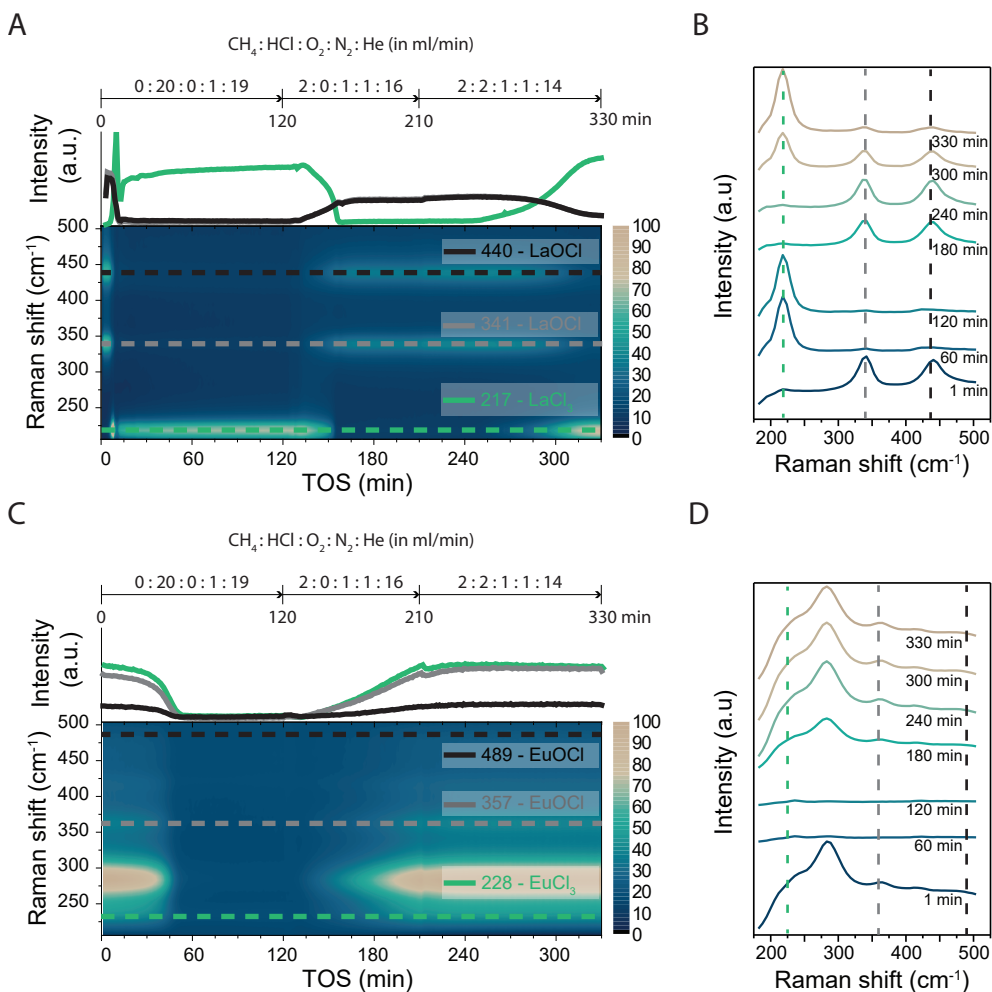
Figure 2.10. Chlorination (minute 0 - 120, CH$_4$:HCl:O$_2$:N$_2$:He 0:20:0:1:19, T = 450 °C), dechlorination (minute 120-210, CH$_4$:HCl:O$_2$:N$_2$:He 2:0:1:1:16, T = 500 °C) and oxychlorination (minute 210-330, CH$_4$:HCl:O$_2$:N$_2$:He 2:2:1:1:14, T = 500 °C) steps were investigated with operando Raman spectroscopy for (A) LaOCl and (C) EuOCl materials. The Raman spectra are plotted as contour plots versus the time-on-stream (TOS) and the intensity of key vibrations are plotted above. Individual spectra with 30-60 min time intervals and the last spectrum of the experiment are given in (B) for LaOCl and (D) EuOCl materials.

is most probably caused by the probed catalyst bed height. It is hypothesized that HCl is completely consumed by the top of the catalyst bed before a steady state consumption of HCl is reached and HCl travels further through the catalyst bed. Here, a more gradual transition between the LaOCl to $LaCl_3$ is observed, starting after 270 min of reaction. As already expected from the chlorination and dechlorination steps, the rate of chlorination exceeded the rate of dechlorination. After 330 min of reaction, vibrational modes corresponding to LaOCl and $LaCl_3$ are both visible, indicating that the catalyst material is in between a LaOCl-$LaCl_3$ state. However, at the end of the experiment, the intensity of the LaOCl bands almost disappeared in the background. At 330 min, the catalyst is comprised of almost pure $LaCl_3$ and it is expected that the remaining LaOCl would be converted to $LaCl_3$ over prolonged reaction times. Thus, even at low HCl concentrations (10%), the catalyst chlorination rate exceeded the dechlorination rate.

The same chlorination-dechlorination-oxychlorination experiment was performed for the EuOCl material. The Raman data of EuOCl is visualized as a contour plot in Figure 2.10C and individual spectra are plotted in Figure 2.10D. Above the contour plot, the intensity of three vibrations at 228 cm^{-1} ($2E_{2g} + A_g$ of $EuCl_3$), 357 cm^{-1} (A_{1g}, B_{2g} of EuOCl) and 489 cm^{-1} (E_g of EuOCl) are plotted versus time-on-stream (TOS). In the Raman spectrum of EuOCl, two bands at 282 cm^{-1} (λ = 540 nm) and 423 cm^{-1} (λ = 544 nm) cannot be ascribed to specific Raman vibrations. These peaks correspond to the $^5D_1 \rightarrow {}^7F_{0-2}$ (λ = 525-584 nm) emission lines of Eu^{3+}.[50,51] For the 0-120 min time period, a gradual decrease of all Raman vibration intensities is observed and it appeared that the final state is only reached after 50 min of reaction. Considering that LaOCl was fully chlorinated to $LaCl_3$ within 15 min, it can be stated that EuOCl is less susceptible to be chlorinated into $LnCl_3$ than LaOCl. The typical vibration of $EuCl_3$ at 228 cm^{-1} also decreased in intensity since it overlaps with the more intense 282 cm^{-1} emission line, which decreased over time. The observed intensity of the $EuCl_3$ vibration at the tested temperature is very weak, probably due to the weakening of the Eu-Cl bond and the loss of coordination number near the T_{melt}.[49] Not only is the Raman signal lost upon chlorination, the photoluminescence signal of $EuCl_3$ is also quenched upon heating. In Figures 2.11A and 2.11B, a temperature ramp on EuOCl/$EuCl_3$ was performed. A gradual change from the $EuCl_3$ spectrum to the EuOCl spectrum is observed, heating from 20 °C to 350 °C. No difference can be observed between the reference EuOCl and the EuOCl/$EuCl_3$ spectrum (Figure 2.11C), even though the composition of the heated sample did not change during the temperature ramp (Figure 2.11D). The loss of signal, both in the Raman and photoluminescence spectrum, indicated the chlorination of EuOCl to $EuCl_3$. Hence, the photoluminescence intensity is directly correlated to the degree of catalyst chlorination. For the 120-210 min time period, the intensities of all Raman bands were restored during the dechlorination step. Again, the Raman signal of the $2E_{2g} + A_g$ vibration of $EuCl_3$ at 235 cm^{-1} increased in intensity due to the rise of the relatively broad $^5D_1 \rightarrow {}^7F_1$ emission line. However, no formation of Eu_2O_3 was observed as its distinct vibration at 345 cm^{-1} was not detected in the Raman spectrum.[52,53] For the 210-330 min time period, the Raman spectra did not change during the oxychlorination step. A small variation in Raman peak intensity was observed in the beginning of the ex-
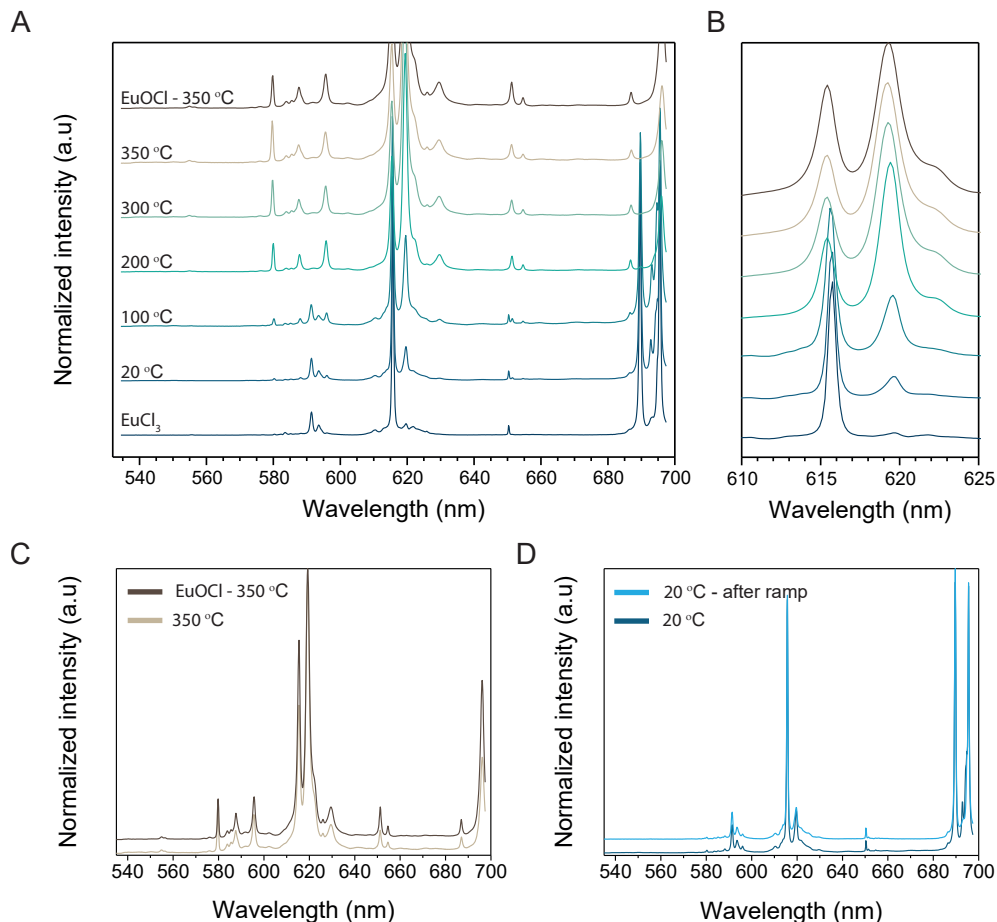
Figure 2.11. (A) The temperature induced quenching of the photoluminescence signal corresponding to $EuCl_3$, resulting in the photoluminescence spectrum of EuOCl which is formed due to hydrolysis. (B) Zoom-in of the region between 610 - 625 nm. (C) Comparison between the photoluminscence spectra of $EuCl_3$/EuOCl and EuOCl at 350 °C where no difference is observed. (D) Photoluminescence spectrum of the $EuCl_3$/EuOCl sample before and after the ramp to show that little changes occurred during the temperature ramp.

periment, but from the intensity plot it is apparent that no major changes occur. Hence, little bulk chlorination takes place. The high rate of CH_4 chlorination, and thus surface dechlorination, results in that EuOCl does not bulk chlorinate. Evident from the reaction mechanism (Figure 2.5) is that the surface chlorination must occur for the reaction to take place. In combination with the fact that the activity is increased with increasing HCl concentration, we can conclude that the surface chlorination is rate limiting, and not the activation of O_2 or CH_4. An increase in the HCl concentration is therefore beneficial for the catalytic activity of EuOCl since surface chlorination occurs more readily.

2.2.4 Operando Photoluminescence Spectroscopy

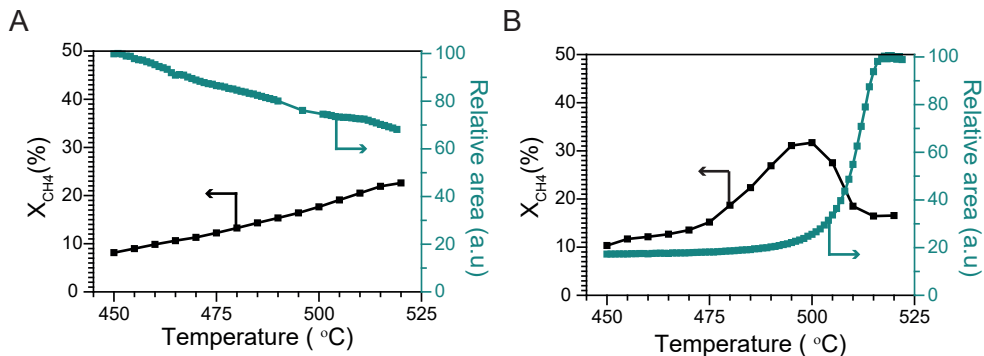The activity profiles of EuOCl under 10% and 80% HCl in Figures 2.8A and 2.8B showed

A

B

Figure 2.12. Temperature ramp experiments between 450 – 520 °C at 1 °C/min for EuOCl at CH_4:HCl:O_2:N_2:He of 2:2:1:1:14 with a 2 h pretreatment of (A) CH_4:HCl:O_2:N_2:He 2:2:1:1:14 at 450 °C and (B) CH_4:HCl:O_2:N_2:He 0:4:0:1:15 at 450 °C. The photoluminescence spectra were collected, normalized to the highest peak and integrated. The relative spectral area and the CH_4 conversion (X_{CH4}) were plotted versus the temperature.

similar behavior as both profiles contained a drop in the activity after which the activity is restored at higher temperatures. At 10% HCl, the onset of the drop occurred at ~ 475 °C and the minimum is reached at ~ 500 °C. At 80% HCl, the onset of the drop is delayed from 480 °C to 500 °C and a maximum X_{CH4} of 42% is reached. At 550 °C, EuOCl reached the same X_{CH4} of ~ 38% for both conditions. As this drop is reproducible with different newly synthesized EuOCl catalysts and for the same EuOCl catalyst when the same experiment is repeated, the role of the degree of catalyst chlorination on the drop in catalytic activity is investigated. Temperature ramp experiments from 450 - 520 °C were performed with the same catalyst, but the pretreatment step was varied. Furthermore, photoluminescence spectra of EuOCl were collected with the operando Raman probe. The collected spectra were normalized to the highest signal of the series, and integrated over the entire spectral range. The relative spectral area is used as a measure for the degree of chlorination, as the chlorination of EuOCl to $EuCl_3$ quenched the signal, as described in section 2.2.3 of this chapter. The X_{CH4} and relative spectral area are plotted versus the temperature. In Figure 2.12A, standard oxychlorination at 450 °C was applied as pretreatment step (CH_4:HCl:O_2:N_2:He 2:2:1:1:14). The X_{CH4} increased linearly with increasing reaction temperature, while the opposite trend is present for the relative spectral area. No spectral changes occurred during the temperature ramp, only the intensity of the signal decreased with increasing temperature. The gradual decrease in relative area is expected, as the overall photoluminescence intensity is negatively correlated with the temperature. Subsequently, the catalyst was cooled to 450 °C and chlorinated for 2 h prior to the temperature ramp (CH_4:HCl:O_2:N_2:He 0:4:0:1:15), as shown in Figure 2.12B. Now the drop in activity is observed, starting at 500 °C, which coincided with the temperature of the drop observed in Figure 2.8B for EuOCl tested at 80% HCl. Simultaneous with the sharp decrease in activity is the exponential growth of the relative spectral area, indicating that bulk $EuCl_3$ is rapidly converted to EuOCl, as mostly the state of the catalyst bulk is probed with photoluminescence spectroscopy. Both the X_{CH4} as well as the relative spectral area stabilized at 515 °C, indicating that the catalyst reached a steady state. The

53

reaction temperature played a crucial role in the degree of catalyst chlorination. In a scenario where excess HCl was present in the feed, bulk chlorination occurred at lower temperatures. Once the temperature was increased to > 480 °C, bulk chlorination becomes unfavorable, and the bulk Cl^- migrates to the surface, temporarily increasing the degree of surface chlorination. Hence, an increase in the activity is observed, as the Cl^- is forced out of the catalyst. Once the free Cl^- in the catalyst depletes, activity and selectivity are restored to the same levels as observed when no drop in activity was observed. The pretreatment step applied in Figures 2.12A and 2.12B additionally revealed that the presence of CH_4 also plays a vital role in the degree of catalyst chlorination. Evident from Figure 2.9A is that the HCl oxidation rate at 450 °C and 10% HCl is low, and dechlorination of the catalyst material via HCl oxidation is thus a slow process. Furthermore, the HCl oxidation rate is limited by the HCl concentration in the feed, as the rate could be significantly enhanced when excess HCl was fed (Figure 2.9B). In Figure 2.12, it is showcased that with and without the presence of CH_4 in the feed, the catalyst is either in a dechlorinated or in a chlorinated state, respectively. We can therefore conclude that the state of the catalyst material is determined by both the reaction temperature, as well as the $HCl:CH_4$ ratio in the feed.

2.2.5 Stability of Europium Oxychloride as Catalyst Material

Finally, EuOCl was tested for its stability under oxychlorination conditions at 450 C. Over a period of 48 h, the catalyst material was exposed to increasing HCl concentrations with constant CH_4 and O_2 concentration and total flow. The X_{CH4}, product yields and reaction selectivity are plotted in Figure 2.13A. At the start, a drop in the X_{CH4} and yields of CH_3Cl and CO are visible. This effect is most probably caused by the decrease of surface area of the catalyst since no prechlorination step was performed.[22] After 2 h of reaction, the CH_3Cl yield stabilized, while the CO yield gradually decreased. This is also visible from the selectivity plot in Figure 2.13A where the S_{CO} decreased from 44% to 37%, while the S_{CH3Cl} increased with the same percentage and the S_{CH2Cl2} remained constant. Subsequently, the HCl concentration was increased to 20% without increasing the total flow. An immediate jump in CH_3Cl (+2.2%), CH_2Cl_2 (+0.6%) and CO (+0.8%) yield occurs due to the increased chlorination rate of the catalyst surface. However, now the CH_3Cl yield dropped over time (-0.8%) while the CO yield remained constant.

Again, a jump in yield is observed when increasing the HCl concentration to 40% for CH_3Cl (+2%), CH_2Cl_2 (+1.1%) and CO (+1%). The selectivity of all the reaction products stayed fairly constant over the duration of 10 h. The yields of the reaction products decrease slightly. Up to this point, the catalyst material behaved in the same fashion. However, when the HCl concentration is further increased from 40% to 60%, a different catalytic behavior is observed.

Right from the moment that the HCl concentration was further increased, the CO yield dropped gradually (-1.1%), while the CM yields did not show any downward trend. The S_{CO} is reduced from 26% to 20%, a relative decrease of 23%. Under these conditions, a low $CHCl_3$ yield of 0.4% was observed, which correlated to a S_{CHCl3} of 2.4%. Near the end, the

A
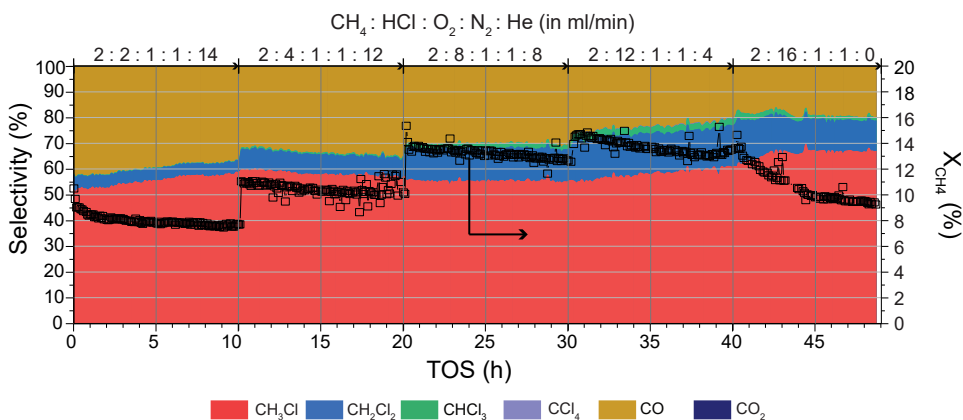
B
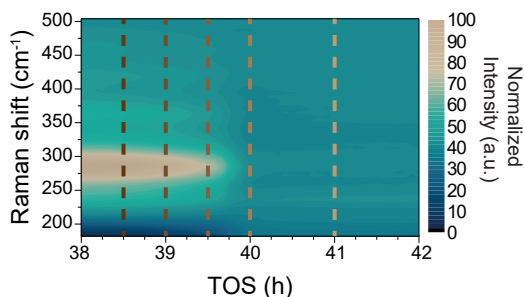
C
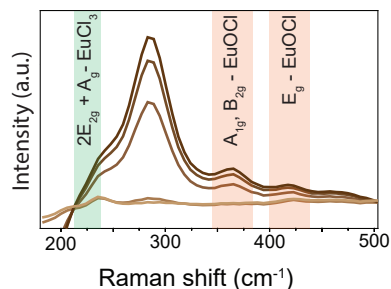
Figure 2.13. (A) The CH_4 conversion (X_{CH4}) and the selectivity towards CH_3Cl (S_{CH3Cl}), CH_2Cl_2 (S_{CH2Cl2}), $CHCl_3$ (S_{CHCl3}), CCl_4 (S_{CCl4}), CO (S_{CO}) and CO_2 (S_{CO2}) plotted versus time-on-stream (TOS). (B) Operando Raman spectra plotted versus the TOS between 38-42 h. The vertical lines in (B) are plotted individually in (C) to show the loss of Raman peak intensity of the vibrations corresponding to EuOCl.

production of CH_3Cl increased slightly after which it started to drop when the HCl concentration is further increased to 80%. Just before the feed ratio is adjusted to 80% HCl, we observe a change of the catalyst property, as analyzed with operando Raman spectroscopy. The operando Raman spectra in the spectral range of 180 - 500 cm^{-1} are plotted versus TOS in Figure 2.13B. Furthermore, some individual operando Raman spectra are plotted of moments before and after changing the feed ratio to 80% HCl in Figure 2.13C. After 38 h, the Raman spectra start to change and the overall intensity decreased, indicative of the transition from EuOCl to $EuCl_3$.

The full chlorination of the catalyst material had severe effects on the catalytic behavior. While the selectivity of the reaction did not seem to be affected by the changing catalyst properties, the catalyst deactivated. The decreasing CO yield trend is continued but now also the CH_3Cl yield is negatively affected over time. From previous experiments, it is known that EuOCl is difficult to chlorinate, especially under oxychlorination conditions. Here, bulk transformation of EuOCl to $EuCl_3$ occurred under very high HCl concentrations ($\geq$ 60%) over prolonged reaction times. However, bulk chlorination is unwanted since a decrease in product yield was observed. A balanced HCl concentration in the feed mix-

ture is therefore crucial to enhance the surface chlorination rate but also prevent bulk chlorination. An HCl concentration between 40% - 60% appears to be optimal, in terms of catalyst stability as well as catalytic performance.

2.3. CONCLUSIONS

In this chapter, a series of lanthanide oxide chloride (i.e., LnOCl with Ln = La, Pr, Nd, Sm, Eu, Gd, Tb, Dy or Ho) and Er- and Yb-based catalyst materials, which turned to be all active in the catalytic oxychlorination of CH_4. Based on their catalytic activity, the following ranking was made: Eu > Tb > Gd ~ Ho ~ Er > Dy > Sm > Pr ≈ Nd ≈ La ≈ Yb. Furthermore, from all the catalyst materials under investigation, EuOCl exhibited the highest activity and the best selectivity towards CH_3Cl. The catalytic performance of EuOCl could be further improved by altering the HCl concentration as an excess of HCl doubled the activity and lowered the CO selectivity. Exceptionally high conversion levels (~ 40%) could be reached, while maintaining a low CO_x selectivity (< 15%). Operando Raman spectroscopy revealed that the surface chlorination of the catalyst surface is rate limiting, hence the activity of both the MOC as well as the HCl oxidation is boosted when an excess of HCl is present. Operando photoluminescence spectroscopy of Eu^{3+} revealed that the bulk of EuOCl was subjected to major changes, and the state of the catalyst is determined by the CH_4:HCl ratio. However, if high HCl concentrations are applied at low X_{CH4} over prolonged reaction times, EuOCl does chlorinate fully and the catalyst activity is lowered. The tuneable activity and selectivity by altering the HCl concentration in the feed and the reaction make EuOCl a very interesting candidate as catalytic material for a viable CH_4 oxychlorination process.

2.4. ACKNOWLEDGEMENTS

2.5. EXPERIMENTAL METHODS

2.5.1. Catalyst Synthesis

The LnOCl (where Ln = La, Pr, Nd, Sm, Eu, Gd, Tb, Dy and Ho) and Er- and Yb-based catalyst materials under study were prepared by dissolving the corresponding lanthanide (III) chloride salt ($LnCl_3 \cdot xH_2O$, Fisher scientific, > 99%) in ethanol (absolute, VWR) followed by a precipitation using stoichiometric amounts of ammonium hydroxide (Fisher Scientific, 25% in H_2O) at room temperature. After the drop-wise addition, the precipitates were stirred for an additional hour and subsequently centrifuged to obtain the gel. Then, the obtained gel was washed with ethanol (absolute, VWR) and dried at 80 °C. Lastly, the dried solids were calcined in a static oven at 500 °C for 3 h using a ramp rate of 5 °C/min.

2.5.2. Catalyst Characterization

X-ray diffraction (XRD) patterns were obtained with a Bruker-AXS D2 Phaser powder x-ray

diffractometer in Bragg–Brentano geometry, using Co Kα1,2 = 1.79026 Å, operated at 30 kV. The measurements were carried out between 10 and 80° using a step size of 0.05° and a scan speed of 1 s, with a 2 mm slit for the source. N_2 adsorption isotherms were measured at 77 K on a Micromeritics TriStar II Plus instrument. Prior to all measurements, samples were dried at 573 K under a flow of N_2. Specific surface areas were calculated using the multipoint Brunauer Emmett Teller (BET) method (0.05 < p/p0 < 0.25). Pore volumes were calculated by the t-plot method; pore size distributions were obtained by BJH analysis. Transmission electron microscopy (TEM) was performed on a FEI Tecnai 20 instrument operating at 200kV.

Operando Raman spectroscopy measurements were performed with an AvaRaman-532 Hero-Evo instrument (λ = 532 nm, laser output 50 mW, spectral resolution of 10 cm^{-1}) equipped with an AvaRaman-PRB-FC-532 probe, capable of withstanding temperatures up to 500 °C. Spectra were collected every minute with the AvaSoft 8 software. The data was subsequently baseline corrected and normalized. The initial Raman intensity was optimized to obtain at least 50% of the saturation value. The operando Raman experiments, described in section 2.2.3 of this chapter, were performed by a sequential chlorination, dechlorination and oxychlorination step. The chlorination reaction was performed at 450 °C with $HCl:N_2$ 20:20 (ml/min) for 2 h. Subsequently, the reactor was heated to 500 °C under N_2 and then flows $CH_4:HCl:O_2:N_2:He$ of 2:0:1:1:16 and $CH_4:HCl:O_2:N_2:He$ of 2:2:1:1:14 were applied for the dechlorination (90 min) and oxychlorination (2 h), respectively. For the in situ photoluminescence spectroscopy in which the quenching of the $EuCl_3$ signal was investigated in section 2.2.3 of the chapter, $EuCl_3 \cdot 6H_2O$ was loaded in a quartz reactor and dried at 350 °C (5 °C/min, 20 ml/min N_2). The dehydration of the $EuCl_3$ causes the water to partly hydrolyse $EuCl_3$ to EuOCl, thereby obtaining a mixed $EuCl_3$/EuOCl.[54] The $EuCl_3$ was cooled to room temperature and again heated to 350 °C (5 °C/min, 20 ml/min N_2). During the temperature ramp, photoluminescent spectra were obtained. Lastly, the sample was cooled to room temperature and the spectrum was obtained. The $EuCl_3$ reference sample was made by heating $EuCl_3 \cdot 6H_2O$ to 350 °C in HCl atmosphere (5 °C/min, 4:16 $HCl:N_2$ in ml/min) and the spectrum was obtained at room temperature. The operando photoluminescence spectroscopy in section 2.2.4 of the chapter experiments were performed by two sequential ramp experiments from 450 °C to 520 °C at 1 °C/min under $CH_4:HCl:O_2:N_2:He$ of 2:2:1:1:14. Prior to the first ramp experiment, the catalyst was subjected to $CH_4:HCl:O_2:N_2:He$ of 2:2:1:1:14 for 2 h at 450 °C. Prior to the second ramp experiment, the catalyst was subjected to $CH_4:HCl:O_2:N_2:He$ of 0:4:0:1:14.

2.5.3. Catalyst Testing

All the catalytic tests and operando Raman measurements were performed in a lab scale continuous-flow fixed-bed reactor quartz reactor. Details of the setup, including a schematic and some pictures, are shown in Figure 2.14.

The quartz reactor (bed dimensions L x W x D: 30 x 6.3 x 2.7 mm) was placed vertically in a home-made oven with a one-sided horizontal hole reaching the center where the high-temperature Raman probe could be inserted. The temperature was regulated
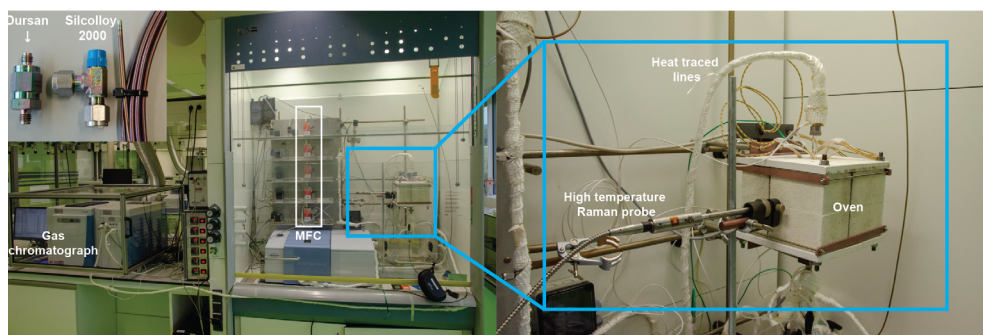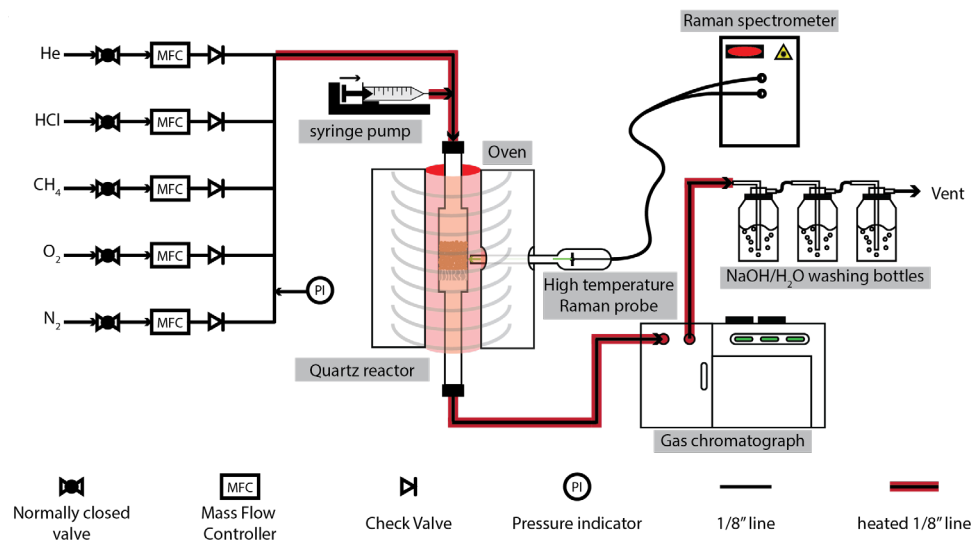
Figure 2.14. Schematic of the lab scale continuous flow set-up equipped with a high temperature Raman probe to study the catalyst during the reaction thereby making it possible to perform operando spectroscopy; and pictures of the set-up with key components indicated.

with a K-type thermocouple of which the tip reached the center of the oven. Flows of HCl (Linde 5.0), CH_4 (Linde 5.0), O_2 (Linde 5.0), N_2 (Linde 5.0, internal standard) and He (Linde 5.0, diluent) were regulated with digital mass-flow controllers (Bronkhorst) to obtain the desired feed ratio mixture. The reaction products were analyzed with an online custom build Trace 1300 gas chromatograph (GC) equipped with two FID (CH_4, CH_3Cl, CH_2Cl_2, $CHCl_3$ & CCl_4) and two TCD channels (permanent gases). Separation of reactants and products prior to detection was performed over the following columns: Rt-Silicabond (FID) and Rt-Qbond (FID), molsieve 5A (TCD) and Haysep Q (TCD). 1/8" Lines (Swagelok with Silcolloy 2000) were heated to 130 °C to prevent water condensation and resulting corrosion problems. Other steel components were coated with Dursan (Swagelok). Three gas washing bottles, first two filled with water and the last one filled with 4M NaOH, were used to remove any unreacted HCl and other reactive Cl-containing molecules, such as $COCl_2$ and Cl_2 gas. The syringe pump was used for the calibration of CH_2Cl_2, $CHCl_3$ and

CCl_4.

In a typical experiment, 500 mg of catalyst material (with a 125 - 425 μm size fraction) was loaded in a quartz reactor and heated to 450 °C under N_2 with 10 °C/min. The catalyst was activated in a 20% HCl/N_2 for 2 h prior to catalysis. For the isothermal experiments, the temperature was adjusted to reach X_{CH4} = 10% for CH_4:HCl:O_2:N_2:He of 2:2:1:1:14. When stable conversion was reached, the HCl:He ratio was adjusted so that the HCl concentration was increased to 20%, 40%, 60% and 80%, while keeping a constant flow of 20 ml/min. For the ramp experiments, the reactor was brought to 350 °C and the desired feed mixture (i.e., CH_4:HCl:O_2:N_2:He of 2:2:1:1:14 or 2:16:1:1:0 in ml/min) was fed into the reactor. A stabilization period of 30 min was applied and then the ramp experiment of 1 °C/min was commenced to 550 °C. For the stability test, the reactor was brought to 450 °C under N_2. After a stabilization period of 15 min, the flow was adjusted to CH_4:HCl:O_2:N_2:He 2:2:1:1:14 (in ml/min) and commenced for 10 h. Subsequently, the HCl:He ratio was adjusted so that the HCl concentration was increased to 20%, 40%, 60% and finally 80% HCl, while keeping a constant flow of 20 ml/min. Every feed ratio was tested for 10 h, except for 80% HCl which was tested for 8 h. During the stability test, operando Raman spectroscopy measurements were performed.

The CH_4 conversion, X_{CH4}, and O_2 conversion, X_{O2}, are calculated according to

$$(Eq.\,2.1)\ X_a(\%) = \frac{x_{a,inlet} - (x_{a,outlet} * ISCF)}{x_{a,inlet}} * 100\%$$

where $x_{a,inlet/outlet}$ and ISCF stand for the volumetric concentration of compound a at the inlet and outlet of the reactor and the Internal Standard Correction Factor, respectively. The yield of product i, Y_i, is calculated according to

$$(Eq.\,2.2)\ Y_i(\%) = \frac{x_i}{x_{CH4,inlet}} * 100\% * ISCF$$

where x_i stands for the volumetric concentration of carbon containing product i. The selectivity of product i, S_i, is calculated according to

$$(Eq.\,2.3)\ S_i(\%) = \frac{Y_i}{X_{CH4}} * 100\%$$

The CH_4 reaction rate is calculated according to

$$(Eq.\,2.4)\ R_{CH4}\left(\frac{mmol}{h * g_{cat}}\right) = \frac{P * F_T * x_{CH4,inlet} * \frac{X_{CH4}}{100}}{R * T * W_{cat}}$$

where P, F_T, R, T and W_{cat} stand for the pressure, total flow, gas constant, ambient temperature and catalyst weight. Finally, the carbon balance was calculated and measurements with their carbon balance > ± 5% were removed. The carbon balance was calculated according to

$$(Eq.\,2.5)\ Carbon\ balance = \sum\ Y(i) + 100 - X_{CH4}$$

2.6. REFERENCES

(1)   BP Energy Outlook. 2019.

(2)   Wang, B.; Albarracín-Suazo, S.; Pagán-Torres, Y.; Nikolla, E. Advances in Methane Conversion Processes. Catal. Today 2017, 285, 147–158. https://doi.org/10.1016/J.CATTOD.2017.01.023.

(3)   Jiao, F.; Li, J.; Pan, X.; Xiao, J.; Li, H.; Ma, H.; Wei, M.; Pan, Y.; Zhou, Z.; Li, M.; Miao, S.; Li, J.; Zhu, Y.; Xiao, D.; He, T.; Yang, J.; Qi, F.; Fu, Q.; Bao, X. Selective Conversion of Syngas to Light Olefins. Science 2016, 351, 1065–1068. https://doi.org/10.1126/science.aaf1835.

(4)   Alvarez-Galvan, M. C.; Mota, N.; Ojeda, M.; Rojas, S.; Navarro, R. M.; Fierro, J. L. G. Direct Methane Conversion Routes to Chemicals and Fuels. Catal. Today 2011, 171, 15–23. https://doi.org/10.1016/j.cattod.2011.02.028.

(5)   Taifan, W.; Baltrusaitis, J. CH_4 Conversion to Value Added Products: Potential, Limitations and Extensions of a Single Step Heterogeneous Catalysis. Appl. Catal. B Environ. 2016, 198, 525–547. https://doi.org/10.1016/j.apcatb.2016.05.081.

(6)   Zichittella, G.; Aellen, N.; Paunović, V.; Amrute, A. P.; Pérez-Ramírez, J. Olefins from Natural Gas by Oxychlorination. Angew. Chem. Int. Ed. 2017, 56, 13670–13674. https://doi.org/10.1002/anie.201706624.

(7)   Kim, J.; Ryou, Y.; Hwang, G.; Bang, J.; Jung, J.; Bang, Y.; Kim, D. H. Oxychlorination of Methane over FeO_x/CeO_2 Catalysts. Korean J. Chem. Eng. 2018, 35, 2185–2190. https://doi.org/10.1007/s11814-018-0135-4.

(8)   Paunović, V.; Zichittella, G.; Hemberger, P.; Bodi, A.; Pérez-Ramírez, J. Selective Methane Functionalization via Oxyhalogenation over Supported Noble Metal Nanoparticles. ACS Catal. 2019, 9, 1710–1725. https://doi.org/10.1021/acscatal.8b04375.

(9)   He, J.; Xu, T.; Wang, Z.; Zhang, Q.; Deng, W.; Wang, Y. Transformation of Methane to Propylene: A Two-Step Reaction Route Catalyzed by Modified CeO_2 Nanocrystals and Zeolites. Angew. Chem. Int. Ed. 2012, 51, 2438–2442. https://doi.org/10.1002/anie.201104071.

(10)   Peringer, E.; Podkolzin, S. G.; Jones, M. E.; Olindo, R.; Lercher, J. A. $LaCl_3$-Based Catalysts for Oxidative Chlorination of CH_4. Top. Catal. 2006, 38, 211–220. https://doi.org/10.1007/s11244-006-0085-7.

(11)   Peringer, E.; Salzinger, M.; Hutt, M.; Lemonidou, A. A.; Lercher, J. A. Modified Lanthanum Catalysts for Oxidative Chlorination of Methane. Top. Catal. 2009, 52, 1220–1231. https://doi.org/10.1007/s11244-009-9265-6.

(12)   Paunovic, V.; Zichittella, G.; Moser, M.; Amrute, A. P.; Pérez-Ramírez, J. Catalyst Design for Natural-Gas Upgrading through Oxybromination Chemistry. Nat. Chem. 2016, 8, 803–809. https://doi.org/10.1038/nchem.2522.

(13)   Paunović, V.; Lin, R.; Scharfe, M.; Amrute, A. P.; Mitchell, S.; Hauert, R.; Pérez-Ramírez, J. Europium Oxybromide Catalysts for Efficient Bromine Looping in Natural Gas Valorization. Angew. Chem. Int. Ed. 2017, 56, 9791–9795. https://doi.org/10.1002/anie.201704406.

(14)   Zichittella, G.; Paunović, V.; Amrute, A. P.; Pérez-Ramírez, J. Catalytic Oxychlorination versus Oxybromination for Methane Functionalization. ACS Catal. 2017, 7, 1805–1817. https://doi.org/10.1021/acscatal.6b03600.

(15)   Paunović, V.; Artusi, M.; Verel, R.; Krumeich, F.; Hauert, R.; Pérez-Ramírez, J. Lanthanum Vanadate Catalysts for Selective and Stable Methane Oxybromination. J. Catal. 2018, 363, 69–80. https://doi.org/10.1016/j.jcat.2018.04.001.

(16)   Lin, R.; Amrute, A. P.; Pérez-Ramírez, J. Halogen-Mediated Conversion of Hydrocarbons to Commodities. Chem. Rev. 2017, 117, 4182–4247. https://doi.org/10.1021/acs.chemrev.6b00551.

(17)   Van Der Heijden, A. W. A. M.; Bellière, V.; Alonso, L. E.; Daturi, M.; Manoilova, O. V.; Weckhuysen, B. M. Destructive Adsorption of CCl_4 over Lanthanum-Based Solids: Linking Activity to Acid-Base Properties. J. Phys. Chem. B 2005, 109, 23993–24001. https://doi.org/10.1021/jp054689b.

(18)   Schweizer, A. E.; Jones, M. E.; Hickman, D. A. Oxidative Halogenation of C1 Hydrocarbons to Halogenated C1 Hydrocarbons and Integrated Processes Related Thereto. United States Patent 6,452,058 B1, 2002.

(19)   Scharfe, M.; Zichittella, G.; Paunović, V.; Pérez-Ramírez, J. Ceria in Halogen Chemistry. Chin. J. Catal. 2020, 41, 915–927. https://doi.org/10.1016/S1872-2067(19)63528-X.

(20)   Sabnis, K. D.; Fickel, D. W.; Shou, H.; Casper, M. D.; Kulkarni, N.; Araujo, A.; Mamedov, E. Selective Monochlorination of Methane via Elimination of Dichloromethane from the Oxychlorination Product Stream. React. Kinet. Mech. Catal. 2019, 127, 413–423. https://doi.org/10.1007/s11144-019-01550-8.

(21)   Podkolzin, S. G.; Stangland, E. E.; Jones, M. E.; Peringer, E.; Lercher, J. A. Methyl Chloride Production from Methane over Lanthanum-Based Catalysts. J. Am. Chem. Soc. 2007, 129, 2569–2576. https://doi.org/10.1021/ja066913w.

(22)   Peringer, E.; Tejuja, C.; Salzinger, M.; Lemonidou, A. A.; Lercher, J. A. On the Synthesis of $LaCl_3$ Catalysts for Oxidative Chlorination of Methane. Appl. Catal. A Gen. 2008, 350, 178–185. https://doi.org/10.1016/j.apcata.2008.08.009.

(23)   Stauffer, J. E. Methane to Olefins. United States Patent 7,091,391 B2, 2006.

(24)   Clarke, W. D.; Haymon, T. D.; Henley, J. P.; Hickman, D. A.; Jones, M. E.; Miller, M. C.; Morris, T. E.; Reed, D. J.; Samson, L. J.; Schweizer, A. E.; Smith, S. A.

Production of Vinyl Halide from Single Carbon Feedstocks. United States Patent 2005/0,027,084 A1, 2005.

(25)   Gulotty, R. J.; Jones, M. E.; Hickman, D. A. Oxyhalogenation Process Using Catalyst Having Porous Rare Earth Halide Support. United States Patent 6,680,415 B1, 2004.

(26)   Nubel, P. O.; Satek, L. C.; Spangler, M. J.; Lutman, C. A.; Michaels, G. O. Halogen-Assisted Conversion of Lower Alkanes. United States Patent 5,087,786, 1991.

(27)   Podkolzin, S. G.; Stangland, E. E.; Schweizer, A. E.; Jones, M. E. Oxidative Halogenation of C1 Hydrocarbons to Halogenated C1 Hydrocarbons. United States Patent 2008/0,275,279 A1, 2008.

(28)   Bowman, R. G.; Stangland, E. E.; Jones, M. E.; Millar, D. M.; Podkolzin, S. G.; Stears, B. A.; Wehmeyer, R. M. Oxidative Mono-Halogenation of Methane. United States Patent 8,674,149 B2, 2014.

(29)   Saadun, A. J.; Zichittella, G.; Paunović, V.; Markaide-Aiastui, B. A.; Mitchell, S.; Pérez-Ramírez, J. Epitaxially Directed Iridium Nanostructures on Titanium Dioxide for the Selective Hydrodechlorination of Dichloromethane. ACS Catal. 2020, 10, 528–542. https://doi.org/10.1021/acscatal.9b04467.

(30)   Olah, G. A.; Gupta, B.; Felberg, J. D.; Ip, W. M.; Husain, A.; Karpeles, R.; Lammertsma, K.; Melhotra, A. K.; Trivedi, N. J. Electrophilic Reactions at Single Bonds. 20. Selective Monohalogenation of Methane over Supported Acidic or Platinum Metal Catalysts and Hydrolysis of Methyl Halides over Gamma-Alumina-Supported Metal Oxide/Hydroxide Catalysts. A Feasible Path for the O. J. Am. Chem. Soc. 1985, 107, 7097–7105. https://doi.org/10.1021/ja00310a057.

(31)   van der Heijden, A. W. A. M.; Podkolzin, S. G.; Jones, M. E.; Bitter, J. H.; Weckhuysen, B. M. Catalytic Hydrogen-Chlorine Exchange between Chlorinated Hydrocarbons under Oxygen-Free Conditions. Angew. Chem. Int. Ed. 2008, 47, 5002–5004. https://doi.org/10.1002/anie.200800270.

(32)   Treger, Y. A.; Rozanov, V. N.; Sokolova, S. V; Murashova, O. P. Producing Ethylene and Propylene from Natural Gas via the Intermediate Synthesis of Methyl Chloride and Its Subsequent Catalytic Pyrolysis. Catal. Ind. 2012, 4, 231–235. https://doi.org/10.1134/S2070050412040186.

(33)   Van der Avert, P.; Weckhuysen, B. M. Low-Temperature Catalytic Destruction of CCl_4, $CHCl_3$ and CH_2Cl_2 over Basic Oxides. Phys. Chem. Chem. Phys. 2004, 6, 5256–5262. https://doi.org/10.1039/b413876g.

(34)   Pyykkö, P. Relativistic Effects in Structural Chemistry. Chem. Rev. 1988, 88, 563–594. https://doi.org/10.1021/cr00085a006.

(35)   Garcia, E.; Corbett, J. D.; Ford, J. E.; Vary, W. J. Low-Temperature Routes to New Structures for Yttrium, Holmium, Erbium, and Thulium Oxychlorides. Inorg. Chem. 1985, 24, 494–498. https://doi.org/10.1021/ic00198a013.

(36)   van der Heijden, A. W. A. M.; Garcia Ramos, M.; Weckhuysen, B. M. Intermediates in the Destruction of Chlorinated C1 Hydrocarbons on La-Based Materials: Mechanistic Implications. Chem. Eur. J. 2007, 13, 9561–9571. https://doi.org/10.1002/chem.200700901.

(37)   van der Heijden, A. W. A. M.; Mens, A. J. M.; Bogerd, R.; Weckhuysen, B. M. Dehydrochlorination of Intermediates in the Production of Vinyl Chloride over Lanthanum Oxide-Based Catalysts. Catal. Lett. 2008, 122, 238–246. https://doi.org/10.1007/s10562-008-9436-2.

(38)   Van der Avert, P.; Podkolzin, S. G.; Manoilova, O.; de Winne, H.; Weckhuysen, B. M. Low-Temperature Destruction of Carbon Tetrachloride over Lanthanide Oxide-Based Catalysts: From Destructive Adsorption to a Catalytic Reaction Cycle. Chem. Eur. J. 2004, 10, 1637–1646. https://doi.org/10.1002/chem.200305442.

(39)   Zichittella, G.; Polyhach, Y.; Tschaggelar, R.; Jeschke, G.; Pérez-Ramírez, J. Quantification of Redox Sites during Catalytic Propane Oxychlorination by Operando EPR Spectroscopy. Angew. Chem. Int. Ed. 2021, 60, 3596–3602. https://doi.org/10.1002/anie.202013331.

(40)   McBee, E. T.; Hass, H. B.; Neher, C. M.; Strickland, H. Chlorination of Methane. Ind. Eng. Chem. 1942, 34, 296–300. https://doi.org/10.1021/ie50387a009.

(41)   Milligan, B. A.; Dumesic, J. A. Physical, Adsorptive, and Catalytic Properties of Platinum Supported on Silica Modified with Europium Oxide. J. Catal. 1989, 115, 180–193. https://doi.org/10.1016/0021-9517(89)90017-1.

(42)   Van der Avert, P.; Weckhuysen, B. M. Low-Temperature Destruction of Chlorinated Hydrocarbons over Lanthanide Oxide Based Catalysts. Angew. Chem. Int. Ed. 2002, 41, 4730–4732. https://doi.org/10.1002/anie.200290030.

(43)   Rioux, R. M.; Song, H.; Hoefelmeyer, J. D.; Yang, P.; Somorjai, G. A. High-Surface-Area Catalyst Design: Synthesis, Characterization, and Reaction Studies of Platinum Nanoparticles in Mesoporous SBA-15 Silica. J. Phys. Chem. B 2005, 109, 2192–2202. https://doi.org/10.1021/jp048867x.

(44)   Vogt, C.; Groeneveld, E.; Kamsma, G.; Nachtegaal, M.; Lu, L.; Kiely, C. J.; Berben, P. H.; Meirer, F.; Weckhuysen, B. M. Unravelling Structure Sensitivity in CO_2 Hydrogenation over Nickel. Nat. Catal. 2018, 1, 127–134. https://doi.org/10.1038/s41929-017-0016-y.

(45)   Haeuseler, H. Raman Spectra of Single Crystals of LaOCl. J. Raman Spectrosc. 1984, 15, 120–121. https://doi.org/10.1002/jrs.1250150210.

(46)   Weckhuysen, B. M.; Rosynek, M. P.; Lunsford, J. H. Destructive Adsorption of Carbon Tetrachloride on Lanthanum and Cerium Oxides. Phys. Chem. Chem. Phys. 1999, 1, 3157–3162. https://doi.org/10.1039/a901847f.

(47)   Kim, D.; Jeong, J. R.; Jang, Y.; Bae, J. S.; Chung, I.; Liang, R.; Seo, D. K.; Kim, S. J.; Park, J. C. Self-Emitting

2

Blue and Red EuOX (X = F, Cl, Br, I) Materials: Band Structure, Charge Transfer Energy, and Emission Energy. Phys. Chem. Chem. Phys. 2019, 21, 1737–1749. https://doi.org/10.1039/c8cp06470a.

(48)   She, C. Y.; Broberg, T. W.; Edwards, D. F. Raman Spectra of Tetragonal Lanthanide Oxychlorides Obtained from Polycrystalline and Single-Crystal Samples. Phys. Rev. B 1971, 4, 1580–1583. https://doi.org/10.1103/PhysRevB.4.1580.

(49)   Zakir'yanova, I. D.; Salyulev, A. B.; Khokhlov, V. A. Raman Spectroscopy Study of the Phase Transitions in Rare-Earth Metal Trichlorides. Russ. Metall. 2011, 2011, 754–759. https://doi.org/10.1134/S0036029511080167.

(50)   Hölsä, J.; Porcher, P. Free Ion and Crystal Field Parameters for REOCl:Eu^{3+}. J. Chem. Phys. 1981, 75, 2108–2117. https://doi.org/10.1063/1.442314.

(51)   Rabouw, F. T.; Prins, P. T.; Norris, D. J. Europium-Doped NaYF$_4$ Nanocrystals as Probes for the Electric and Magnetic Local Density of Optical States throughout the Visible Spectral Range. Nano Lett. 2016, 16, 7254–7260. https://doi.org/10.1021/acs.nanolett.6b03730.

(52)   Lui, R.; Yan, Q.; Zhai, Y.; QI, H.; Hsia, Y.; Jiang, J.; Gonser, U. Investigation of the Solid-Solid Surface Adsorption of Eu$_2$O$_3$ on Amorphous Al$_2$O$_3$. Hyperfine Interact. 1992, 69, 847–850. https://doi.org/10.1007/BF02401959.

(53)   Quesada, A.; Del Campo, A.; Fernández, J. F. Stabilization of Cubic Phase in Dense Eu$_2$O$_3$ Ceramics. Mater. Lett. 2015, 157, 77–80. https://doi.org/10.1016/j.matlet.2015.05.085.

(54)   Lyle, S. J.; Westall, W. A. A Study of the Thermal Decomposition of Hydrated Europium(III) Chloride and Europrium(III) Bromide. Thermochim. Acta 1983, 68, 51–58. https://doi.org/10.1016/0040-6031(83)80379-7.

2

Revealed by Operando Spectroscopy

3
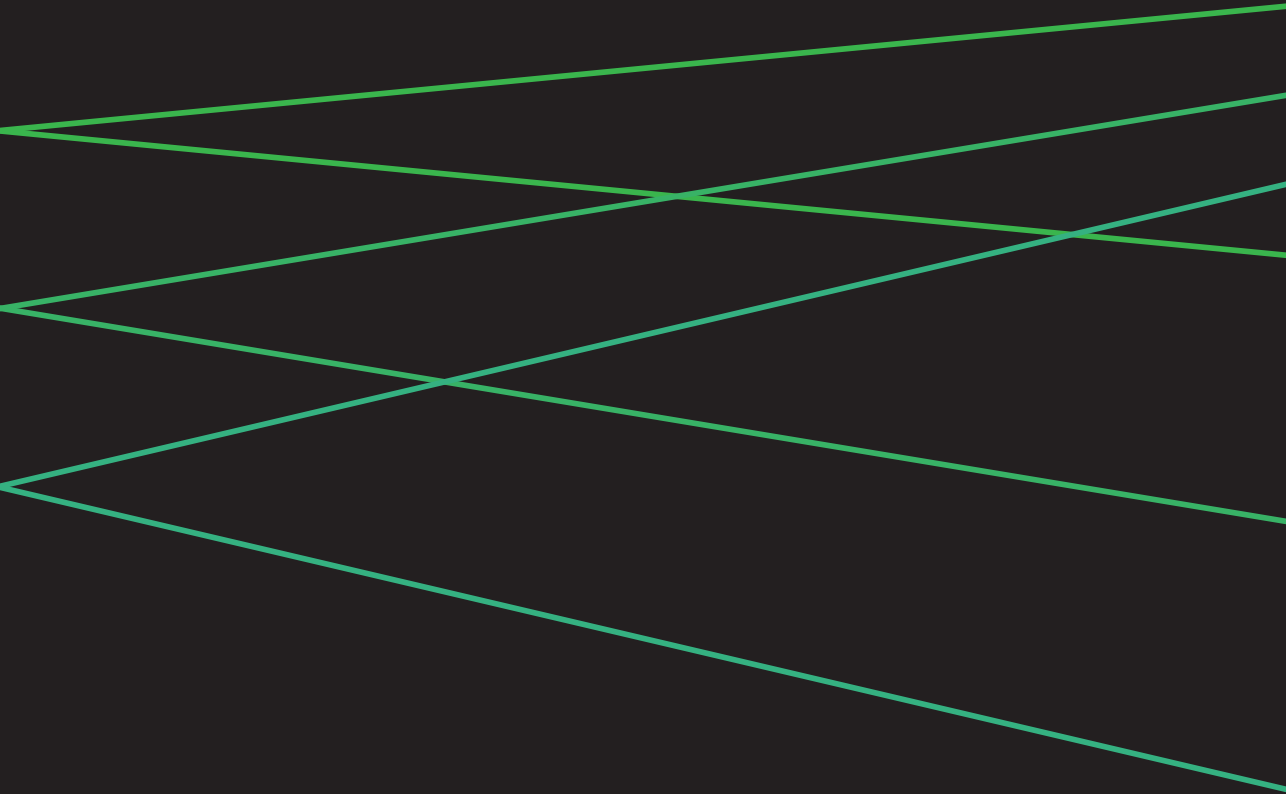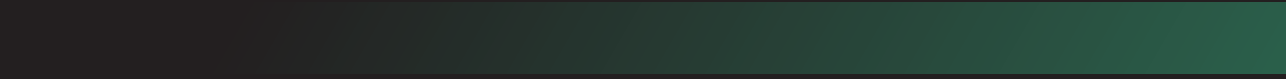
Favoring the Methane Oxychlorination Reaction over EuOCl by Synergistic Effects with Lanthanum

Abstract

The direct conversion of CH_4 into fuels and chemicals produces less waste, requires smaller capital investments and has improved energy efficiency compared to multistep processes. While the CH_4 oxychlorination (MOC) reaction has been given little attention, it offers the potential to achieve high CH_4 conversion levels at high selectivities. In a continuing effort to design commercially interesting MOC catalysts, in this chapter the catalyst design of EuOCl is improved by the partial replacement of Eu^{3+} by La^{3+}. More specifically, a set of catalytic solid solutions of La^{3+} and Eu^{3+} (i.e., $La_xEu_{1-x}OCl$ where x = 0, 0.25, 0.50, 0.75 and 1) were synthesized, characterized and tested in the MOC reaction. The La^{3+}-Eu^{3+} catalysts exhibited an increased CH_3Cl selectivity (i.e., 54 – 66% vs 41 – 52%), lower CH_2Cl_2 selectivity (i.e., 8 – 24% vs 18 – 34%) and comparable CO selectivity (i.e., 11 – 28% vs 14 – 28%) compared to EuOCl under the same reaction conditions and varying HCl concentrations in the feed. The La^{3+}-Eu^{3+} catalysts possessed a higher CH_4 conversion rate than when the individual activities of LaOCl and EuOCl are summed with a similar La^{3+}:Eu^{3+} ratio (i.e., the linear combination). In the solid solution, La^{3+} is readily chlorinated and acts as a Cl^- buffer which can transfer Cl^- to the active Eu^{3+} phase, thereby enhancing the activity. The improved catalyst design enhanced the CH_3Cl yield and selectivity, reduced catalyst cost and the separation cost of unreacted HCl. These results showcase that, by matching intrinsic material properties, catalyst design can be altered to overcome reaction bottlenecks.

3.1. INTRODUCTION

CH_4 is a relatively cheap and widely available natural resource, but it requires, as outlined in chapter 1, multi-step processes to produce fuels and base chemicals from it.[1] Single-step processes conceptually produce less waste, require smaller capital investments and have improved energy efficiency.[2,3] However, practical considerations make that none of the direct CH_4 conversion routes have seen industrialization so far.[2] The key challenges with direct conversion routes that need to be addressed, e.g., low conversion levels and/or poor selectivity, all require better catalyst design.[4,5] Of the direct conversion routes, CH_4 oxyhalogenation (MOH) reaction has one of the highest potential to see industrialization due to the moderate reaction temperatures and high conversion levels of CH_4.[6] Moreover, a high selectivity towards the desired CH_3X (where X = Cl, Br or I) can be achieved.[7,8] Being able to produce CH_3X selectively in high quantities is of great interest. The chemical analogy between CH_3OH and CH_3X is remarkable,[2,9–11] and makes CH_3X as valuable as CH_3OH.[5,12,13] However, relatively little research has been performed on the MOH reaction.[6,12,14]

From the perspective of a circular economy approach, CH_4 oxychlorination (MOC) has the additional advantage of being able to utilize HCl, a by-product of other chlorination reactions.[15,16] However, the corrosive and oxidative environment under which the MOC catalysts must operate pose technological challenges and hinder industrialization of the process.[6,17,18] A commercially interesting catalyst must be able to operate over prolonged times with a high CH_3Cl selectivity and CH_4 conversion level.[19] Furthermore, the selectivity to CO_x needs to be minimized to make optimal use of the chemical feedstock and to lower separation costs.[14] These aforementioned requirements are challenging and very little is known about how to fulfill these catalyst requirements.[20,21] Hence, more work is required to develop suitable MOC catalysts for commercial applications.

A number of catalyst compositions are published in the academic and patent literature, which can be divided into transition metal-based catalysts (e.g., TiO_2[8,22], VPO[8,22], $FePO_4$[8], Fe/K[23], ZrO_2[24] and Nb_2O_5[22]), noble metal-based catalysts (e.g., RuO_2[8,22], NM/MO[14] where NM = Ru, Rh, Pd, Ir, Pt and MO = Metal Oxide support material), lanthanide-based catalysts (e.g., $LaOCl$[25–27], CeO_2[8,12,22,28] and $EuOCl$[29]) and bimetallic catalysts (e.g., $Cu/K/La$[8,30,31], FeO_x/CeO_2[28,32], $LaVO_4$[22], $Ce/LaOCl$[17], $Ni/LaOCl$[17] and $Co/LaOCl$[17]). None of these groups of catalyst materials outperforms any of the other groups by definition and only a handful of individual solid catalyst materials were studied in depth. A more fundamental approach on catalyst design needs to be adopted to understand the kinetic and thermodynamic bottlenecks encountered when operating certain catalyst materials.

In chapter 2, EuOCl has been reported as a promising candidate for the MOC reaction as its performance is stable and, by varying the reaction temperature and feed mixture, also highly tunable.[33] EuOCl is suitable to be studied under working conditions with operando spectroscopy because of the Raman active modes of the material and the photoluminescent properties of Eu^{3+}. By doing so, we were able to reveal that the chlorination of

the catalyst surface was rate limiting. While EuOCl outperformed the other lanthanide oxychloride catalyst materials tested in our work, a number of improvements need to be made to the catalyst design in order to have a potential industrial catalyst: 1) improve CH_3Cl selectivity (S_{CH3Cl}), preferably at higher CH_4 conversion levels (X_{CH4}); 2) reduce catalyst cost by lowering the Eu^{3+} content in the catalyst; and 3) lower the HCl concentration in the feed, while still maintaining a high degree of surface chlorination. A large excess of HCl and unreacted feed are undesired as they result in high separation costs.

In this chapter, we explore the effect of the partial replacement of Eu^{3+} by La^{3+} on the catalytic performance in the MOC and investigate the apparent synergistic effect between La^{3+} and Eu^{3+}. Operando Raman spectroscopy previously revealed that the chlorination of EuOCl to $EuCl_3$ is a slow process, and can be rate limiting during the MOC reaction.[33] Based on thermodynamic calculations and experimental evidence, LaOCl was selected as a Cl^- reservoir for Eu^{3+} as the chlorination from LaOCl to $LaCl_3$ occurs readily at low HCl concentrations. $La_{1-x}Eu_xOCl$ (where x = 0, 0.25, 0.50, 0.75 or 1) solid solution catalysts were synthesized and characterized. Incorporation of La^{3+} into EuOCl crystal lattice was favored, since La^{3+} has the same oxidation state and a comparable ionic radius to Eu^{3+}. The performance of $La_{1-x}Eu_xOCl$ materials in the MOC reaction was tested, and compared to the benchmark EuOCl. The addition of La^{3+} improved the degree of chlorination of the catalyst, thereby improving the CH_3Cl yield, while preserving the excellent CO selectivity compared to monometallic EuOCl. Furthermore, operando luminescence spectroscopy was applied to provide further insight in the chlorination behavior of La^{3+}-Eu^{3+} solid solutions. Lastly, physical mixtures of LaOCl and EuOCl were used as catalytic material, showcasing the importance of intimate contact between La^{3+} and Eu^{3+} in the MOC reaction. This resulted in the enhancement of the catalytic performance, approaching the performance of the La^{3+}-Eu^{3+} solid solution. Thus, we showcase that, by matching intrinsic material properties, catalyst design can be altered to overcome reaction bottlenecks.

3.2. RESULTS AND DISCUSSION

3.2.1 Physicochemical Properties of the Lanthanide Oxychlorides

The synthesized $La_{1-x}Eu_xOCl$ catalyst materials were characterized by N_2 physisorption, inductively coupled plasma-optical emission spectroscopy (ICP-OES) and X-ray diffraction (XRD) to gain insights into their physicochemical properties (Table 3.1). The applied base precipitation method yielded catalyst materials with specific surface area (S_{BET}) and pore volume (V_{pore}) of the same order of magnitude. The S_{BET} ranged between 24.4 and 41.5 m^2/g, while the V_{pore} ranged between 0.06 and 0.23 cm^3/g. Furthermore, the experimental $La^{3+}:Eu^{3+}$ molar ratio obtained from ICP-OES after the precipitation for the bimetallic catalysts is in good agreement with the desired theoretical ratio (Table 3.1).

While ICP-OES provided the elemental ratio of the bulk materials, it did not provide information on the distribution of the two elements throughout the material. XRD was applied to investigate if the desired metal phase was obtained, and if solid solutions of La^{3+} and Eu^{3+} were obtained. The XRD patterns of the as-synthesized catalyst materials are given

with Lanthanum

Table 3.1. Physicochemical properties of the as-synthesized LaOCl, La$_{0.75}$Eu$_{0.25}$OCl, La$_{0.50}$Eu$_{0.50}$OCl, La$_{0.25}$Eu$_{0.75}$OCl and EuOCl. Specific surface area (S$_{BET}$) and pore volume (V$_{pore}$) were derived based on N$_2$ physisorption results. The La^{3+}:Eu^{3+} ratios obtained from Inductively Coupled Plasma-Optical Emission spectroscopy (ICP-OES) corresponded well with the theoretical values. Positions of the deconvoluted (110) x-ray diffraction (XRD) peak, the corresponding La^{3+}:Eu^{3+} ratio and relative area as calculated with Vegard's Law for as-synthesized La$_{0.75}$Eu$_{0.25}$OCl, La$_{0.50}$Eu$_{0.50}$OCl, La$_{0.25}$Eu$_{0.75}$OCl are also tabulated.

Catalyst material LnOCl where Ln =	Physisorption results		La^{3+}:Eu^{3+} molar ratio (ICP-OES)	Phase 1 (La^{3+} rich)			Phase 2 (Eu^{3+} rich)		
	S$_{BET}$ (m²/g)	V$_{pore}$ (cm³/g)		Position (°)	La^{3+}:Eu^{3+}	Relative area (%)	Position (°)	La^{3+}:Eu^{3+}	Relative area (%)
La	24.4	0.06	-	30.62	-	-	-	-	-
La$_{0.75}$Eu$_{0.25}$	39.6	0.22	74:26	30.80	86:14	54	31.02	68.1:31.9 ±1.2	46
La$_{0.50}$Eu$_{0.50}$	41.1	0.18	50:50	30.88	79:21	47	31.42	34.5:65.5 ± 1.3	53
La$_{0.25}$Eu$_{0.75}$	41.5	0.16	24:76	30.99	70:30	21	31.69	16.0:84.0 ±1.7	79
Eu	37.4	0.23	-	-	-	-	31.91	-	-
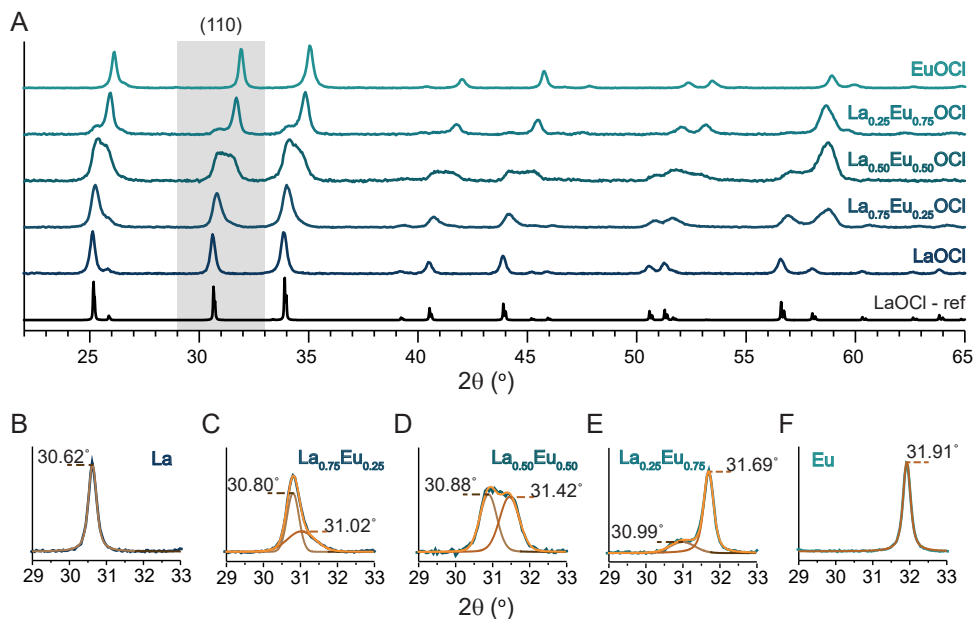
Figure 3.1. (A) X-ray Diffraction (XRD) patterns of the as-synthesized LnOCl catalyst materials under study, including LaOCl, La$_{0.75}$Eu$_{0.25}$OCl, La$_{0.50}$Eu$_{0.50}$OCl, La$_{0.25}$Eu$_{0.75}$OCl and EuOCl and LaOCl reference pattern (ICDD 00-00800477). (B-F) The zoom-in of the (110) XRD peaks displays the fitted peaks used for determining the degree of La^{3+}-Eu^{3+} mixing in Table 3.1 according to Vegard's law (see section 3.5.4 of this chapter for the applied procedure).

in Figure 3.1A. As previously reported, LaOCl and EuOCl are easily synthesized in the oxychloride phase without any noticeable contaminations from other crystalline phases.[33] Since LaOCl and EuOCl have the same space group, P4/nmm, and comparable ionic

radii[34], solid-state ion mixing of the two elements is expected to occur.[35,36] By deconvolution of the (110) XRD peaks of the as-synthesized LnOCl catalysts (Figures 3.1B–3.1F) and applying Vegard's law (see section 3.5.4 of this chapter for more details on the applied procedure), at least two mixed phases were distinguished with varying $La^{3+}:Eu^{3+}$ ratios, referred to as phase 1 and phase 2 (Table 3.1). Noticeable is that for every bimetallic La^{3+}-Eu^{3+} catalyst, we have obtained one La^{3+}-rich phase (x > 70%, referred to as phase 1) and one phase with a larger distribution in La^{3+}-Eu^{3+} ratio (phase 2). We hypotesize that LaOCl is precipitated at a higher rate than EuOCl during the synthesis, thereby always obtaining one La^{3+}-rich phase. The synthesized catalyst materials, with known molar ratio's and comparable S_{BET} and V_{pore}, enabled us to investigate the role of the $La^{3+}:Eu^{3+}$ ratio in the MOC reaction.

3.2.2 Catalytic Performances

Temperature ramp experiments under MOC reaction conditions were performed to study the catalytic activity trends of the bimetallic La^{3+}-Eu^{3+} catalysts. An overview of the catalytic performance of the La^{3+}-Eu^{3+} catalysts is given in Figure 3.2. The catalytic performance of pure LaOCl and EuOCl are presented in chapter 2, but the plots are given for facile comparison. The reaction temperature at which the catalyst becomes active, referred to as the onset temperature, is determined as the reaction temperature at which the X_{CH4} > 2%.

The La^{3+}-Eu^{3+} catalyst materials showed many resemblances with respect to each other in terms of catalytic performance as the same qualitative trends could be observed. In general, the bimetallic catalysts showed a steady increase in the X_{CH4} up to ~ 450 °C (Figure 3.2A), after which the X_{CH4} curve leveled off (Figure 3.2B). With increasing Eu^{3+} content in the catalyst, the flattening of the X_{CH4} curve was more pronounced, but also started at a higher reaction temperature and thus a higher overall activity was obtained. Also in terms of product yield, the same qualitative trends were observed. The Y_{CH3Cl} reached a maximum at a reaction temperature between 450 °C and 475 °C and CH_3Cl is the dominant product below 500 °C (Figure 3.2C). The Y_{CH2Cl2} was overall quite low, with a maximum yield of ~ 3% at 480 °C (Figure 3.2D). Lastly, the Y_{CO} increased steadily over the entire reaction temperature range, reaching its maximum value at 550 °C (Figure 3.2E). CH_3Cl and CCl_4 were detected in minor quantities, with selectivities < 3%. No CO_2 was detected under these reaction conditions.

The bimetallic catalysts showed different catalytic performances compared to their monometallic counterparts. The most striking difference is that the X_{CH4} of the bimetallic catalyst materials levels off above 500 °C, while a large increase in X_{CH4} is observed for both LaOCl and EuOCl (Figure 3.2A). Furthermore, the observed X_{CH4} drop for EuOCl, attributed to the dechlorination of $EuCl_3$ to EuOCl, is not present when a solid solution is formed between La^{3+} and Eu^{3+} (Figure 3.2B). Interestingly, the highest Y_{CH3Cl} of all catalysts was obtained for $La_{0.50}Eu_{0.50}OCl$ and $La_{0.25}Eu_{0.75}OCl$, reaching a maximum value of 11% at 460 °C. This was significantly higher than the 8% Y_{CH3Cl} of EuOCl at the same reaction temperature. This difference was caused by the lower Y_{CH2Cl2} for the La^{3+}-Eu^{3+} catalyst compared to
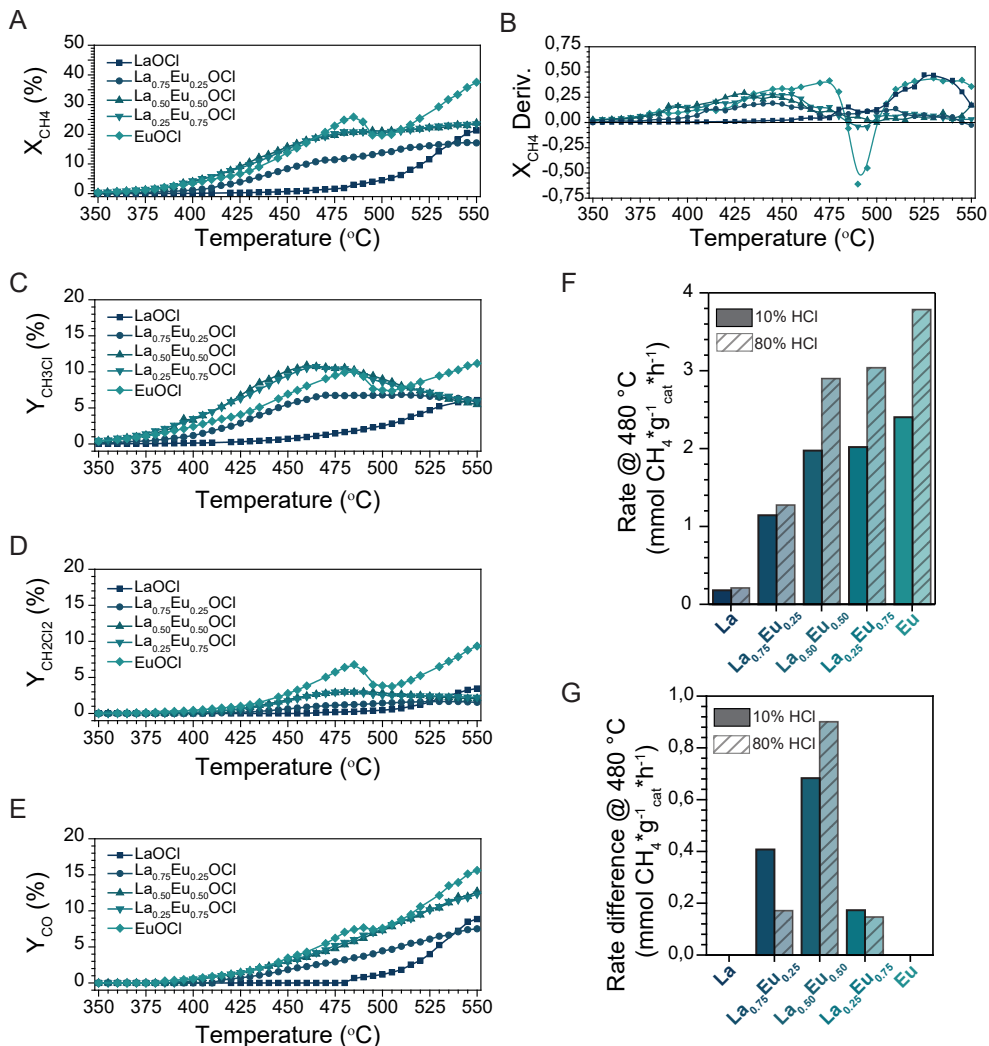
Figure 3.2. CH$_4$ oxychlorination (MOC) experiments for the synthesized La^{3+}-Eu^{3+} catalysts. (A) CH$_4$ conversion (X$_{CH4}$) plotted versus the reaction temperature for LaOCl, La$_{0.75}$Eu$_{0.25}$OCl La$_{0.50}$Eu$_{0.50}$OCl, La$_{0.25}$Eu$_{0.75}$OCl and EuOCl under 10% HCl. The derivative of the X$_{CH4}$ versus reaction temperature is plotted in (B). The yield of (C) CH$_3$Cl, (D) CH$_2$Cl$_2$ and (E) CO are plotted versus the reaction temperature under 10% HCl. The CH$_4$ conversion rate normalized to the amount of catalyst is given in (F). Lastly, the rate difference with respect to the linear combination of LaOCl and EuOCl with the same La^{3+}:Eu^{3+} ratio is given in (G). The temperature-dependent X$_{CH4}$ over LaOCl and EuOCl are obtained from chapter 2.

EuOCl, as the X$_{CH4}$ and Y$_{CO}$ were similar. One additional advantage of using the bimetallic La^{3+}-Eu^{3+} catalysts was that no CO$_2$ was detected over the entire tested range, unlike with other catalyst materials reported in the literature.[8,14,32]

The most balanced performance was observed for La$_{0.50}$Eu$_{0.50}$OCl. The observed X$_{CH4}$, Y$_{CH3Cl}$, Y$_{CH2Cl2}$ and Y$_{CO}$ were similar to La$_{0.25}$Eu$_{0.75}$ and significantly improved compared to

A

B
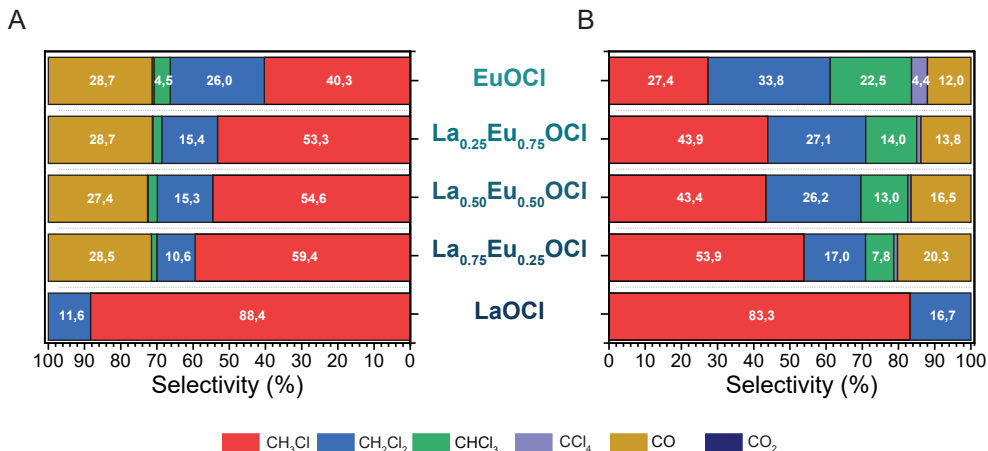
Figure 3.3. Selectivity towards CH_3Cl, CH_2Cl_2, $CHCl_3$, CCl_4, CO, and CO_2 for LaOCl, $La_{0.75}Eu_{0.25}OCl$ $La_{0.50}Eu_{0.50}OCl$, $La_{0.25}Eu_{0.75}OCl$ and EuOCl tested under (A) 10% HCl and (B) 80% HCl in the feed for the CH_4 oxychlorination (MOC) reaction. La^{3+}-Eu^{3+} solid solution catalysts show very similar selectivity under the same conditions for both the 10% and 80% HCl in the feed. The observed selectivity in both cases varies drastically compared to the selectivity observed for LaOCl and EuOCl. Reaction conditions: CH_4:HCl:O_2:N_2:He of 2:2:1:1:14 (10% HCl, in mL/min) or 2:16:1:1:0 (80% HCl, in mL/min), T = 480 °C.

$La_{0.75}Eu_{0.25}OCl$. This is visualized by normalizing the CH_4 conversion rate at 480 °C to the amount of catalyst (Figure 3.2F). A clear trend between the Eu^{3+} content in the catalyst material and the obtained conversion rate is apparent when the activity is normalized to the amount of catalyst and S_{BET}. The following activity ranking was obtained: EuOCl > $La_{0.25}Eu_{0.75}OCl$ ~ $La_{0.50}Eu_{0.50}OCl$ >> $La_{0.75}Eu_{0.25}OCl$ >> LaOCl. Large increments in conversion rates were observed going from LaOCl to $La_{0.75}Eu_{0.25}OCl$ and to $La_{0.50}Eu_{0.50}OCl$, while the CH_4 conversion rate increments decreased going from $La_{0.50}Eu_{0.50}OCl$ to EuOCl. Conversely, when the observed activity was corrected for the activity of the linear combination of LaOCl and EuOCl, a synergistic effect between La^{3+} and Eu^{3+} was observed (Figure 3.2G). The addition of La^{3+} to EuOCl enhanced the activity of Eu^{3+} as all the La^{3+}-Eu^{3+} catalysts possessed a higher conversion rate than when the individual activities of LaOCl and EuOCl are summed with a similar La^{3+}:Eu^{3+} ratio (i.e., the linear combination). An optimum was found when an equal amount of La^{3+} and Eu^{3+} was present, as the observed rate difference was the largest. Since monometallic LaOCl showed little activity at this reaction temperature by itself, we hypothesize that LaOCl acts as a Cl^- buffer, supplying Cl^- to the active Eu^{3+} phase. This effect is caused by the facile chlorination of LaOCl, which increases the degree of chlorination of the catalyst material and hence the activity. The role of La^{3+} and Eu^{3+} is further discussed in section 3.2.3 of this chapter. Nevertheless, the observed selectivities for the bimetallic catalysts were not significantly influenced by the catalyst composition (Figure 3.3). The S_{CH3Cl} lied between 53% and 60% for the bimetallic catalysts, which is much better than the S_{CH3Cl} of 40% obtained for EuOCl. The S_{CO} in all cases is ~ 28% and seems to be governed by the reaction conditions, and not by the catalyst composition.

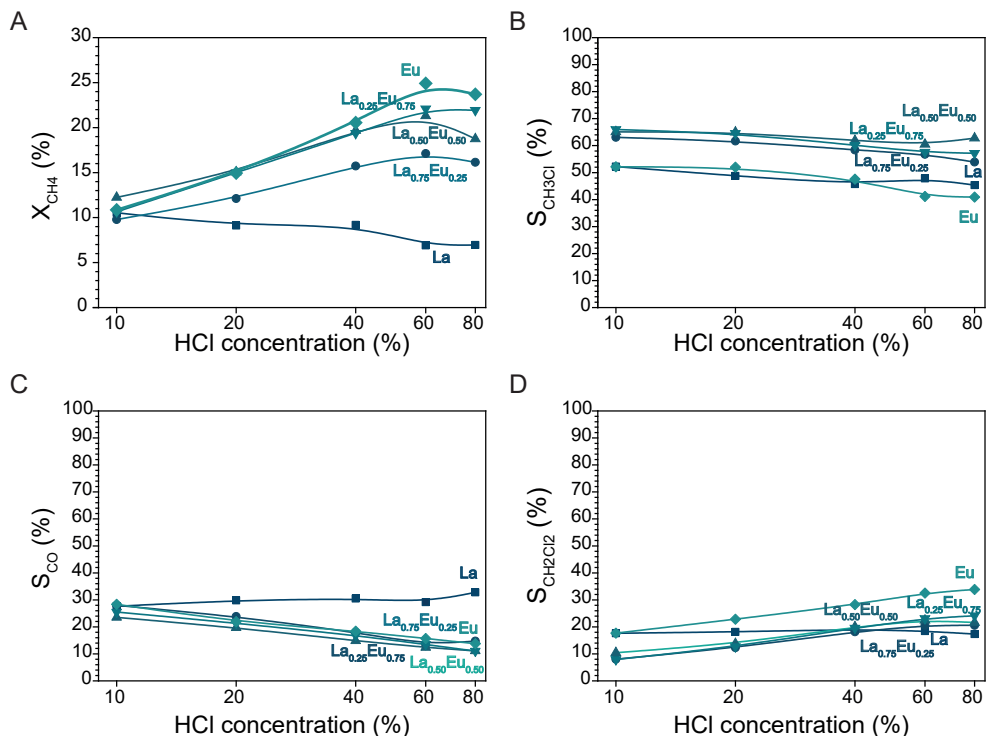The results presented in Figure 3.2 show that La^{3+} had a major influence on the activity

Figure 3.4. (A) CH_4 conversion (X_{CH4}) and the selectivity towards (B) CO (S_{CO}), (C) CH_3Cl (S_{CH3Cl}), and (D) CH_2Cl_2 (S_{CH2Cl2}) versus the HCl concentration for LaOCl (T = 520 °C), $La_{0.75}Eu_{0.25}OCl$ (T = 475 °C), $La_{0.50}Eu_{0.50}OCl$ (T = 450 °C), $La_{0.25}Eu_{0.75}OCl$ (T = 450 °C) and EuOCl (T = 450 °C) in the CH_4 oxychlorination (MOC) reaction. The La^{3+}-Eu^{3+} catalyst materials all show increasing X_{CH4} with increasing HCl concentration. The S_{CH3Cl} is higher compared to LaOCl and EuOCl over the entire HCl concentration range tested. The temperature was adjusted to reach X_{CH4} = 10% for CH_4:HCl:O_2:N_2:He of 2:2:1:1:14. When stable conversion was reached, the HCl:He ratio was adjusted so that the HCl concentration was increased to 20%, 40%, 60% and 80%, while keeping a constant flow of 20 mL/min.

and selectivity in the MOC reaction. Previously, we applied higher HCl concentrations, i.e., 10 – 80% HCl in the feed, to boost the catalytic performance of EuOCl.[33] The catalytic destruction of chloromethanes was circumvented by the high degree of surface chlorination, resulting in improved product selectivity.[9,10,37–41] With the incorporation of La^{3+}, a similar functionality is incorporated into the catalyst design, and the question arises whether an increment in the HCl concentration is still needed to boost the catalytic performance of La^{3+}-Eu^{3+} solid solution catalysts. To investigate the effect of HCl concentration on the La^{3+}-Eu^{3+} solid solution catalysts, the reaction temperature was adjusted to obtain X_{CH4} = 10% after which the HCl concentration in the feed was increased. The X_{CH4}, S_{CH3Cl}, S_{CO} and S_{CHCl2} are plotted versus the HCl concentration in Figures 3.4A-3.4D, respectively. All Eu-containing catalysts were still positively influenced in terms of X_{CH4} by the increment in HCl concentration. A clear trend in the activity profile was observable going from LaOCl to EuOCl. With increasing Eu^{3+} concentration in the catalyst materials, the X_{CH4} is also proportionally more influenced by the increase in HCl concentration. The reaction selec-
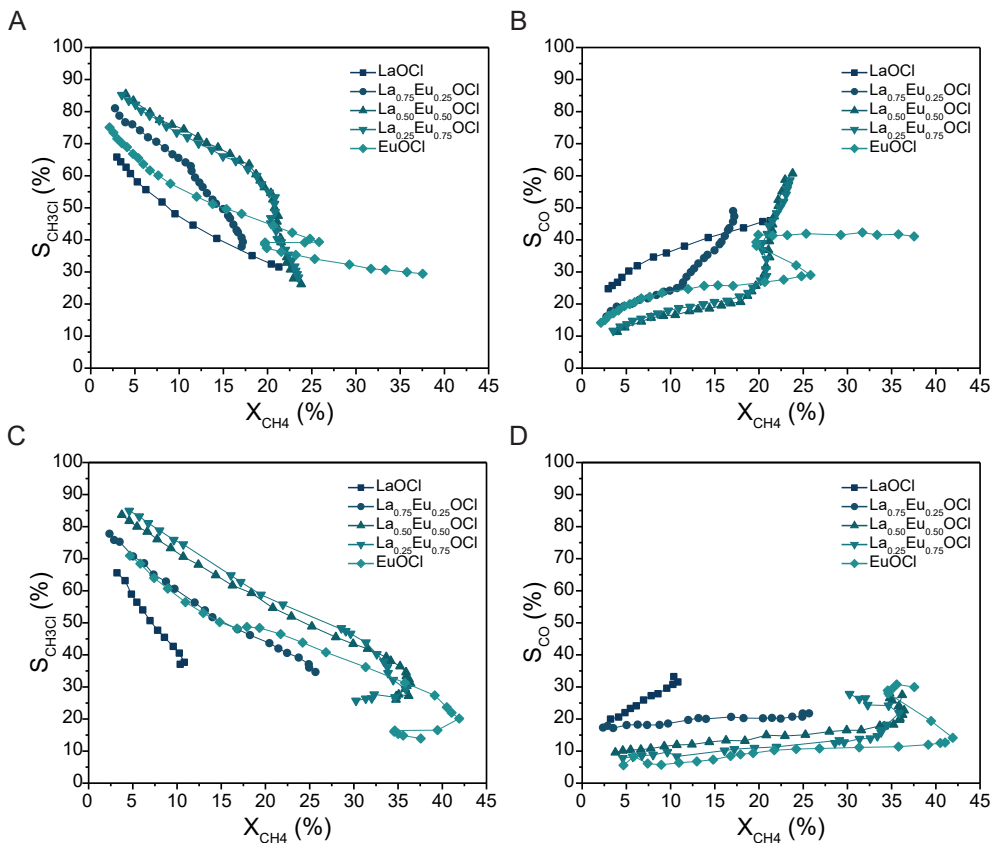
Figure 3.5. Non-isothermal conversion-selectivity plots for LaOCl, $La_{0.75}Eu_{0.25}OCl$ $La_{0.50}Eu_{0.50}OCl$, $La_{0.25}Eu_{0.75}OCl$ and EuOCl for the CH_4 oxychlorination (MOC) reaction. The CH_4 conversion (X_{CH4}) - CH_3Cl selectivity (S_{CH3Cl}) is given for (A) 10% HCl in the feed and (C) 80% HCl in the feed. The corresponding X_{CH4} - CO selectivity (S_{CO}) is also given for (B) 10% HCl in the feed and (D) 80% HCl in the feed.

tivity was not influenced drastically by the change in HCl concentration. In general, very small distinctions in terms of selectivity are found comparing the La^{3+}-Eu^{3+} catalysts. The La^{3+}-Eu^{3+} catalysts follow the same qualitative trend as EuOCl, only the quantitative performance is more suited for commercial application. Compared to EuOCl, the La^{3+}-Eu^{3+} catalysts have an increased S_{CH3Cl} (i.e., 54 – 66% vs 41 – 52%), lower S_{CH2Cl2} (i.e., 8 – 24% vs 18 – 34%) and comparable S_{CO} (i.e., 11 – 28% vs 14 – 28%).

To truly compare the catalytic performance of the catalyst material under study, the non-isothermal conversion-selectivity relation was given plotted towards CH_3Cl and CO (Figure 3.5). In general, the $La_xEu_{1-x}OCl$ catalyst materials performed significantly better compared to EuOCl at 10% HCl concentrations as the S_{CH3Cl} (Figure 3.5A) and S_{CO} (Figure 3.5B) were drastically improved at the same conversion level. For example, at X_{CH4} = 10%, the S_{CH3Cl} and S_{CO} of EuOCl were 54% and 25% while for the $La_{0.50}Eu_{0.50}OCl$ values of 74% and 17% were obtained. Only at high conversion levels (X_{CH4} > 20%), the EuOCl catalyst performed better than the $La_xEu_{1-x}OCl$ catalyst materials, with the important caveat that
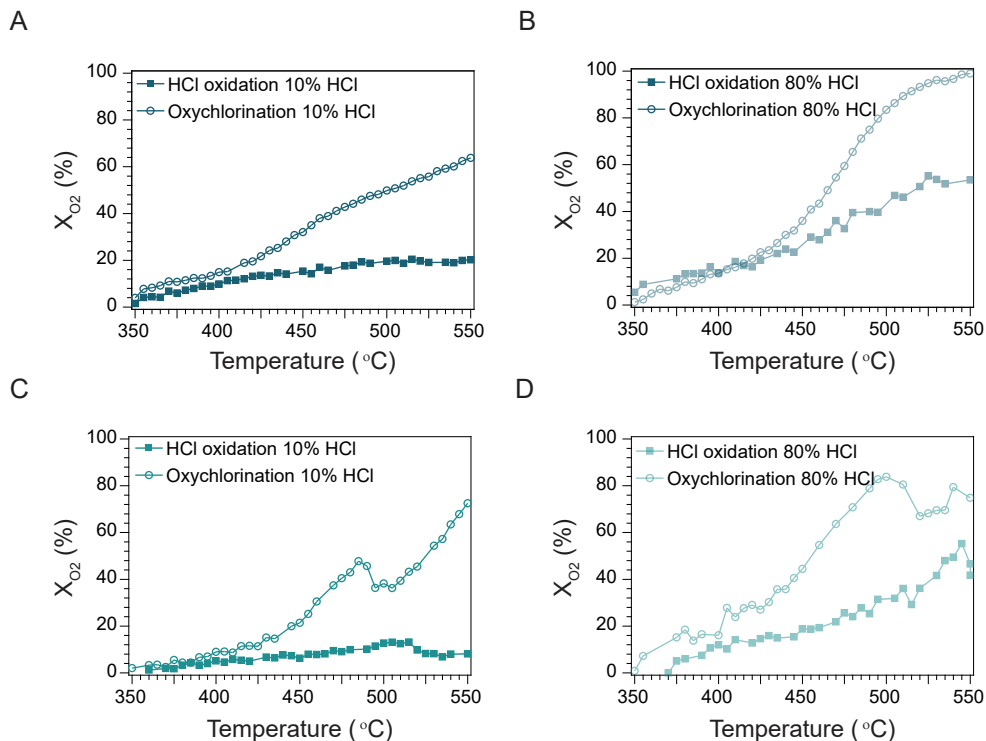
Figure 3.6. Temperature ramp experiments where the oxygen conversion (X_{O2}) is plotted versus the reaction temperature for the HCl oxidation reaction (filled squares) and CH_4 oxychlorination (MOC) reaction (open circles) for (A) $La_{0.50}Eu_{0.50}OCl$ 10% HCl and (B) $La_{0.50}Eu_{0.50}OCl$ 80% HCl (C) EuOCl 10% HCl and (D) EuOCl 80% HCl in the feed. The temperature-dependent X_{O2} over EuOCl was obtained from chapter 2.

the S_{CH3Cl} became too low for practical applications. In the extreme case where the HCl concentration was increased to 80%, the performance of the $La_xEu_{1-x}OCl$ catalyst materials was still superior to the performance of EuOCl in terms of S_{CH3Cl} (Figure 3.5C) while the S_{CO} (Figure 3.5D) were fairly comparable. Here, the $La_{0.25}Eu_{0.75}OCl$ catalyst performed slightly better than the other $La_xEu_{1-x}OCl$ catalyst materials with an S_{CH3Cl} and S_{CO} of 74% and 8% at X_{CH4} = 10%. At the same conversion level, the S_{CH3Cl} and S_{CO} of EuOCl were 56% and 6%. The main difference in product selectivity at 80% HCl concentration is that the CH_3Cl is not further chlorinated to higher chloromethanes for $La_xEu_{1-x}OCl$ catalysts.

Lastly, the change in chemical composition of the catalyst material may alter the reaction mechanism that is responsible for the chlorination of CH_4. Gas-phase chlorination via tandem reactions, HCl oxidation and free radical chlorination, are in competition with the surface-driven MOC reaction. To investigate the contribution of the gas-phase chlorination to the observed activity, the HCl oxidation performance of $La_{0.50}Eu_{0.50}OCl$ was tested. The oxygen conversion (X_{O2}) of the HCl oxidation was compared to the X_{O2} of the MOC reaction under 10% and 80% HCl in the feed in Figures 3.6A and 3.6B, respectively. For facile comparison, the same plots are given for EuOCl obtained from chapter 2 in Figures

Calculated reaction equation:
LnOCl(s) + 2HCl(g) -> LnCl$_3$(s) + H$_2$O
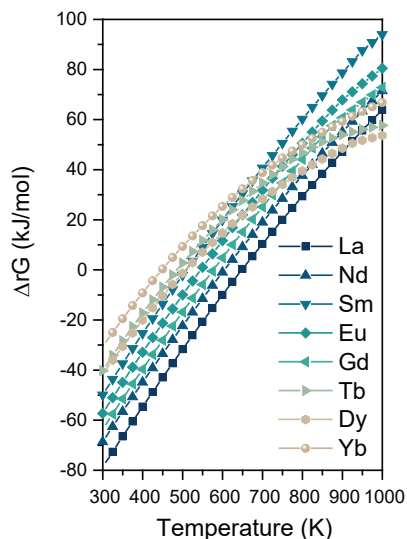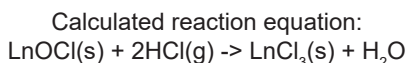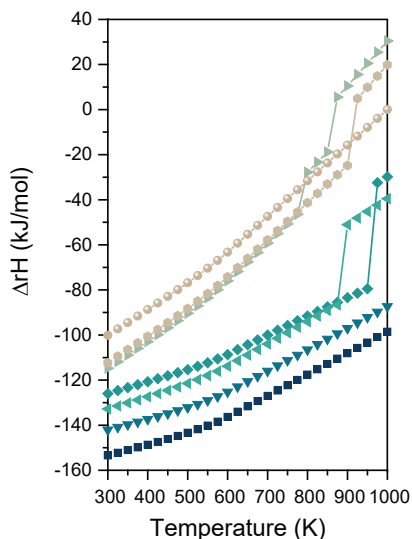
Figure 3.7. Calculated (A) Gibbs free energy (Δ_rG) and (B) enthalpy (Δ_rH) of the chlorination of LnOCl to LnCl$_3$. Of all the lanthanides available in HSC Chemistry for the chlorination reaction given above, La^{3+} was found to have the lowest Δ_rG and Δ_rH. This indicated that the chlorination of LaOCl to LaCl$_3$ is the most facile compared to the other lanthanides. Thermodynamic calculations were performed with HSC chemistry 7.1. The reaction equation given in the figure was filled in for every lanthanide element as input in the Chemical Reactions Calculator and the Δ_rG and Δ_rH between 300 K and 1000 K with steps of 25 K were calculated.

3.6C and 3.6D, respectively. At 10% HCl, the X_{O_2} for La$_{0.50}$Eu$_{0.50}$OCl increased to a reaction temperature of 500 °C, after which it stabilized at the final X_{O_2} value of ~ 20%. This was significantly less than the X_{O_2} during MOC reaction, which gradually increased to a final X_{O_2} value of ~ 62%. A discrepancy between the X_{O_2} of the HCl oxidation and MOC was already observed from 405 °C onwards, evidencing that the surface-driven CH$_4$ chlorination is the dominant pathway during MOC at 10% HCl. When the HCl concentration was increased to 80% HCl, thereby also increasing the activity of the catalyst material in the MOC, a steeper increase in the X_{O_2} was observed for the HCl oxidation, which gradually increased up to a final X_{O_2} value of ~ 53% at 550 °C. The X_{O_2} was significantly higher when the HCl concentration was increased and the thermal chlorination had a larger contribution to the overall activity. These trends in both HCl oxidation and MOC match well with the trends observed for monometallic EuOCl. The addition of La^{3+} does not influence the HCl oxidation capability of EuOCl qualitatively.

3.2.3 Understanding the Working Mechanism

The catalytic performance of La^{3+}-Eu^{3+} solid catalysts showed clear synergetic behavior when compared to either LaOCl or EuOCl. The premise of making La^{3+}-Eu^{3+} solid solutions
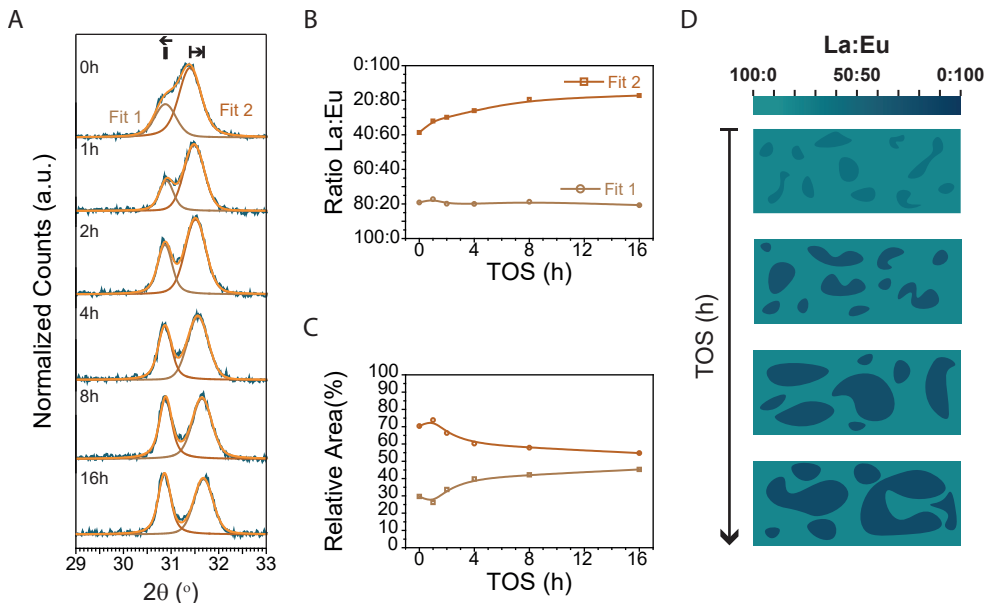
Figure 3.8. Time series of $La_{0.50}Eu_{0.50}OCl$ exposed to CH_4 oxychlorination (MOC) conditions to study the phase segregation behavior of La^{3+}-Eu^{3+} solid solutions. $La_{0.50}Eu_{0.50}OCl$ was tested for 1, 2, 4, 8 and 16 h time-on-stream (TOS) at 450 °C and the catalyst material was characterized with x-ray diffraction (XRD). Fresh catalyst was loaded into the reactor for every measurement. (A) The zoom in of the (110) XRD peaks displays phase segregation over time. The obtained (B) La^{3+}:Eu^{3+} ratio and (C) relative area of Fit 1 and Fit 2 indicate that the phase segregation predominantly occurs within the first 8 h of reaction. A schematic representation of the phase segregation is depicted in (D), where the La^{3+}-rich phase starts to increase in La^{3+} concentration and relative amount.

was to improve the chlorination rate of EuOCl, as this chlorination step was found to be rate limiting.[33] High HCl concentrations in the feed were needed to boost the activity of EuOCl, which is unfavorable in terms of product separation and size of recycle streams. The chlorination and dechlorination behavior of La^{3+} was studied and we observed that La^{3+} was readily chlorinated to $LaCl_3$. Thermodynamic calculations are consistent with this observation, as the chlorination of LnOCl (Ln = lanthanide) to $LnCl_3$ is the most facile for LaOCl (Figure 3.7). Thus, LaOCl most probably functions as a Cl^- acceptor/capacitator for the active EuOCl. However, the harsh reaction conditions under which these solid catalysts operate cause many changes in the physicochemical properties over time, and the intimate contact between La^{3+} and Eu^{3+} could be lost. The loss of intimate contact between La^{3+} and Eu^{3+} implies that the exchange of ions between La^{3+} and Eu^{3+} is made more difficult, thereby losing the synergistic effect. Hence, catalyst stability could pose an issue.

To analyze whether further phase segregation occurs over time, $La_{0.50}Eu_{0.50}OCl$ was subjected to MOC conditions for 1, 2, 4, 8 and 16 h and the post characterization results of the chemical composition and structure are presented in Figure 3.8. The as-synthesized $La_{0.50}Eu_{0.50}OCl$ displayed two XRD reflections in the region where the (110) lies (Figure 3.8A), both consisted of La^{3+} as well as Eu^{3+} (Figure 3.8B). Over time, the Eu^{3+}-rich phase starts to move to higher angles, indicating the further enrichment of this phase with Eu^{3+}.

The La^{3+}-rich phase however, does not change in chemical composition (± 2% over the entire duration). Simultaneous to the segregation is the change in relative peak area where the La^{3+}-rich phase gained in relative peak area. The largest differences were observed in the first 8 h, where the La^{3+}:Eu^{3+} ratio of the Eu^{3+}-rich phase changed from 39:61 to 20:80. After 16 h time-on-stream (TOS), the La^{3+}:Eu^{3+} ratio reached 17:83 for the Eu^{3+}-rich phase.

The observed phase segregation suggests that total phase segregation could occur over prolonged reaction times or harsher reaction conditions, thereby losing the intimate contact between La^{3+} and Eu^{3+}. It is unclear if the segregation of these two phases would result in the loss of the synergistic effect between La^{3+} and Eu^{3+}. Therefore, to investigate whether this synergistic effect between La^{3+} and Eu^{3+} also exists when the two phases are completely segregated, two physical mixtures of LaOCl and EuOCl were prepared and tested under the same reaction conditions as La$_{0.50}$Eu$_{0.50}$OCl. Physical mixture 1 (PM1) was prepared by sonicating a mixture of LaOCl and EuOCl nano-powders in ethanol, after which the solvent was evaporated and the powder mixture was sieved (125 - 425 μm size fraction). Intimate mixing of the powders is achieved, but no solid solution was formed. Physical mixture 2 (PM2) was prepared by mixing sieved LaOCl and EuOCl particles (125 - 425 μm size fraction), hence no intimate contact is expected. PM1 and PM2 were tested performing temperature ramp experiments under 10% HCl, and post characterized with XRD. The X$_{CH4}$, Y$_{CH3Cl}$ and the (110) XRD peak of PM1 are presented in Figures 3.9A-3.9C, respectively and compared to La$_{0.50}$Eu$_{0.50}$OCl. The same plots as for PM1 were made for PM2 and presented in Figures 3.9D-3.9F, respectively. A comparison between PM2 and the linear combination of LaOCl and EuOCl is made.

A clear distinction between the observed performance of PM1 and PM2 was apparent. When intimate contact was achieved, thus in the case of PM1, the X$_{CH4}$ and Y$_{CH3Cl}$ much resemble the same trend as observed for La$_{0.50}$Eu$_{0.50}$OCl. Even though some quantitative differences exist, and the overall performance is slightly lower, an enhancement of the activity compared to the linear combination was present (Figure 3.9G). The drop in catalytic activity, unique for EuOCl, was not observed, indicating that an intimate contact is established between La^{3+} and Eu^{3+}. Surprisingly, mixing of Eu^{3+} in the La^{3+}-rich phase occurred, indicated by the shift to higher angles for the La^{3+}-rich phase. The La^{3+}:Eu^{3+} ratio changed from 100:0 to 88:12. No La^{3+} was incorporated in the EuOCl crystal structure, but migration of Eu^{3+} into LaOCl occurred, possibly because of the higher thermodynamic stability of such phase. The enhancement of activity and mixing of phases did not occur in PM2, when no intimate contact between La^{3+} and Eu^{3+} was present. The activity profile and selectivity of PM2 much resembled a linear combination of the activity of monometallic LaOCl and EuOCl. The drop in catalytic activity does occur for this catalyst, which is characteristic for monometallic EuOCl. Furthermore, XRD patterns reveals that no mixing of Eu^{3+} and La^{3+} occurred at these reaction conditions and reaction times. The premise of mixing La^{3+} and Eu^{3+} was to accelerate the chlorination rate of the catalyst material, and hence the activity of Eu, by incorporating a Cl$^-$ accepting element in the material. At this point, we have observed a synergistic effect between La^{3+} and Eu^{3+} and established the fact that the intimate contact between La^{3+} and Eu^{3+} responsible for this synergistic effect
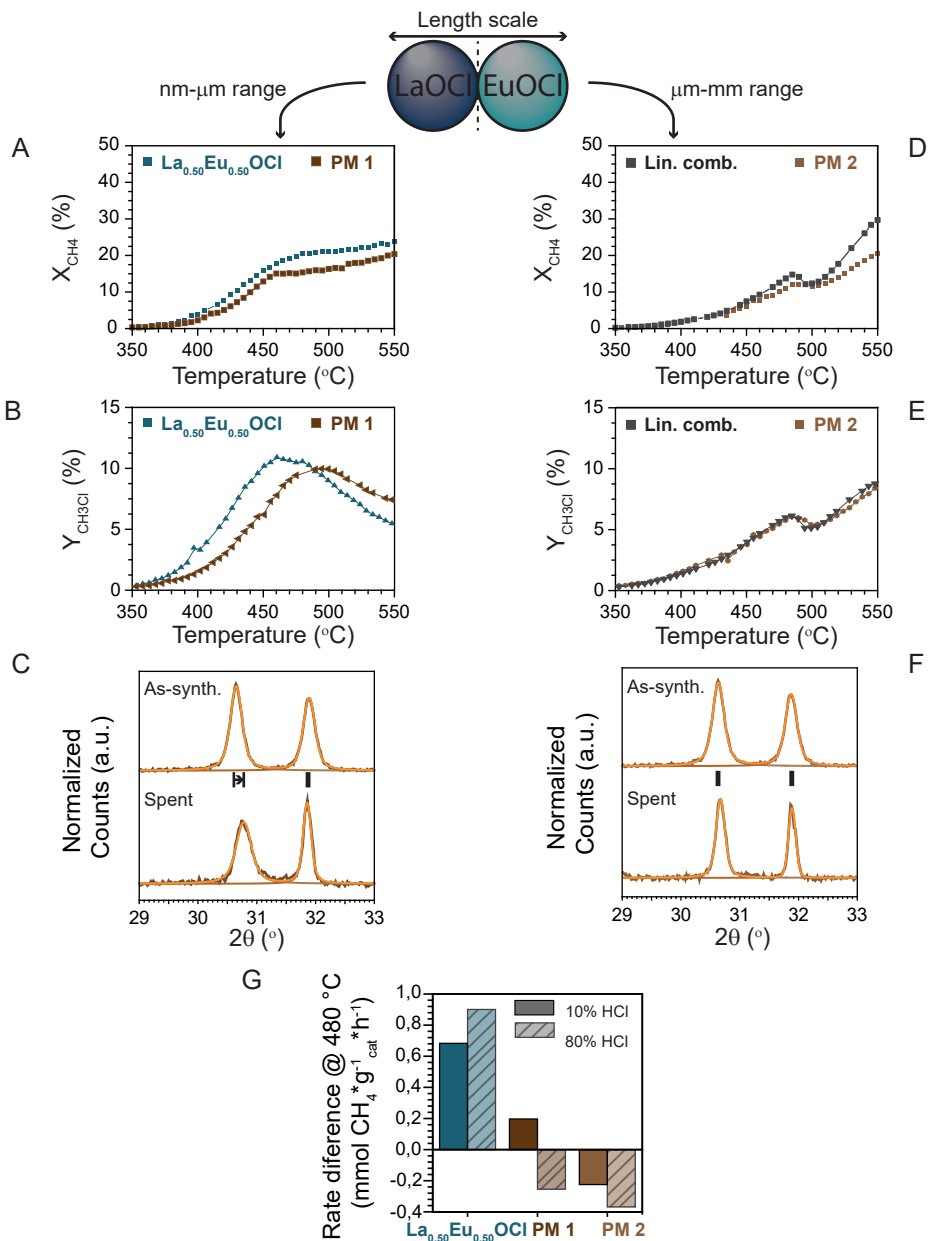
Figure 3.9. Catalytic performance of PM1 compared to La$_{0.50}$Eu$_{0.50}$OCl and the performance of PM2 compared to the linear combination of LaOCl and EuOCl. The (A) CH$_4$ conversion (X$_{CH4}$), (B) CH$_3$Cl yield (Y$_{CH3Cl}$) and (C) analysis of the (110) X-ray Diffraction (XRD) peak of PM1 indicate that the performance of PM1 is very comparable to La$_{0.50}$Eu$_{0.50}$OCl if intimate contact between LaOCl and EuOCl is established. The (D) X$_{CH4}$, (E) Y$_{CH3Cl}$ and (F) analysis of the (110) XRD peak of PM2 reveal that similar performance to the linear combination of LaOCl and EuOCl is obtained when no intimate contact is established. (G) The rate difference of La$_{0.50}$Eu$_{0.50}$OCl, PM1 and PM2 with respect to the linear combination of LaOCl and EuOCl.

will be preserved. However, it is yet unclear what the mechanism behind this synergistic effect is. Furthermore, during reaction, a La^{3+}-rich oxychloride phase with minor amounts of Eu^{3+} and an (almost) pure EuOCl phase were obtained. In order to unravel the active phase, we have looked at the chlorination behavior of Eu^{3+} in different Eu-containing catalysts.

Structural information, combined with the observed activity in the MOC reaction, provide crucial insight in the working mechanism of these MOC catalyst materials. According to

$$\text{(Eq. 3.1)} \; LnOCl + 2\,HCl \xrightarrow{k_1} LnCl_3 + H_2O$$
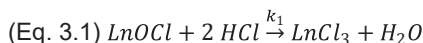
our understanding, the oxychlorination reaction consists of two non-catalytic reactions combined to form a catalytic cycle; the chlorination of the lanthanide oxychloride

$$\text{(Eq. 3.2)} \; LnCl_3 + 2CH_4 + O_2 \xrightarrow{k_2} LnOCl + CH_3Cl + H_2O.$$
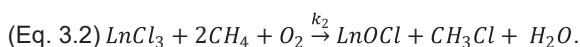
and the dechlorination of the lanthanide chloride

Many more chemical reactions occur in the complex MOC reaction, as e.g., the dechlorination can also occur via the reaction with H_2O.[40,41] For simplicity reasons the two reaction equations that make up the standard oxychlorination reaction to CH_3Cl are given as the main point is the concept of catalyst chlorination and dechlorination. From (Eq. 3.1) and (Eq. 3.2) it becomes apparent that the state of the catalyst, or the degree of catalyst chlorination, is controlled by . By altering the feed composition, either k_1 or k_2 is directly influenced, which is represented by a change in catalytic performance.

The structural information was obtained with operando luminescence spectroscopy. The area of the Eu^{3+} luminescence signal was used as a measure for the degree of Eu^{3+} chlorination in chapter 2.[33] Since $EuCl_3$ shows no luminescence at elevated temperatures, the decrease in luminescence intensity can be correlated to the degree of chlorination. The Eu^{3+} luminescence spectra of $La_{0.50}Eu_{0.50}OCl$ and PM1 showed the same emissions as Eu^{3+} in EuOCl and responded in the same manner to a change in degree of chlorination (Figure 3.10A). Thus, the same analysis can be performed to show the qualitative trends in the degree of chlorination of Eu^{3+} in La^{3+}-Eu^{3+} catalyst materials.

When considering EuOCl, very high HCl concentrations and prolonged reaction times were needed to convert EuOCl into $EuCl_3$. The relative spectral area of the Eu^{3+} luminescence signal (Figure 3.10B) and the X_{CH4} (Figure 3.10C) are plotted versus the TOS, where the HCl concentration in the feed is gradually increased. Here, the first signs of catalyst chlorination started after 10 h, and reached its final state after 12 h. The X_{CH4} gradually increased up to 60% HCl and a steady downward trend in the X_{CH4} of EuOCl was visible at when the final HCl concentration of 80% was fed, which coincides with previously reported observations that full chlorination deactivates the catalyst material. For EuOCl, only at these very high HCl concentrations the $k_1/k_2 > 1$, combined with the fact that the activity correlated with the HCl concentration, indicated that the chlorination of the EuOCl surface is the rate-determining step. Any Cl^- present on the surface had reacted before
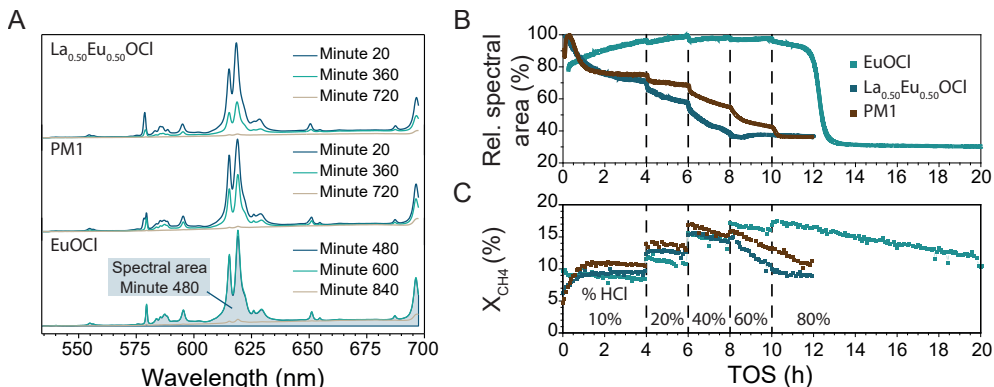
Figure 3.10. (A) Photoluminescence spectra of La$_{0.50}$Eu$_{0.50}$OCl, PM1 and EuOCl corresponding to the runtimes in (B) show the same behavior to the response in degree of chlorination as observed for EuOCl. The only change appeared in the spectral intensity and not in the shape of the spectrum. The applied integrated spectral area is graphically depicted for EuOCl by the blue area. (B) Relative spectral area of the Eu^{3+} luminescence signal observed during CH$_4$ oxychlorination (MOC) reaction under varying reaction conditions at 450 °C and (C) the corresponding X$_{CH4}$ plotted versus time-on-stream (TOS). Incorporation of La^{3+} caused a faster chlorination of the Eu^{3+}. Reaction conditions: CH$_4$:HCl:O$_2$:N$_2$:He of 2:2:1:1:14 (10% HCl, in mL/min), at 450 °C. Subsequently, the HCl:He ratio was altered to obtain 20, 40, 60 and 80 vol% HCl, while keeping a constant flow of 20 mL/min.

it could diffuse to the bulk, hence no phase change was observed. If the surface chlorination would not be rate-limiting, increasing the HCl concentration would not result in an increase in the activity.

We have applied the same principle for La^{3+}-Eu^{3+} catalysts, to show that La^{3+} addition heavily affects the rate of EuOCl chlorination, and thus the rate-determining step. When La^{3+} was in close proximity to Eu^{3+}, more facile catalyst chlorination was observed. The highest chlorination rate was observed for La$_{0.50}$Eu$_{0.50}$OCl, as the integrated spectral area already shows a decreasing trend with 10% HCl in MOC reaction conditions. Right from the start, k$_1$/k$_2$ > 1. This is remarkable, as EuOCl was proven to be difficult to chlorinate under these conditions. The chlorination continued with an increasing rate when the HCl concentration was further increased up to 8 h, where it reached its final state. Complete chlorination was achieved, as no emissions from EuOCl could be detected anymore. Interestingly, up to 8 h, the X$_{CH4}$ increased from 9% to 15%, after which it decreased back to 9% after reaching full chlorination. Qualitatively, the same trend was observed for PM1, but chlorination of the catalyst material occurred at a slower rate. The catalyst material was fully chlorinated after 10 h.

A crucial observation is that a fast chlorination of Eu^{3+} was expected for La$_{0.50}$Eu$_{0.50}$OCl, but not for PM1. PM1 showed no incorporation of La^{3+} into the EuOCl phase (Figure 3.9) and therefore the same trend as for pure EuOCl would be expected. However, the excellent particle mixing of LaOCl and EuOCl heavily influenced the rate of chlorination of the pure EuOCl. This showcases that the ions in these materials are very mobile, and that facile exchange of ions occurs when the two phases are within close proximity. The apparent activation energy (E$_{app}$) of La$_{0.50}$Eu$_{0.50}$OCl (126 kJ/mol) was very comparable to the E$_{app}$ of

A

B

Pure EuOCl

Synergistic effect between EuOCl and LaOCl
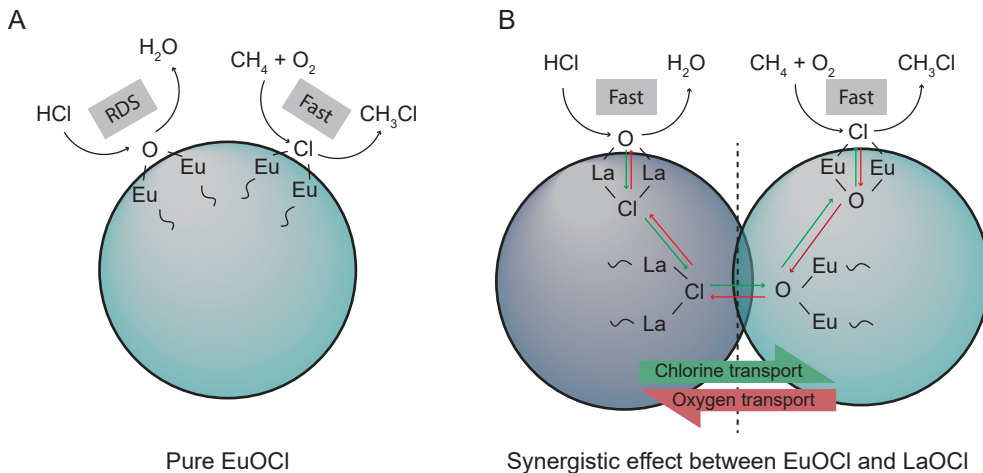
Scheme 3.1. Schematic representation of the role of (A) EuOCl and (B) the combination of LaOCl and EuOCl exhibiting a synergistic effect in the CH_4 oxychlorination (MOC) reaction. For EuOCl, the rate determining step (RDS) is the chlorination of the catalyst surface. When an La^{3+}-rich and Eu^{3+}-rich phase are in close proximity to each other, exchange of ions can occur. The rate-determining step, the chlorination of EuOCl, is accelerated by the presence of LaOCl. The oxygen on the LaOCl surface is replaced with Cl by the reaction with HCl. Subsequently, the excess Cl is transferred to the Cl-deficient EuOCl after which it is transferred to the surface of the EuOCl phase. The Cl is reacted with CH_4 and O_2 on the catalyst surface, leaving an O^{2-} group. Conversely, O^{2-} travels the reverse path.

EuOCl (120 kJ/mol), suggesting that the energy needed for the reaction was not altered. A hypothesis on the process of ion exchange is schematically depicted in Scheme 3.1, responsible for the observed synergistic effect in catalysis. In the case where only EuOCl is present (Scheme 3.1A), the rate determining step (RDS) is (Eq. 3.1). The dechlorination of the catalyst surface is rapid and therefore the bulk stays in the dechlorinated state. In the case where both Eu^{3+} and La^{3+} are present (Scheme 3.1B), ion exchange through the bulk occurs. LaOCl, acting as a Cl^- acceptor/capacitator, is rapidly chlorinated by the reaction with HCl. Subsequently, the mobile excess Cl^- is transferred to the Cl-deficient EuOCl where an exchange with O^{2-} occurs. The Cl^- is reacted with CH_4 and O_2 on the EuOCl catalyst surface, replenishing the O^{2-} group. While LaOCl and EuOCl individually are active in the MOC, both capable of surface chlorination and CH_4 activation, the process of ion exchange is accelerated. Hence, PM1 also exhibited synergistic effects when tested for its MOC performance.

Lastly, the stability of $La_{0.50}Eu_{0.50}OCl$ under MOC conditions was tested for 48 h at 450 °C under varying HCl concentration in the feed. Every 10 h, the HCl concentration was increased to find the upper limit under which the catalyst material still exhibited stable performance. Simultaneously, the photoluminescent properties of Eu^{3+} were again used to monitor the degree of EuOCl chlorination. The activity/selectivity in the MOC reaction and the corresponding spectral data are plotted versus TOS in Figures 3.11A and 3.11B, respectively. $La_{0.50}Eu_{0.50}OCl$ exhibited very stable X_{CH4} under 10% and 20% HCl in the MOC reaction, with values of 12% and 16%, respectively. At 40% HCl, a slight downward trend
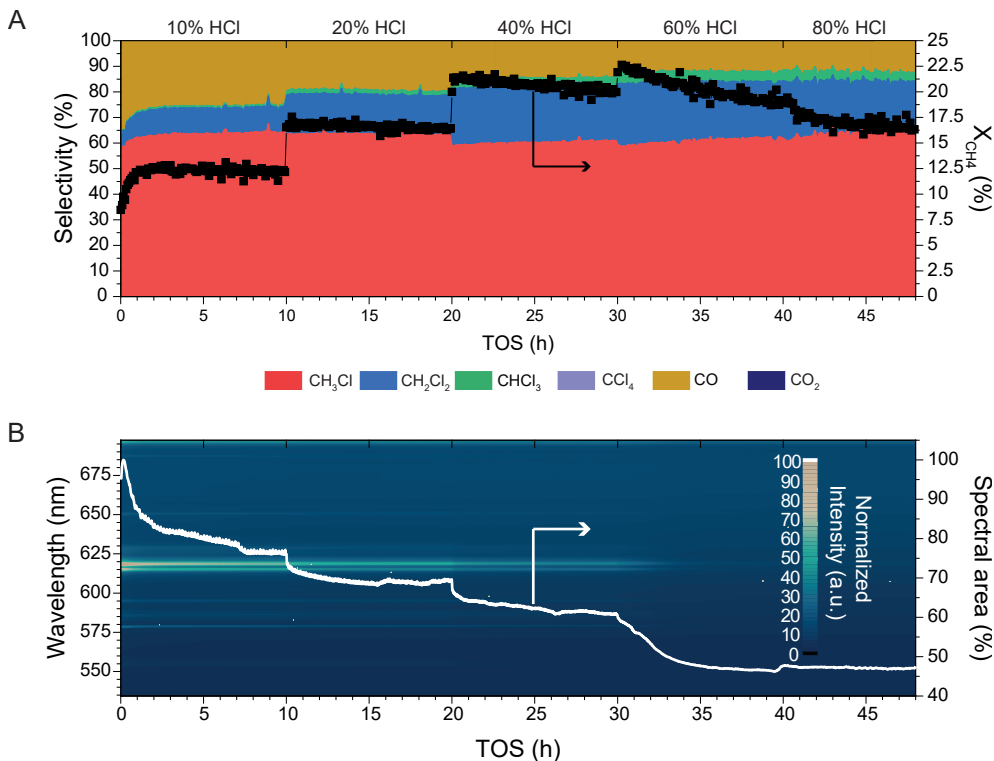
Figure 3.11. Stability test of La$_{0.50}$Eu$_{0.50}$OCl at 450 °C, while varying the HCl concentration in the feed every 10 h for the CH$_4$ oxychlorination (MOC) reaction. (A) The CH$_4$ conversion (X$_{CH4}$) and the selectivity towards CH$_3$Cl (S$_{CH3Cl}$), CH$_2$Cl$_2$ (S$_{CH2Cl2}$), CHCl$_3$ (S$_{CHCl3}$), CCl$_4$ (S$_{CCl4}$), CO (S$_{CO}$), and CO$_2$ (S$_{CO2}$) are plotted versus time-on-stream (TOS). (B) Operando luminescence spectroscopy of Eu^{3+} where the spectra are plotted as a heat map versus the TOS. Furthermore, the integrated spectral area is plotted versus the TOS as a measure for the degree of catalyst chlorination. With increasing HCl concentration up to 60%, the X$_{CH4}$ increased while the S$_{CO}$ and S$_{CH3Cl}$ decreased. When 60% HCl was fed in the reactor, the X$_{CH4}$ sloped down while simultaneously the catalyst fully chlorinated. Reaction conditions: CH$_4$:H-Cl:O$_2$:N$_2$:He of 2:2:1:1:14 (10% HCl, in mL/min), at 450 °C. Subsequently, the HCl:He ratio was altered to obtain 20, 40, 60 and 80 vol% HCl, while keeping a constant flow of 20 mL/min.

in the X$_{CH4}$ was observable, going from 21% to 19%. The decline was accelerated when the HCl concentration was further increased to 60%. A final X$_{CH4}$ of 16% was achieved after 48 h. The selectivity in the MOC reaction showed the same stability as observed for X$_{CH4}$. At 10% and 20% HCl in the feed, an S$_{CH3Cl}$ of ~ 64% was achieved. When the X$_{CH4}$ showed a decreasing trend, from 60% HCl onwards till the end of the experiment, the S$_{CH3Cl}$ slightly increased from 59 to 64% in favor of S$_{CH2Cl2}$ and S$_{CHCl3}$. The S$_{CO}$ remained unaltered under these reaction conditions at ~ 13%. This is in line with the trends, observable for X$_{CH4}$ were the observed changes in the spectral intensity. After an initial stabilization period of ~ 8 h in which the catalyst is slowly chlorinated, a steady state composition of the catalyst was achieved as the spectral area did not change until the HCl concentration was further increased to 20%. Again, a stabilization period was observed which now took roughly 3 h whereafter a steady state was achieved. At 40%, where the X$_{CH4}$ slowly decreased
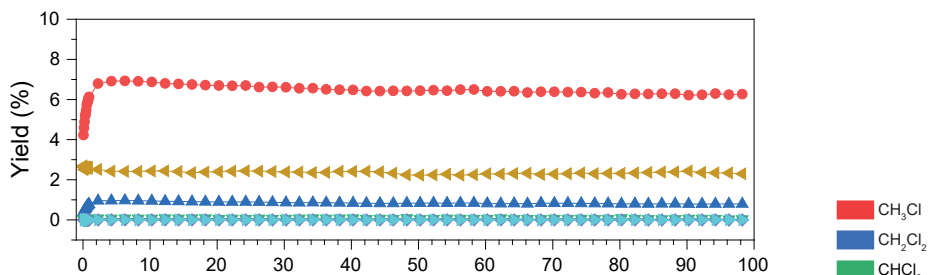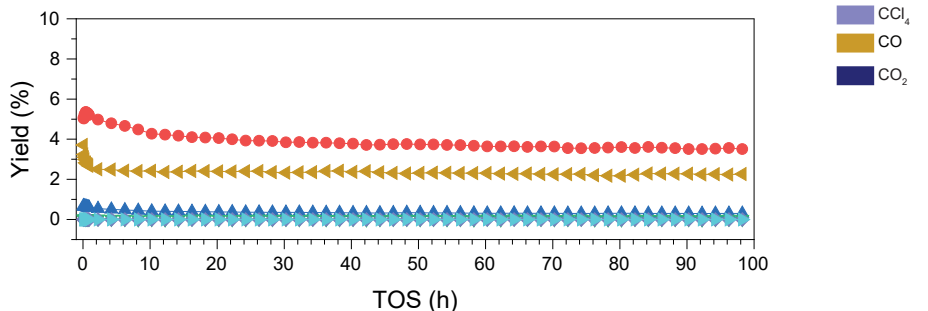
Figure 3.12. Catalytic stability of (A) $La_{0.50}Eu_{0.50}OCl$ and (B) EuOCl in the CH_4 oxychlorination reaction tested for 100 h time-on-stream (TOS) at 450 °C. The yields are plotted versus the TOS. Both catalyst materials show stable performance during the duration of the experiment. Reaction conditions: CH_4:HCl:O_2:N_2:He of 2:2:1:1:14 (10% HCl, in mL/min), temperature 450 °C.

over time, the integrated spectral area also showed a slightly decreasing slope. From 60% HCl onwards, the catalyst was gradually chlorinated almost to completion. These results suggest that $La_{0.50}Eu_{0.50}OCl$ is stable in the MOC reaction under the condition that EuOCl is not fully chlorinated to $EuCl_3$. This was further evidenced by the performing a 100 h during stability test under the same conditions. The results of this experiment are summarized in Figure 3.12. As can be noted no sign of deactivation was observed for $La_{0.50}Eu_{0.50}OCl$ under 10% HCl at 450 °C. Furthermore, the catalytic benefits arising from the synergistic effect between La^{3+} and Eu^{3+}, i.e., increased S_{CH3Cl}, lower S_{CH2Cl2} and similar S_{CO} and X_{CH4}, were preserved.

3.3. CONCLUSIONS

In this chapter, a set of $La_xEu_{1-x}OCl$ (where x = 0, 0.25, 0.50, 0.75 and 1) solid solutions with comparable physicochemical properties were synthesized. Intimate contact between La^{3+} and Eu^{3+} was achieved, as La^{3+} and Eu^{3+} were incorporated into the same crystal structure. However, CH_4 oxychlorination (MOC) conditions caused phase segregation into two phases; a La^{3+}-rich phase and an Eu^{3+}-rich phase. These phases were still in close contact with one another, exhibiting synergistic effects in the MOC reaction. LaOCl, which readily chlorinates, acts as a Cl^- buffer in the EuOCl catalyst and accelerates the catalyst chlorination rate. Transport of chlorides from the La^{3+}-rich phase to the active EuOCl is suspected to take place, facilitating the difficult EuOCl chlorination step. This synergistic effect resulted in the fact that all La^{3+}-Eu^{3+} solid solution catalysts possessed enhanced activity as compared to the linear combination of LaOCl and EuOCl. Even in absolute terms, the activity of e.g., $La_{0.50}Eu_{0.50}OCl$ approached the activity of EuOCl, even though the material contains 50% less of the active Eu^{3+}. Furthermore, mixing La^{3+} and Eu^{3+} also significantly improved the observed selectivity. Compared to EuOCl, the La^{3+}-Eu^{3+} catalysts have an increased S_{CH3Cl} (i.e., 54 – 66% vs. 41 – 52%), lower S_{CH2Cl2} (i.e., 8 – 24% vs 18 –3 4%) and comparable S_{CO} (i.e., 11 – 28% vs 14 – 28%) under the same reaction conditions and varying HCl concentrations in the feed. Finally, the synergistic effect between La^{3+} and Eu^{3+} can be assured over extended reaction times as the same synergistic effect can be reached by physically mixing LaOCl and EuOCl. This physical mixture showed qualitatively the same trends as the $La_{0.50}Eu_{0.50}OCl$, and after reaction, incorporation of Eu^{3+} in the LaOCl crystal structure was found. The improved catalyst design by the partial replacement of Eu^{3+} by La^{3+} makes Eu-based catalyst materials even more attractive for commercial applications as better CH_3Cl yield and selectivity could be achieved, while also reducing the raw material cost of the MOC catalyst.

3.4. ACKNOWLEDGEMENTS

3.5. EXPERIMENTAL METHODS

3.5.1. Catalyst Synthesis

The $La_{1-x}Eu_xOCl$ (where x = 0, 0.25, 0.5, 0.75 or 1) catalyst materials under study were prepared by dissolving lanthanum (III) chloride hydrate ($LaCl_3 \cdot xH_2O$, Alfa Aesar, > 99,9%) and/or europium (III) chloride hydrate ($EuCl_3 \cdot xH_2O$, Alfa Aesar, > 99,9%) in ethanol (absolute, VWR), followed by a precipitation using stoichiometric amounts of ammonium hydroxide (Fisher Scientific, 25% in H_2O) at room temperature. After the drop-wise addition, the precipitates were stirred for an additional hour and subsequently centrifuged to obtain the gel. Then, the obtained gel was washed with ethanol (absolute, VWR) and dried at 80 °C in air. Lastly, the dried solids were calcined in a static oven at 500 °C for 3

h using a ramp rate of 5 °C/min.

3.5.2. Catalyst Characterization

X-ray diffraction (XRD) patterns were obtained with a Bruker-AXS D8 powder x-ray diffractometer in Bragg–Brentano geometry, using Cu $K_{\alpha1,2}$ = 1.54184 Å, operated at 40 kV. The measurements were carried out between 22 and 65 ° using a step size of 0.02 ° and a scan speed of 1 s, with a 2 mm slit for the source.

N_2 adsorption isotherms were measured at -196 °C on a Micromeritics TriStar II Plus instrument. Prior to all measurements, samples were dried at 300 °C in a flow of N_2. Specific surface areas were calculated using the multipoint Brunauer Emmett Teller (BET) method (0.05 < p/p_0 < 0.25). Pore volumes were calculated by the t-plot method; pore size distributions were obtained by the Barrett Joyner Halenda (BJH) analysis; Harkins and Jura thickness model was applied for the t-plot and BJH methods.

Inductively coupled plasma-optical emission spectroscopy (ICP-OES) was applied to determine the chemical composition of the catalyst materials, using a SPECTRO CIROS[CCD] instrument. ICP-OES samples were prepared by destructing the solids in aqua regia.

Operando spectroscopy determination of the qualitative $EuOCl/EuCl_3$ signal ratio by luminescence spectroscopy was performed with an AvaRaman-532 Hero-Evo instrument (λ = 532 nm, laser output 50 mW, spectral resolution of 10 cm^{-1}) equipped with an Ava-Raman-PRB-FC-532 probe, capable of withstanding temperatures up to 500 °C. Spectra were collected every minute with the AvaSoft 8 software. The data were subsequently dark corrected. The initial signal was optimized to obtain at least 50% of the saturation value.

3.5.3. Catalyst Testing

All the catalytic tests and operando spectroscopy characterization experiments were performed in a lab scale continuous-flow fixed-bed reactor quartz reactor. Details on the experimental set-up as well as definitions and calculations are reported in chapter 2.

CH_4 oxychlorination (MOC) reaction: 500 mg of catalyst material (125 – 425 μm sieve fraction) was loaded in a quartz reactor and heated to 450 °C under N_2 with a 10 °C/min heating rate. The catalyst was activated in 20% HCl/N_2 for 2 h prior to catalysis. For the isothermal experiments, the reaction temperature was adjusted to reach X_{CH4} = 10% for $CH_4{:}HCl{:}O_2{:}N_2{:}He$ of 2:2:1:1:14. When stable conversion was reached, the HCl:He ratio was adjusted so that the HCl concentration was increased to 20, 40, 60 and 80 vol%, while keeping a constant flow of 20 mL/min. For the ramp experiments, the reactor was brought to 350 °C and the desired feed mixture (i.e., $CH_4{:}HCl{:}O_2{:}N_2{:}He$ of 2:2:1:1:14 or 2:16:1:1:0 in mL/min) was fed into the reactor. A stabilization period of 30 min was applied and then the ramp experiment of 1 °C/min was commenced to 550 °C. For the stability tests, the reactor was brought to 450 °C and $CH_4{:}HCl{:}O_2{:}N_2{:}He$ of 2:2:1:1:14 was fed into the reactor for 4 h. Subsequently, the HCl concentration was increased to 20, 40, 60 and 80 vol%, while keeping a constant flow of 20 mL/min. Every HCl concentration was

fed for 2 h. To characterize the spent catalysts, the catalyst materials were dechlorinated at 550 °C for 5 h under CH_4:HCl:O_2:N_2:He of 2:0:4:1:13. Background of this dechlorination step is provided in section 3.5.5 of this chapter. For the determination of the apparent activation energy, 250mg of catalyst (125 – 425 µm sieve fraction) was loaded in a quartz reactor to 350 °C under N_2 with a 10°C/min heating rate. The catalyst was subjected to CH_4:HCl:O_2:N_2:He of 2:2:1:1:14 (in mL/min) for 1 h. The temperature was increased to 550 °C with increments of 10 °C with a heating rate of 5 °C/min and kept at every temperature step for 45 min to obtain the steady state activity. Only the datapoints where the CH_4 conversion level was below 10% were considered for fitting the apparent activation energy to avoid heat and mass transfer limitations.

HCl oxidation: 500 mg of catalyst material (125 – 425 µm sieve fraction) was loaded in a quartz reactor and heated to 450 °C under N_2 with 10 °C/min. The catalyst was activated in 20% HCl/N_2 for 2 h prior to catalysis. Temperature ramp experiment were performed from 350 °C to 550 °C at a ramp rate of 1 °C/min under the desired feed mixture (i.e., CH_4:HCl:O_2:N_2:He of 0:2:1:1:16 or 0:16:1:1:2 in mL/min).

3.5.4 Elemental Ratio Determination with Vegard's Law

The Origin 2017 multi peak fit tool was used to fit Voigt peaks functions, which in turn were used to determine the (110) x-ray diffraction (XRD) peak positions. This was done for the monometallic catalysts (references) as well as for the bimetallic catalysts and the results are given in Table 3.1. From the peak position, the interplanar distance d (nm) was calculated according to braggs law

$$(Eq.\,3.3)\ \lambda = 2d * \sin(\theta)$$

where λ and θ are the wavelenght of the x-ray source (nm) and the angle of the incident light (°) to the plane respectively. With the use of the interplanar distance and the Miller indices, the lattice parameters were then calculated. For the tetragonal LnOCl crystal system, the lattice parameters a and c (nm) are determined by

$$(Eq.\,3.4)\ \frac{1}{d^2} = \frac{(h^2 + k^2)}{a^2} + \frac{l^2}{c^2}\,.$$

For simplicity, either (hk0) can be used to give a or (00l) can be used to give c. The signal splitting is pronounced for the (110) reflection in the region of 29 – 33° and this reflection was used to calculate the La^{3+}:Eu^{3+} ratio. The contribution of both elements to each peak was determined via Vegard's law since both diffractions are the same crystal structure. According to Vegard's law, the lattice parameters of a solid solution is approximately the mean of the two lattice parameters, expressed by[1–3]

$$(Eq.\,3.5)\ a_{La+Eu} = (1 - x) * a_{La} + x * a_{Eu}$$

where a_{La+Eu} is the average lattice parameter of the alloy, a_{La} the La lattice parameter and a_{Eu} the Eu lattice parameter. The elemental fraction is expressed by x.

3.5.5 Characterization of Spent Catalyst Materials

During the MOC reaction, catalyst chlorination occurs and a bulk phase transition

from LnOCl to LnCl$_3$ can take place (or at least partly). A dechlorination step in 2:4:1:15 CH$_4$:O$_2$:N$_2$:He was performed at 550 °C to induce a phase transition of the material from the chlorinated phase to LnOCl, thereby removing excess Cl$^-$ in the catalyst material and making the sample air-stable. Subsequently, post-characterization of the catalyst materials with N$_2$ physisorption, XRD and TEM is performed. However, the physicochemical properties obtained after the post-characterization of the active catalyst material might not be representative of the active catalyst material in the reaction. Nevertheless, the dechlorination step has practical considerations, and without, no post-characterization could be performed. Lanthanide chlorides are hygroscopic in nature and, when exposed to air, form their corresponding hydrates. Upon rehydration, the structure of the catalyst material can be lost as e.g., LaCl$_3$ dissolves from moisture in the air. TEM measurements cannot be performed under inert conditions. Furthermore, for XRD and N$_2$ physisorption, it implies that the catalyst material has to be transported to an inert atmosphere to guarantee the preservation of the physicochemical properties of the active catalyst material. The reactor set-up does not allow us to close the reaction tube and prevent rehydration. Even though the reactor tube can be transferred to a glovebox, we cannot assure that rehydration did not occur. The potential rehydration raises an issue as sorption samples are typically dried at elevated temperatures under vacuum conditions. During this pretreatment, the thermal dehydration can cause hydrolysis of the lanthanide chloride to the lanthanide oxychloride and release HCl.[4,5] The sorption apparatus used in our laboratory is not corrosion resistant and thus the experiment would perform harm to the equipment. XRD can be performed under inert conditions, but its XRD pattern is difficult to analyze as there are many unidentifiable diffractions. Due to these practical considerations, we chose to perform the dechlorination step, as we believe that still some qualitative trends can be deducted from these results. However, we do acknowledge the fact that the physicochemical properties of the catalyst material could be altered during this dechlorination step.

with Lanthanum

3.6. REFERENCES

(1)   Torres Galvis, H. M.; De Jong, K. P. Catalysts for Production of Lower Olefins from Synthesis Gas: A Review. ACS Catal. 2013, 3, 2130–2149. https://doi.org/10.1021/cs4003436.

(2)   Ravi, M.; Ranocchiari, M.; van Bokhoven, J. A. The Direct Catalytic Oxidation of Methane to Methanol—A Critical Assessment. Angew. Chem. Int. Ed. 2017, 56, 16464–16483. https://doi.org/10.1002/anie.201702550.

(3)   Bai, S.; Liu, F.; Huang, B.; Li, F.; Lin, H.; Wu, T.; Sun, M.; Wu, J.; Shao, Q.; Xu, Y.; Huang, X. High-Efficiency Direct Methane Conversion to Oxygenates on a Cerium Dioxide Nanowires Supported Rhodium Single-Atom Catalyst. Nat. Commun. 2020, 11, 954. https://doi.org/10.1038/s41467-020-14742-x.

(4)   Guo, Z.; Liu, B.; Zhang, Q.; Deng, W.; Wang, Y.; Yang, Y. Recent Advances in Heterogeneous Selective Oxidation Catalysis for Sustainable Chemistry. Chem. Soc. Rev. 2014, 43, 3480–3524. https://doi.org/10.1039/c3cs60282f.

(5)   Taifan, W.; Baltrusaitis, J. CH_4 Conversion to Value Added Products: Potential, Limitations and Extensions of a Single Step Heterogeneous Catalysis. Appl. Catal. B Environ. 2016, 198, 525–547. https://doi.org/10.1016/j.apcatb.2016.05.081.

(6)   Lin, R.; Amrute, A. P.; Pérez-Ramírez, J. Halogen-Mediated Conversion of Hydrocarbons to Commodities. Chem. Rev. 2017, 117, 4182–4247. https://doi.org/10.1021/acs.chemrev.6b00551.

(7)   Treger, Y. A.; Rozanov, V. N.; Sokolova, S. V; Murashova, O. P. Producing Ethylene and Propylene from Natural Gas via the Intermediate Synthesis of Methyl Chloride and Its Subsequent Catalytic Pyrolysis. Catal. Ind. 2012, 4, 231–235. https://doi.org/10.1134/S2070050412040186.

(8)   Zichittella, G.; Paunović, V.; Amrute, A. P.; Pérez-Ramírez, J. Catalytic Oxychlorination versus Oxybromination for Methane Functionalization. ACS Catal. 2017, 7, 1805–1817. https://doi.org/10.1021/acscatal.6b03600.

(9)   van der Heijden, A. W. A. M.; Garcia Ramos, M.; Weckhuysen, B. M. Intermediates in the Destruction of Chlorinated C1 Hydrocarbons on La-Based Materials: Mechanistic Implications. Chem. Eur. J. 2007, 13, 9561–9571. https://doi.org/10.1002/chem.200700901.

(10)   Van Der Heijden, A. W. A. M.; Bellière, V.; Alonso, L. E.; Daturi, M.; Manoilova, O. V.; Weckhuysen, B. M. Destructive Adsorption of CCl_4 over Lanthanum-Based Solids: Linking Activity to Acid-Base Properties. J. Phys. Chem. B 2005, 109, 23993–24001. https://doi.org/10.1021/jp054689b.

(11)   EuroChlor. The Chlorine Tree; Brussels, 2016.

(12)   Scharfe, M.; Zichittella, G.; Paunović, V.; Pérez-Ramírez, J. Ceria in Halogen Chemistry. Chin. J. Catal. 2020, 41, 915–927. https://doi.org/10.1016/S1872-2067(19)63528-X.

(13)   Lunsford, J. H. Catalytic Conversion of Methane to More Useful Chemicals and Fuels: A Challenge for the 21st Century. Catal. Today 2000, 63, 165–174. https://doi.org/10.1016/S0920-5861(00)00456-9.

(14)   Paunović, V.; Zichittella, G.; Hemberger, P.; Bodi, A.; Pérez-Ramírez, J. Selective Methane Functionalization via Oxyhalogenation over Supported Noble Metal Nanoparticles. ACS Catal. 2019, 9, 1710–1725. https://doi.org/10.1021/acscatal.8b04375.

(15)   Kwon, S.; Chae, H. J.; Na, K. Control of Methane Chlorination with Molecular Chlorine Gas Using Zeolite Catalysts: Effects of Si/Al Ratio and Framework Type. Catal. Today 2020, 352, 111–117. https://doi.org/10.1016/j.cattod.2020.01.014.

(16)   Wegener, G.; Brandt, M.; Duda, L.; Hofmann, J.; Klesczewski, B.; Koch, D.; Kumpf, R.-J.; Orzesek, H.; Pirkl, H.-G.; Six, C.; Steinlein, C.; Weisbeck, M. Trends in Industrial Catalysis in the Polyurethane Industry. Appl. Catal. A Gen. 2001, 221, 303–335. https://doi.org/10.1016/S0926-860X(01)00910-3.

(17)   Peringer, E.; Salzinger, M.; Hutt, M.; Lemonidou, A. A.; Lercher, J. A. Modified Lanthanum Catalysts for Oxidative Chlorination of Methane. Top. Catal. 2009, 52, 1220–1231. https://doi.org/10.1007/s11244-009-9265-6.

(18)   Aglulin, A. G. Mechanism of the Formation of Carbon Oxides under Conditions of the Oxidative Chlorination of Methane: IV. Kinetics of the Reaction of CCl_4 with Oxygen on Copper-Containing Salt Catalysts for Methane Oxychlorination at Reduced Partial Pressures. Kinet. Catal. 2009, 50, 427–434. https://doi.org/10.1134/S0023158409030148.

(19)   Sanchez-Sanchez, M.; Lercher, J. A. Oxidative Functionalization of Methane on Heterogeneous Catalysts. In Alkane Functionalization; John Wiley & Sons, Ltd: Chichester, UK, 2018; pp 141–157. https://doi.org/10.1002/9781119379256.ch8.

(20)   Wang, B.; Albarracín-Suazo, S.; Pagán-Torres, Y.; Nikolla, E. Advances in Methane Conversion Processes. Catal. Today 2017, 285, 147–158. https://doi.org/10.1016/J.CATTOD.2017.01.023.

(21)   Alvarez-Galvan, M. C.; Mota, N.; Ojeda, M.; Rojas, S.; Navarro, R. M.; Fierro, J. L. G. Direct Methane Conversion Routes to Chemicals and Fuels. Catal. Today 2011, 171, 15–23. https://doi.org/10.1016/j.cattod.2011.02.028.

(22)   Paunović, V.; Zichittella, G.; Verel, R.; Amrute, A. P.; Pérez-Ramírez, J. Selective Production of Carbon Monoxide via Methane Oxychlorination over Vanadyl Pyrophosphate. Angew. Chem. Int. Ed. 2016, 55, 15619–

15623. https://doi.org/10.1002/anie.201608165.

(23)   Ohtsuka, Y.; Tamai, Y. Oxychlorination of Methane in the Presence of Molten Metallic Chlorides. J. Catal. 1978, 51, 169–172. https://doi.org/10.1016/0021-9517(78)90290-7.

(24)   Huang, J.; Wang, W.; Li, D.; Xu, S.; Liu, Q.; Chen, X.; Fei, Z.; Zhang, Z.; Cui, M.; Tang, J.; Qiao, X. Facile Construction of Non-Crystalline ZrO_2 as an Active yet Durable Catalyst for Methane Oxychlorination. J. Sol-Gel Sci. Technol. 2019, 92, 163–172. https://doi.org/10.1007/s10971-019-05089-x.

(25)   Peringer, E.; Tejuja, C.; Salzinger, M.; Lemonidou, A. A.; Lercher, J. A. On the Synthesis of $LaCl_3$ Catalysts for Oxidative Chlorination of Methane. Appl. Catal. A Gen. 2008, 350, 178–185. https://doi.org/10.1016/j.apcata.2008.08.009.

(26)   Podkolzin, S. G.; Stangland, E. E.; Jones, M. E.; Peringer, E.; Lercher, J. A. Methyl Chloride Production from Methane over Lanthanum-Based Catalysts. J. Am. Chem. Soc. 2007, 129, 2569–2576. https://doi.org/10.1021/ja066913w.

(27)   Peringer, E.; Podkolzin, S. G.; Jones, M. E.; Olindo, R.; Lercher, J. A. $LaCl_3$-Based Catalysts for Oxidative Chlorination of CH_4. Top. Catal. 2006, 38, 211–220. https://doi.org/10.1007/s11244-006-0085-7.

(28)   He, J.; Xu, T.; Wang, Z.; Zhang, Q.; Deng, W.; Wang, Y. Transformation of Methane to Propylene: A Two-Step Reaction Route Catalyzed by Modified CeO_2 Nanocrystals and Zeolites. Angew. Chem. Int. Ed. 2012, 51, 2438–2442. https://doi.org/10.1002/anie.201104071.

(29)   Zichittella, G.; Aellen, N.; Paunović, V.; Amrute, A. P.; Pérez-Ramírez, J. Olefins from Natural Gas by Oxychlorination. Angew. Chem. Int. Ed. 2017, 56, 13670–13674. https://doi.org/10.1002/anie.201706624.

(30)   Rozanov, V. N.; Treger, Y. A.; Silina, I. S. Stability of Catalysts for the Oxidative Chlorination of Methane. Catal. Ind. 2016, 8, 336–340. https://doi.org/10.1134/S2070050416040085.

(31)   García, C. L.; Resasco, D. E. High-Temperature Oxychlorination Catalysts: Role of $LaCl_3$ as an Inhibitor of the Segregation of Active Species during Heating/Cooling Cycles. J. Catal. 1990, 122, 151–165. https://doi.org/10.1016/0021-9517(90)90267-N.

(32)   Kim, J.; Ryou, Y.; Hwang, G.; Bang, J.; Jung, J.; Bang, Y.; Kim, D. H. Oxychlorination of Methane over FeO_x/CeO_2 Catalysts. Korean J. Chem. Eng. 2018, 35, 2185–2190. https://doi.org/10.1007/s11814-018-0135-4.

(33)   Terlingen, B.; Oord, R.; Ahr, M.; Hutter, E.; van Lare, C.; Weckhuysen, B. M. Mechanistic Insights into the Lanthanide-Catalyzed Oxychlorination of Methane as Revealed by Operando Spectroscopy. ACS Catal. 2021, 11, 10574–10588. https://doi.org/10.1021/acscatal.1c00393.

(34)   Shannon, R. D. Revised Effective Ionic Radii and Systematic Studies of Interatomic Distances in Halides and Chalcogenides. Acta Crystallogr. Sect. A 1976, 32, 751–767. https://doi.org/10.1107/S0567739476001551.

(35)   Zhu, X.; Yu, Y.; Yuan, J.; Zhang, X.; Yu, H.; Zhang, W.; Du, A.; Zhou, B. Synthesis, Characterization and Mechanism of Formation of Carbon Aerogels Incorporated with Highly Crystalline Lanthanum Oxychloride Particles. RSC Adv. 2017, 7, 39635–39640. https://doi.org/10.1039/c7ra05454h.

(36)   Aitasalo, T.; Hölsä, J.; Lastusaari, M.; Legendziewicz, J.; Lehto, L.; Lindén, J.; Maryško, M. Structural, Magnetic and Spectroscopic Investigations of Europium Oxychloride, EuOCl. J. Alloys Compd. 2004, 380, 296–302. https://doi.org/10.1016/j.jallcom.2004.03.057.

(37)   Podkolzin, S. G.; Manoilova, O. V.; Weckhuysen, B. M. Relative Activity of La_2O_3, LaOCl, and $LaCl_3$ in Reaction with CCl_4 Studied with Infrared Spectroscopy and Density Functional Theory Calculations. J. Phys. Chem. B 2005, 109, 11634–11642. https://doi.org/10.1021/jp050680y.

(38)   Weckhuysen, B. M.; Rosynek, M. P.; Lunsford, J. H. Destructive Adsorption of Carbon Tetrachloride on Lanthanum and Cerium Oxides. Phys. Chem. Chem. Phys. 1999, 1, 3157–3162. https://doi.org/10.1039/a901847f.

(39)   Van der Avert, P.; Weckhuysen, B. M. Low-Temperature Catalytic Destruction of CCl_4, $CHCl_3$ and CH_2Cl_2 over Basic Oxides. Phys. Chem. Chem. Phys. 2004, 6, 5256–5262. https://doi.org/10.1039/b413876g.

(40)   Van der Avert, P.; Podkolzin, S. G.; Manoilova, O.; de Winne, H.; Weckhuysen, B. M. Low-Temperature Destruction of Carbon Tetrachloride over Lanthanide Oxide-Based Catalysts: From Destructive Adsorption to a Catalytic Reaction Cycle. Chem. Eur. J. 2004, 10, 1637–1646. https://doi.org/10.1002/chem.200305442.

(41)   Van der Avert, P.; Weckhuysen, B. M. Low-Temperature Destruction of Chlorinated Hydrocarbons over Lanthanide Oxide Based Catalysts. Angew. Chem. Int. Ed. 2002, 41, 4730–4732. https://doi.org/10.1002/anie.200290030.

(42)   King, H. W. Quantitative Size-Factors for Metallic Solid Solutions. J. Mater. Sci. 1966, 1, 79–90. https://doi.org/10.1007/BF00549722.

(43)   Vegard, L. Die Konstitution Der Mischkristalle Und Die Raumfullung Der Atome. Z. fur Phys. 1921, 5, 17–26. https://doi.org/10.1007/BF01349680.

(44)   Zhong, X.; Feng, Y.; Knoll, W.; Han, M. Alloyed $Zn_xCd_{1-x}S$ Nanocrystals with Highly Narrow Luminescence Spectral Width. J. Am. Chem. Soc. 2003, 125, 13559–13563. https://doi.org/10.1021/ja036683a.

(45)   Lyle, S. J.; Westall, W. A. A Study of the Thermal Decomposition of Hydrated Europium(III) Chloride and Euprium(III) Bromide. Thermochim. Acta 1983, 68, 51–58. https://doi.org/10.1016/0040-6031(83)80379-7.

(46)   Roy, R. J.; Kipouros, G. J. Estimation of Vapour Pressures of Neodymium Trichloride Hydrates. Thermochim. Acta 1991, 178, 169–183. https://doi.

with Lanthanum

3

4
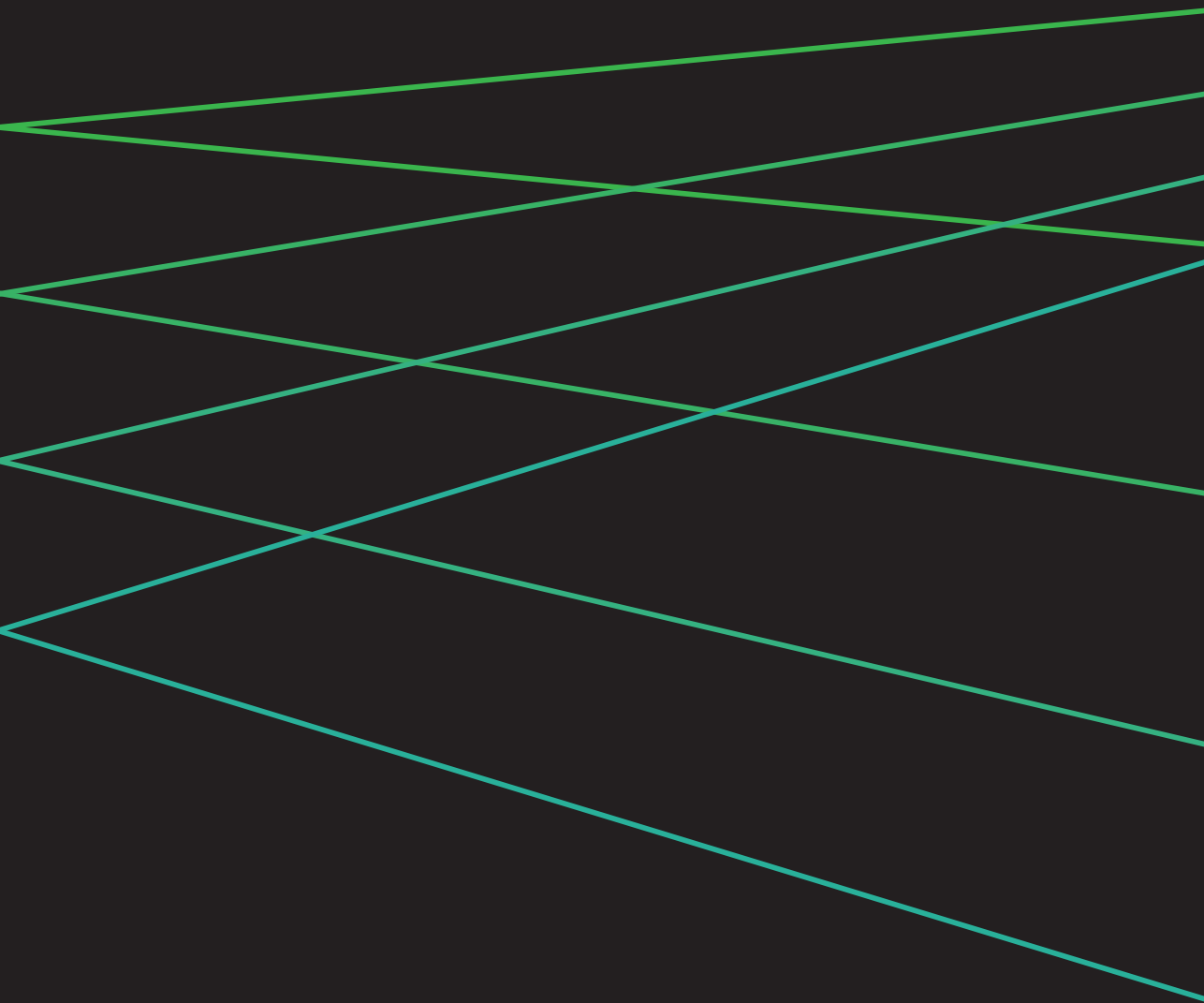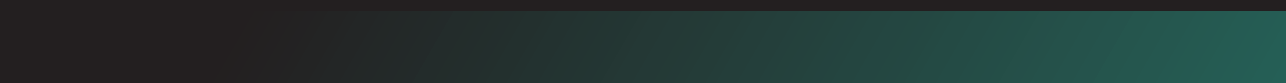
Bifunctional Europium for *Operando* Catalyst Thermometry in an Exothermic Chemical Reaction

Abstract

Often the reactor temperature or the temperature of the reaction medium is reported in the field of heterogeneous catalysis, even though it could vary significantly from the temperature of the reactive catalyst surface under reaction conditions. The influence of the catalyst temperature on the observed catalytic performance and vice versa is therefore not accurately known. In this chapter, we apply EuOCl as both solid catalyst and thermometric material, allowing for operando temperature determination of the catalyst particle in a direct manner. The interplay between reaction conditions and the catalyst temperature dynamics in the exothermic CH_4 oxychlorination reaction is studied. Under isothermal oven temperature conditions, significant catalyst heating was observed due to the exothermicity of the reaction, with a maximum temperature difference between the reactor and the catalyst of 16 °C. Heat dissipation by means of radiation appears dominating compared to convection in this set-up, explaining the observed uniform catalyst bed temperature. Application of operando catalyst thermometry could provide a deeper mechanistic understanding of catalyst performances and allow for safer process operation in chemical industries.

4

4.1. INTRODUCTION

Temperature is arguably the most important parameter in catalysis as it dominates the reaction kinetics, thermodynamics and stability of the catalyst.[1,2] These phenomena determine the overall feasibility of a chemical process. Almost all publications in the field consider only the temperature of the reactor or reaction medium, thereby assuming that the catalyst bodies have the same temperature. The influence of the reaction thermodynamics and kinetics is not considered in most cases, undermining the dynamic temperature changes of the catalyst bodies under reaction conditions. It is somewhat surprising that, after more than a century of heterogeneous catalysis research, very limited information is available on the local temperature of the catalyst bodies under working conditions.[3–8]

In the handful of articles published on operando catalyst thermometry, large discrepancies between the set reactor temperature and the catalyst temperature were reported.[6,7] Previous research evidenced that local temperature was highly influenced by the reaction mixture fed in the reactor, inducing heat generation (+80 °C from set point)[6] or heat removal (-65 °C from set point)[7]. These results stress the importance of monitoring the local temperature as precise control is crucial for stable, safe, and efficient catalytic conversion processes.[9–12] Operando determination of the catalyst temperature is especially interesting in exothermic reactions. As a case study, we chose the CH_4 oxychlorination (MOC) reaction, which has to potential to see commercialization, but operating this potentially hazardous reaction is not trivial.[13–20] The reaction $CH_4 + HCl + \frac{1}{2}O_2 \rightarrow CH_3Cl + H_2O$ is highly exothermic, with a reaction enthalpy of $\Delta H^0_{773K} = -157.6$ kJ mol^{-1}, operated at > 400 °C, the reaction feed/products mixtures are corrosive, potentially explosive, and toxic.[21,22] Process safety is thus a top priority for this chemical reaction.

EuOCl is a unique MOC catalyst because it is not only catalytically active, but also shows temperature-sensitive luminescence. This bifunctionality enables local temperature measurements at the active catalytic site. The application of operando catalyst thermometry in the MOC reaction enables real-time control over the catalyst performance and process safety. A hazardous thermal runaway can be identified in an early stage, without the temperature detection delay from which traditional temperature measurement techniques suffer.[23–25]

In this chapter, EuOCl is applied as catalytic material as well as operando thermometer for the MOC reaction. The interplay between catalyst heating and cooling is investigated by varying the reaction conditions. Firstly, the thermometric properties of EuOCl are determined as well as experimental limits and specifics. Subsequently, operando thermometry is performed under MOC reaction conditions where either the reaction temperature or the feed composition is varied. The reaction rate correlates positively with the increase in catalyst temperature, both for varying temperature as well as feed composition, and a maximum temperature increase of 16 °C was detected. Heat transfer calculations evidenced that heat dissipation by means of radiation is dominant compared to convection,

4

supported by the observed uniform catalyst bed temperature. Operando catalyst thermometry enabled the coupling of the catalyst temperature to the catalytic performance in the MOC reaction and study its dynamic behavior.

4.2. RESULTS AND DISCUSSION

4.2.1 Characterization of Europium Oxychloride as Thermometer

The bifunctional EuOCl catalyst was synthesized in the desired EuOCl crystal phase (Figure 4.1A).[20,22,26] The excitation of EuOCl with 375 nm light yielded sharp emissions (Figure 4.1B), which could all be assigned according to the energy diagram of Eu^{3+} (Figure 4.1C).[27,28] The EuOCl catalyst material showed temperature-dependent emission in the temperature range from 400 to 550 °C (Figure 4.1D). We observe variations in the relative emission intensity from the thermally coupled $^5D_0$ and $^5D_1$ states, specifically the $^5D_1 \rightarrow$ $^7F_{1-2}$ and $^5D_0 \rightarrow$ $^7F_2$ emissions, denoted I_2 and I_1, respectively (Figure 4.1E). The temperature-dependent emission was calibrated in inert conditions (20 mL/min N_2, 1 °C/min) and could be described according to the Boltzmann model. This yielded an energy difference between the two thermally coupled states of 1804 cm^{-1} corresponding to the expected value of 1760 cm^{-1}.[27]

Furthermore, the catalyst temperature as determined by the Boltzmann model (T_{cat}) was not influenced by the gas flow (Figure 4.2A). We therefore assume that the temperature of the feed gas is equal to T_{oven}. Bulk chlorination of EuOCl to $EuCl_3$ can occur under reaction conditions when the chlorination reaction occurs at a faster rate than the dechlorination reaction.[21,22] This must be avoided, because the luminescence of $EuCl_3$ differs from EuOCl, causing errors in temperature readout.[29] Since the luminescence of $EuCl_3$ is relatively weak, we can use the emission intensity as an indication for the undesired formation of $EuCl_3$. Indeed, we observed a loss of luminescence signal at temperatures below 500 °C under chlorinating conditions, which is likely caused by formation of $EuCl_3$ (Figures 4.2B-4.2D). To prevent bulk chlorination and ensure accurate temperature measurements, we will carry out the experiments at temperatures at or above 500 °C.

The performed operando thermometry measurements provide an average temperature of numerous particles. The spot size of the laser is in the millimeter range, measuring the temperature of numerous catalyst bodies (125 - 425 mm sieve fraction) that are agglomerates of individual EuOCl catalyst particles (< 500 nm). Hence, an average temperature of numerous catalyst particles is obtained. At the surface of an individual catalyst particle, the methane oxychlorination reaction proceeds and heat is generated due to the exothermicity of the possible reactions (section 4.5.6 of this chapter). Under reaction conditions, Eu^{3+} is excited with a 375 nm laser, penetrating the surface of the individual catalyst particle. This generates luminescence both at the surface and in the interior part of the catalyst, enabling temperature measurements of the entire catalyst particle. UV-light typically has a penetration depth of < 100 mm in strongly scattering media such as a bed of micrometre-sized particles.Hence, penetration of the laser through the catalyst bed is not expected. We confirmed this by performing absorbance and transmittance
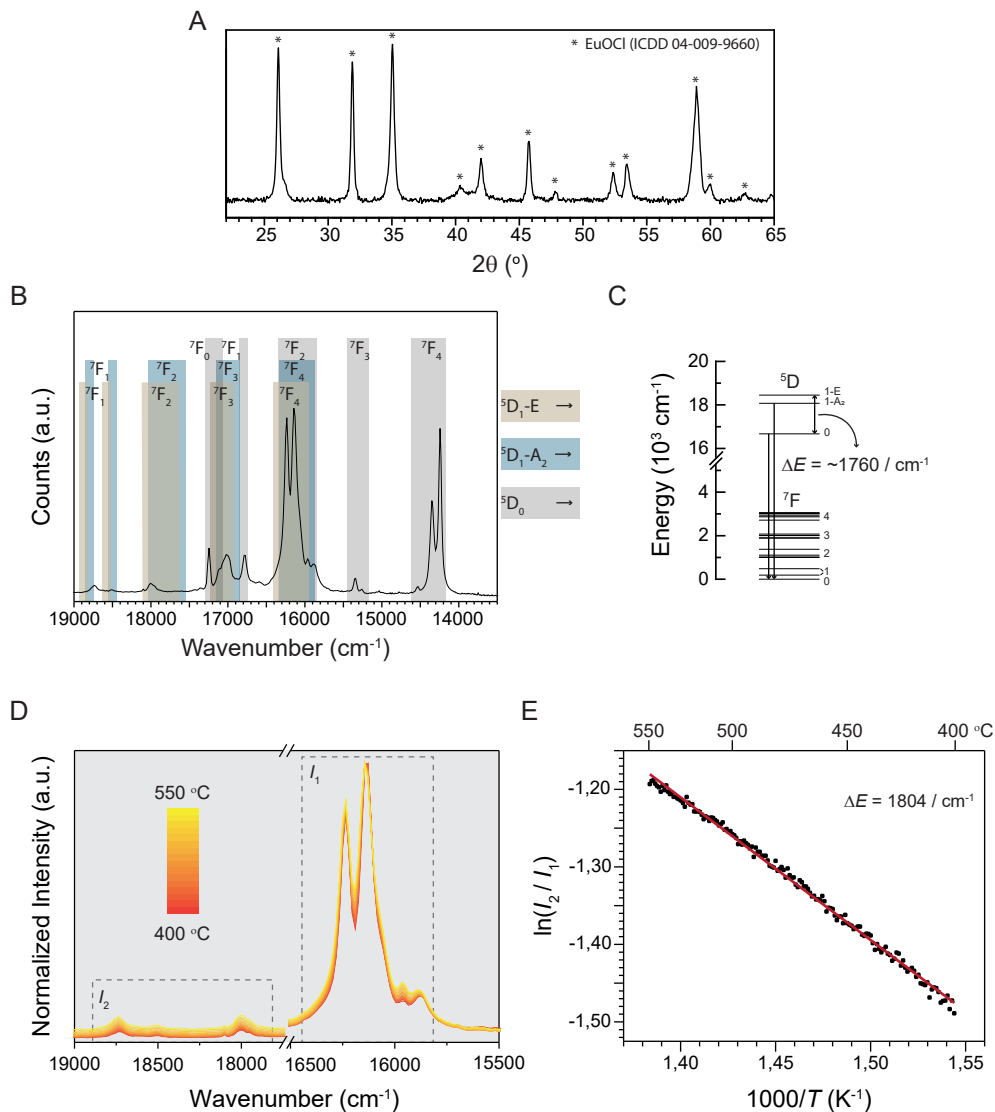
Figure 4.1. (A) X-ray Diffractogram (XRD) performed on the as-synthesized EuOCl. All XRD patterns could be assigned to the reference EuOCl (ICDD 04-009-9660). (B) Emission spectrum of EuOCl where the Eu^{3+} emissions are labelled according to (C) Energy diagram of Eu^{3+} where the energy gap (ΔE) between the $^5D_1$ and $^5D_0$ states is indicated. (D) Emission spectra of EuOCl upon excitation at 375 nm from 400 °C (red) to 550 °C (yellow) with increments of 10 °C, where the $^5D_1$ and $^5D_0$ emissions are indicated by I_2 and I_1 respectively. (E) The ratio of integrated emission intensities of the $^5D_1$ and $^5D_0$ states (see section 4.5.4 and 4.5.5 of this chapter for details on data analysis) as a function of the inverse temperature. The straight line is a fit to the Boltzmann model, yielding a $^5D_1$ - $^5D_0$ ΔE of 1804 cm^{-1}.

measurements (results not shown for brevity). The absorption at 375nm was relatively high and less than 1% of the incident beam could pass through the EuOCl-filled quartz reactor.
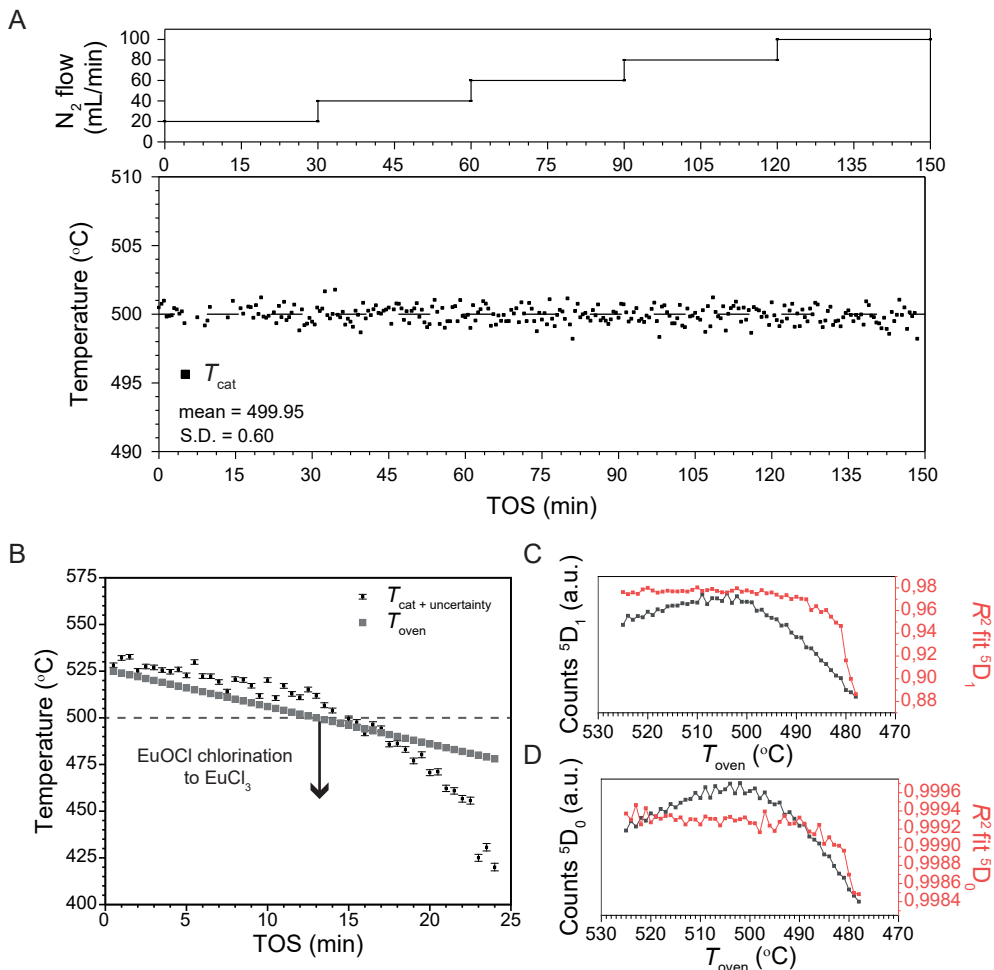
Figure 4.2. (A) The catalyst temperature as determined by the Boltzmann model (T_{cat}) is plotted versus time-on-stream (TOS) at an oven temperature (T_{oven}) of 500 °C. No cooling of the catalyst with increasing gas flow (20 - 100 mL/min N_2) was observed, indicating that the inlet gas was already heated to the T_{oven} before contacting the catalyst. (B) T_{cat} and T_{oven} plotted versus the TOS. The T_{oven} was gradually decreased by 1 °C/min from 525 °C under 50 % HCl/He (20 mL/min total flow). From 0 - 12 min TOS, the T_{cat} followed the T_{oven} closely. After 12 min TOS, the T_{cat} dropped below the T_{oven}. The fitted (C) $^5D_1$ and (D) $^5D_0$ revealed that at 500 °C, a maximum in the counts was obtained, after which it rapidly decreased at lower temperatures. Chlorination of the catalyst at a temperature below 500 °C quenched the luminescence signal, reducing the counts. The decrease in counts was also reflected in the R_2 of the fits, which decrease rapidly, especially at temperatures lower than 490 °C.

4.2.2 Operando Thermometry Under Varying Oven Temperature

The catalyst temperature was significantly increased due to the heat generation under MOC reaction conditions (Figure 4.3). A temperature ramp-up and ramp-down between 500 °C and 550 °C revealed a significant discrepancy between the T_{oven} and T_{cat}, further denoted as ΔT, where catalyst heating was observed over the entire temperature range
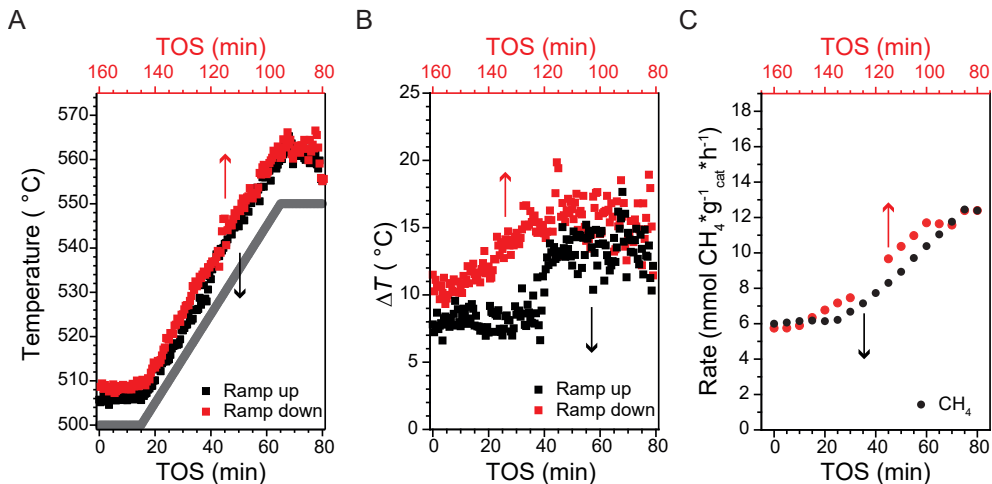
Figure 4.3. (A) Temperature ramp-up and ramp-down between 500 °C and 550 °C where the catalyst temperature as determined by the Boltzmann model (T_{cat}) and oven temperature (T_{oven}) are plotted versus time-on-stream (TOS). (B) ΔT defined as the difference between T_{cat} and T_{oven} plotted versus TOS. (C) Simultaneous to the temperature measurements, the activity was measured and the CH_4 conversion rate is given. In all cases, the black data points correspond to the bottom x-axis and the red data points correspond to the upper x-axis. Reaction conditions: CH_4:HCl:O_2:N_2:He of 8:8:4:4:0 (in mL/min), T_{oven} = 500 – 550 °C with a ramp rate of 1 °C/min, W_{cat} = 500 mg.

(Figure 4.3A). At T_{oven} = 500 °C (0 - 15 min), a ΔT of 8 °C was observed, which increased to 13 °C at T_{oven} = 550 °C (65 min, Figure 4.3B). When the temperature was kept at 550 °C, the ΔT increased further to ~ 16°C. Once T_{oven} was ramped down from 550 – 500 °C (95 – 145 min), the ΔT gradually decreased from 16 to 10 °C. The ΔT showed a positive correlation with the observed activity in the reaction (Figure 4.3C). Interestingly, an asymmetry in the ΔT between the ramp up and ramp down was observed. The ΔT was higher at the same T_{oven} during the ramp down compared to the ramp up, coinciding with the higher observed activity at the same T_{oven} (Figure 4.3C). As a constant gas hourly space velocity (GHSV) was used, the change in ΔT can be ascribed to the positive feedback between reaction rate and local temperature.

4.2.3 Operando Thermometry under Varying Feed Compositions

To shed light on the interplay between catalyst cooling and heat generation, three different variations in the feed composition were investigated. The response on the activity and local temperature was analyzed. Increasing the GHSV, while keeping the feed composition unaltered resulted in an increase in the ΔT (Figure 4.4A). The increase in ΔT can be explained by the increase in reaction rate of both O_2 and CH_4. The higher flow of reactive gas generated more reaction heat than was removed by the higher gas flow rate. The opposite effect was observed when the feed was diluted with inert He (Figure 4.4B). The increasing GHSV lowered the ΔT, while also decreasing the reaction rate of O_2 and CH_4. Note that at low reaction rates, the ΔT was roughly 0 °C. Finally, the GHSV was kept constant while the activity was increased (Figure 4.4C). This was achieved by varying the HCl:He ratio while keeping a constant total flow.[22] Again, the reaction rate of CH_4 and O_2

A Constant feed composition, varying GHSV

ΔT (°C)

GHSV (h^{-1})

Rate (mmol*g^{-1}_{cat}*h^{-1})

O$_2$
CH$_4$

B Constant CH$_4$:HCl:O$_2$, varying He diluent

ΔT (°C)

GHSV (h^{-1})

Rate (mmol*g^{-1}_{cat}*h^{-1})

O$_2$
CH$_4$

C Constant GHSV, varying He:HCl ratio

ΔT (°C)

GHSV (h^{-1})

Rate (mmol*g^{-1}_{cat}*h^{-1})

O$_2$
CH$_4$
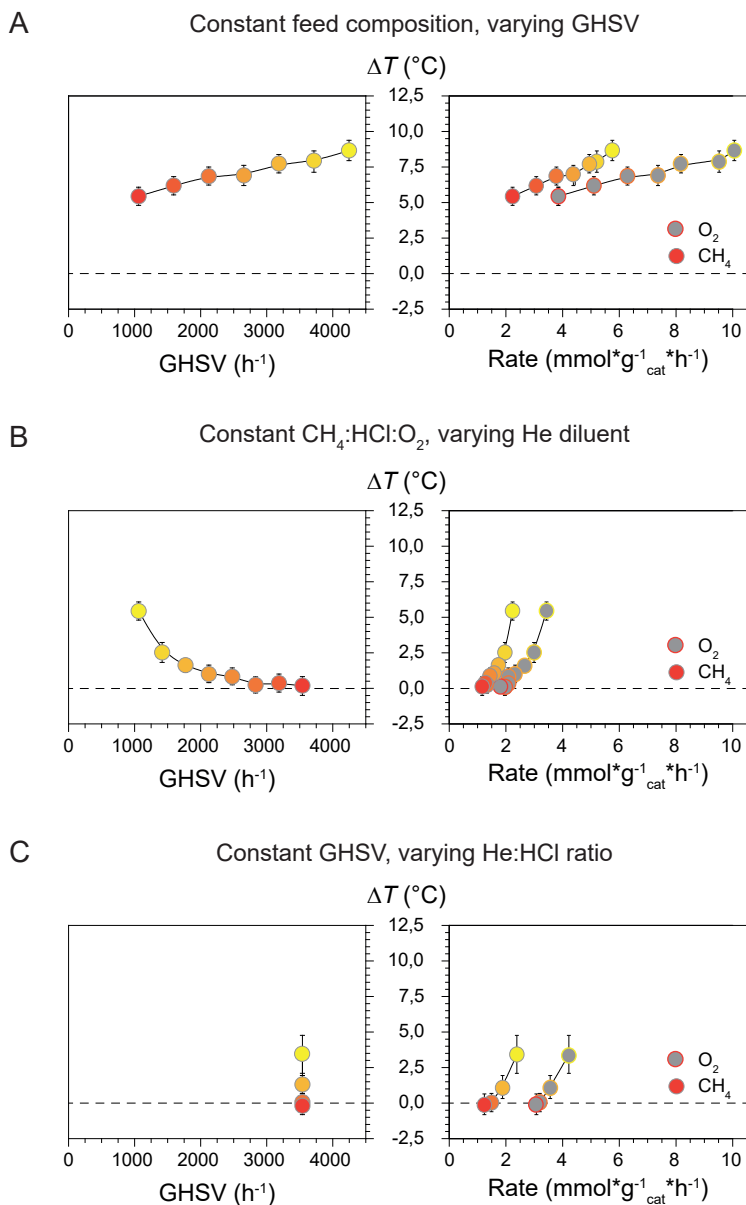
Figure 4.4. Temperature difference between the T_{oven} and T_{cat}, defined as ΔT, plotted versus the variable parameter gas hourly space velocity (GHSV, left window) and the resulting reaction rate for CH$_4$ and O$_2$ (right window). (A) The total flow was increased without altering the gas feed composition (CH$_4$:HCl:O$_2$:N$_2$:He 2:2:1:1:0). Feed composition was unaltered but the flow was increased. (B) The reaction mixture was diluted with inert He (CH$_4$:HCl:O$_2$:N$_2$:He 2:2:1:1:x (in mL/min) where x = 0 – 14 with increments of 2). (C) The HCl:He ratio in the feed was altered while maintaining the same total flow (CH$_4$:HCl:O$_2$:N$_2$:He 2:16-x:1:1:x (in mL/min) where x = 0 (yellow), 4 (orange), 8 (dark orange), 14 (red)). Reaction conditions: T_{oven} = 500 °C, W_{cat} = 500 mg, V_{cat} = 0.34 cm^3.

A

$CH_4:HCl:O_2:N_2:He$
2:2:1:1:0

GHSV 1061 h^{-1} GHSV 4247 h^{-1}

Rate
(mmol $CH_4 * g_{cat}^{-1} * h^{-1}$)

- Top
- Bottom

ΔT (°C)

- Top
- Bottom

TOS (min)

B

Feed

Top

Bottom

Products

C

X_{CH_4} (%)

- 250 mg
- 500 mg

Temperature (°C)

4
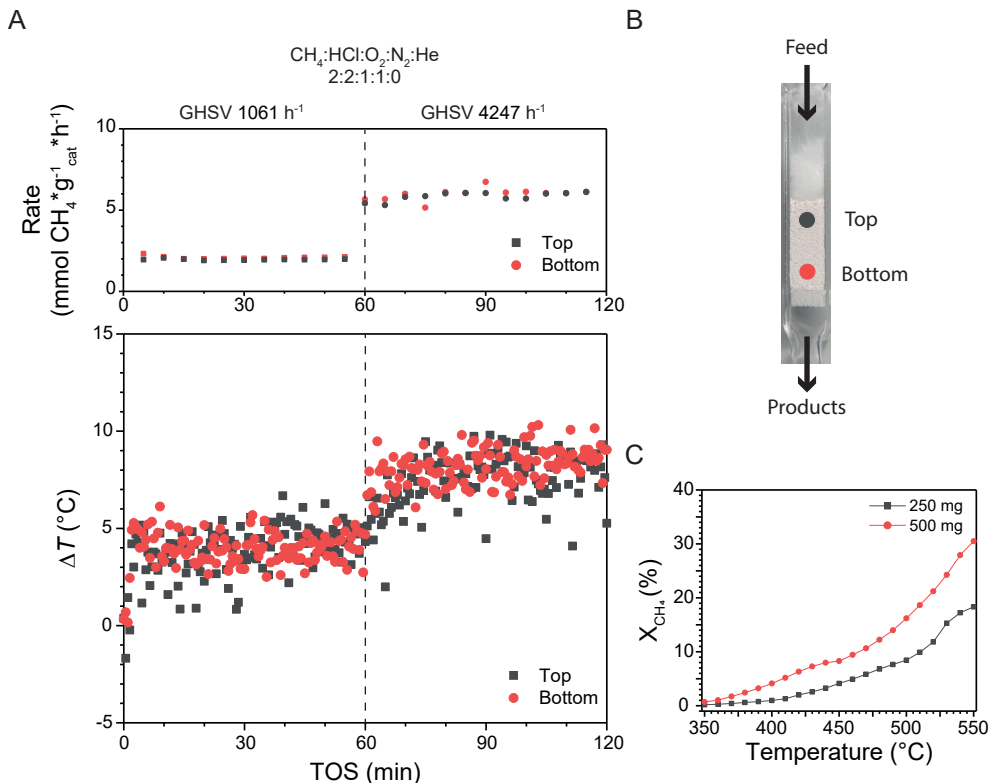
Figure 4.5. (A) The reaction rate and the temperature difference between the T_{oven} and T_{cat}, defined as ΔT, plotted versus the time-on-stream (TOS). Catalyst temperature was determined at different bed heights, separated 9 mm apart. After a stabilization period of 30 min under N_2, the reaction mixture was introduced. (B) The temperature of the top part and bottom part were measured sequentially. Reaction conditions: $CH_4:HCl:O_2:N_2:He$ of 2:2:1:1:0 (total flow 6 or 24 mL/min), T_{oven} = 500 °C, W_{cat} = 500 mg, V_{cat} = 0.34 cm³. (C) CH_4 conversion (X_{CH_4}) plotted versus the temperature for EuOCl tested with different weight loadings of catalyst. The activity of the 500 mg is roughly double that of the 250mg weight loading. Reaction conditions: T_{oven} = 350 - 550 °C with steps of 10 °C, stabilized for 45 min, $CH_4:HCl:O_2:N_2:He$ 2:2:1:1:14 (in mL/min).

were positively correlated to the ΔT. Here, the change in ΔT is purely a kinetic effect as the cooling rate by convection can be regarded constant.

4.2.4 Thermal Radiation as Dominant Heat Dissipation Mechanism

Both under varying oven temperatures (Figure 4.3) as well as under varying reaction gas feed compositions (Figure 4.4), the reaction rate was positively correlated to the ΔT. Furthermore, an increase in the GHSV did not always result in enhanced heat removal, as the reaction rate was not correlated to the GHSV. Heat transfer calculations (section 4.5.6 of this chapter) evidenced that heat loss due to convection is negligible compared to radiation. Any heat generated by the reaction will quickly be dissipated by radiation until an equilibrium temperature is reached. Hence, a uniform catalyst temperature over the length of the bed is expected. Our qualitative approach was able to explain the observed trends, but we were unable to describe the change in temperature quantitatively. To ver-

ify the uniformity of the catalyst bed temperature, the T_{cat} was determined at the top and bottom of the catalyst bed (Figure 4.5A) under MOC conditions where the GSHV was varied. As the experimental set-up did not allow for simultaneous temperature determination of the catalyst at the top and bottom of the bed (Figure 4.5B), the temperatures were determined in a sequential manner. First the top of the catalyst was probed and subsequently the bed height with respect to the probe was altered to enable the temperature determination of the bottom part. A constant reaction rate confirmed that the catalyst activity was the same in subsequent experiments. Furthermore, the bottom part of the catalyst bed was roughly as active as the top part, since a decrease in the catalyst loading by half resulted in a reduction of the X_{CH4} by the same amount (Figure 4.5C). Overall, we observed no significant difference in temperature between the top and the bottom of the reactor, consistent with radiation as the dominant heat dissipation mechanism.

4.3. CONCLUSIONS

In this chapter, the bifunctionality of EuOCl, i.e., the catalytic activity in the MOC reaction and its temperature-dependent luminescence, enabled the rapid, stable, and direct temperature determination of catalyst particles under reaction conditions. The apparent heat balance between heat generation and heat loss was investigated by varying the feed composition and the reaction temperature. Under various conditions we have observed a higher catalyst temperature compared to the oven set temperature. This temperature difference ΔT correlated strongly to the reaction rate. The maximum ΔT observed was 16 °C. Heat-balance calculations were able to describe the observed trends qualitatively and identified radiation as the dominant heat dissipation mechanism. This was consistent with the measured uniform catalyst bed temperature. To be able to describe the temperature increase quantitatively, a more detailed model must be constructed and more carefully controlled experiments must be conducted, which will form the basis of a follow-up study. We anticipate that the concept of operando thermometry in chemical reactions can be transferred to other fields where lanthanide-based catalysts are used. These fields include reactions where a lanthanide acts as catalytic center, e.g., reactions involving halogens[30–35], or promotor, e.g., reforming reactions[36,37] and methanol synthesis[38] in which La^{3+} would be (partially) substituted by Eu^{3+}. Lastly, the application of thermometric support materials[39–42] opens up the possibility to perform operando thermometry in reactions where lanthanides typically do not play a role.

4.4. ACKNOWLEDGEMENTS

4.5. EXPERIMENTAL METHODS

4.5.1 Catalyst Synthesis

EuOCl powders were synthesized by dissolving europium (III) chloride hydrate (EuCl$_3$ · xH$_2$O, Alfa Aesar, > 99.9%) in ethanol (absolute, VWR). Subsequently, stoichiometric

amounts of ammonium hydroxide (Fisher Scientific, 25% in H_2O) were added in drop-wise fashion at room temperature. The precipitates were stirred for 1 h, centrifuged and washed with ethanol (absolute, VWR) three times, dried at 80 °C in air and calcined at 500 °C for 3 h (5 °C/min ramp rate).[22]

4.5.2 Catalyst Characterization

X-ray diffraction (XRD) patterns were obtained with a Bruker-AXS D8 powder x-ray dif-fractometer in Bragg–Brentano geometry, using Cu $K_{\alpha 1,2}$ = 1.54184 Å, operated at 40 kV. The measurements were carried out between 22 and 65 ° using a step size of 0.02 ° and a scan speed of 1 s, with a 2 mm slit for the source. Operando luminescence spectroscopy was performed with an Cobolt-06-01 laser (λ = 375 nm, max laser output 75 mW) ex-citation source, coupled to an Avantes FCR-7UVIR400-2.5-bx-6x350-HTX reflection probe, capable of withstanding temperatures up to 550 °C. Detection was performed with an AvaSpec-ULS2048CL-EVO with a 10 mm grating. Spectra were collected with the AvaSoft 8 software. For the data processing procedure, see sections 4.5.4 and 4.5.5 of this chapter.

4.5.3 Catalyst Testing

All the catalytic tests and operando spectroscopy characterization experiments were per-formed in a lab scale continuous-flow fixed-bed reactor quartz reactor. Details on the experimental set-up as well as definitions and calculations are reported in chapter 2. In a typical MOC experiment, 500 mg of the catalyst material (125 – 425 μm sieve fraction) was loaded in a quartz reactor and heated to 500 °C with a ramp rate of 10 °C/min in 20 ml/min N_2. Subsequently, the feed was changed to the desired CH_4:HCl:O_2:N_2:He ratio specified in the caption of every figure.

4.5.4 Thermometric Performance and Temperature Determination

The Boltzmann equation

$$(Eq.\,4.1)\frac{I_{5D1}}{I_{5D0}} = A * e^{\frac{-\Delta E}{k_B T}}$$

where I ($^5D_1/^5D_0$) is the intensity ratio of the two thermally coupled states, here the $^5D_1$ and $^5D_0$ of Eu^{3+}, and A is a constant including geometric factors and intrinsic properties of the emitting states, is applied to calculate the energy gap between the thermally coupled states for calibration measurements and for the determination of the catalyst temper-ature. When Boltzmann thermometers are applied, the relative sensitivity of the ther-mometer can be expressed as

$$(Eq.\,4.2)\,S_R = \frac{\Delta E}{k_B T^2}\,(in\,\%\,K^{-1})$$

where ΔE is energy gap between the two thermally coupled states, k_B is the Boltzmann constant and T is the temperature in K. The temperature uncertainty can be expressed by

$$(Eq.\,4.3)\,\sigma_T = \frac{1}{S_R}\sqrt{\frac{1}{A} + \frac{1}{B}}\,(in\,K)$$

where A and B are the integrals of the region of interest.

4.5.5 Data Analysis Procedure

The raw spectral data was converted before it was suited for thermometric applications. The first step was the dark subtraction to correct for stray light and detector noise. Subsequently, any faulty measurements, i.e., saturated measurements or below 10% of the saturation value, were removed from the dataset. Next, the wavelength was converted to energy scale by

$$(Eq.\,4.4)\; E = \frac{1}{\lambda} * 10^{-7}\; (in\; cm^{-1})$$

where λ is the wavelength in nm. As the x-axis went from evenly spaced intervals to non-evenly spaced intervals, the spectral intensity has to be corrected accordingly.[43] The Jacobian transformation

$$(Eq.\,4.5)\; I_{corrected}(\lambda) = \frac{I_{spectrum}(\lambda)}{E(\lambda)^2}$$

was applied where I and E are the intensity and energy at a specific wavelength. Next, the spectra were normalized to 100 and the regions of interest were fitted with multiple Lorentzian functions and a baseline, given by the basic function

$$(Eq.\,4.6)\; I_{fit} = \sum_i \frac{a_i * w_i^2}{(E(\lambda) - c_i)^2 * w_i^2} + z$$

where a, w, c and z are the peak amplitude, peak width, peak center and a constant. The area of the sum of the Lorentzian (without z) was applied as input for the Boltzmann equation (Eq. 4.1).

4.5.6 Heat Transfer Calculations by Convection and Radiation

Heat generated by the reaction

$$(Eq.\,4.7)\; Q_r = X C_{CH_4} F_g \Delta H_r \approx 0.02\, W$$

with a CH$_4$ conversion $X \approx 0.3$, inlet CH$_4$ concentration $C_{CH4} \approx 1.5$ mol m^{-3}, gas flow $F_g = 3 \cdot 10^{-7}$ m^{3}s^{-1} and reaction enthalpy $\Delta H_r = 158 \cdot 10^3$ J mol^{-1} was calculated. If all heat would be withdrawn by reaction gas mixture, the temperature increase of the gas

$$(Eq.\,4.8)\; \Delta T_g = \frac{Q_r}{F_g \rho_g C p_g} = \frac{X C_{CH4} \Delta H_r}{\rho_g C p_g} \approx 120\, K$$

with a gas density $\rho_g \approx 0.5$ kg m^{-3} and a heat capacity of the gas $C_{p,g} \approx 1150$ J kg^{-1}K^{-1}. As the inlet gas temperature is assumed to be equal to the oven temperature (Figure 4.2A), convection by reaction mixture is presumably not the predominant cooling mechanism due to the large calculated ΔT_g. Therefore, Q_r needs to be withdrawn radially outwards by either conduction or radiation. The heat generated by reaction per sieved catalyst

particle can be expressed as

$$(Eq.\,4.9)\; Q_{r,p} = \frac{Q_r}{n_p}$$

Assuming spherical catalyst particles, the number of particles, n_p, is approximated by

$$(Eq.\,4.10)\; n_p = \frac{V_{bed}(1 - \epsilon_{bed})}{V_p} = \frac{V_{bed}(1 - \epsilon_{bed})}{\frac{1}{6}\pi d_p^3}$$

with a particle diameter d_p = 275 $\cdot 10^{-6}$ m, packing factor ϵ_{bed} ≈ 0.43, bed volume v_{bed} = 3.4$\cdot 10^{-7}$ m^3 and the number of particles n_p ≈ 17700, resulting in $Q_{r,p}$ = 1.2$\cdot 10^{-6}$ W. At 773K (500 °C), the particle emission

$$(Eq.\,4.11)\; Q_{e,p} = \sigma T^4 \pi d_p^2 = 4.8 * 10^{-3} W$$

where σ is the Stefan-Boltzmann constant (σ = 5.6703*10^{-8} Wm^{-2}K^{-4}). Even at extremely low values of material emissivity, particle emission $Q_{e,p}$ is at least 2 orders of magnitude larger than the heat generated per particle $Q_{r,p}$. Hence, any increase in particle tempera-ture due to reaction would immediately be lost by radiation to the environment. There-fore, the temperature is likely to be uniform throughout the bed. At the walls of the reactor, heat is lost to the environment (i.e., the oven), most likely by radiation as well as

$$(Eq.\,4.12)\; Q_{e,reactor} = \sigma T^4 A = 6.7\, W$$

with the outer reactor surface A = 3.3$\cdot 10^{-4}$ m^2 and T = 773K. Again, $Q_{e,reactor}$ is more than 2 orders of magnitude larger than Q_r. Hence, any temperature increase due to reaction will quickly be emitted by radiation, until equilibrium at oven temperature is reached. It can therefore be concluded that the bed temperature most likely is constant throughout its volume, at oven temperature. Still, heat is generated by the reaction and the catalyst bed temperature must be higher than the surrounding as

$$(Eq.\,4.13)\; Q_{e,reactor} - Q_{e,0} = Q_r = \epsilon_m \sigma A(T^4 - T_0^4)$$

with $Q_{e,0}$ the total mission without reaction. However, the material emissivity of EuOCl is unknown and determination is outside the scope of this work. Nevertheless, assuming an ϵ_m of 0.1 would result in a ΔT of 5K, which is in the right order of magnitude. The cal-culations enabled us to explain the trends qualitatively but a more detailed model and more carefully controlled experiments are needed for the quantitative description of the temperature increase.

4.5.7 Reaction Enthalpies

Chlorination reaction of EuOCl:
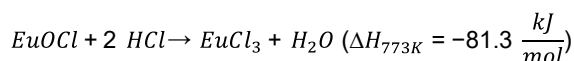
$$EuOCl + 2\; HCl \rightarrow EuCl_3 + H_2O \; (\Delta H_{773K} = -81.3\; \frac{kJ}{mol})$$

Dechlorination reaction of $EuCl_3$:

$$EuCl_3 + 2\ CH_4 + O_2 \rightarrow EuOCl + 2\ CH_3Cl + H_2O\ (\Delta H_{773K} = -233.9\ \frac{kJ}{mol})$$

Oxychlorination reaction of C_1:

$$2\ CH_4 + 2\ HCl + O_2 \rightarrow 2\ CH_3Cl + 2\ H_2O\ (\Delta H_{773K} = -315.2\ \frac{kJ}{mol})$$

$$2\ CH_3Cl + 2\ HCl + O_2 \rightarrow 2\ CH_2Cl_2 + 2\ H_2O\ (\Delta H_{773K} = -324.8\ \frac{kJ}{mol})$$

$$2\ CH_2Cl_2 + 2\ HCl + O_2 \rightarrow 2\ CHCl_3 + 2\ H_2O\ (\Delta H_{773K} = -307.5\ \frac{kJ}{mol})$$

$$2\ CHCl_3 + 2\ HCl + O_2 \rightarrow 2\ CCl_4 + 2\ H_2O\ (\Delta H_{773K} = -281.8\ \frac{kJ}{mol})$$
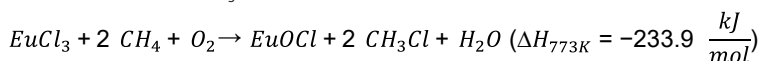
Catalytic destruction with H_2O:

$$CH_3Cl + H_2O \rightarrow CO + HCl + 2\ H_2\ (\Delta H_{773K} = 132.9\ \frac{kJ}{mol})$$

$$CH_2Cl_2 + H_2O \rightarrow CO + 2\ HCl + H_2\ (\Delta H_{773K} = 49.2\ \frac{kJ}{mol})$$

$$CHCl_3 + H_2O \rightarrow CO + 3\ HCl\ (\Delta H_{773K} = -43.1\ \frac{kJ}{mol})$$

$$CCl_4 + 2\ H_2O \rightarrow CO_2 + 4\ HCl\ (\Delta H_{773K} = -185.6\ \frac{kJ}{mol})$$

Oxidation of chloromethanes:

$$CH_3Cl + O_2 \rightarrow CO + HCl + H_2O\ (\Delta H_{773K} = -359.3\ \frac{kJ}{mol})$$

$$2\ CH_2Cl_2 + O_2 \rightarrow 2\ CO + 4\ HCl\ (\Delta H_{773K} = -393.7\ \frac{kJ}{mol})$$

$$2\ CHCl_3 + O_2 \rightarrow 2\ CO + 2\ HCl + 2\ Cl_2\ (\Delta H_{773K} = -203.4\ \frac{kJ}{mol})$$

$$CCl_4 + O_2 \rightarrow CO_2 + 2\ Cl_2\ (\Delta H_{773K} = -302.8\ \frac{kJ}{mol})$$
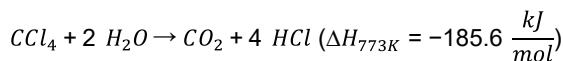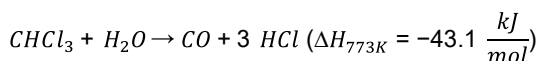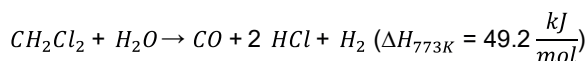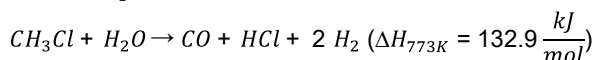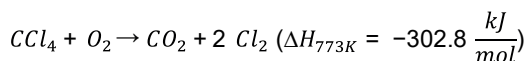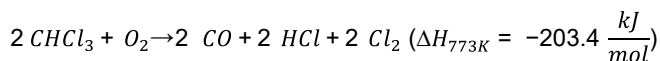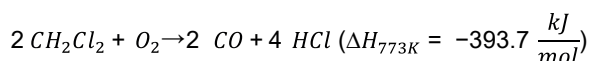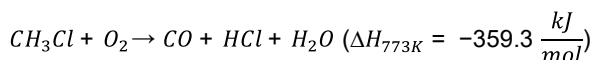
4.6. REFERENCES

(1)   Ertl, G.; Knözinger, H.; Weitkamp, J. Handbook of Heterogeneous Catalysis, 2nd ed.; Wiley-VCH Verlag: Weinheim, 2008. https://doi.org/10.1002/9783527610044.

(2)   Somorjai, G. A.; Li, Y. Introduction to Surface Chemistry and Catalysis, 2nd ed.; Wiley: Hoboken, 2010.

(3)   Krishnaraj, C.; Rijckaert, H.; Jena, H. S.; Van Der Voort, P.; Kaczmarek, A. M. Upconverting Er³⁺-Yb³⁺ Inorganic/Covalent Organic Framework Core-Shell Nanoplatforms for Simultaneous Catalysis and Nanothermometry. ACS Appl. Mater. Interfaces 2021, 13, 47010–47018. https://doi.org/10.1021/acsami.1c11314.

(4)   Kaczmarek, A. M.; Jena, H. S.; Krishnaraj, C.; Rijckaert, H.; Veerapandian, S. K. P.; Meijerink, A.; Van Der Voort, P. Luminescent Ratiometric Thermometers Based on a 4f–3d Grafted Covalent Organic Framework to Locally Measure Temperature Gradients During Catalytic Reactions. Angew. Chem. Int. Ed. 2021, 60, 3727–3736. https://doi.org/10.1002/anie.202013377.

(5)   Jena, H. S.; Rijckaert, H.; Krishnaraj, C.; Van Driessche, I.; Van Der Voort, P.; Kaczmarek, A. M. Hybrid Nanocomposites Formed by Lanthanide Nanoparticles in Zr-MOF for Local Temperature Measurements during Catalytic Reactions. Chem. Mater. 2021, 33, 8007–8017. https://doi.org/10.1021/acs.chemmater.1c02126.

(6)   Geitenbeek, R. G.; Nieuwelink, A.-E.; Jacobs, T. S.; Salzmann, B. B. V.; Goetze, J.; Meijerink, A.; Weckhuysen, B. M. In Situ Luminescence Thermometry To Locally Measure Temperature Gradients during Catalytic Reactions. ACS Catal. 2018, 8, 2397–2401. https://doi.org/10.1021/acscatal.7b04154.

(7)   Hartman, T.; Geitenbeek, R. G.; Whiting, G. T.; Weckhuysen, B. M. Operando Monitoring of Temperature and Active Species at the Single Catalyst Particle Level. Nat. Catal. 2019, 2, 986–996. https://doi.org/10.1038/s41929-019-0352-1.

(8)   van Ravenhorst, I. K.; Geitenbeek, R. G.; van der Eerden, M. J.; Tijn van Omme, J.; Peréz Garza, H. H.; Meirer, F.; Meijerink, A.; Weckhuysen, B. M. In Situ Local Temperature Mapping in Microscopy Nano-Reactors with Luminescence Thermometry. ChemCatChem 2019, 11, 5505–5512. https://doi.org/10.1002/cctc.201900985.

(9)   Tsakoumis, N. E.; Rønning, M.; Borg, Ø.; Rytter, E.; Holmen, A. Deactivation of Cobalt Based Fischer-Tropsch Catalysts: A Review. Catal. Today 2010, 154, 162–182. https://doi.org/10.1016/j.cattod.2010.02.077.

(10)   Gygax, R. Chemical Reaction Engineering for Safety. Chem. Eng. Sci. 1988, 43, 1759–1771. https://doi.org/10.1016/0009-2509(88)87040-4.

(11)   Werther, J. Measurement Techniques in Fluidized Beds. Powder Technol. 1999, 102, 15–36. https://doi.org/10.1016/S0032-5910(98)00202-2.

(12)   Moodley, D.; Claeys, M.; van Steen, E.; van Helden, P.; Kistamurthy, D.; Weststrate, K. J.; Niemantsverdriet, H.; Saib, A.; Erasmus, W.; van de Loosdrecht, J. Sintering of Cobalt during FTS: Insights from Industrial and Model Systems. Catal. Today 2020, 342, 59–70. https://doi.org/10.1016/j.cattod.2019.03.059.

(13)   Sun, L.; Wang, Y.; Guan, N.; Li, L. Methane Activation and Utilization: Current Status and Future Challenges. Energy Technol. 2020, 8, 1900826. https://doi.org/10.1002/ente.201900826.

(14)   Olivos-Suarez, A. I.; Szécsényi, À.; Hensen, E. J. M.; Ruiz-Martinez, J.; Pidko, E. A.; Gascon, J. Strategies for the Direct Catalytic Valorization of Methane Using Heterogeneous Catalysis: Challenges and Opportunities. ACS Catal. 2016, 6, 2965–2981. https://doi.org/10.1021/acscatal.6b00428.

(15)   Scharfe, M.; Zichittella, G.; Paunović, V.; Pérez-Ramírez, J. Ceria in Halogen Chemistry. Chin. J. Catal. 2020, 41, 915–927. https://doi.org/10.1016/S1872-2067(19)63528-X.

(16)   Paunović, V.; Zichittella, G.; Hemberger, P.; Bodi, A.; Pérez-Ramírez, J. Selective Methane Functionalization via Oxyhalogenation over Supported Noble Metal Nanoparticles. ACS Catal. 2019, 9, 1710–1725. https://doi.org/10.1021/acscatal.8b04375.

(17)   Zichittella, G.; Aellen, N.; Paunović, V.; Amrute, A. P.; Pérez-Ramírez, J. Olefins from Natural Gas by Oxychlorination. Angew. Chem. Int. Ed. 2017, 56, 13670–13674. https://doi.org/10.1002/anie.201706624.

(18)   Zichittella, G.; Paunović, V.; Amrute, A. P.; Pérez-Ramírez, J. Catalytic Oxychlorination versus Oxybromination for Methane Functionalization. ACS Catal. 2017, 7, 1805–1817. https://doi.org/10.1021/acscatal.6b03600.

(19)   He, J.; Xu, T.; Wang, Z.; Zhang, Q.; Deng, W.; Wang, Y. Transformation of Methane to Propylene: A Two-Step Reaction Route Catalyzed by Modified CeO_2 Nanocrystals and Zeolites. Angew. Chem. Int. Ed. 2012, 51, 2438–2442. https://doi.org/10.1002/anie.201104071.

(20)   Peringer, E.; Podkolzin, S. G.; Jones, M. E.; Olindo, R.; Lercher, J. A. $LaCl_3$-Based Catalysts for Oxidative Chlorination of CH_4. Top. Catal. 2006, 38, 211–220. https://doi.org/10.1007/s11244-006-0085-7.

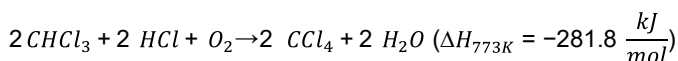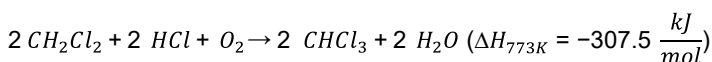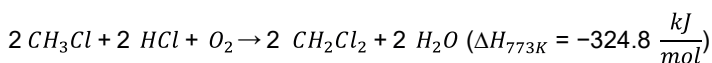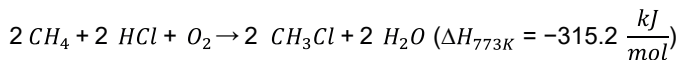(21)   Terlingen, B.; Oord, R.; Ahr, M.; Hutter, E. M.; van Lare, C.; Weckhuysen, B. M. Favoring the Methane Oxychlorination Reaction over EuOCl by Synergistic Effects with Lanthanum. ACS Catal. 2022, 12, 5698–5710. https://doi.org/10.1021/acscatal.2c00777.

(22)   Terlingen, B.; Oord, R.; Ahr, M.; Hutter, E.; van Lare, C.; Weckhuysen, B. M. Mechanistic Insights into the Lanthanide-Catalyzed Oxychlorination of Methane as Revealed by Operando Spectroscopy. ACS Catal. 2021, 11, 10574–10588. https://doi.org/10.1021/acscatal.1c00393.

(23)   Kummer, A.; Varga, T. What Do We Know

Already about Reactor Runaway? – A Review. Process Saf. Environ. Prot. 2021, 147, 460–476. https://doi.org/10.1016/j.psep.2020.09.059.

(24)   Juncheng, J.; Dan, W.; Lei, N.; Gang, F.; Yong, P. Inherent Thermal Runaway Hazard Evaluation Method of Chemical Process Based on Fire and Explosion Index. J. Loss Prev. Process Ind. 2020, 64, 104093. https://doi.org/10.1016/j.jlp.2020.104093.

(25)   Liu, B.; Huang, Q.; Wang, P. Influence of Surrounding Gas Temperature on Thermocouple Measurement. Case Stud. Therm. Eng. 2020, 19, 100627. https://doi.org/10.1016/j.csite.2020.100627.

(26)   Peringer, E.; Salzinger, M.; Hutt, M.; Lemonidou, A. A.; Lercher, J. A. Modified Lanthanum Catalysts for Oxidative Chlorination of Methane. Top. Catal. 2009, 52, 1220–1231. https://doi.org/10.1007/s11244-009-9265-6.

(27)   Deshazer, L. G.; Dieke, G. H. Spectra and Energy Levels of Eu^{3+} in $LaCl_3$. J. Chem. Phys. 1963, 38, 2190–2199. https://doi.org/10.1063/1.1733949.

(28)   Hölsä, J.; Porcher, P. Free Ion and Crystal Field Parameters for $REOCl:Eu^{3+}$. J. Chem. Phys. 1981, 75, 2108–2117. https://doi.org/10.1063/1.442314.

(29)   Geitenbeek, R. G.; de Wijn, H. W.; Meijerink, A. Non-Boltzmann Luminescence in $NaYF_4:Eu^{3+}$: Implications for Luminescence Thermometry. Phys. Rev. Appl. 2018, 10, 064006. https://doi.org/10.1103/PhysRevApplied.10.064006.

(30)   Scharfe, M.; Lira-Parada, P. A.; Amrute, A. P.; Mitchell, S.; Pérez-Ramírez, J. Lanthanide Compounds as Catalysts for the One-Step Synthesis of Vinyl Chloride from Ethylene. J. Catal. 2016, 344, 524–534. https://doi.org/10.1016/j.jcat.2016.10.026.

(31)   Ma, H.; Wang, Y.; Qi, Y.; Rout, K. R.; Chen, D. Critical Review of Catalysis for Ethylene Oxychlorination. ACS Catal. 2020, 10, 9299–9319. https://doi.org/10.1021/acscatal.0c01698.

(32)   Zichittella, G.; Polyhach, Y.; Tschaggelar, R.; Jeschke, G.; Pérez-Ramírez, J. Quantification of Redox Sites during Catalytic Propane Oxychlorination by Operando EPR Spectroscopy. Angew. Chem. Int. Ed. 2021, 60, 3596–3602. https://doi.org/10.1002/anie.202013331.

(33)   Paunović, V.; Lin, R.; Scharfe, M.; Amrute, A. P.; Mitchell, S.; Hauert, R.; Pérez-Ramírez, J. Europium Oxybromide Catalysts for Efficient Bromine Looping in Natural Gas Valorization. Angew. Chem. Int. Ed. 2017, 56, 9791–9795. https://doi.org/10.1002/anie.201704406.

(34)   de Rivas, B.; Guillén-Hurtado, N.; López-Fonseca, R.; Coloma-Pascual, F.; García-García, A.; Gutiérrez-Ortiz, J. I.; Bueno-López, A. Activity, Selectivity and Stability of Praseodymium-Doped CeO_2 for Chlorinated VOCs Catalytic Combustion. Appl. Catal. B Environ.

2012, 121–122, 162–170. https://doi.org/10.1016/j.apcatb.2012.03.029.

(35)   Van Der Heijden, A. W. A. M.; Bellière, V.; Alonso, L. E.; Daturi, M.; Manoilova, O. V.; Weckhuysen, B. M. Destructive Adsorption of CCl_4 over Lanthanum-Based Solids: Linking Activity to Acid-Base Properties. J. Phys. Chem. B 2005, 109, 23993–24001. https://doi.org/10.1021/jp054689b.

(36)   Haryanto, A.; Fernando, S.; Murali, N.; Adhikari, S. Current Status of Hydrogen Production Techniques by Steam Reforming of Ethanol: A Review. Energy and Fuels 2005, 19, 2098–2106. https://doi.org/10.1021/ef0500538.

(37)   Charisiou, N. D.; Siakavelas, G.; Papageridis, K. N.; Baklavaridis, A.; Tzounis, L.; Avraam, D. G.; Goula, M. A. Syngas Production via the Biogas Dry Reforming Reaction over Nickel Supported on Modified with CeO_2 and/or La_2O_3 Alumina Catalysts. J. Nat. Gas Sci. Eng. 2016, 31, 164–183. https://doi.org/10.1016/j.jngse.2016.02.021.

(38)   Ban, H.; Li, C.; Asami, K.; Fujimoto, K. Influence of Rare-Earth Elements (La, Ce, Nd and Pr) on the Performance of Cu/Zn/Zr Catalyst for CH_3OH Synthesis from CO_2. Catal. Commun. 2014, 54, 50–54. https://doi.org/10.1016/j.catcom.2014.05.014.

(39)   Hirata, G.; Perea, N.; Tejeda, M.; Gonzalez-Ortega, J. A.; McKittrick, J. Luminescence Study in Eu-Doped Aluminum Oxide Phosphors. Opt. Mater. 2005, 27, 1311–1315. https://doi.org/10.1016/j.optmat.2004.11.029.

(40)   Geitenbeek, R. G.; Prins, P. T.; Albrecht, W.; Van Blaaderen, A.; Weckhuysen, B. M.; Meijerink, A. $NaYF_4:Er^{3+},Yb^{3+}/SiO_2$ Core/Shell Upconverting Nanocrystals for Luminescence Thermometry up to 900 K. J. Phys. Chem. C 2017, 121, 3503–3510. https://doi.org/10.1021/acs.jpcc.6b10279.

(41)   Myint, T.; Gunawidjaja, R.; Eilers, H. Spectroscopic Properties of Nanophase Eu-Doped ZrO_2 and Its Potential Application for Fast Temperature Sensing under Extreme Conditions. J. Phys. Chem. C 2012, 116, 21629–21634. https://doi.org/10.1021/jp307092b.

(42)   Geitenbeek, R. G.; Salzmann, B. B. V.; Nieuwelink, A.-E.; Meijerink, A.; Weckhuysen, B. M. Chemically and Thermally Stable Lanthanide-Doped Y_2O_3 Nanoparticles for Remote Temperature Sensing in Catalytic Environments. Chem. Eng. Sci. 2019, 198, 235–240. https://doi.org/10.1016/j.ces.2018.10.004.

(43)   Mooney, J.; Kambhampati, P. Get the Basics Right: Jacobian Conversion of Wavelength and Energy Scales for Quantitative Analysis of Emission Spectra. J. Phys. Chem. Lett. 2013, 4, 3316–3318. https://doi.org/10.1021/jz401508t.

4

in an Exothermic Chemical Reaction
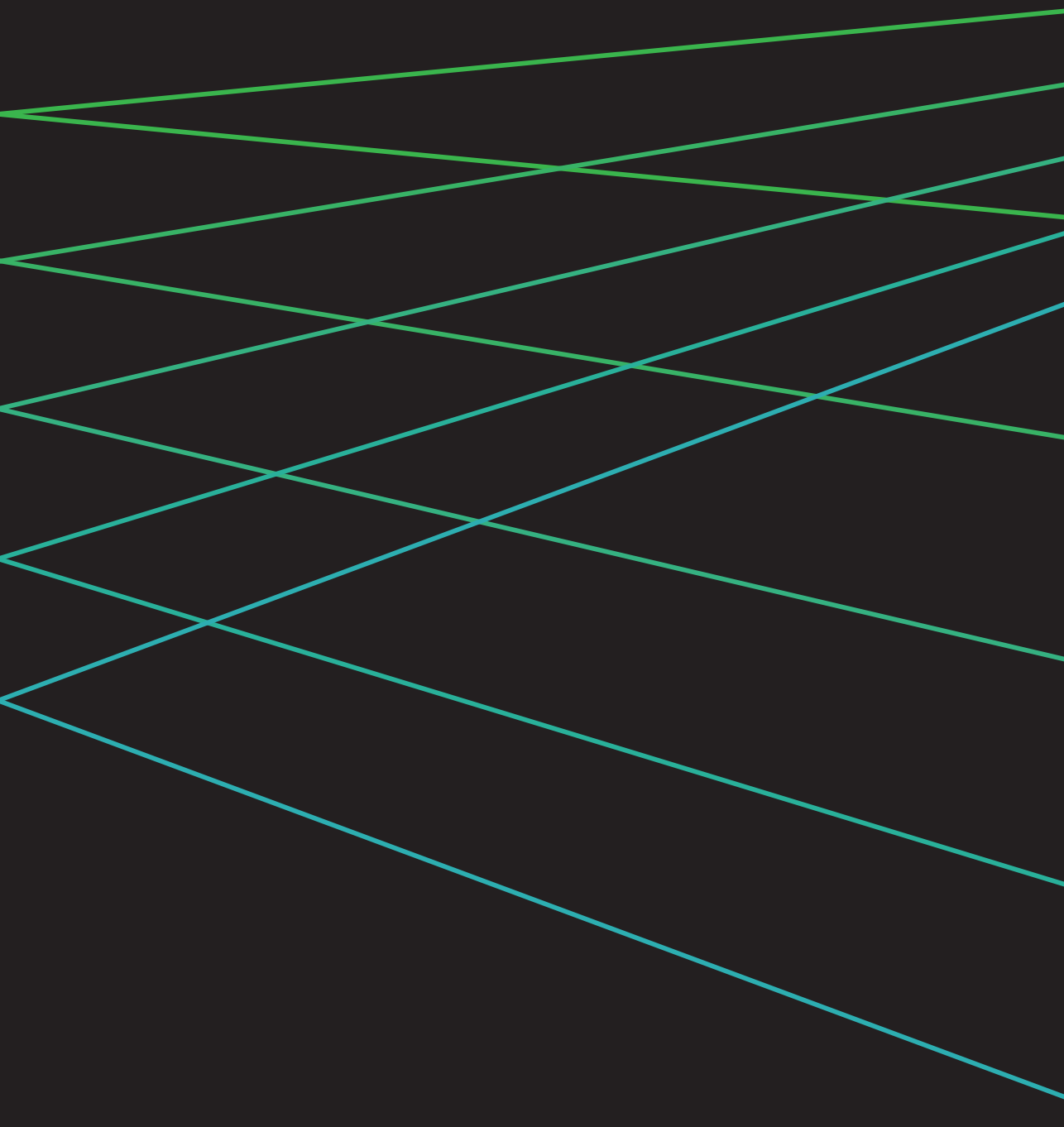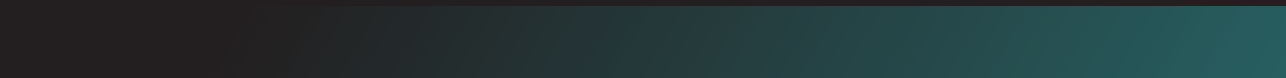
5

Europium-Magnesium-Aluminium-based Mixed Metal Oxides as Highly Active Methane Oxychlorination Catalysts

Abstract

The methane oxychlorination (MOC) process is a promising reaction for the production of liquefied CH_4 derivatives. Even though catalyst design is still in its early stages, the general trend is that benchmark catalyst materials have a redox active site, with e.g., Cu^{2+}, Ce^{4+} and Pd^{2+} as prominent showcase examples. However, with the identification of irreducible LaOCl moiety as an active centre for MOC, it was demonstrated that a redox active couple is not a requirement to establish a high activity. In this chapter, we show that Mg^{2+}-Al^{3+} mixed-metal oxide (MMO) materials are highly active and stable MOC catalysts. The synergistic interaction between Mg^{2+} and Al^{3+} could be exploited due to the fact that a homogeneous distribution of the chemical elements was achieved. This interaction was found to be crucial for the unexpected high MOC activity as reference MgO and γ-Al_2O_3 materials did not show any significant activity. Operando Raman spectroscopy revealed that Mg^{2+} acted as a Cl^- buffer and as a chlorinating agent for Al^{3+}, which was the active metal centre in the CH_4 activation step. The addition of the redox active Eu^{3+} to the irreducible Mg^{2+}-Al^{3+} mixed metal oxide catalyst enabled further tuning of the catalytic performance and made the $EuMg_3Al$ catalyst as one of the most active MOC catalyst materials reported so far. Combined operando Raman/luminescence spectroscopy revealed that the chlorination behaviour of Mg^{2+} and Eu^{3+} were correlated, and we therefore hypothesize that Mg^{2+} also acted as a chlorinating agent for Eu^{3+}. These results indicate that both redox activity as well as synergistic effects between Eu, Mg and Al are required to obtaining high catalytic performance. The importance of elemental synergy and redox properties are expected to be translated to the oxychlorination of other hydrocarbons, such as light alkanes, due to large similarities in catalytic chemistry.

5

5.1. INTRODUCTION

The world energy outlook from 2021 states that CH_4 has contributed to around 30% of the global rise in temperature today, either directly as greenhouse gas or indirectly in the form of CO_2.[1] The energy sector is one of the largest emitters of CH_4, mostly through non-emergency flaring, venting, and leakages of equipment.[1] While flaring and venting are not sustainable practices, they are allowed by current regulations, and no economically viable alternatives are available. However, CH_4 utilization offers great potential for sustainable production of renewable chemicals, also after the fossil fuel era.[2–4] Carbon capture utilization and storage (CCUS) technology is advancing[5–7] and many point sources emitting CO_2 can be found across different industries.[7,8] The CO_2 from these processes can be converted to CH_4 via thermocatalysis[9,10], electrocatalysis[8] and photocatalysis[8,11], thus providing a renewable stream of CH_4. Furthermore, the production of CH_4 (then named bio- CH_4) from the anaerobic digestion of biomass, including agricultural and municipal waste, has seen industrialization, providing another renewable source of CH_4.[3]

Efficient conversion processes for the production of liquefied CH_4 derivatives is pivotal for the feasibility of the entire conversion process.[12] On-site production of CH_4-derived liquids would allow for cost-efficient transportation, which is currently one of the largest economic obstacles.[3,4] The design criteria for an efficient CH_4 conversion process consist of a high CH_4 conversion at a high selectivity to the desired product, preferably at low energy consumption. The CH_4 oxychlorination (MOC) reaction has the potential to fulfil these design criteria.[13–21]

Several reported catalyst materials show promising catalytic behaviour in the MOC reaction.[13,15,17,22] High conversion levels of CH_4 and good selectivity to the desired CH_3Cl reaction product are achieved at relatively mild temperature and pressure for benchmark catalysts. Even though the development of MOC catalysts is still in an early phase, a redox active centre apparently seems essential for enhanced catalytic performance in MOC chemistry. The readily reducible elements Cu^{2+}, Ce^{4+} and Pd^{2+} all show great activity in the MOC reaction.[15,17,22–24] Even for the more difficult to reduce Eu^{3+}, redox properties are likely to play a significant role in the reaction mechanism.[25]

With the field focusing on redox-active elements, catalyst compositions based on non-reducible elements are being somewhat overlooked. With the finding of an irreducible LaOCl as an active catalytic centre, it was demonstrated that a stable redox active couple is not pivotal for high MOC activity.[18–21] Interestingly, $LaCl_3$ can even perform a Cl^- atom exchange reaction between CH_2Cl_2 and CCl_4.[26] Furthermore, synergistic effects between La^{3+} and Eu^{3+} were crucial to overcome the rate-determining step of Eu^{3+} in the MOC reaction.

In this chapter, the working hypothesis that irreducible, synergistic chemical elements can be used to obtain a very active MOC catalyst is proven by the design of irreducible Mg^{2+}-Al^{3+} mixed-metal oxide (MMO) catalyst materials. Mg^{2+} and Al^{3+} both have been successfully applied in catalytic materials for reactions involving halogens, including olefin polymerization catalysis.[14,17,27–32] The MMO class of materials offers a wide range of op-

portunities in which the chemical composition and redox properties can be tuned without altering the main physicochemical characteristics, i.e., crystal structure and surface area. The Mg^{2+}-Al^{3+} MMO's under study were all highly active. Furthermore, stable performance was observed over a 100 h period, revealing that long-term stability could be achieved. Considering that the MgO and γ-Al_2O_3 reference materials did not show significant MOC performance, the exceptionally high activity of the Mg^{2+}-Al^{3+} MMO was highly unexpected. Operando Raman spectroscopy evidenced that Mg^{2+} acts as a Cl^- buffer and makes the Cl^- accessible for Al^{3+}, which is the active element in the CH_4 activation step. However, the selectivity in the reaction did not meet the standard reported in literature and was also not tuneable by varying the HCl concentration. However, the layered double hydroxide (LDH) precursor composition to make the MMO materials can be altered to fit the desired application.[33–41] This feature was exploited in this chapter to showcase that an redox active site, namely Eu^{3+}, could significantly improve the catalytic performance of the MMO-type MOC materials. Hence, the Mg^{2+}-Al^{3+} was functionalized by the partial substitution of Al^{3+} by redox active Eu^{3+}. The incorporation of Eu^{3+} caused the activity to be enhanced significantly. Furthermore, the activity was also preserved when operated under high HCl concentrations in the feed. This resulted in the fact that the CO selectivity could be significantly lowered compared to the undoped Mg^{2+}-Al^{3+} MMO materials.

5.2. RESULTS AND DISCUSSION

5.2.1 Catalyst Materials Synthesis and Characterization

In this chapter, the synergistic concept reported for the La^{3+}-Eu^{3+} system in the CH_4 oxychlorination (MOC) reaction, as outlined in chapter 3, where La^{3+} acted as a chlorinating agent and Eu^{3+} as an active element, was translated to the Mg^{2+}-Al^{3+} system. This is shown in Figure 5.1A. However, one significant difference is that both Mg^{2+} and Al^{3+} are irreducible under the applied reaction conditions of the MOC reaction. Hence, any observed activity relies on the acid-base properties of the material, as redox-type chemistry can be excluded. Thermodynamic calculations evidenced the chemical similarities between Mg^{2+} and La^{3+} as their equilibria composition in the presence of HCl compose of roughly the same metal oxide/chloride ratio (Figure 5.1B). Eu^{3+} and Al^{3+} are also thought to fulfil the same function as both chemical elements are difficult to chlorinate under reaction conditions. To exploit the mutual interaction between Mg^{2+} and Al^{3+}, intimate contact between the chemical elements is desired. The applied approach in this chapter is based on the synthesis of layered double hydroxides (LDHs) (Figure 5.1C), followed by a calcination step to obtain mixed-metal oxide (MMO) catalyst materials (Figure 5.1D).[42–45] The modifiable building units (Figure 5.1E) allowed for the facile replacement of Al^{3+} by the redox active Eu^{3+}, thereby functionalizing the material with redox properties. Furthermore, the MMO matrix can be synthesized with varying elemental compositions/ratios, while still obtaining a high surface area material with a homogeneous distribution of elements. This approach enables a fair comparison between elements and compositions, without drastically altering the physicochemical properties of the material, such as surface area, pore volume, and crystal structure.
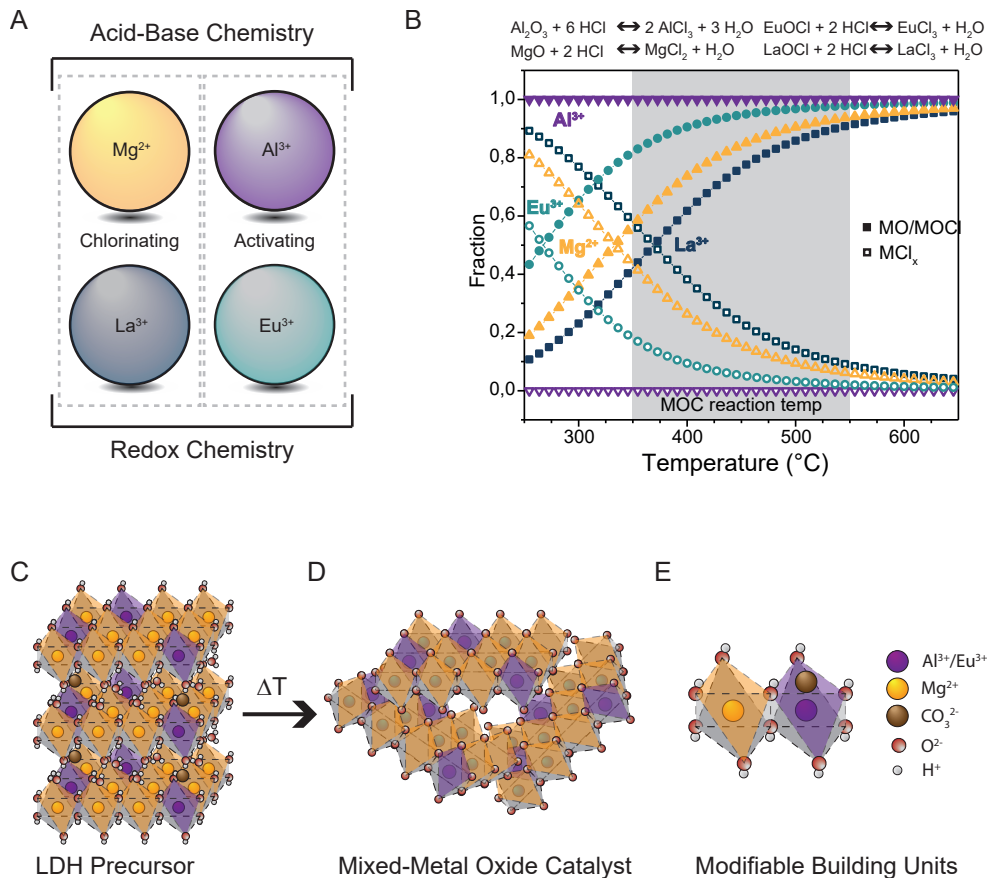
Figure 5.1. (A) The synergistic concept reported for redox active La^{3+}-Eu^{3+}, where La^{3+} acted as a chlorinating agent and Eu^{3+} as an active element, was copied for catalyst materials based on irreducible Mg^{2+} and Al^{3+}. (B) Thermodynamic equilibria calculations performed with the HSC Chemistry 9.1 program revealed that Mg^{2+} could fulfil a similar role as La^{3+}. The same holds for Al^{3+} as it is difficult to chlorinate, just as Eu^{3+}. The synthesis approach applied here exploits the tuneable character of the layered double hydroxide (LDH) composition to yield the mixed-metal oxide (MMO) catalyst material with a homogeneous distribution of chemical elements. (E) The octahedral building units that up the LDH can be readily modified without changing the physicochemical properties drastically. This approach allows for a fair comparison of different catalyst compositions.

Two sets of MMO catalyst materials were prepared and we refer to the section 5.5.1 of this chapter for details on the synthesis procedure. The first set of MMO catalyst materials contained irreducible Mg^{2+} and Al^{3+}, i.e., $Mg_2AlO_{3.5}$, $Mg_3AlO_{4.5}$ and $Mg_4AlO_{5.5}$, which will be further denoted in the form of Mg_xAl. For the second set of MMO catalyst materials, Al^{3+} was partially substituted for the reducible Eu^{3+}, i.e., $Eu_{0.06}Mg_2Al_{0.94}O_{3.5}$, $Eu_{0.08}Mg_3Al_{0.92}O_{4.5}$ and $Eu_{0.10}Mg_4Al_{0.90}O_{5.5}$, which will be further denoted in the form of $EuMg_xAl$. An overview of the catalyst compositions and their corresponding physicochemical properties is provided in Table 5.1. The Brunauer Emmett Teller (BET) surface area (S_{BET}) and pore volume (V_{pore}) of the MMO materials were quite comparable with S_{BET} values between 206.2 and

Table 5.1. Overview of the physicochemical properties of the mixed-metal oxide (MMO) catalyst materials and reference materials. For all catalyst materials, the BET surface area (S_{BET}), pore volume (V_{pore}), the lattice parameter a as determined with x-ray diffraction (XRD) (section 5.5.4 of this chapter) and the molar ratio as determined with inductively coupled plasma-optical emission spectroscopy (ICP-OES) are given.

Catalyst material	Further denoted as	N_2 Physisorption		(Eu^{3+}:)Mg^{2+}:Al^{3+} molar ratio (ICP-OES)	Lattice parameter a (Å)
		S_{BET} (m^2/g)	V_{pore} (cm^3/g)		
$Mg_2AlO_{3.5}$	Mg_2Al	212.1	0.74	2:0.95	4.168
$Mg_3AlO_{4.5}$	Mg_3Al	257.8	1.27	3:0.96	4.183
$Mg_4AlO_{5.5}$	Mg_4Al	229.6	0.98	4:0.95	4.194
$Eu_{0.06}Mg_2Al_{0.94}O_{3.5}$	$EuMg_2Al$	221.9	0.92	0.06:2:0.89	4.172
$Eu_{0.08}Mg_3Al_{0.92}O_{4.5}$	$EuMg_3Al$	275.0	1.53	0.08:3:0.90	4.195
$Eu_{0.1}Mg_4Al_{0.90}O_{5.5}$	$EuMg_4Al$	206.2	0.50	0.10:4:0.9	4.191
Reference Materials					
MgO	MgO	167.9	0.51	-	-
γ-Al_2O_3	γ-Al_2O_3	261.5	0.85	-	-
$EuMg_3O_{4.5}$	Mg_3Eu	175.0	0.51	1.01:3:0	-
$Eu_{0.16}Mg_3Al_{0.84}O_{4.5}$	$EuMg_3Al-4\%$	247.3	0.82	0.16:3:0.82	-
$MgAl_2O_4$	$MgAl_2O_4$	67.4	0.14	-	-

275.0 m^2/g, while the V_{pore} ranged between 0.50 and 1.53 cm^3/g. The catalyst with an Mg^{2+}:Al^{3+} ratio of 3 gave the highest S_{BET} and V_{pore} for both sets of MMO catalysts. In all cases, phase-pure MMO materials were synthesized, as shown by the characteristic defective MgO periclase reflections (COD 5000225), i.e., (111), (200) and (220) (Figure 5.2A). A shift to lower angles in the X-ray diffraction (XRD) was observed with increasing Mg^{2+}/Al^{3+} ratio (Figure 5.2B), coinciding with the increase of the lattice parameter a (Table 5.1) as a higher ratio of the larger Mg^{2+} and Eu^{3+} are incorporated into the crystal structure.[46] No XRD reflections corresponding to segregated Eu^{3+}, Mg^{2+} and or Al^{3+} phases were observed. Also, no extra framework phases were observed with elemental mapping (Figure 5.2C), as obtained with scanning transmission electron microscopy-energy dispersive x-ray spectroscopy (STEM-EDS) analysis. The synthesis procedure yielded the desired molar ratio for all catalyst materials, as evidenced by inductively coupled plasma-optical emission spectroscopy (ICP-OES) (Table 5.1). A theoretical dopant concentration of 2 atom % Eu^{3+} was used, as a too high lanthanide concentration in combination with a mismatch in ionic radii and charge yielded extra-framework phases (Figure 5.2D).[35] Extra-framework phases add another degree of complexity when trying to study these catalyst materials, and were therefore regarded as undesirable for the aim of this chapter. Hence, the Eu^{3+} content was kept at 2 atom %, enabling a fair comparison of the Mg^{2+}:Al^{3+} ratio and the effect of Eu^{3+} doping.

5.2.2. Methane Oxychlorination Properties of Mg^{2+}-Al^{3+} Mixed-Metal Oxides

The Mg^{2+}-Al^{3+} MMO catalyst materials clearly showed catalytic synergy in the MOC reaction, which was unexpected considering that that the reference MgO and γ-Al_2O_3 did not
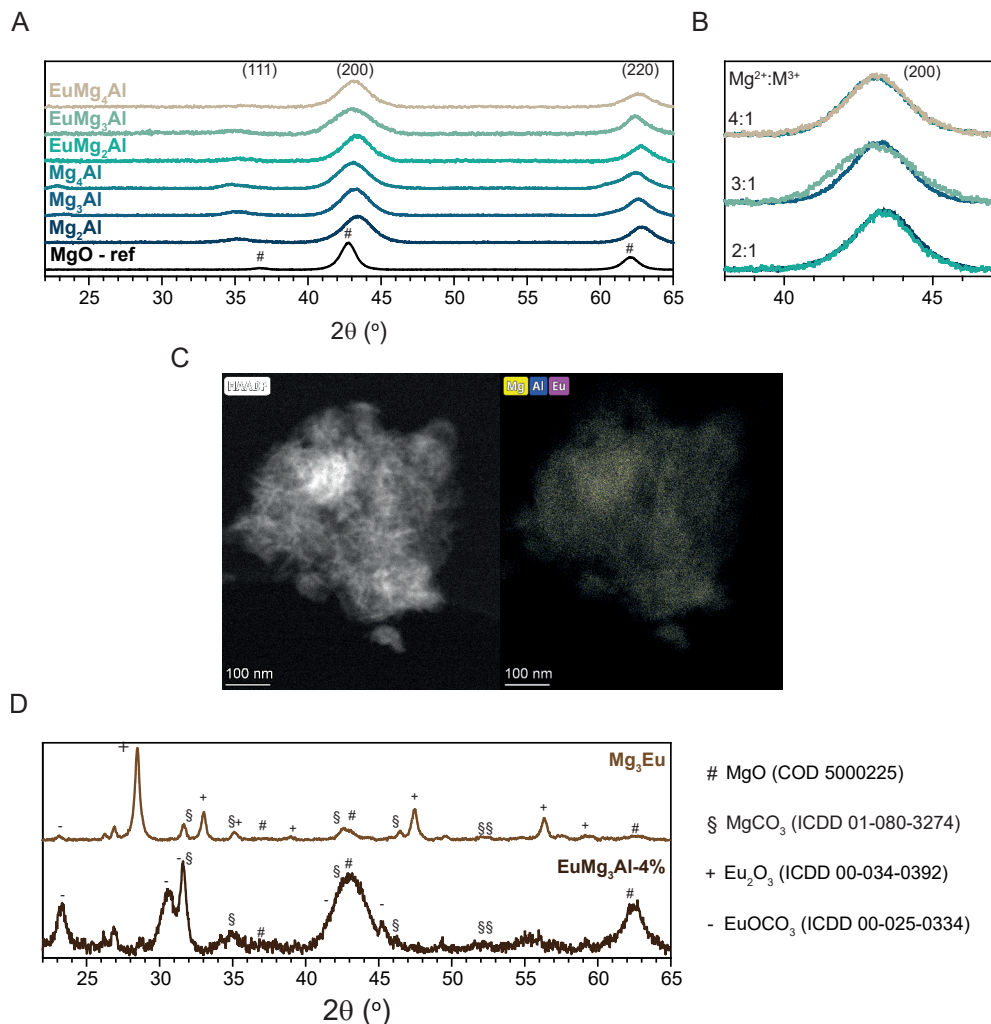
Figure 5.2. (A) X-ray Diffraction (XRD) patterns of the as-synthesized mixed-metal oxide (MMO) catalyst materials. The reflections of the MMO materials are indicated in the graph. (B) A zoom-in of the (200) where the diffractions are ordered based on the $Mg^{2+}:M^{3+}$ ratio where the Eu-doped MMO is plotted together with the corresponding non-doped MMO. (C) High-angle annular dark field-scanning transmission electron microscopy (HAADF-STEM) with energy dispersive x-ray spectroscopy (EDS) analysis revealed the uniform distribution on the nanoscale of Mg, Al and Eu of the MMO with 2 atom % Eu^{3+}. (D) For the reference catalyst materials synthesized with an Eu^{3+} content above 2 atom %, extra framework phases are obtained.

show any significant activity (Figure 5.3A). The synergistic interaction between Mg^{2+} and Al^{3+} appears to be the main descriptor for the observed activity. When a homogeneous mixing of Mg^{2+} and Al^{3+} throughout the catalyst is realized, as is the case for Mg_xAl and $MgAl_2O_4$, significant CH_4 conversion (X_{CH4}) was observed. However, for a physical mixture of MgO and γ-Al_2O_3 with Mg^{2+}/Al^{3+} ratio of 3, only minimal enhancement of activity was observed. The synergy between Mg^{2+} and Al^{3+} will be further discussed in section 5.2.4

Figure 5.3. Overview of the catalytic performance of Mg_xAl mixed-metal oxide (MMO) catalyst materials and reference materials in the CH_4 oxychlorination (MOC) reaction. (A) The CH_4 conversion (X_{CH4}) is plotted versus the reaction temperature under 10% HCl in the feed. (B) The CH_4 conversion rate normalized to the amount of catalyst at 480 °C under 10% HCl. The selectivity at 480 °C is indicated in the bar. (C) The non-isothermal activity is plotted versus the CO selectivity (S_{CO}, square) and the CH_3Cl selectivity (S_{CH3Cl}, circle) under 10% (filled) and 80% (open) HCl in the feed. (D) The Mg_xAl catalyst materials were stable under prolonged periods as Mg_4Al did not show deactivation over a 100 h period time-on-stream (TOS) in terms of X_{CH4} and CH_3Cl yield (Y_{CH3Cl}).

of this chapter. The conversion curve of Mg_2Al differed quite significantly from the other Mg_xAl catalysts in the region above 475 °C. The activity of Mg_2Al levelled off to a final value of 9% while for Mg_3Al, Mg_4Al and $MgAl_2O_4$, the X_{CH4} increased steadily up to a temperature of 510 °C after which it levelled off to 15%. Further research is needed to clarify the nature of the lower activity of Mg_2Al compared to Mg_3Al and Mg_4Al at elevated temperatures.

The highest activity was observed for the Mg_4Al catalyst material, which had a CH_4 conversion rate of 4.63 mmol*g_{cat}*h^{-1} at 480 °C, though the activities of Mg_xAl and $MgAl_2O_4$ were all in the same range (Figure 5.3B). These values are significantly higher than reported for most MOC catalyst materials, which can be ascribed to the low density of the MMO ($\rho_{sieve} \approx 0.67$ g/cm³). Nevertheless, a poor selectivity was observed for all Mg_xAl catalysts at 480 °C (Figure 5.3B). This was further evidenced by the activity-selectivity plot, where

a maximum CH_3Cl selectivity (S_{CH3Cl}) of 70% at X_{CH4} < 1% under 10% HCl was obtained for Mg_3Al (Figure 5.3C, filled symbols). This performance does not meet the standard that is reported in literature where S_{CH3Cl} > 70% at X_{CH4} > 10% is typically achieved.[15,17,47,48] A large part of the CH_4 is converted to CO, which was the dominant product at temperatures above 490 °C. A strategy to minimize the CO selectivity applied for EuOCl was to enhance the HCl concentration in the feed, see chapter 2 and 3. Here, the same strategy did not result in an improved activity/selectivity relation for Mg_3Al MMO's (Figure 5.3C, open symbols). Actually, the increase in HCl only resulted in loss of activity. Increasing the HCl concentration from 10% to 80% resulted in a drop in activity from 4.08 mmol*g_{cat}*h^{-1} to 1.17 mmol*g_{cat}*h^{-1} at 480 °C for Mg_3Al, a trend that is observable for the entire tested temperature range for all Mg^{2+}-Al^{3+} catalyst materials (results not shown for brevity). The nature of this deactivation under increased HCl concentrations in the feed is further in-vestigated in section 5.2.4 of the chapter. Lastly, the Mg_xAl catalysts were stable over 100 h time-on-stream (TOS), being a good indication that these MMO catalysts could possess long-term stability in the MOC reaction (Figure 5.3D).

5.2.3. Effect of Eu-doping of the Mg-Al Matrix on the Methane Oxychlorination Reaction

Even though the irreducible Mg_xAl MMO materials were active and stable catalysts, a good selectivity in the reaction is crucial for eventual application. The addition of a redox active element could further improve the catalytic properties and enable the tuning of the activity-selectivity relation. The catalyst synthesis procedure of the MMO materials allowed for facile partial replacement of Al^{3+} by the redox active Eu^{3+} without altering the crystal structure and S_{BET}/V_{pore} (Table 5.1, Figure 5.2A). The choice for Eu^{3+} was made as the working principles of Eu^{3+} in the MOC reactions are relatively well studied. Typically, increasing the HCl concentration in the feed leads to a lower CO selectivity for Eu^{3+}-based catalysts, even at increased conversion levels.[13,47] The Mg_xAl catalyst itself performed poorly under such conditions in terms of S_{CO} and conversion rate. Thus, the functional-ization of the Mg_xAl MMO with Eu^{3+} could add the functionalities which the Mg_xAl MMO lacked.

First of all, the addition of the redox functionality was reflected in the fact that the EuM-g_3Al was able to perform the HCl oxidation reaction, i.e., 4 HCl + O_2 → Cl_2 + 2 H_2O, while the Mg_3Al was not (Figure 5.4A). This indicates that the reaction over Mg_3Al is purely a surface driven reaction as evolution of Cl_2 is excluded. With the incorporation of Eu^{3+}, the reaction can occur over or via a redox active site, enabling the formation of (some) Cl_2 during oxychlorination. The doping of the Mg_xAl MMO catalysts with only 2 atom % of Eu^{3+} greatly improved the catalytic activity in the MOC reaction. Generally speaking, the activity is doubled over the entire tested temperature range compared to the undoped MMO materials (Figure 5.4B). All three $EuMg_xAl$ catalysts behaved very similarly over the entire tested temperature range in terms of X_{CH4}, again revealing that the Mg:Al ratio did not influence the catalytic properties significantly. The highest activity was achieved for $EuMg_3Al$, possessing a CH_4 conversion rate of 10.56 mmol*g_{cat}*h^{-1}, a doubling compared
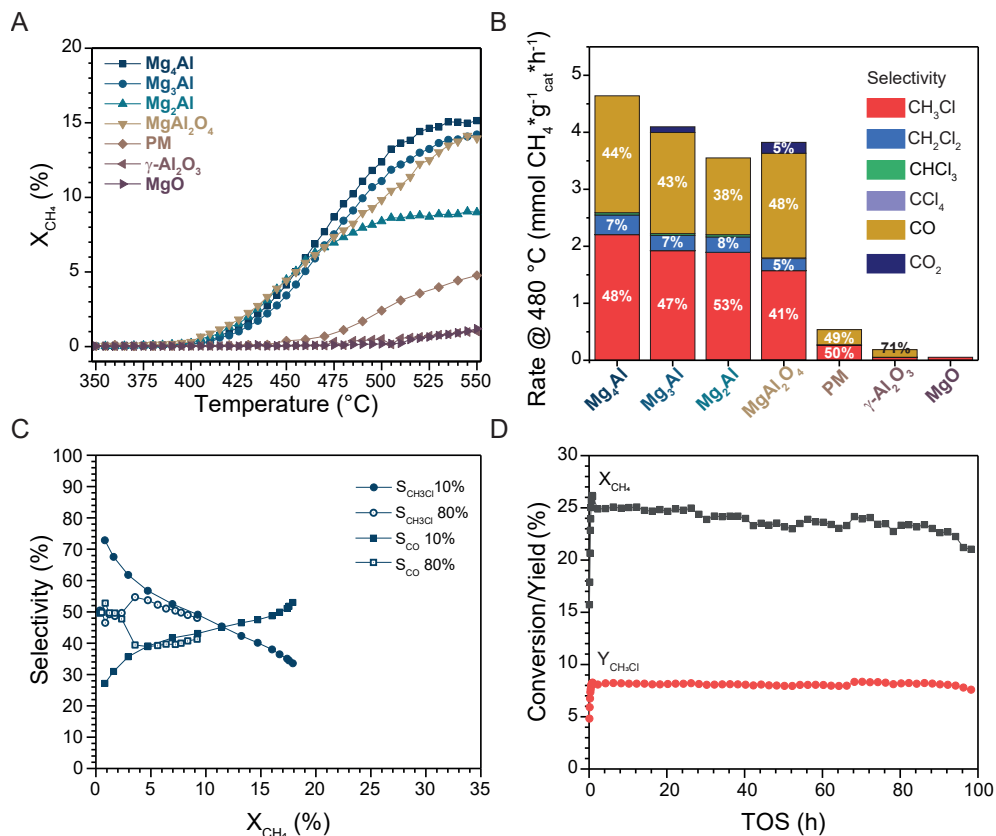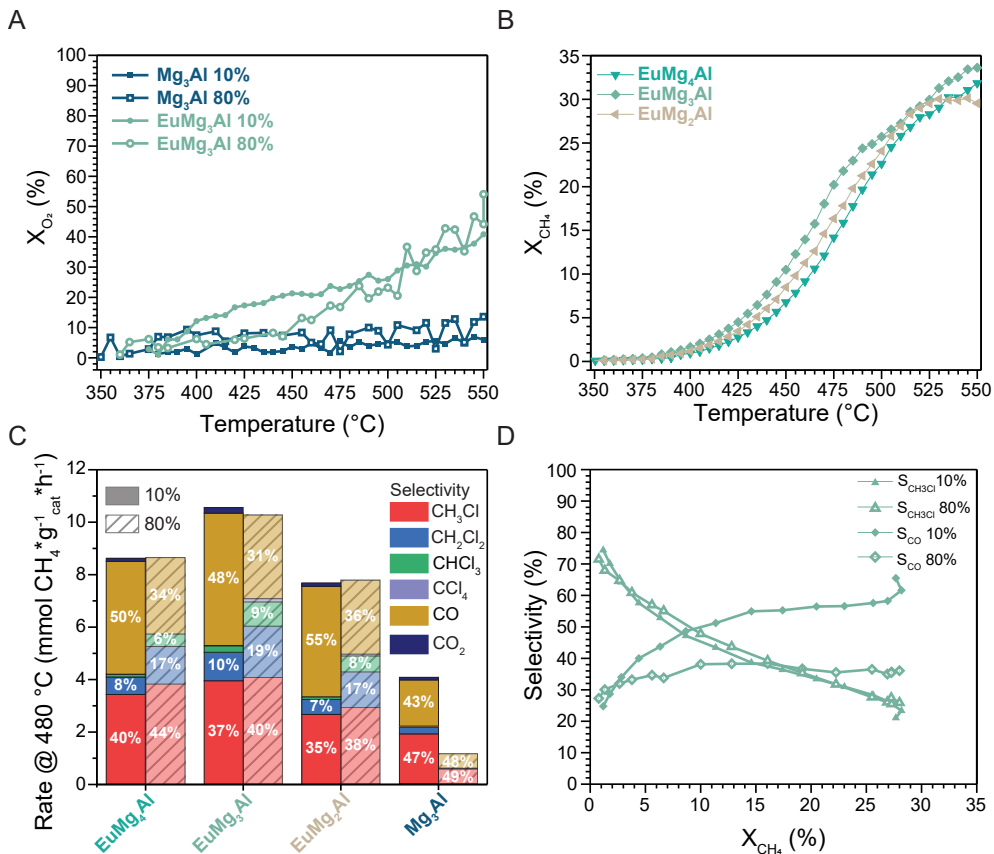
Figure 5.4. Overview of the catalytic performance of EuMg$_x$Al mixed-metal oxide (MMO) catalyst materials in the CH$_4$ oxychlorination (MOC) reaction. (A) The O$_2$ conversion (X$_{O_2}$) is plotted versus the temperature for the HCl oxidation under 10% and 80% HCl over Mg$_3$Al and EuMg$_3$Al. (B) The CH$_4$ conversion (X$_{CH_4}$) is plotted versus the temperature under 10% HCl in the feed. (C) The CH$_4$ conversion rate normalized to the amount of catalyst at 480 °C under 10% and 80% HCl in the feed. The selectivity at 480 °C is indicated in the bar. (D) The non-isothermal activity is plotted versus the CO selectivity (S$_{CO}$, diamond) and the CH$_3$Cl selectivity (S$_{CH3Cl}$, triangle) under 10% (filled) and 80% (open) HCl in the feed.

to the undoped Mg$_3$Al (Figure 5.4C). To put this conversion rate into a broader context, EuMg$_3$Al is one of the most active catalyst reported, approaching FeO$_x$-CeO$_2$ with a CH$_4$ conversion rate of roughly 15.7 mmol*g$_{cat}$*h^{-1} under similar conditions.[17] The functionalization of the Mg$_x$Al MMO was further evidenced by the preservation of the activity under 80% HCl, conditions under which the Mg$_x$Al MMO did not perform well. The addition of Eu^{3+} enhanced the CH$_4$ conversion rate from 1.17 mmol*g$_{cat}$*h^{-1} for Mg$_3$Al to 10.27 mmol*g$_{cat}$*h^{-1} for EuMg$_3$Al, a 9-fold increment. The selectivity could be varied by altering the HCl concentration, as the S$_{CO}$ is reduced for the Eu^{3+}-doped catalysts (Figure 5.4C). This was also evidenced by the activity-selectivity relation, where a reduction of the S$_{CO}$ by as much as 30% point was observed when increasing the HCl concentration (Figure 5.4D). However, the S$_{CH3Cl}$ did not respond to the varying HCl concentration as the 10% and 80%
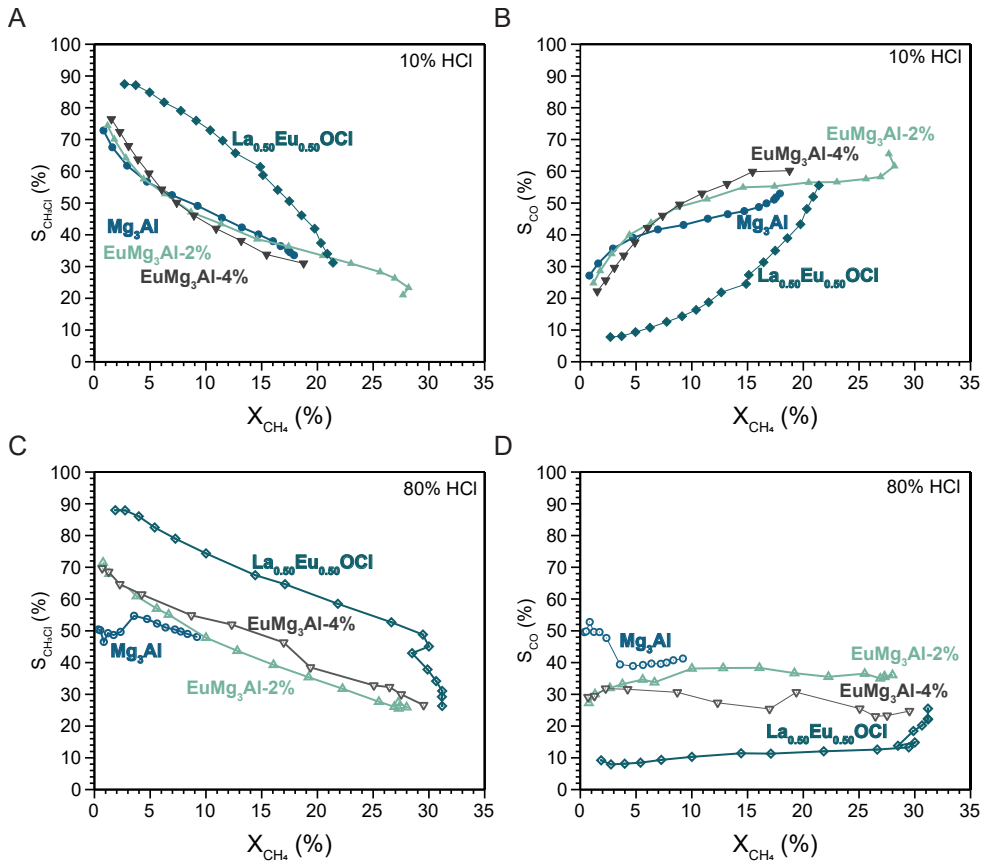
Figure 5.5. Non-isothermal activity-selectivity (X-S) relation for the CH_4 oxychlorination (MOC) reaction plotted for Mg_3Al and $EuMg_3Al$-2%, $EuMg_3Al$-4% and $La_{0.50}Eu_{0.50}OCl$ from chapter 3 under (A, B) 10% HCl and (C, D) 80% HCl in the feed. The selectivity of (A, C) CH_3Cl and (B, D) CO is given.

are almost exact overlays.

A plateau in the S_{CO} was observed from $X_{CH_4} > 10\%$ at a value of ~ 35%. We hypothesize that this effect is caused by the fact that the undoped Mg_xAl MMO displays low activity under these conditions, suppressing the poorer X-S relation of Mg_3Al, while Eu^{3+} becomes more active, resulting in improved catalytic performance. If this hypothesis is true, an increase in the Eu^{3+} content would further improve the X-S relation. Therefore, the non-isothermal X-S relation was also measured for the reference $EuMg_3Al$ with 4 atom-% Eu^{3+} (Figure 5.5). For facile comparison, the X-S relation of the benchmark $La_{0.50}Eu_{0.50}$ from chapter 3 is also plotted. The increase in Eu^{3+} content from 2 to 4 atom-% did not significantly improve the catalytic performance under 10% HCl. However, under 80% HCl, an increase in the S_{CH3Cl} was achieved, while a lowering of the S_{CO} was observed at the same time. The S_{CH3Cl} gradually decreased with increasing X_{CH_4} but the S_{CO} revealed a plateau between 23 - 30%. Thus, the catalytic performance positively correlated to the Eu^{3+} content in the catalyst, but the excellent X-S of $La_{0.50}Eu_{0.50}OCl$ could not be matched.
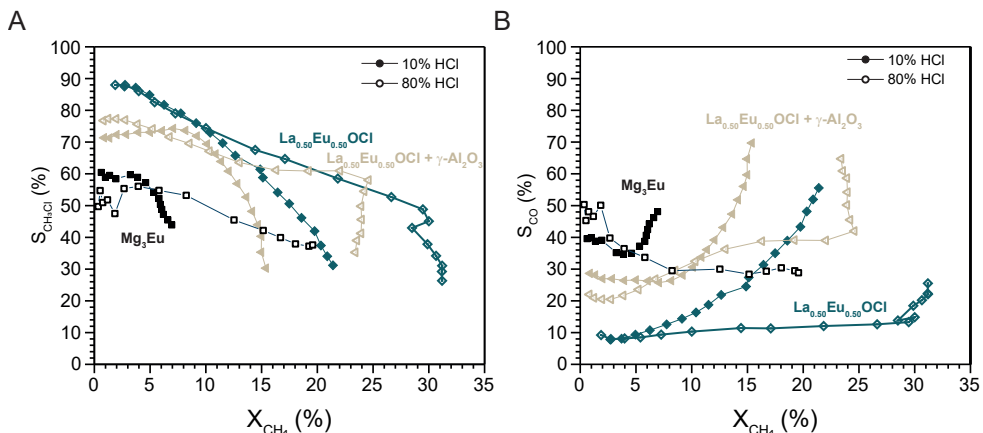
Figure 5.6. Non-isothermal activity-selectivity (X-S) relation for the CH_4 oxychlorination (MOC) plotted for and $La_{0.50}Eu_{0.50}OCl$ from chapter 3, $La_{0.50}Eu_{0.50}OCl + \gamma$-$Al_2O_3$ and Mg_3Eu under 10% HCl (filled symbols) and 80% HCl (open symbols) in the feed. The $La_{0.50}Eu_{0.50}OCl + \gamma$-$Al_2O_3$ was a dual catalyst bed with 500 mg $La_{0.50}Eu_{0.50}OCl$ first contacting the gas feed and then 100 mg of γ-Al_2O_3, separated by quartz wool to prevent mixing. The selectivity of (A) CH_3Cl (S_{CH3Cl}) and (B) CO (S_{CO}) is given.

The CO formation was already quite pronounced at $X_{CH4} < 5\%$ for Al^{3+} containing catalysts, which proved difficult to improve by altering the reaction conditions and catalyst composition. To show that Al^{3+} was the main contributor the poor CO selectivity, a dual catalyst bed was made. At the top, the gas stream first contacted the active $La_{0.50}Eu_{0.50}OCl$, producing a mix of chloromethanes. Subsequently, the product mix contacted 100mg of γ-Al_2O_3 before being analysed with GC (Figure 5.6). Clear from the X-S graphs is that the CO selectivity drastically deteriorated when compared to $La_{0.50}Eu_{0.50}OCl$. Interestingly, the sum of S_{CH3Cl} and S_{CO} made up almost 100% of the total product formation over the entire X_{CH4} range, revealing that the γ-Al_2O_3 catalytically destructed any formed polychlorinated C_1 molecules to CO. However, without the presence of Al^{3+} in the MMO, the catalytic performance is underwhelming. For the reference Mg_3Eu catalyst the X_{CH4} did not exceed 8% with a minimum S_{CO} of 35%. The catalyst performed better under 80% HCl, where minimum S_{CO} of 28% could be reached at the maximum X_{CH4} of 20%. Nevertheless, based on the absence of Al^{3+}, better X-S performance was expected.

5.2.4. Operando Spectroscopy Study on the Mg^{2+}-Al^{3+} Synergy Concept

The high activity of the Mg^{2+}-Al^{3+} MMO catalysts came to us as a surprise due to the fact that Mg^{2+} and Al^{3+} can be regarded irreducible under the applied conditions. This is reflected in the fact that Mg_3Al was proven inactive in the HCl oxidation reaction to Cl_2, where typically a redox couple is needed for Mars-van Krevelen-type of reactions.[49] Most of the active oxychlorination catalyst compositions reported in literature possess an active redox couple, e.g., Cu^{22}, Pd^{15} and $Ce^{17,48}$. Moreover, the absence of a redox couple and synergistic effects caused monometallic MgO and γ-Al_2O_3 to be relatively inactive. Hence, intimate contact between Mg^{2+} and Al^{3+} appears crucial for enhancement of activity and a non-redox MOC reaction mechanism must exist in which the functionalities of Mg^{2+} and

5
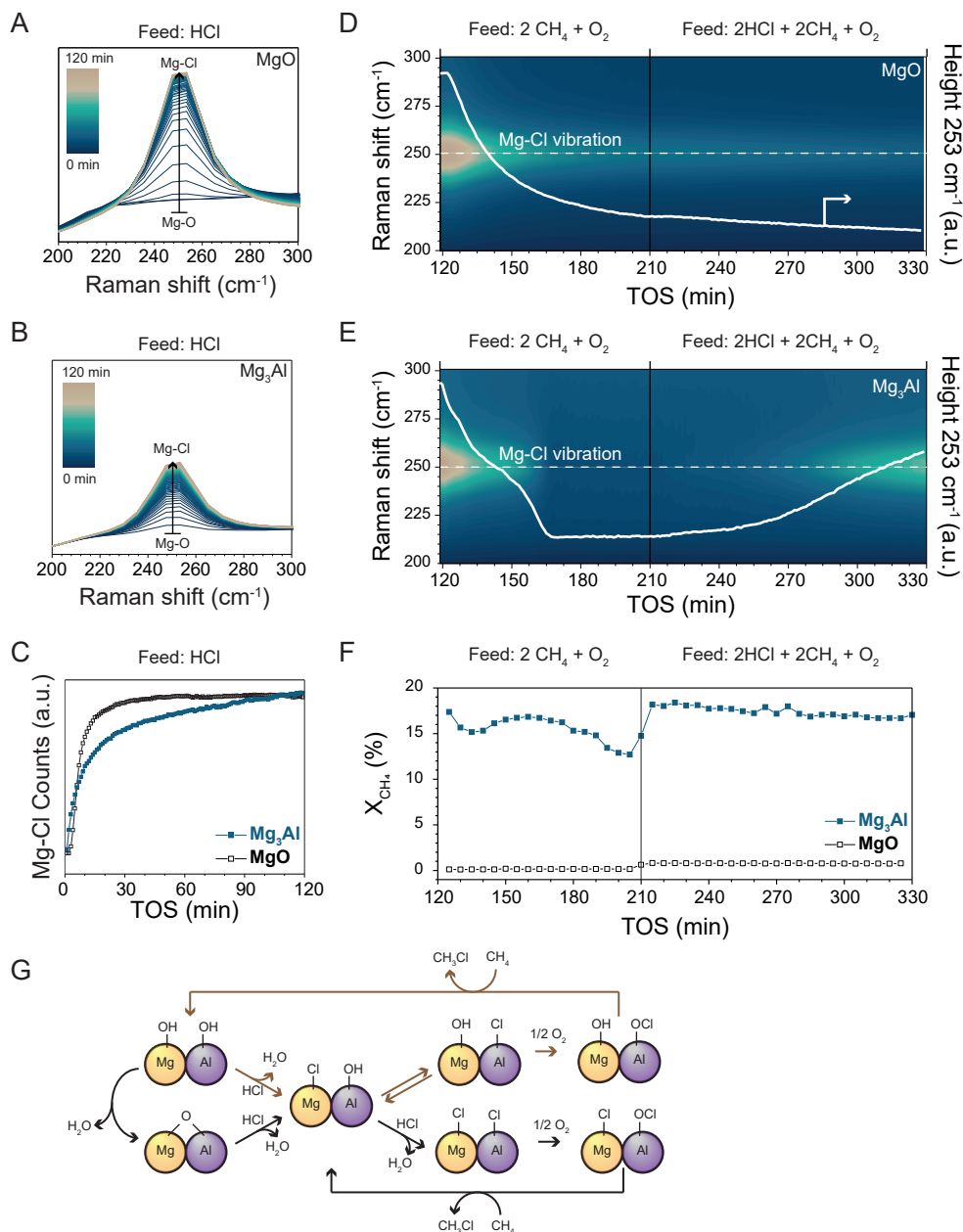
Figure 5.7. Operando Raman spectroscopy measurements performed during chlorination, dechlorination and oxychlorination where the Mg^{2+}-Cl Raman stretching vibration is probed. The Mg-Cl Raman vibration during the chlorination step is plotted for (A) MgO and (B) Mg_3Al. (C) The height of the peak is plotted versus the time-on-stream (TOS) for the both. The Mg-Cl Raman vibration is plotted versus the TOS during the dechlorination and oxychlorination step for (D) MgO and (E) Mg_3Al. Furthermore, the height profile of the Mg-Cl vibration at 253 cm^{-1} is given. Lastly, (F) CH_4 conversion (X_{CH4}) was plotted versus the TOS during the dechlorination and oxychlorination step for both catalysts. (G) Proposed acid-base reaction mechanism for Mg^{2+}-Al^{3+}-based catalysts.

5

Al^{3+} are complementary.

To gain insights in the reaction over the Mg_xAl MMO's, Operando Raman spectroscopy was performed to study the (de)chlorination behaviour of Mg^{2+} in MgO and Mg_3Al under varying reaction conditions (Figure 5.7). In the chlorination step, the catalysts were subjected to 50 v/v% HCl/N_2, which caused the formation of $MgCl_2$ in both cases, as indicated by the emergence of the Mg-Cl vibration at 253 cm^{-1} (Figures 5.7A-5.7B). Important to note is that no other spectral changes were observed (Figure 5.8A). Any formation of $AlCl_3$ would not be detectable with Raman due to the low boiling point of 180 °C. The formation of bulk $AlCl_3$ was however excluded as γ-Al_2O_3 was proven stable under 24 h of oxychlorination conditions, as no weight loss, S_{BET} loss, phase change or reactor staining was observed. The final state was reached faster in the case of MgO compared to Mg_3Al (Figure 5.7C). We hypothesize that the chlorination of Mg^{2+} in Mg_3Al is more difficult due to the interaction with Al^{3+}, as γ-Al_2O_3 is resistant to bulk chlorination under the applied conditions. Subsequently, the catalysts were subjected to dechlorinating conditions to remove the Cl^- by the reaction with CH_4 and O_2. In the case of MgO, partial dechlorination was observed, still preserving some of the Mg^{2+}-Cl peak (Figure 5.7D). At the same time, no products were formed (Figure 5.7F). Our theory is that the dechlorination of $MgCl_2$ to MgO is solely a thermodynamic effect as thermodynamic equilibrium $MgCl_2$:MgO ratio is pushed towards MgO with decreasing HCl present (Figure 5.8B). For Mg_3Al however, the Cl^- was completely removed from the catalyst, indicated by the complete disappearance of the Mg-Cl vibration (Figure 5.7E). During the dechlorination step, significant X_{CH4} was observed, indicating that Cl^- was stored in the form of $MgCl_2$ and released by the active Al^{3+}. During the dechlorination step, the activity gradually dropped as the Mg^{2+}-Cl signal dropped as well, an indication that the Cl^- stored in the catalyst was depleting. The fact that the catalyst was still active while the Cl^- was depleted could be ascribed to the fact that the middle of the catalyst bed was probed while the bottom of the catalyst bed could still hold Cl^-. Lastly, MOC conditions were applied. The MgO catalyst did not show any significant spectral change as it was still in the partially chlorinated state. We hypothesize that the thermodynamic equilibrium composition was reached. Furthermore, the product formation was negligible. The dechlorinated Mg^{2+} in Mg_3Al was partially chlorinated, and at the same time a stable X_{CH4} of ~ 17% was observed. Hence, the element specific properties of Mg^{2+} and Al^{3+} are complementary. Mg^{2+} was readily chlorinated by HCl and could be (partially) converted from MgO to $MgCl_2$. Cl^- could be stored and transferred to Mg^{2+}-Al^{3+} boundary. The available Cl^- was readily reacted away by Al^{3+} with CH_4 and O_2, enabling a catalytic cycle of chlorination and dechlorination. Hence, due to the importance of the Mg^{2+}-Al^{3+} interaction and the irreducibility of the two elements, our theory is that surface Mg-O-Al is chlorinated to Mg-Cl-Al, which then follows the same acid-base reaction mechanism as proposed for the irreducible LaOCl (Figure 5.7G).[21] Furthermore, Cl^- transfer from Mg^{2+} to Al^{3+} can occur, in which Mg^{2+} acts as a chlorine capacitator.

Lastly, the activity of the Mg_xAl was significantly reduced when the HCl concentration in the feed was increased. Operando Raman spectroscopy on Mg_3Al evidenced a correlation between the degree of Mg^{2+} chlorination and catalyst deactivation (Figure 5.9).
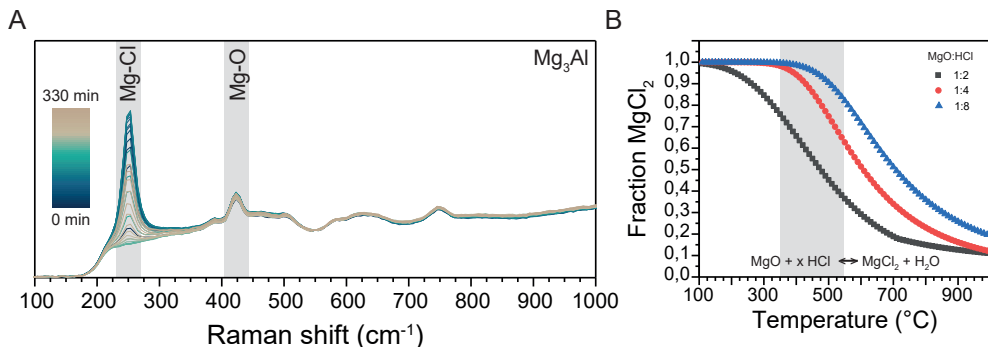
Figure 5.8. (A) Raman spectra of Mg$_3$Al corresponding to the chlorination-dechlorination-oxychlorination experiment presented in Figure 5.7. No spectral changes except for the appearance of the Mg-Cl vibration at 253 cm^{-1} were observed. (B) Thermodynamic equilibria composition calculations revealed that an increment in the HCl concentration in the feed increases the fraction of Mg^{2+} that is chlorinated in the CH$_4$ oxychlorination temperature range (grey box). Calculations were made with HSC Chemistry 9 equilibrium composition package from 100 - 1000°C.
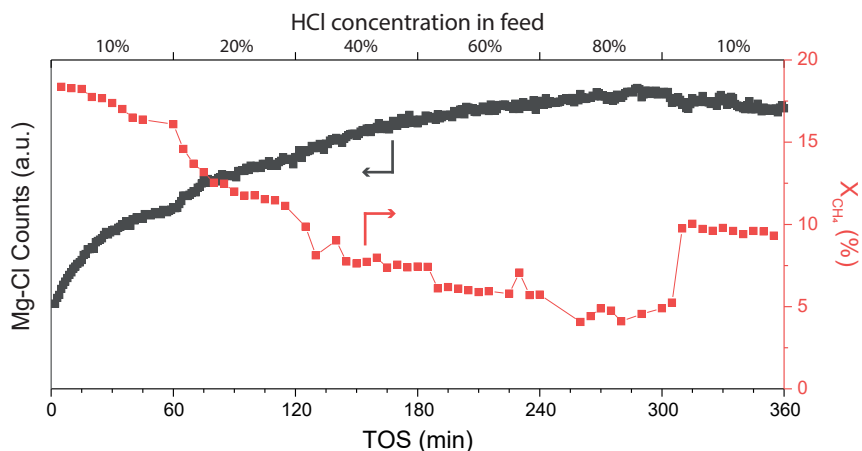
Figure 5.9. Influence of the HCl concentration in the feed on the Mg-Cl Raman intensity (left axis) and the CH$_4$ conversion (X$_{CH4}$, right axis) plotted versus the time-on-stream (TOS). The HCl concentration was adjusted every 60 min.

Under 10% HCl (0 - 60 min), the chlorination rate and dechlorination of MgO moved to a steady state, where only partial Mg^{2+} chlorination was achieved. When the HCl was further increased to 20% (60 - 120 min), an acceleration in the Mg^{2+} chlorination rate was observed, coinciding with a dip in X$_{CH4}$. No sign of stabilization of the Mg-Cl Raman signal or the X$_{CH4}$ was apparent under 20% HCl. This deactivation/Mg^{2+} chlorination trend was continued until the final HCl concentration of 80% was fed (120 - 300 min). Thereafter, the HCl concentration in the feed was lowered, causing a partial and gradual dechlorination and at the same time a partial and sudden recovery of the activity. Hence, the catalytic performance of Mg$_3$Al was quite sensitive to an increase in HCl concentration, caused by catalyst chlorination.
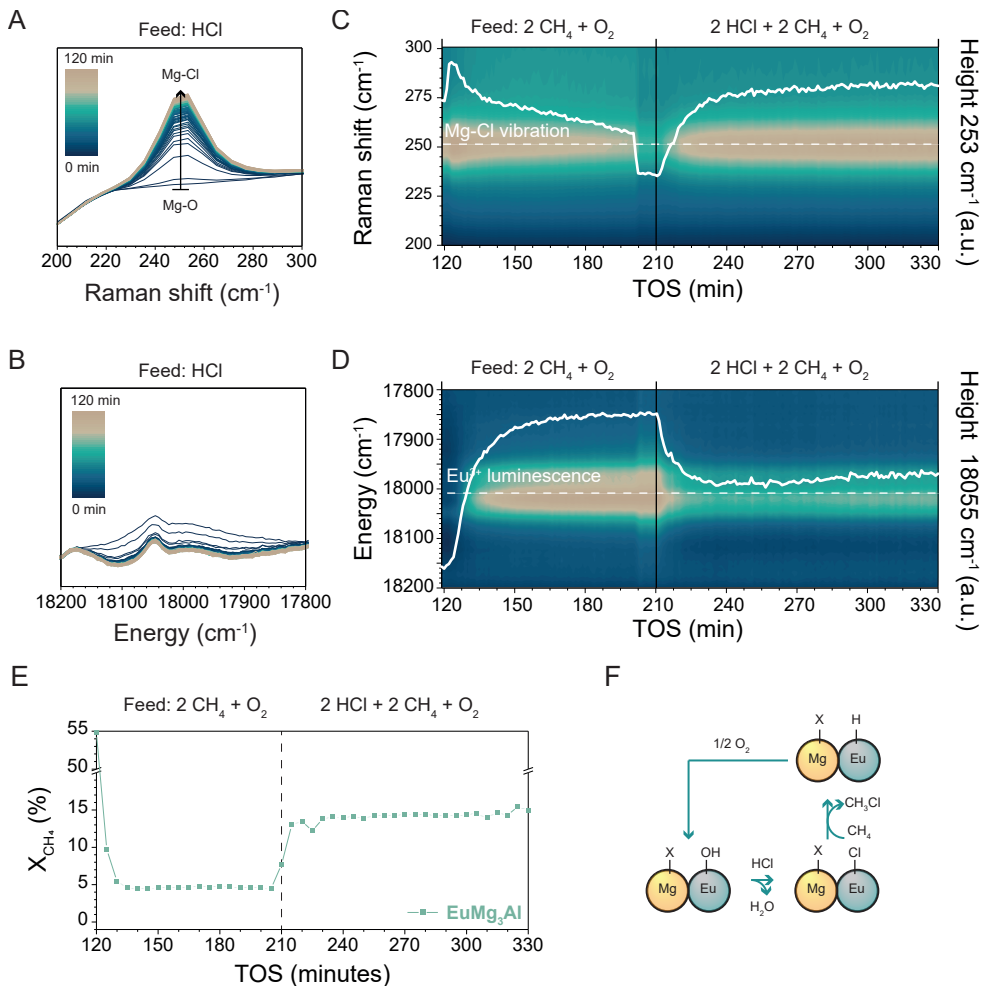
Figure 5.10. *Operando* measurements performed on EuMg$_3$Al where the Mg^{2+}-Cl Raman vibration and the $^5D_1 \rightarrow {}^7F_2$ emission of Eu^{3+} are plotted as a function of reaction time. (A) The Mg^{2+}-Cl Raman vibration and the (B) $^5D_1 \rightarrow {}^7F_2$ emission during the chlorination step are plotted. Furthermore the (C) Mg^{2+}-Cl Raman vibration and the (D) $^5D_1 \rightarrow {}^7F_2$ emission during the dechlorination and oxychlorination are plotted as a function of time-on-stream (TOS). The height profiles of the Mg-Cl Raman vibration or the Eu^{3+} luminescence are given. (E) CH$_4$ conversion (X$_{CH4}$) was plotted versus the TOS during the dechlorination and oxychlorination step.

5.2.5. Combined Operando Luminescence and Raman Spectroscopy on the Eu-Mg$_3$Al Catalyst Material

For the EuMg$_3$Al material, it was possible to analyse the chlorination-dechlorination behaviour of Eu^{3+}, alongside the chlorination-dechlorination behaviour of MgO. This was done by detecting the luminescence signal of Eu^{3+}, which is quenched at high temperatures when Eu^{3+} is in the chlorinated state, as evidenced in chapter 2 and 3.[13,47] The Raman vibration of Mg^{2+}-Cl and the luminescence signal of the $^5D_1 \rightarrow {}^7F_2$ transition were plotted

during a chlorination, dechlorination and oxychlorination step. During the chlorination step, a significant increase in the signal of the Mg^{2+}-Cl Raman vibration at 253 cm^{-1} was observable (Figure 5.10A). This observation is in line with the trends observed for MgO and Mg_3Al. The luminescence signal from the as-synthesized catalyst was, however, hardly detectable and did not alter during the chlorination step (Figure 5.10B). The absence of luminescence signal is most probably caused by the lack of symmetry of the Eu^{3+} centre in the defective periclase-type structure.[50] The chlorinated Eu^{3+} luminescence signal is also quenched at 500 °C, hence the chlorination step was not observable. Subsequently, the dechlorination step caused the catalyst to dechlorinate as the Mg-Cl vibration (Figure 5.10C) decreased in intensity and the Eu^{3+} luminescence signal increased (Figure 5.10D). The increase in luminescence can explained by the fact that the material restructured during the chlorination reaction, enhancing the symmetry of the Eu^{3+} centre. Simultaneously, the X_{CH4} revealed a fast discharge of Cl^-, as indicated by the high initial X_{CH4} of 55% which quickly dropped to a steady-state X_{CH4} of 5% (Figure 5.10E). This coincided with the fact that the Eu^{3+} signal rose quickly in the first 15 min of the dechlorination step (Figure 5.10D, 120–135 min). During the same period, the dechlorination of Mg^{2+} did show an increased rate but it was much less rapid than for Eu^{3+}. A discrepancy in the dechlorination behaviour was observed when comparing the Mg^{2+}-Cl Raman and the Eu^{3+} luminescence, as Eu^{3+} approached a dechlorinated state already after 30 min while the Mg^{2+}-Cl Raman steadily decreased. Lastly, during the oxychlorination step, both Mg^{2+} (Figure 5.10C) and Eu^{3+} (Figure 5.10D) were partially chlorinated, an indication that the addition of Mg^{2+} did not only chlorinate Al^{3+}, but also facilitated the rate determining chlorination of Eu^{3+}. We hypothesize that Mg^{2+} performed the same role as La^{3+} had in $La_{0.50}Eu_{0.50}OCl$. We anticipate that the methane oxychlorination reaction over the Eu^{3+}-containing catalysts occurs via the same mechanism as proposed for Al^{3+}, for which the Al^{3+} can be replaced with Eu^{3+} (Figure 5.7G). In addition to this acid-base mechanism, a redox cycle is proposed for Eu^{3+} in which the Eu^{3+} is reduced by the uptake of a H-atom (Figure 5.10F). The high dispersity of Eu^{3+} throughout the material in combination with the chlorinating effect of Mg^{2+} make that the $EuMg_3Al$ was highly active in the MOC reaction.

5.3. CONCLUSIONS

In this chapter, the concept that irreducible, synergistic elements can make up a very active catalyst for the CH_4 oxychlorination (MOC) reaction is demonstrated by the application of Mg^{2+}-Al^{3+} mixed-metal oxide (MMO) catalysts. Two sets of catalyst materials were synthesized, characterized and tested for their catalytic performance in the MOC reaction. The first set of materials consisted of irreducible Mg^{2+}-Al^{3+} MMO's, where the Mg^{2+}:Al^{3+} ratio was varied from 2 - 4. The Mg_4Al MMO possessed a high CH_4 conversion rate of 4.63 $mmol*g_{cat}*h^{-1}$ and good stability over a 100 h period. A homogeneous distribution of Mg^{2+} and Al^{3+} was required for the synergy in the reaction. However, the S_{CO} and S_{CH3Cl} could not meet the standard reported in literature, as the $S_{CO} > 40\%$ and the $S_{CH3Cl} < 50\%$ at $X_{CH4} \sim 10\%$. Hence, the MMO was functionalized with the redox active Eu^{3+} by the partial replacement with Al^{3+}, adding complementary Eu^{3+} properties to the Mg_xAl MMO.

For Mg^{2+}-Al^{3+} MMO's doped with 2 atom-% of Eu, the CH_4 conversion rate was boosted to 10.56 mmol*g_{cat}*h^{-1}, making it one of the most active catalyst materials reported. The redox active Eu^{3+} made the catalyst active in the HCl oxidation, while the undoped catalyst was not. Furthermore, the activity was preserved under high HCl concentrations in the feed, making the catalyst more resistant to HCl. The S_{CO} became tuneable by varying the HCl concentration in the feed, and could be suppressed by as much as 30%. Even though Al^{3+} was needed for the activity in the reaction, the metal was also highly active in the catalytic destruction of polychlorinated C_1, greatly influencing the activity-selectivity relation. Hence, the $EuMg_3Al$ MMO was not competitive in terms of selectivity to other benchmark catalysts reported in literature. Operando Raman spectroscopy shed light on the synergy between Mg^{2+} and Al^{3+}. Mg^{2+} acted as a Cl^- buffer and chlorinating agent for Al^{3+}, which was the active metal in the CH_4 activation step. Lastly, combined operando Raman/luminescence spectroscopy revealed that the chlorination behaviour of Mg^{2+} and Eu^{3+} were correlated, and we therefore hypothesize that Mg^{2+} also acted as a chlorinating agent for Eu^{3+}. The high dispersity of Eu^{3+} throughout the material in combination with the chlorinating effect of Mg^{2+} make that the $EuMg_3Al$ exhibited even great activity in the MOC reaction than Mg_3Al. The fact that a highly active catalyst material could be made of irreducible Mg^{2+} and Al^{3+} sheds new light on the importance of synergistic effects and the addition of Eu^{3+} showcases the importance of redox properties in oxychlorination chemistry.

5.4. ACKNOWLEDGEMENTS

5.5. EXPERIMENTAL METHODS

5.5.1 Catalyst Synthesis

The layered double hydroxide (LDH) precursor materials were synthesized by the co-precipitation method.[35,39,51] A round bottom flask was filled with 50 mL of demineralized water and the pH was adjusted to pH 10 by the addition of a prepared 1M $Na_2CO_3 \cdot 10\ H_2O$ (> 99%, Sigma Aldrich) solution in demineralized water. The metal chloride salts, i.e., $MgCl_2 \cdot 6H_2O$ (> 99%, Acros Organics), $AlCl_3 \cdot 6H_2O$ (99%, Acros Organics), $EuCl_3 \cdot xH_2O$ (> 99,9%, Alfa Aesar), were dissolved in 18 mL demineralized water and added to a syringe. The amount of metal chloride salts was calculated to yield 1 gram of MMO per batch. Next, the metal chloride salt solution was added with a rate of 1 mL/min and the pH was kept between 9.9 and 10.1 by adding 18 mL of 1M Na_2CO_3. Once the Na_2CO_3 was added, the pH was corrected by adding a premade 1M NaOH (pellets, 98%, Alfa Aesar) solution in demineralized water. Next, the precipitates were aged for 20 h at 75 °C before being washed 3 times with demineralized water. Finally, the LDH materials were dried at 120 °C for 3 h and finally calcined at 450 °C in static air for 8 h to yield the MMO. The ratio of Eu^{3+}:Mg^{2+}:Al^{3+} was calculated to yield the following final MMO's: $Mg_2AlO_{3.5}$, $Mg_3AlO_{4.5}$,

Mg$_4$AlO$_{5.5}$, Eu$_{0.06}$Mg$_2$Al$_{0.94}$O$_{3.5}$, Eu$_{0.08}$Mg$_3$Al$_{0.92}$O$_{4.5}$ and Eu$_{0.1}$Mg$_4$Al$_{0.90}$O$_{5.5}$, to obtain catalyst materials with an Mg^{2+}:Al^{3+} ratio of 2, 3 or 4 with an Eu^{3+} doping of 2 atom-%. Reference MgO, Eu$_{0.16}$Mg$_3$Al$_{0.84}$O$_{4.5}$ and Mg$_3$EuO$_{4.5}$ were made according to the same procedure. γ-Al$_2$O$_3$ (high surface area catalyst support, Alfa Aesar) and MgAl$_2$O$_4$ (Spinel, < 50nm particle size, Sigma Aldrich) was used in the catalytic tests without any pre-treatment or modification.

5.5.2 Catalyst Characterization

X-ray diffraction (XRD) patterns were obtained with a Bruker-AXS D8 powder x-ray diffractometer in Bragg–Brentano geometry, using Cu K$_{α1,2}$ = 1.54184 Å, operated at 40 kV. The measurements were carried out between 22 and 65 ° using a step size of 0.02 ° and a scan speed of 0.5 s, with a 2 mm slit for the source. N$_2$ adsorption isotherms were measured at -196 °C on a Micromeritics TriStar II Plus instrument. Prior to all measurements, samples were dried at 300 °C in a flow of N$_2$. Specific surface areas were calculated using the multipoint Brunauer Emmett Teller (BET) method (0.05 < p/p$_0$ < 0.25). Pore volumes were calculated by the t-plot method; pore size distributions were obtained by the Barrett Joyner Halenda (BJH) analysis; the Harkins and Jura thickness model was applied for the t-plot and BJH methods. Inductively coupled plasma-optical emission spectroscopy (ICP-OES) was applied to determine the chemical composition of the catalyst materials, using a SPECTRO CIROS^{CCD} instrument. ICP-OES samples were prepared by destructing the solids in aqua regia. High-resolution transmission electron microscopy (HR-TEM) and high-angle annular dark field-scanning transmission electron microscopy (HAADF-STEM) were performed on a Talos F200x equipped with 4 in-column SDD Super-X detectors to perform energy dispersive x-ray spectroscopy (EDS) analysis.

5.5.3 Catalyst Testing

All the catalytic tests and operando spectroscopy characterization experiments were performed in a lab scale continuous-flow fixed-bed reactor quartz reactor. Details on the experimental set-up as well as definitions and calculations are reported in chapter 2.

CH$_4$ oxychlorination (MOC) reaction: 100 mg of catalyst (125–425 µm sieve fraction) was loaded in a quartz reactor and heated to 350 °C and the desired feed mixture (i.e., CH$_4$:HCl:O$_2$:N$_2$:He of 2:2:1:1:14 or 2:16:1:1:0 in mL/min) was fed into the reactor. A stabilization period of 15 min was applied and then the ramp experiment of 1 °C/min was commenced to 550 °C. For the stability tests, 250 mg of catalyst (125–425 µm sieve fraction) was loaded in a quartz reactor and heated to 450 °C under N$_2$ with a 10 °C/min heating rate. The feed was adjusted to CH$_4$:HCl:O$_2$:N$_2$:He of 2:2:1:1:14 (in mL/min) and the experiment was performed for 100h. For the determination of the activity-selectivity relation, 100mg of catalyst (125–425 µm sieve fraction) was loaded in a quartz reactor to 350 °C under N$_2$ with a 10°C/min heating rate. The catalyst was subjected to CH$_4$:HCl:O$_2$:N$_2$:He of 2:2:1:1:14 (in mL/min) for 45 min. The temperature was increased to 550 °C with increments of 10 °C with a heating rate of 5 °C/min and kept at every temperature step for 45 min to obtain the steady state activity. The subsequent chlorination-dechlorination-oxychlorination experiments were carried out at 500 °C. The applied CH$_4$:HCl:O$_2$:N$_2$:He ratio was 0:20:0:20:0

(chlorination step, in mL/min), 2:0:1:1:16 (dechlorination step, in mL/min) or 2:1:1:1:14 (oxychlorination step, in mL/min).

HCl oxidation (4 HCl + O_2 → 2 Cl_2 + 2 H_2O): 100 mg of catalyst (125–425 µm sieve fraction) was loaded in a quartz reactor. Temperature ramp experiment were performed from 350 °C to 550 °C at a ramp rate of 1 °C/min under the desired feed mixture (i.e., CH_4:HCl:O_2:N_2:He of 0:2:1:1:16 or 0:16:1:1:2 in mL/min).

5.5.4. Lattice Parameter Calculations

The lattice parameter a was calculated according to the following procedure and the results are summarized in Table 5.2. First, Origin 2017 multi peak fit tool was used to fit Voigt peaks functions, which in turn were used to determine the (200) x-ray diffraction (XRD) positions. From the peak position, the interplanar distance d (Å) was calculated according to Bragg's law

$$(Eq.\,5.1)\; \lambda = 2\,d * \sin(\theta)$$

where λ and θ are the wavelength of the x-ray source (Å) and the angle of the incident light (°) to the plane respectively. With the use of the interplanar distance and the Miller indices, the lattice parameters were then calculated. For the cubic MgO crystal system, the lattice parameter a (Å) can be calculated according to

$$(Eq.\,5.2)\; \frac{1}{d^2} = \frac{(h^2+k^2+l^2)}{a^2}.$$

Table 5.2. The 2θ of the (200) reflection, the interplanar distance d and the lattice parameter a are tabulated. The interplanar distance d and lattice parameter a are calculated according to (Eq. 5.1) and (Eq. 5.2), respectively.

Catalyst material	2θ (°)	Interplanar distance d (Å)	Lattice parameter a (Å)
MgO	42.80	2.11	4.22
$Mg_2AlO_{3.5}$	43.37	2.08	4.17
$Mg_3AlO_{4.5}$	43.20	2.09	4.18
$Mg_4AlO_{5.5}$	43.08	2.10	4.19
$Eu_{0.06}Mg_2Al_{0.94}O_{3.5}$	43.32	2.09	4.17
$Eu_{0.08}Mg_3Al_{0.92}O_{4.5}$	43.07	2.10	4.20
$Eu_{0.1}Mg_4Al_{0.90}O_{5.5}$	43.12	2.10	4.19

5.6. REFERENCES

(1)   International Energy Agency. World Energy Outlook 2021; Paris, 2021.

(2)   Zichittella, G.; Pérez-Ramírez, J. Status and Prospects of the Decentralised Valorisation of Natural Gas into Energy and Energy Carriers. Chem. Soc. Rev. 2021, 50, 2984–3012. https://doi.org/10.1039/D0CS01506G.

(3)   Schwach, P.; Pan, X.; Bao, X. Direct Conversion of Methane to Value-Added Chemicals over Heterogeneous Catalysts: Challenges and Prospects. Chem. Rev. 2017, 117, 8497–8520. https://doi.org/10.1021/acs.chemrev.6b00715.

(4)   Guo, X.; Fang, G.; Li, G.; Ma, H.; Fan, H.; Yu, L.; Ma, C.; Wu, X.; Deng, D.; Wei, M.; Tan, D.; Si, R.; Zhang, S.; Li, J.; Sun, L.; Tang, Z.; Pan, X.; Bao, X. Direct, Nonoxidative Conversion of Methane to Ethylene, Aromatics, and Hydrogen. Science 2014, 344, 616–619. https://doi.org/10.1126/science.1253150.

(5)   Wang, N.; Akimoto, K.; Nemet, G. F. What Went Wrong? Learning from Three Decades of Carbon

Capture, Utilization and Sequestration (CCUS) Pilot and Demonstration Projects. Energy Policy 2021, 158, 112546. https://doi.org/10.1016/j.enpol.2021.112546.

(6)   Park, J. H.; Yang, J.; Kim, D.; Gim, H.; Choi, W. Y.; Lee, J. W. Review of Recent Technologies for Transforming Carbon Dioxide to Carbon Materials. Chem. Eng. J. 2022, 427, 130980. https://doi.org/10.1016/j.cej.2021.130980.

(7)   Alper, E.; Yuksel Orhan, O. CO_2 Utilization: Developments in Conversion Processes. Petroleum 2017, 3, 109–126. https://doi.org/10.1016/j.petlm.2016.11.003.

(8)   Kondratenko, E. V.; Mul, G.; Baltrusaitis, J.; Larrazábal, G. O.; Pérez-Ramírez, J. Status and Perspectives of CO_2 Conversion into Fuels and Chemicals by Catalytic, Photocatalytic and Electrocatalytic Processes. Energy Environ. Sci. 2013, 6, 3112–3135. https://doi.org/10.1039/c3ee41272e.

(9)   Vogt, C.; Groeneveld, E.; Kamsma, G.; Nachtegaal, M.; Lu, L.; Kiely, C. J.; Berben, P. H.; Meirer, F.; Weckhuysen, B. M. Unravelling Structure Sensitivity in CO_2 Hydrogenation over Nickel. Nat. Catal. 2018, 1, 127–134. https://doi.org/10.1038/s41929-017-0016-y.

(10)   Vrijburg, W. L.; Moioli, E.; Chen, W.; Zhang, M.; Terlingen, B. J. P.; Zijlstra, B.; Filot, I. A. W.; Züttel, A.; Pidko, E. A.; Hensen, E. J. M. Efficient Base-Metal NiMn/TiO_2 Catalyst for CO_2 Methanation. ACS Catal. 2019, 9, 7823–7839. https://doi.org/10.1021/acscatal.9b01968.

(11)   Chang, X.; Wang, T.; Gong, J. CO_2 Photo-Reduction: Insights into CO_2 Activation and Reaction on Surfaces of Photocatalysts. Energy Environ. Sci. 2016, 9, 2177–2196. https://doi.org/10.1039/C6EE00383D.

(12)   Zichittella, G.; Paunović, V.; Pérez-Ramírez, J. Mechanistic Understanding of Halogen-Mediated Catalytic Processes for Selective Natural Gas Functionalization. Chim. Int. J. Chem. 2019, 73, 288–293. https://doi.org/10.2533/chimia.2019.288.

(13)   Terlingen, B.; Oord, R.; Ahr, M.; Hutter, E.; van Lare, C.; Weckhuysen, B. M. Mechanistic Insights into the Lanthanide-Catalyzed Oxychlorination of Methane as Revealed by Operando Spectroscopy. ACS Catal. 2021, 11, 10574–10588. https://doi.org/10.1021/acscatal.1c00393.

(14)   Scharfe, M.; Zichittella, G.; Paunović, V.; Pérez-Ramírez, J. Ceria in Halogen Chemistry. Chin. J. Catal. 2020, 41, 915–927. https://doi.org/10.1016/S1872-2067(19)63528-X.

(15)   Paunović, V.; Zichittella, G.; Hemberger, P.; Bodi, A.; Pérez-Ramírez, J. Selective Methane Functionalization via Oxyhalogenation over Supported Noble Metal Nanoparticles. ACS Catal. 2019, 9, 1710–1725. https://doi.org/10.1021/acscatal.8b04375.

(16)   Kim, J.; Ryou, Y.; Hwang, G.; Bang, J.; Jung, J.; Bang, Y.; Kim, D. H. Oxychlorination of Methane over FeO_x/CeO_2 Catalysts. Korean J. Chem. Eng. 2018, 35, 2185–2190. https://doi.org/10.1007/s11814-018-0135-4.

(17)   He, J.; Xu, T.; Wang, Z.; Zhang, Q.; Deng, W.; Wang, Y. Transformation of Methane to Propylene: A Two-Step Reaction Route Catalyzed by Modified CeO_2 Nanocrystals and Zeolites. Angew. Chem. Int. Ed. 2012, 51, 2438–2442. https://doi.org/10.1002/anie.201104071.

(18)   Peringer, E.; Salzinger, M.; Hutt, M.; Lemonidou, A. A.; Lercher, J. A. Modified Lanthanum Catalysts for Oxidative Chlorination of Methane. Top. Catal. 2009, 52, 1220–1231. https://doi.org/10.1007/s11244-009-9265-6.

(19)   Peringer, E.; Tejuja, C.; Salzinger, M.; Lemonidou, A. A.; Lercher, J. A. On the Synthesis of $LaCl_3$ Catalysts for Oxidative Chlorination of Methane. Appl. Catal. A Gen. 2008, 350, 178–185. https://doi.org/10.1016/j.apcata.2008.08.009.

(20)   Podkolzin, S. G.; Stangland, E. E.; Jones, M. E.; Peringer, E.; Lercher, J. A. Methyl Chloride Production from Methane over Lanthanum-Based Catalysts. J. Am. Chem. Soc. 2007, 129, 2569–2576. https://doi.org/10.1021/ja066913w.

(21)   Peringer, E.; Podkolzin, S. G.; Jones, M. E.; Olindo, R.; Lercher, J. A. $LaCl_3$-Based Catalysts for Oxidative Chlorination of CH_4. Top. Catal. 2006, 38, 211–220. https://doi.org/10.1007/s11244-006-0085-7.

(22)   Zichittella, G.; Paunović, V.; Amrute, A. P.; Pérez-Ramírez, J. Catalytic Oxychlorination versus Oxybromination for Methane Functionalization. ACS Catal. 2017, 7, 1805–1817. https://doi.org/10.1021/acscatal.6b03600.

(23)   Garcia, C. L.; Resasco, D. E. Effects of the Support and the Addition of a Second Promoter on Potassium Chloride-Copper(II) Chloride Catalysts Used in the Oxychlorination of Methane. Appl. Catal. 1989, 46, 251–267. https://doi.org/10.1016/S0166-9834(00)81121-5.

(24)   Ma, H.; Wang, Y.; Qi, Y.; Rout, K. R.; Chen, D. Critical Review of Catalysis for Ethylene Oxychlorination. ACS Catal. 2020, 10, 9299–9319. https://doi.org/10.1021/acscatal.0c01698.

(25)   Ro, Y.; Park, S.; Cho, Y.-J.; Kim, D. H. Enhanced Activity and Selectivity of Supported Europium Oxychloride Catalysts for Ethylene Oxychlorination with HCl. Mol. Catal. 2021, 516, 111977. https://doi.org/10.1016/j.mcat.2021.111977.

(26)   van der Heijden, A. W. A. M.; Podkolzin, S. G.; Jones, M. E.; Bitter, J. H.; Weckhuysen, B. M. Catalytic Hydrogen-Chlorine Exchange between Chlorinated Hydrocarbons under Oxygen-Free Conditions. Angew. Chem. Int. Ed. 2008, 47, 5002–5004. https://doi.org/10.1002/anie.200800270.

(27)   Weckhuysen, B. M.; Mestl, G.; Rosynek, M. P.; Krawietz, T. R.; Haw, J. F.; Lunsford, J. H. Destructive Adsorption of Carbon Tetrachloride on Alkaline Earth Metal Oxides. J. Phys. Chem. B 1998, 102, 3773–3778. https://doi.org/10.1021/jp980185k.

(28)   Van der Avert, P.; Weckhuysen, B. M.

Low-Temperature Catalytic Destruction of CCl_4, $CHCl_3$ and CH_2Cl_2 over Basic Oxides. Phys. Chem. Chem. Phys. 2004, 6, 5256–5262. https://doi.org/10.1039/b413876g.

(29)   Paunović, V.; Zichittella, G.; Mitchell, S.; Hauert, R.; Pérez-Ramírez, J. Selective Methane Oxybromination over Nanostructured Ceria Catalysts. ACS Catal. 2018, 8, 291–303. https://doi.org/10.1021/acscatal.7b03074.

(30)   Lane, R. M.; Stacey, M. H. Method of Preparing an Oxychlorination Catalyst. United States Patent 4,273,678, 1981.

(31)   Van der Avert, P.; Weckhuysen, B. M. Low-Temperature Destruction of Chlorinated Hydrocarbons over Lanthanide Oxide Based Catalysts. Angew. Chem. Int. Ed. 2002, 41, 4730–4732. https://doi.org/10.1002/anie.200290030.

(32)   Zichittella, G.; Aellen, N.; Paunović, V.; Amrute, A. P.; Pérez-Ramírez, J. Olefins from Natural Gas by Oxychlorination. Angew. Chem. Int. Ed. 2017, 56, 13670–13674. https://doi.org/10.1002/anie.201706624.

(33)   Fan, G.; Li, F.; Evans, D. G.; Duan, X. Catalytic Applications of Layered Double Hydroxides: Recent Advances and Perspectives. Chem. Soc. Rev. 2014, 43, 7040–7066. https://doi.org/10.1039/c4cs00160e.

(34)   Jun, H.; Zhiliang, Z.; Hongtao, L.; Yanling, Q. Effect of Metal Composition in Lanthanum-Doped Ferric-Based Layered Double Hydroxides and Their Calcined Products on Adsorption of Arsenate. RSC Adv. 2014, 4, 5156–5164. https://doi.org/10.1039/c3ra46680a.

(35)   Bîrjega, R.; Pavel, O. D.; Costentin, G.; Che, M.; Angelescu, E. Rare-Earth Elements Modified Hydrotalcites and Corresponding Mesoporous Mixed Oxides as Basic Solid Catalysts. Appl. Catal. A Gen. 2005, 288, 185–193. https://doi.org/10.1016/j.apcata.2005.04.030.

(36)   Guo, Y.; Zhu, Z.; Qiu, Y.; Zhao, J. Adsorption of Arsenate on Cu/Mg/Fe/La Layered Double Hydroxide from Aqueous Solutions. J. Hazard. Mater. 2012, 239–240, 279–288. https://doi.org/10.1016/j.jhazmat.2012.08.075.

(37)   Liao, Y.; Li, F.; Dai, X.; Zhao, N.; Xiao, F. Solid Base Catalysts Derived from Ca-M-Al (M = Mg, La, Ce, Y) Layered Double Hydroxides for Dimethyl Carbonate Synthesis by Transesterification of Methanol with Propylene Carbonate. Cuihua Xuebao/Chinese J. Catal. 2017, 38, 1860–1869. https://doi.org/10.1016/S1872-2067(17)62898-5.

(38)   Huang, M. X.; Wu, X.; Yi, X. D.; Han, G. Bin; Xia, W. S.; Wan, H. L. Highly Dispersed CoO_x in Layered Double Oxides for Oxidative Dehydrogenation of Propane: Guest-Host Interactions. RSC Adv. 2017, 7, 14846–14856. https://doi.org/10.1039/c7ra01190c.

(39)   Mishra, G.; Dash, B.; Pandey, S. Layered Double Hydroxides: A Brief Review from Fundamentals to Application as Evolving Biomaterials. Appl. Clay Sci. 2018, 153, 172–186. https://doi.org/10.1016/j.clay.2017.12.021.

(40)   Xu, M.; Wei, M. Layered Double Hydroxide-Based Catalysts: Recent Advances in Preparation, Structure, and Applications. Adv. Funct. Mater. 2018, 28, 1–20. https://doi.org/10.1002/adfm.201802943.

(41)   Qu, J.; Sha, L.; Xu, Z.; He, Z.; Wu, M.; Wu, C.; Zhang, Q. Calcium Chloride Addition to Overcome the Barriers for Synthesizing New Ca-Ti Layered Double Hydroxide by Mechanochemistry. Appl. Clay Sci. 2019, 173, 29–34. https://doi.org/10.1016/j.clay.2019.02.017.

(42)   Yang, W.; Kim, Y.; Liu, P. K. T.; Sahimi, M.; Tsotsis, T. T. A Study by in Situ Techniques of the Thermal Evolution of the Structure of a Mg-Al-CO_3 Layered Double Hydroxide. Chem. Eng. Sci. 2002, 57, 2945–2953. https://doi.org/10.1016/S0009-2509(02)00185-9.

(43)   Cavani, F.; Trifirò, F.; Vaccari, A. Hydrotalcite-Type Anionic Clays: Preparation, Properties and Applications. Catal. Today 1991, 11, 173–301. https://doi.org/10.1016/0920-5861(91)80068-K.

(44)   Di Cosimo, J. I.; Díez, V. K.; Xu, M.; Iglesia, E.; Apesteguía, C. R. Structure and Surface and Catalytic Properties of Mg-Al Basic Oxides. J. Catal. 1998, 178, 499–510. https://doi.org/10.1006/jcat.1998.2161.

(45)   Gazzano, M.; Kagunya, W.; Matteuzzi, D.; Vaccari, A. Neutron Diffraction Studies of Polycrystalline Ni/Mg/Al Mixed Oxides Obtained from Hydrotalcite-like Precursors. J. Phys. Chem. B 1997, 101, 4514–4519. https://doi.org/10.1021/jp963761q.

(46)   Shannon, R. D. Revised Effective Ionic Radii and Systematic Studies of Interatomic Distances in Halides and Chalcogenides. Acta Crystallogr. Sect. A 1976, 32, 751–767. https://doi.org/10.1107/S0567739476001551.

(47)   Terlingen, B.; Oord, R.; Ahr, M.; Hutter, E. M.; van Lare, C.; Weckhuysen, B. M. Favoring the Methane Oxychlorination Reaction over EuOCl by Synergistic Effects with Lanthanum. ACS Catal. 2022, 12, 5698–5710. https://doi.org/10.1021/acscatal.2c00777.

(48)   Paunović, V.; Zichittella, G.; Verel, R.; Amrute, A. P.; Pérez-Ramírez, J. Selective Production of Carbon Monoxide via Methane Oxychlorination over Vanadyl Pyrophosphate. Angew. Chem. Int. Ed. 2016, 55, 15619–15623. https://doi.org/10.1002/anie.201608165.

(49)   Hammes, M.; Valtchev, M.; Roth, M. B.; Stöwe, K.; Maier, W. F. A Search for Alternative Deacon Catalysts. Appl. Catal. B Environ. 2013, 132–133, 389–400. https://doi.org/10.1016/j.apcatb.2012.11.034.

(50)   Zhao, Y.; Li, J. G.; Fang, F.; Chu, N.; Ma, H.; Yang, X. Structure and Luminescence Behaviour of As-Synthesized, Calcined, and Restored MgAlEu-LDH with High Crystallinity. Dalt. Trans. 2012, 41, 12175–12184. https://doi.org/10.1039/c2dt31249b.

(51)   Sharma, U.; Tyagi, B.; Jasra, R. V. Synthesis and Characterization of Mg–Al–CO_3 Layered Double Hydroxide for CO_2 Adsorption. Ind. Eng. Chem. Res. 2008, 47, 9588–9595. https://doi.org/10.1021/ie800365t.

5
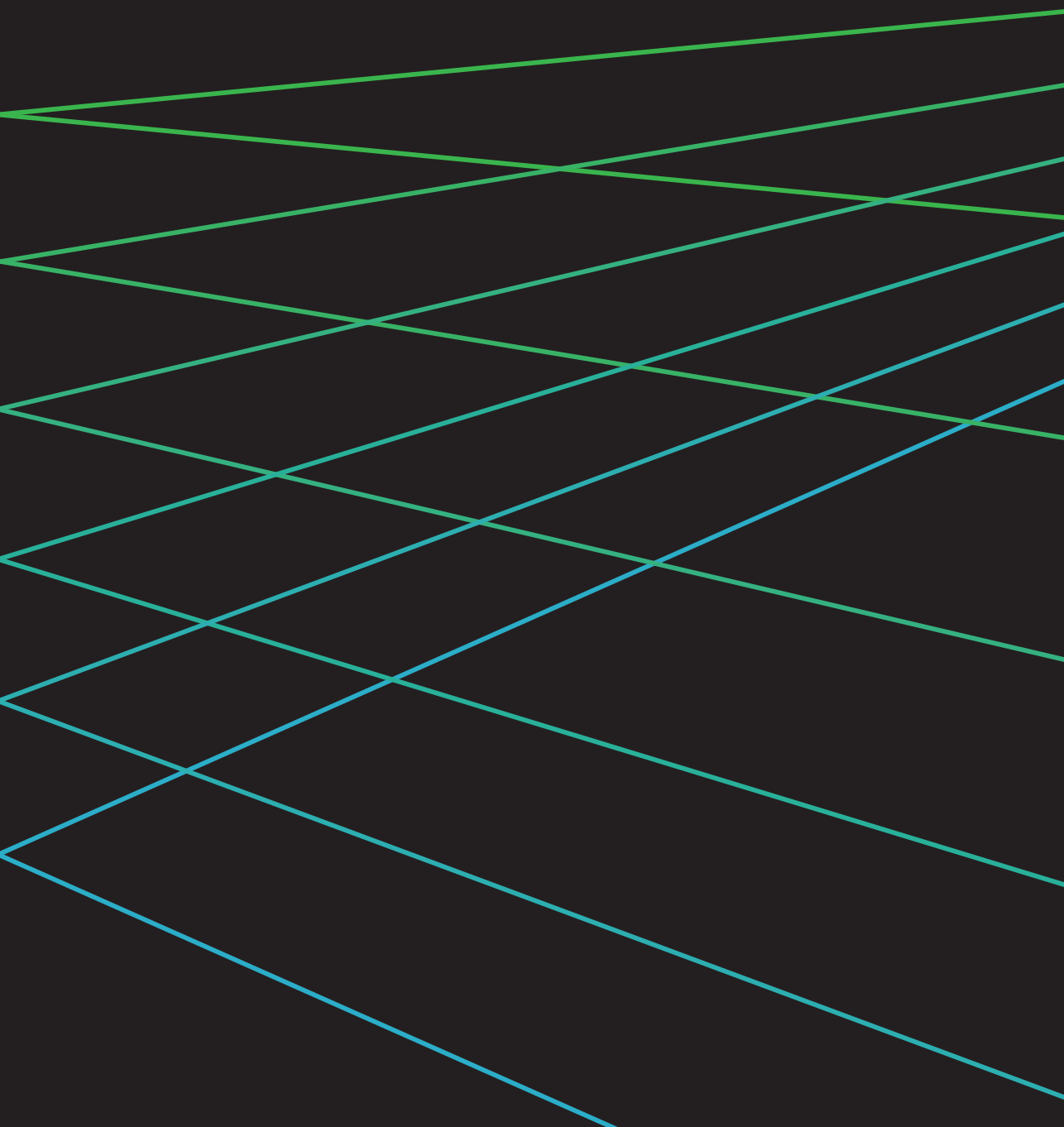
6

**Summary,
Concluding Remarks
and Future Perspectives**

6.1. SUMMARY

The aim of this PhD thesis is to design new catalytic materials for the CH_4 oxychlorination (MOC) reaction and to study these solid catalysts under real working conditions by applying light, i.e., using the operando spectroscopy approach. In this way, the activity and spectroscopic information can be coupled, yielding crucial mechanistic insights to improve the design of the catalytic materials. The presented work reveals that redox properties, bulk and synergistic effects play a crucial role in the working mechanism of bulk MOC catalysts. These features determine the activity, as well as the activity/selectivity relation and the stability of the solid catalysts. Operando spectroscopy did not only provide mechanistic insights, but also made correlations between the catalyst temperature and the reaction rate possible.

The experimental investigation of this study started in chapter 2 with a screening of the lanthanide-series as active metals in the MOC reaction. A set of lanthanide oxychloride (i.e., LnOCl with Ln = La, Pr, Nd, Sm, Eu, Gd, Tb, Dy, Ho) and Er- and Yb-based catalysts were synthesized, characterized and tested. After an initial screening of the catalytic performances, EuOCl came out as the most promising candidate. The EuOCl catalyst possessed the highest MOC activity, the best activity/selectivity relation and was proven to be stable. Moreover, the catalytic performance of EuOCl could be tuned by increasing the HCl concentration in the feed, thereby mitigating the unwanted catalytic destruction of chloromethanes to CO_x. Operando Raman spectroscopy revealed that the chlorination of the catalyst was rate limiting as an increase in the HCl concentration in the feed resulted in enhancement of activity, but did not cause bulk chlorination of the catalyst. This implies that any Cl^- present in the catalyst material reacted away before it could diffuse from the outer surface to the bulk phase. Due to the tuneability of the catalytic performance, the redox properties and ability to deduct spectroscopic information, chapter 3, 4 and 5 focussed on the use of Eu^{3+} in the MOC reaction.

While EuOCl appeared promising as a MOC catalyst, its catalytic performance was limited by the rate of chlorination. The catalyst design was improved in chapter 3 by adding a chlorinating agent for Eu^{3+}. Thermodynamic calculations and operando Raman spectroscopy experiments revealed that the chlorination of LaOCl to $LaCl_3$ was very facile, but LaOCl was not very active. Thus, its properties seemed complementary to those of EuOCl. The La^{3+}-Eu^{3+} catalysts revealed clear synergistic effects in the MOC reaction. The activity of all bimetallic catalysts was significantly higher than anticipated for the linear combination of LaOCl and EuOCl. $La_{0.50}Eu_{0.50}OCl$ is almost as active as EuOCl, even though LaOCl does not show any significant activity under the applied conditions. More important was the fact that the activity/selectivity relationship was significantly improved. A higher CH_3Cl selectivity could be achieved without giving in on the excellent CO selectivity obtained for monometallic EuOCl. The harsh reaction conditions caused phase segregation between the La^{3+} and Eu^{3+}, but the synergy could be assured due to the fact that a physical mixture of pure LaOCl and EuOCl revealed the same synergy as the solid solutions, with the proviso that intimate contact between LaOCl and EuOCl is achieved. Operando lumines-

CHAPTER 2

CHAPTER 3
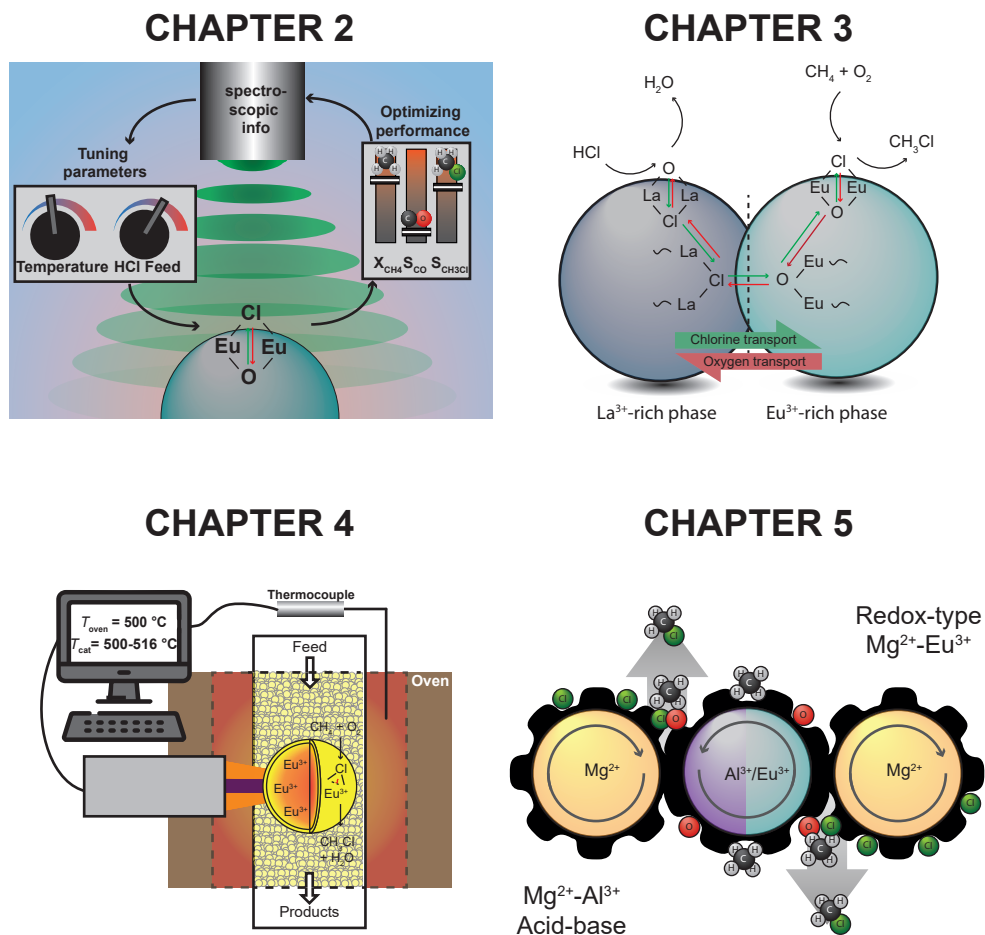
CHAPTER 4

CHAPTER 5

Figure 6.1. Table of content figures of chapter 2, chapter 3, chapter 4 and chapter 5.

cence spectroscopy revealed that La^{3+} acted as a chlorinating agent for Eu^{3+}, even when the phases were completely segregated as in the case for the physical mixture. Actually, when starting from completely segregated phases, incorporation of Eu^{3+} into LaOCl was observed, ensuring the long-term stability of the synergistic effect. Hence, by matching intrinsic material properties, the design of EuOCl could be significantly improved.

The fact that operando luminescence spectroscopy could be performed on Eu^{3+}-based catalysts, opened up the possibility to measure the temperature of the catalyst under reaction conditions. In chapter 4, the bifunctionality of Eu^{3+} as catalytic centre and thermometer was exploited to correlate the catalyst temperature to the applied reaction conditions. The population of two thermally coupled states could be applied as a measure for the catalyst temperature. A catalyst temperature of maximum 16 °C higher compared to the oven temperature was recorded, due to the exothermic nature of the MOC

reaction. The reaction rate was positively correlated to the catalyst temperature, while the gas hourly space velocity (GHSV) did not correlate. Heat dissipation by means of radiation was identified as the main heat loss mechanism, resulting in a uniform catalyst bed temperature. By applying operando catalyst thermometry, the observed catalytic performance could be linked to the actual catalyst temperature, gaining more insights in arguably one of the most important reaction parameters.

Lastly, in chapter 5 a deeper dive is taken into the importance of synergistic effects and redox properties for the design of MOC catalysts. The concept that irreducible elements can make up a very active catalyst for the MOC reaction is proven by the design of irreducible Mg^{2+}-Al^{3+} mixed-metal oxide (MMO) catalysts. The Mg_4Al MMO possessed one of the highest reported activities under the tested reaction conditions, which was all the more surprising considering that MgO and γ-Al_2O_3 did not show any significant activity. Operando Raman spectroscopy revealed that Mg^{2+} acted as a Cl^- buffer and as a chlorinating agent for Al^{3+}, which was the active metal in the CH_4 activation step. Even though exceptional activity was obtained, the activity/selectivity relation did not meet benchmark standards and could not be tuned by altering the feed. Additionally, the Mg^{2+}-Al^{3+} MMO's deactivated under increasing HCl concentrations. A third element, Eu^{3+}, was homogeneously incorporated into the MMO structure by the partial replacement of Al^{3+}. Adding 2 atom-% of the redox active Eu^{3+} in the material doubled the activity, made the activity/selectivity relation tuneable and preserved the activity under high HCl concentrations. Combined operando Raman and luminescence spectroscopy revealed that the chlorination behaviour of Mg^{2+} and Eu^{3+} were correlated, and we therefore hypothesize that Mg^{2+} also acted as a chlorinating agent for Eu^{3+}. These results indicate that both redox activity as well as synergistic effects are required to obtaining benchmark performance.

6.2. CONCLUDING REMARKS

With the development of several new catalytic materials in this PhD thesis, it is important to reflect on how these solid catalysts compare to benchmark catalysts in the academic literature. For the benchmark catalysts reported in literature and the catalyst materials reported in this PhD thesis, the CH_3Cl selectivity (S_{CH3Cl}) was plotted versus the temperature at which the X_{CH4} reached 10%, while the color indicates the reaction rate (Figure 6.2A). While many catalytic systems show a S_{CH3Cl} above 70% at $X_{CH4} = 10\%$, a large portion of these catalytic systems are not stable or were not tested for their stability. To comply with the stability criterium reported in chapter 1.4.1., only the catalysts reported as stable in terms of chemical, structural and catalytic stability are considered (Figure 6.2B). Now, only a few catalytic systems show S_{CH3Cl} above 70% at $X_{CH4} = 10\%$, making $La_{0.50}Eu_{0.50}OCl$ a benchmark catalyst. The (Eu)MgAl MMO catalyst materials however cannot compete with the benchmark catalysts reported in the open literature. Even though these catalysts exhibit a high reaction rate, the S_{CH3Cl} does not meet the required standard.

The true value of the presented work lies in the obtained mechanistic insights by per-
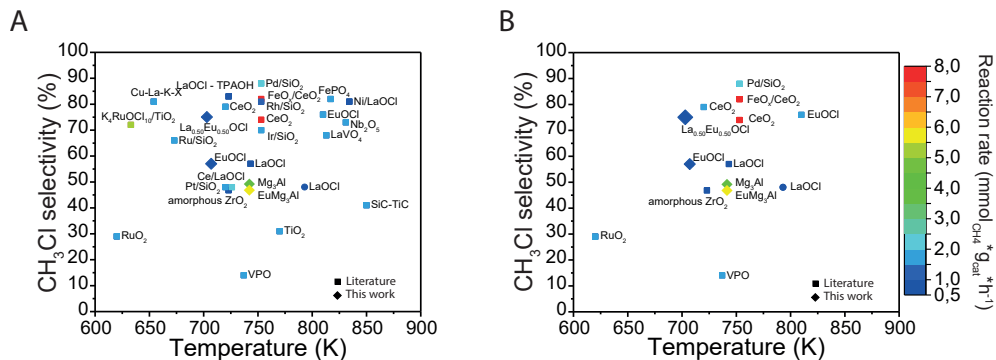
Figure 6.2. (A) The CH$_3$Cl selectivity plotted versus the temperature at which 10% CH$_4$ conversion is reached for the catalyst systems reported after 2006 in the academic literature including the catalysts reported in this PhD thesis. The colour of the symbol represents the reaction rate, normalized to the catalyst weight (g$_{catalyst}$). (B) The CH$_3$Cl selectivity plotted versus the temperature at which 10% CH$_4$ conversion is reached for the catalytic systems in (A) for which stable (chemical, structural and/ or catalytic) performance is reported.

forming operando spectroscopy. The concepts of bulk ion diffusion, synergistic effects and redox properties are central to this PhD thesis, but were not very well-known concepts in the field of MOC. The investigation into these concepts for other benchmark catalysts, e.g., Ce^{4+}-based, could advance the fields of oxychlorination chemistry.

The industrial application of bulk lanthanide-based catalyst materials would impose a serious supply chain risk as all the lanthanide elements are on the list of critical elements, mostly because of geopolitical reasons.[1] The bulk lanthanide-based catalysts presented in this study did not meet the activity/selectivity and production rates required for industrial application, but research is still in its infancy. The use of lanthanides as catalyst materials cannot be excluded as active catalyst compositions can be made. If an industrial catalyst would constitute of lanthanide elements, care must be taken to limit their use in order to minimize the dependance on geopolitics.

In a broader perspective, the MOC reaction presents a serious use-case for the on-site production of liquefied CH$_4$. The desired CH$_3$Cl is a valuable product and can be regarded as a chemical building block. It is therefore a pity to note that only a handful of articles are published in the academic literature in the last five years. The niche business, safety hazards, environmental issues and the challenging experimental set-up result in the fact that the MOC is an unpopular reaction to work on. However, in my opinion, the MOC reaction deserves to be investigated more thoroughly. Even though little research has been performed on the topic, already a fairly good activity-selectivity relation can be obtained compared to other direct CH$_4$ conversion processes. The fact that performing the reaction is experimentally challenging and potentially hazardous should not hold back research from being conducted. Pivotal in the intensification of the research is that knowledge must be transferred between parties. In this work, the close collaboration with the industrial partner Nobian accelerated the research as the input from industry helped to set clear catalyst design criteria. The knowledge transfer made the construc-

tion of an experimental set-up safer and more robust. I truly hope that, preferably in the form of collaborations, more research will be conducted towards this interesting reaction as it could have a bright future ahead.

6.3. FUTURE PERSPECTIVES

6.3.1. Fundamental Understanding of the Methane Oxychlorination and Side Reactions

The rational design of new catalyst materials in the MOC reaction is still in its infancy, but benchmark catalysts for this process based on Ce^{4+}, Eu^{3+} and Pd^{2+} seem very promising for further development.[2–4] However, the full reaction mechanism under reaction conditions is clearly very complex. Besides the surface MOC reaction, the catalytic destruction of chloromethanes, gas-phase chlorination via Cl_2 evolution and bulk effects occur simultaneously. These reactions need to be studied individually to understand how e.g., the catalytic destruction of chloromethanes can be prevented, thereby directly improving the overall activity/selectivity relation. An important note is that the role of the support in these reactions must be included in the analysis, as most of the commonly used supports, e.g., SiO_2, γ-Al_2O_3 and TiO_2, are not innocent and can catalyse some of the (side) reactions. Hence, their inertness to a certain reaction determines their applicability as support material.

In order to obtain a fundamental understanding of the different reactions, the operando characterization toolbox for the MOC reaction needs to be expanded. In this PhD thesis, mainly bulk effects were studied by the application of operando Raman and luminescence spectroscopy which was proven a powerful analytical approach. However, operando characterization of surface species and redox properties would be great additions to get a more complete view of the mechanisms at play, thereby enabling the construction of more detailed reaction mechanisms. Diffuse reflectance infrared Fourier transform spectroscopy (DRIFTS) was tried in this PhD thesis to gain more information on surface species. However, chemical degradation of the DRIFTS cell and windows occurred within one experiment due to the corrosive reaction conditions of the MOC reaction, making the practical applicability of DRIFTS in oxychlorination reactions cumbersome, if not simply improbable. Hence, alternative techniques need to be developed to be able to deduct valuable information on the surface composition. The use of shell-isolated nanoparticle-enhanced Raman spectroscopy (SHINERS) could be a viable option (Figure 6.3A). The plasmonic resonance between two shell-isolated nanoparticles (SHINs) boosts the Raman scattering significantly and thereby enabling the study of species with low Raman signal or short lived lifetimes.[5] In this way, the Raman scattering intensity of surface species dominates over the bulk Raman scattering and adsorbates/intermediate species can be observed. As SiO_2 is stable under the challenging operating conditions, it would be possible to deposit the catalytically active material on SiO_2-coated plasmonic nanoparticles (SiO_2-NP). SHINs are reported to be able to withstand temperatures up to 400°C, which overlaps with the lower operating temperature of the MOC reaction.[5] The great ad-

A

Enhanced Surface Raman Signal

SiO$_2$

Eu^{3+}

Au

B

X-ray Source

Eu^{3+} Eu^{3+}
Eu^{2+}
Eu^{2+} Eu^{3+}
Eu^{2+} Eu^{3+} Eu^{2+}
Eu^{3+} Eu^{3+} Eu^{3+}
Eu^{3+} Eu^{2+}
Eu^{3+} Eu^{3+} Eu^{2+}
Eu^{3+}
Eu^{2+}

To detector
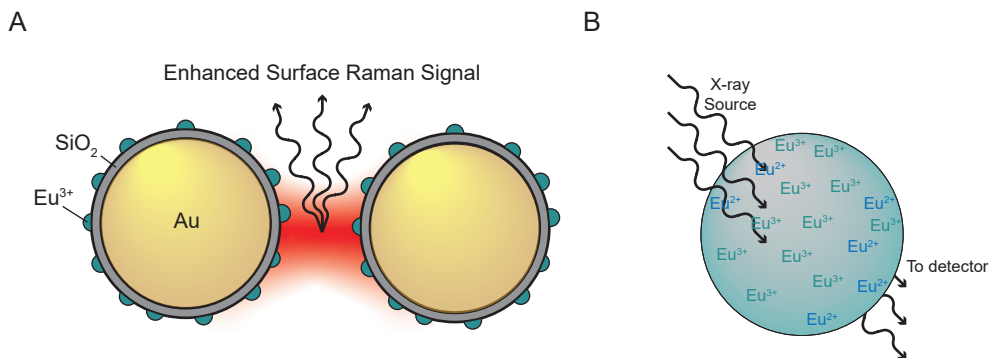
Figure 6.3. The expansion of the operando characterization toolbox could be achieved by applying (a) Surface-Enhanced Raman Spectroscopy (SERS) and (b) X-ray Absorption Spectroscopy in the field of CH$_4$ oxychlorination (MOC).
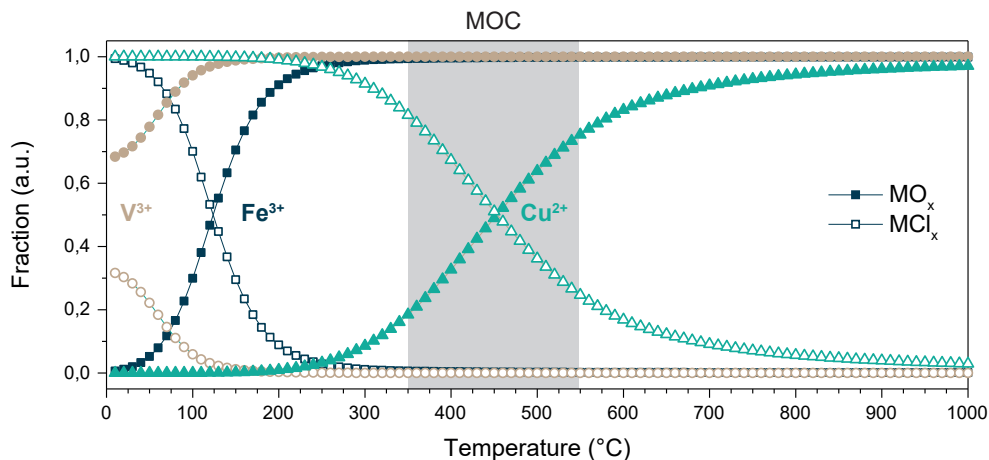
Figure 6.4. Thermodynamic equilibria compositions from 100 - 1000 °C of the chlorination of the metal oxide with stoichiometric amounts of HCl as calculated with HSC chemistry 9 equilibrium compositions package. Under CH$_4$ oxychlorination reaction conditions (grey box), V^{3+} and Fe^{3+} are in the dechlorinated state. Reference Cu^{2+} is still in a partially chlorinated state.

vantage of this analytical technique is that it would be possible to perform these Raman spectroscopy experiments within the designated catalytic set-up, that is resistant to the corrosive environment.

Clear from chapter 5 is that redox properties play an important role in the reaction mechanism and can drastically boost the activity. Pioneering work by Pérez-Ramírez et al. has shown that operando electron paramagnetic resonance (EPR) is a powerful tool to analyse the redox dynamics under reaction conditions.[6] For EuOCl, Eu^{2+}/Eu^{3+} redox couple exists in C$_{2+}$ oxychlorination, even under oxidative conditions at elevated temperatures.[7] The balanced redox properties of Eu^{2+}/Eu^{3+} are held accountable for the high activity while maintaining a low CO selectivity for C$_{2+}$ oxychlorination. Besides operando EPR, operando x-ray absorption spectroscopy (XAS) would be highly interesting, providing information about the oxidation state as well as the local environment during the

MOC reaction (Figure 6.3B).[8] This would be pioneering work since the oxychlorination reactions have never been performed, while performing XAS to our knowledge. More general applicability of these high-end techniques in the MOC reaction could provide the required mechanistic insights that are currently lacking.

6.3.2. Mixed Metal Oxide as Matrix for Development of Methane Oxychlorination Catalysts

It is obvious that the "shotgun" approach, classically applied in the field for the discovery of interesting catalytic materials, needs to be replaced by a more methodical approach in which a more fundamental understanding of the catalysis is deducted. The mixed-metal oxide (MMO) offers a matrix in which specific elemental properties and functionalities can be investigated. This approach seems promising due to the wide variety in chemical compositions that can be synthesized with ease, while obtaining relatively comparable physicochemical properties. In chapter 5 the synergistic effect between Mg^{2+} and Al^{3+} could be investigated as well as the effect of adding Eu^{3+}, introducing redox properties and allowing for tunability of the activity/selectivity. Hence, the MMO allows for the rational design of new catalyst materials, which is especially interesting in the field of MOC where little is known about elemental properties and reaction mechanisms. It becomes clear from the results described in chapter 5 that Al^{3+} might not be the best choice due to the fact that it is highly active in the catalytic destruction of chloromethanes, making the suppression of the CO selectivity virtually impossible. However, Al^{3+} is needed for obtaining the exceptionally high activity. The (partial) substitution of Al^{3+} for another trivalent element, e.g., Fe^{3+} or V^{3+}, could circumvent the issues associated with the use of Al^{3+}, while still preserving the activity and MMO structure. Even though both $FeCl_3$ and VCl_3 both exhibit low boiling points, the chlorination of these trivalent metals is not facile at elevated temperatures, just as in the case of Al^{3+} (Figure 6.4). Hence, rapid loss of catalytic material under reaction conditions is not expected, but the stability of the solid catalysts must be analysed carefully. Furthermore, MMO compositions including a tetravalent element have been reported, including Ti^{4+}, Ce^{4+} and Zr^{4+}, which could all be interesting options for a potential MOC catalyst as these metals were proven stable under oxychlorination conditions.[9–12] The divalent Ca^{2+}, Mn^{2+}, Fe^2, Ni^{2+} and noble metals (e.g., Pd^{2+} and Ru^{2+}) are potential (partial) replacements for the Mg^{2+}. The analysis of benchmark Ce^{4+} and Pd^{2+} within the MMO matrix could provide additional insights in their catalytic behaviour compared to Eu^{3+}.

6.2.3. Development and Application of Operando Thermometry for Catalysis

Even though it sounds very trivial, the applied reaction conditions hugely influence the catalyst temperature; a fact that is often not considered. The implications on reaction kinetics, thermodynamics and catalyst stability can be drastic, but this is still a largely unexplored field in catalysis research. A critical problem often encountered is that published results cannot be exactly reproduced. The field of the MOC reaction is certainly no exception, as both LaOCl and EuOCl were tested in this PhD thesis, but the results did not match well with LaOCl and EuOCl from the literature (Figure 6.2). Similar problems

are encountered during the upscaling of a process, where typically the catalyst performance does not match with the performance obtained in lab-scale experiments. In both cases, multiple factors vary between these experiments, e.g., reactor dimensions and design, feed composition, method of temperature read-out, etc.. Comparing the activity at the same catalyst temperature might reduce the error obtained between results. Hence, testing the validity of reporting the performance not only versus the reaction temperature, but also versus the catalyst temperature, could advance the field.
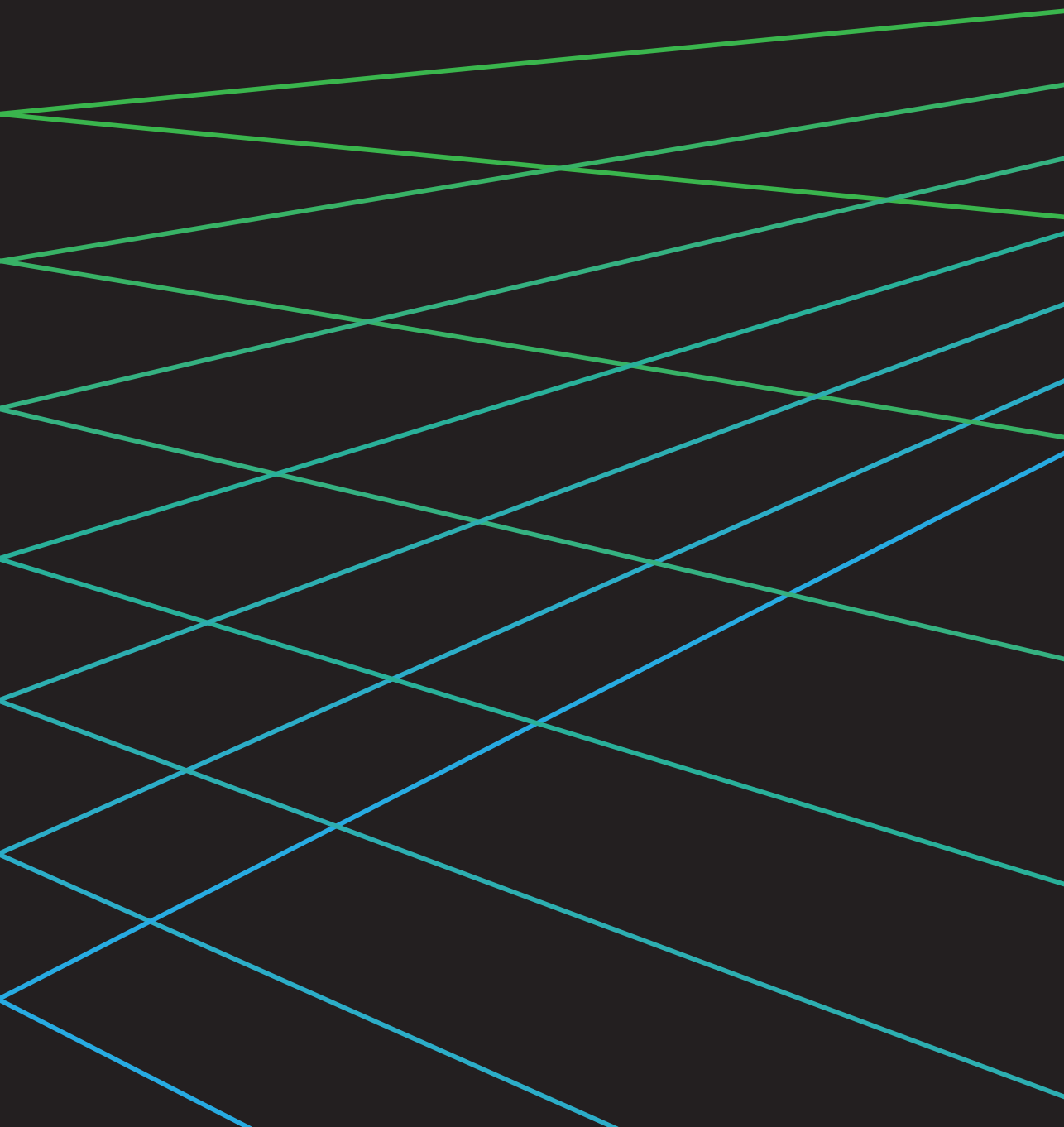
In order to do so, thermometric (catalyst) materials must be developed for a wide variety of applications. Thermometric particles, e.g., $NaYF_4:Er^{3+},Yb^{3+}/SiO_2$, offer a solution that is already proven viable for catalytic reactions.[13] The alternative approach is that the thermometric functionality is built in the catalyst. The bifunctionality of EuOCl, reported in chapter 4, is quite unique in the sense that not many luminescent materials exhibit great catalytic activity. Nevertheless, the oxyhalogenation reactions are very well suited to be studied in such a manner as benchmark solid catalysts can be synthesized from lanthanide elements.[14–18] Here, the catalyst itself is also the thermometric material. The second option to incorporate the thermometric functionality is by the partial replacement of a non-luminescent lanthanide with a luminescent lanthanide. Examples include the Ni/La_2O_3/Al_2O_3 reforming catalyst where La^{3+} can be replaced by any other lanthanide, depending on the application/reaction conditions.[19] Lastly, the application of luminescent support materials[19–21] as thermometric material would open up the possibility to perform operando thermometry in reactions where lanthanides typically do not play a role. This would also enable the functionalization of binder materials, commonly used to make catalyst extrudates. Fixating the luminescent probe in the framework of the support might also enhance the stability of the thermometer, making it suitable for long-term application.[13] Thus, expanding the palette of thermometric (catalyst) materials broadens the applicability of operando thermometry in a wide variety of chemical reactions, providing additional insights in reaction kinetics, thermodynamics and stability.

6.4. REFERENCES

(1)   Blengini, G. A.; Latunussa, C. EL; Eynard, U.; Matos, C. T. de; Wittmer, D.; Georgitzikis, K.; Pavel, C.; Carrara, S.; Mancini, L.; Unguru, M.; Blagoeva, D.; Mathieux, F.; Pennington, D. Study on the Eu's List of Critical Raw Materials - Critical Raw Materials Factsheets; 2020. https://doi.org/10.2873/11619.

(2)   Paunović, V.; Zichittella, G.; Hemberger, P.; Bodi, A.; Pérez-Ramírez, J. Selective Methane Functionalization via Oxyhalogenation over Supported Noble Metal Nanoparticles. ACS Catal. 2019, 9, 1710–1725. https://doi.org/10.1021/acscatal.8b04375.

(3)   Paunović, V.; Zichittella, G.; Verel, R.; Amrute, A. P.; Pérez-Ramírez, J. Selective Production of Carbon Monoxide via Methane Oxychlorination over Vanadyl Pyrophosphate. Angew. Chem. Int. Ed. 2016, 55, 15619–15623. https://doi.org/10.1002/anie.201608165.

(4)   He, J.; Xu, T.; Wang, Z.; Zhang, Q.; Deng, W.; Wang, Y. Transformation of Methane to Propylene: A Two-Step Reaction Route Catalyzed by Modified CeO_2 Nanocrystals and Zeolites. Angew. Chem. Int. Ed. 2012, 51, 2438–2442. https://doi.org/10.1002/anie.201104071.

(5)   Hartman, T.; Wondergem, C. S.; Weckhuysen, B. M. Practical Guidelines for Shell-Isolated Nanoparticle-Enhanced Raman Spectroscopy of Heterogeneous Catalysts. ChemPhysChem 2018, 19, 2461–2467. https://doi.org/10.1002/cphc.201800509.

(6)   Zichittella, G.; Polyhach, Y.; Tschaggelar, R.; Jeschke, G.; Pérez-Ramírez, J. Quantification of Redox Sites during Catalytic Propane Oxychlorination by Operando EPR Spectroscopy. Angew. Chem. Int. Ed. 2021, 60, 3596–3602. https://doi.org/10.1002/anie.202013331.

(7)   Zichittella, G.; Aellen, N.; Paunović, V.; Amrute, A. P.; Pérez-Ramírez, J. Olefins from Natural Gas by Oxychlorination. Angew. Chem. Int. Ed. 2017, 56, 13670–

13674. https://doi.org/10.1002/anie.201706624.

(8)   Vrijburg, W. L.; Moioli, E.; Chen, W.; Zhang, M.; Terlingen, B. J. P.; Zijlstra, B.; Filot, I. A. W.; Züttel, A.; Pidko, E. A.; Hensen, E. J. M. Efficient Base-Metal NiMn/TiO$_2$ Catalyst for CO$_2$ Methanation. ACS Catal. 2019, 9, 7823–7839. https://doi.org/10.1021/acscatal.9b01968.

(9)   Roy Chowdhury, P.; Verma, V.; Medhi, H.; Bhattacharyya, K. G. Empirical Modeling of Electron Transport in Fe/Ti Layered Double Hydroxide Using Exponential, Gaussian and Mixed Gauss-Exponential Distribution. ACS Omega 2019, 4, 10599–10609. https://doi.org/10.1021/acsomega.9b01345.

(10)   Qu, J.; Sha, L.; Xu, Z.; He, Z.; Wu, M.; Wu, C.; Zhang, Q. Calcium Chloride Addition to Overcome the Barriers for Synthesizing New Ca-Ti Layered Double Hydroxide by Mechanochemistry. Appl. Clay Sci. 2019, 173, 29–34. https://doi.org/10.1016/j.clay.2019.02.017.

(11)   Li, H.; Wang, X.; Liu, Y.; He, Y.; Feng, J.; Li, D. Pd Nanoparticles Loaded on CoAlCe Layered Double Oxide Nanosheets for Phenol Hydrogenation. ACS Appl. Nano Mater. 2021, 4, 11820–11829. https://doi.org/10.1021/acsanm.1c02398.

(12)   Yan, Z.; Liu, S.; Zhang, Y.; Wang, T.; Luo, S.; Chu, W.; Jing, F. The Role of Zr in NiZrAl Oxides Catalyst and the Evaluation on Steam Reforming of Glycerol for Hydrogen Product. Catal. Today 2019, 319, 229–238. https://doi.org/10.1016/j.cattod.2018.03.055.

(13)   Geitenbeek, R. G.; Prins, P. T.; Albrecht, W.; Van Blaaderen, A.; Weckhuysen, B. M.; Meijerink, A. NaYF$_4$:Er^{3+},Yb^{3+}/SiO$_2$ Core/Shell Upconverting Nanocrystals for Luminescence Thermometry up to 900 K. J. Phys. Chem. C 2017, 121, 3503–3510. https://doi.org/10.1021/acs.jpcc.6b10279.

(14)   Terlingen, B.; Oord, R.; Ahr, M.; Hutter, E. M.; van Lare, C.; Weckhuysen, B. M. Favoring the Methane Oxychlorination Reaction over EuOCl by Synergistic Effects with Lanthanum. ACS Catal. 2022, 12, 5698–5710. https://doi.org/10.1021/acscatal.2c00777.

(15)   Paunović, V.; Lin, R.; Scharfe, M.; Amrute, A. P.; Mitchell, S.; Hauert, R.; Pérez-Ramírez, J. Europium Oxybromide Catalysts for Efficient Bromine Looping in Natural Gas Valorization. Angew. Chem. Int. Ed. 2017, 56, 9791–9795. https://doi.org/10.1002/anie.201704406.

(16)   Zichittella, G.; Paunović, V.; Pérez-Ramírez, J. Mechanistic Understanding of Halogen-Mediated Catalytic Processes for Selective Natural Gas Functionalization. Chim. Int. J. Chem. 2019, 73, 288–293. https://doi.org/10.2533/chimia.2019.288.

(17)   Scharfe, M.; Zichittella, G.; Paunović, V.; Pérez-Ramírez, J. Ceria in Halogen Chemistry. Chin. J. Catal. 2020, 41, 915–927. https://doi.org/10.1016/S1872-2067(19)63528-X.

(18)   Scharfe, M.; Lira-Parada, P. A.; Amrute, A. P.; Mitchell, S.; Pérez-Ramírez, J. Lanthanide Compounds as Catalysts for the One-Step Synthesis of Vinyl Chloride from Ethylene. J. Catal. 2016, 344, 524–534. https://doi.org/10.1016/j.jcat.2016.10.026.

(19)   Haryanto, A.; Fernando, S.; Murali, N.; Adhikari, S. Current Status of Hydrogen Production Techniques by Steam Reforming of Ethanol: A Review. Energy and Fuels 2005, 19, 2098–2106. https://doi.org/10.1021/ef0500538.

(20)   Hirata, G.; Perea, N.; Tejeda, M.; Gonzalez-Ortega, J. A.; McKittrick, J. Luminescence Study in Eu-Doped Aluminum Oxide Phosphors. Opt. Mater. 2005, 27, 1311–1315. https://doi.org/10.1016/j.optmat.2004.11.029.

(21)   Myint, T.; Gunawidjaja, R.; Eilers, H. Spectroscopic Properties of Nanophase Eu-Doped ZrO$_2$ and Its Potential Application for Fast Temperature Sensing under Extreme Conditions. J. Phys. Chem. C 2012, 116, 21629–21634. https://doi.org/10.1021/jp307092b.

(22)   Geitenbeek, R. G.; Salzmann, B. B. V.; Nieuwelink, A.-E.; Meijerink, A.; Weckhuysen, B. M. Chemically and Thermally Stable Lanthanide-Doped Y$_2$O$_3$ Nanoparticles for Remote Temperature Sensing in Catalytic Environments. Chem. Eng. Sci. 2019, 198, 235–240. https://doi.org/10.1016/j.ces.2018.10.004.

6

7

Appendices

List of Abbreviations
Nederlandse Samenvatting
List of Publications and Presentations
Acknowledgements
Curriculum Vitae

APPENDIX A: LIST OF ABBREVIATIONS

AD	Anaerobic Digestion
CCUS	Carbon Capture Utilization And Storage
CFC	Chlorofluorocarbon
CM	Chlorinated Methane
COD	Crystallography Open Database
DFT	Density Functional Theory
DRIFTS	Diffuse Reflectance Infrared Fourier Transform Spectroscopy
Eapp	Apparent Activation Energy
ΔE	Energy Gap
EDS	Electron Dispersive X-Ray Spectroscopy
EPR	Electron Paramagnetic Resonance
FID	Flame Ionization Detector
FTS	Fischer-Tropsch Synthesis
GHSV	Gas Hourly Space Velocity
HAADF-STEM	High-Angle Annular Dark Field-Scanning Transmission Electron Microscopy
ICDD	International Centre For Diffraction Data
ICP-OES	Inductively Coupled Plasma-Optical Emission Spectroscopy
LDH	Layered Double Hydroxide
LNG	Liquefied Natural Gas
MCTO	Methyl Chloride To Methanol
MDA	Methane Dehydroaromatization
MMO	Mixed-Metal Oxide
MOB	Methane Oxybromination
MOC	Methane Oxychlorination
MOH	Methane Oxyhalogenation
MTM	Methane-to-Methanol
NP	Nanoparticle
OCM	Oxidative Coupling Of Methane
ODS	Ozone Depleting Substances
PM	Physical Mixture
RDS	Rate-Determining Step
S_{BET}	Surface Area According to The Brunauer-Emmett-Teller Theory
SHIN	Shell-Isolated Nanoparticles
SHINERS	Shell-Isolated Nanoparticle-Enhanced Raman Spectroscopy
STM	Syngas To Methanol
TCD	Thermal Conductivity Detector
TEM	Transmission Electron Microscopy

TOS	Time-on-Stream
VCM	Vinyl Chloride Monomer
V_{pore}	Pore Volume
XAS	X-Ray Absorption Spectroscopy
X_{CH4}	Methane Conversion
X_{O2}	Oxygen Conversion
XRD	X-Ray Diffraction
$\Delta_r G$	Reaction Gibbs Free Energy
$\Delta_r H$	Reaction Enthalpy

7

APPENDIX B: NEDERLANDSE SAMENVATTING

Het doel van dit proefschrift is om nieuwe katalysatoren te ontwerpen voor de oxidatieve chlorering van methaan (CH_4). De nieuwe katalysatoren worden bestudeert onder werkende condities door gebruik te maken van licht, ook wel *operando* spectroscopie genoemd. Op deze manier kunnen de activiteit van de katalysator en de spectroscopische informatie aan elkaar gekoppeld worden, wat cruciale inzichten geeft om het ontwerp van de katalysator te verbeteren. Het gepresenteerde werk laat zien dat reductie/oxidatie (redox) eigenschappen, bulk en synergetische effecten een belangrijke rol spelen in het werkingsmechanisme van bulk katalysatoren voor de oxidatieve chlorering van CH_4. Deze eigenschappen bepalen de activiteit, stabiliteit en de activiteit-selectiviteit relatie van de katalysator. Het toepassen van *operando* spectroscopie maakte het niet alleen mogelijk om het ontwerp van de katalysator te verbeteren, maar ook om de temperatuur van de katalysator te koppelen aan de reactiesnelheid.

Het onderzoek startte in **hoofdstuk 2** waarin een screening van de lanthaniden serie als actief materiaal in de oxidatieve chlorering gerapporteerd werd. Een set van lanthaniden oxychloriden (*i.e.*, LnOCl waar Ln = La, Pr, Nd, Sm, Eu, Gd, Tb, Dy, Ho) en Er- en Yb-gebaseerde katalysatoren werden gesynthetiseerd, gekarakteriseerd en getest. Uit een initiële screening bleek dat de katalytische eigenschappen van EuOCl het meest belovend waren. De EuOCl katalysator beschikte over de hoogste activiteit, de beste activiteit/selectiviteit relatie en was stabiel over een langere periode in de reactie. Verder konden de katalytische eigenschappen van EuOCl gevarieerd worden door de reactieparameters, zoals de HCl concentratie in de toevoer, te veranderen. De ongewenste katalytische destructie van de geproduceerde chloromethanen naar CO_x kon hierdoor onderdrukt worden. *Operando* Raman spectroscopie bewees dat het chloreren van de katalysator limiterend was in de reactie. Dit bleek uit het feit dat een verhoging van de HCl concentratie in de toevoer resulteerde in een verhoogde activiteit, maar tegelijkertijd niet zorgde voor de faseverandering van EuOCl naar $EuCl_3$. Deze observatie impliceert dat het aanwezige chloor op het oppervlakte van de katalysator weg reageert voordat het chloor het deeltje in diffundeert. Doordat de katalytische eigenschappen van EuOCl makkelijk verandert konden worden, en doordat Eu^{3+} goed te bestuderen valt met *operando* spectroscopie, staat het gebruik van Eu^{3+} centraal als actief element voor de oxidatieve chlorering van CH_4 in **hoofdstukken 3, 4 en 5**.

Alhoewel EuOCl een veelbelovend materiaal lijkt voor de oxidatieve chlorering van CH_4, wordt de katalytische prestatie gehinderd door de snelheid waarmee de katalysator chloreert. Het ontwerp van de katalysator werd verbeterd in **hoofdstuk 3** door een element toe te voegen die de chlorering van Eu^{3+} faciliteert. Thermodynamische berekeningen en *operando* Raman spectroscopie bewezen dat de chlorering van LaOCl naar $LaCl_3$ erg gemakkelijk was. De eigenschappen van La^{3+} lijken daarom complementair aan de eigenschappen van Eu^{3+}. Het paren van de thermodynamische eigenschappen gaf als resultaat dat de La^{3+}-Eu^{3+} katalysatoren synergetische eigenschappen vertoonden in de reactie. De activiteit van alle bimetallische katalysator was aanzienlijk hoger dan verwacht werd voor de lineaire combinatie van de activiteiten van LaOCl en EuOCl. $La_{0.50}Eu_{0.50}OCl$ was bijna even actief als EuOCl, on-

danks dat LaOCl bijna geen activiteit vertoonde onder de dezelfde condities. Belangrijker was het feit dat de activiteit-selectiviteit relatie sterk was verbeterd. Een hogere CH_3Cl opbrengst kon worden verkregen zonder daarbij de selectiviteit naar CO te verhogen. *Operando* luminescentie spectroscopie bewees dat La^{3+} de chlorering van Eu^{3+} faciliteerde, zelfs wanneer er twee compleet gesegregeerde fases van LaOCl en EuOCl bestonden. Verrassend genoeg was er zelfs menging van Eu^{3+} in LaOCl te observeren voor het fysieke mengsel van LaOCl en EuOCl, wat het behoud van het synergetische effect tussen La^{3+} en Eu^{3+} garandeert. Concluderend, door materiaaleigenschappen te paren, was het mogelijk om het ontwerp van EuOCl aanzienlijk te verbeteren.

In **hoofdstuk 4** werden de bifunctionele eigenschappen van Eu^{3+} als katalysator en thermometer geëxploiteerd om de katalysatortemperatuur te correleren aan de reactiecondities. De populatie van twee thermisch gekoppelde energieniveaus kon gebruikt worden als een maat voor de katalysatortemperatuur. Het grootst gemeten verschil tussen de katalysatortemperatuur en de oventemperatuur was 16 °C, veroorzaakt door de exothermiciteit van de reactie. De reactiesnelheid liet een positieve correlatie zien met de katalysator temperatuur, terwijl het debiet per volume katalysator (ook wel gas hourly space velocity ofwel GHSV genoemd) niet correleerde. Warmteverlies door middel van radiatie werd geïdentificeerd als voornaamste reden voor warmteverlies wat voor een uniforme katalysatorbed temperatuur zorgde. Door *operando* katalysator thermometrie toe te passen, werd het mogelijk om de activiteit te koppelen aan de katalysator temperatuur. Dit gaf meer inzicht in misschien wel de belangrijkste, maar vaak over het hoofd geziene parameter, namelijk temperatuur.

Als laatste werd in **hoofdstuk 5** de rol van synergetische effecten en redox eigenschappen onderzocht voor het ontwerp van katalysatoren voor de oxidatieve chlorering van CH_4. De Mg^{2+}-Al^{3+} gemixte metaaloxides (mixed-metal oxide, ofwel MMO) bleken actief als katalysatormateriaal, ondanks dat ze geen redox-actieve elementen bevatten. Het Mg_4Al MMO materiaal beschikte over een van de hoogst gerapporteerde activiteiten onder de geteste reactiecondities, wat des te verrassender was door het feit dat de referentie materialen MgO en γ-Al_2O_3 bijna geen katalytische activiteit vertoonden. *Operando* Raman spectroscopie bewees dat Mg^{2+} als een chloor buffer functioneerde en verantwoordelijk was voor het chloreren van Al^{3+}, welke actief was in de reactie. Alhoewel de activiteit in de reactie exceptioneel hoog was, was de activiteit-selectiviteit relatie niet competitief. Een derde element, het redox actief Eu^{3+}, werd in het materiaal ingebouwd door de partiële substitutie van Al^{3+}. Het toevoegen van 2 atoom % Eu^{3+} resulteerde in een verdubbeling van de activiteit, een variabele activiteit-selectiviteit relatie, en behoud van een hoge activiteit onder hoge HCl concentraties in de toevoer. Gecombineerde *operando* Raman en luminescentie spectroscopie bewees dat de chlorering van Mg^{2+} en Eu^{3+} aan elkaar gekoppeld waren. Daarom wordt verwacht dat Mg^{2+} ook de chlorering van Eu^{3+} faciliteert. Deze resultaten laten zien dat zowel redox activiteit als synergetische effecten nodig zijn om een katalysator te ontwerpen met uitzonderlijke katalytische eigenschappen.

APPENDIX C: LIST OF PUBLICATIONS AND PRESENTATIONS

C.1. This PhD Thesis Is Based on the Following Publications

<u>Bas Terlingen</u>, Ramon Oord, Mathieu Ahr, Eline M. Hutter, Coert van Lare, Bert M. Weckhuysen, "Mechanistic Insights into the Lanthanide-Catalyzed Oxychlorination of Methane as Revealed by Operando Spectroscopy", ACS Catal. 2021, 11, 10574-10588.

<u>Bas Terlingen</u>, Ramon Oord, Mathieu Ahr, Eline M. Hutter, Coert van Lare, Bert M. Weckhuysen, "Favoring the Methane Oxychlorination Reaction over EuOCl by Synergistic Effects with Lanthanum", ACS Catal. 2022, 12, 5698-5710.

<u>Bas Terlingen</u>, Tjom Arens, Thomas P. van Swieten, Freddy T. Rabouw, P. Tim Prins, Michiel M. de Beer, Andries Meijerink, Mathieu Ahr, Eline M. Hutter, Coert van Lare, Bert M. Weckhuysen, "Bifunctional Europium for Operando Catalyst Thermometry in an Exothermic Chemical Reaction", Angew. Chem. Int. Ed. 2022, e2022119911.

<u>Bas Terlingen</u>, Jelle W. Bos, Mathieu Ahr, Matteo M. Monai, Coert E.J. van Lare, Bert M. Weckhuysen, "Importance of Redox Properties and Synergistic Effects for Methane Oxychlorination Catalysts", submitted for publication.

C.2. Other Publications by the Author

Koen W. Bossers, Laurens D.B. Mandemaker, Nikolaos Nikolopoulos, Markus Röhnke, Peter de Peinder, <u>Bas Terlingen</u>, Yuanshuai Liu, Felix Walther, Jürgen Janek, Bert M. Weckhuysen, "A Ziegler-type Spherical Cap Model Reveals Early-Stage Ethylene Polymerization Growth Versus Catalyst Fragmentation Relationships", Nat. Commun. 2022, 13, 1-11.

C.3. Oral Presentations

"Favoring the Methane Oxychlorination Reaction over EuOCl by Synergistic Effects with Lanthanum", 23rd Netherlands' Catalysis and Chemistry Conference (NCCC), Noordwijkerhout, The Netherlands, May 2022.

"Favoring the Methane Oxychlorination Reaction over EuOCl by Synergistic Effects with Lanthanum", 27th North American Catalysis Society Meeting (NAM27), New York City, United States of America, May 2022.

C.4. Poster Presentations

"Improving Methane Oxychlorination Catalysts by Rational Design", 22nd Netherlands' Catalysis and Chemistry Conference (NCCC), Noordwijkerhout, The Netherlands, March 2021.

APPENDIX D: ACKNOWLEDGEMENTS

The expression "save the best for last" is something I did very literally with the writing of my thesis. Personally, I have been very much looking forward to be able to write this section. This is mostly because I now have the opportunity to thank those who made these years as a PhD candidate fun, who challenged me to do better, and who talked me through rough times. I have to confess that I thought it would be much easier to write the acknowledgements, but ironically enough, the writer's block hits me one last time during this process. How do you actually proper thank someone, let alone tens of people who helped you tremendously throughout those four years? Here is my best go!

Bert, you are the first person I would like to sincerely thank! After a bit more than 4 years and many discussions, I think we can look back on a successful project and great time. I think that we had to get used to one another in the beginning, but that changed quite quickly. I have always appreciated your honest opinion and the storm of ideas you always provide when we would have a meeting. In those four years you have always challenged me to do better and present my results better. Looking back, I can conclude that it made me a better and a more confident researcher. I have always felt supported and you have given me the freedom to explore and start collaborations. The thing I enjoyed the most is when I could show you new and exciting results because that could trigger such excitement which shows that you are still a scientist first. I hope you will forever keep this excitement because that is something that motivated me to go on!

Eline, when you started as tenure track assistant professor for ARC-CBBC, I am quite sure that you never expected to get so involved in the topic of this thesis! Half way through my project I asked you if you would want to supervise me, because i was struggling with writing my first article. I don't know how many versions of the first article were sent back and forth, but it must have been more than 10. I sincerely want to thank you for your patience during this process! I remember that for the last article that we published together you told me it was well-written from the start, which I think was a great accomplishment for both of us! Besides supervising the writing process, you always did your best to make sure I was doing well. I felt that I could be honest about anything when we had our meetings and I really enjoyed the fact that I could always walk in to bother you with a question! I am absolutely sure that you will do great as a professor, both scientifically as well as managerial!

This project would not have existed without the industrial partner Nobian. Coert, we have had more than 80 meetings over this 4 year period. Many things have changed during those four years but you were the constant factor in the project. You have put tremendous amounts of time and effort into this project. You have entrusted me with confidential information with the goal to really make an industrial relevant catalyst. I loved the industrial view on the project and it has taught me many things which we normally would not consider in academia. The input you gave helped to focus the work and also to stay motivated. Mathieu, I also want to thank you for the time and effort you have put

in this project. You were always asking critical questions and made sure that the results were sound. Also with the unpublished manuscripts, you always read those very carefully and made sure even the tiniest error was filtered out. Even after you left Nobian, you still wanted to stay involved in the project, which I highly appreciate! Bart and Javier, our collaboration was of short duration, but also my thanks to you for your input!

I would like to thank the rest of the committee, Javier Pérez-Ramírez, Eelco Vogt, Pieter Bruijnincx and Andries Meijerink for reading and correcting my thesis.

I was very fortunate that I did not have to do all the work by myself during these four years. This booklet would have looked much different if it was not for all the co-authors. First, a big thank you to the students who put their trust in me to supervise their bachelor and master theses. Jelle and Tjom, I am very thankful that you were willing to start such challenging master projects with me. It has been a rough ride in both projects but I am super happy that both projects turned out into articles and chapters of my thesis! You both made a significant contribution to this work! I very much enjoyed the fact that it was a true investigation, and you also came up with many ideas! Besides the serious work that had to be done, we found enough time to laugh and discuss things unrelated to work. You both started as PhD's at ICC and I am sure you will do great. I am very much looking forward to your defences (so invite me)! Max, Nadia and Kirsten, thank you for doing your bachelor's thesis under my supervision. It was a pleasure to supervise you and also wish you all the best for the future. Kirsten, good luck with your PhD! I am sure you will also do great!

Matteo, I think you have a body that is 50% science and 50% kindness. You always made time to discuss my results, proof-read many of the manuscripts in this thesis and the support in general! We have had a number of borrels at your place, which I enjoyed very much (and keep giving them)! One last thing, please promise me that you will never put couscous on a croissant again! Freddy and Thomas, thank you for introducing me into the field of luminescence thermometry and helping me with the supervision of Tjom! I am proud of the collaboration and the results that came out of this project! Freddy, I hope it does not turn out that Smintjes are bad for your health.

Ramon, Tim, Jules, Hannie, Fouad, Joris, Oscar, Pascal, Dennie, Jochem and Ad, thank you for all the help. I think I bothered you all with many questions and you were always there to help me out. That really made my life so much easier. Ramon a special thanks to you for building the set-up and helping me to operate it. We spent many hours trying to resolve one blockage after another. It has been a painful learning curve but we managed to get it operable! Tim, thanks for explaining all the ins and outs of the EU^{3+} luminescence! Besides the technical staff, I also want to thank Dymph. You always made sure we filled in the right forms at the right time. Especially at the end of my project, you made sure to organize my defence before you left which I highly appreciate.

Maurice, thanks for all the insightful conversations we had and taking me under your wing. It was always a pleasure to discuss science and things not related to science. Han-

nah, thank you for the effort you put in to make the consortium fun. With every activity, you always put the PhD candidate central and wanted us to have a good time!

Wilbert and Evgeny, you both had a great influence on the decision of doing a PhD. The interest for research really did start when I did my masters project with you. I had a great time in Eindhoven! Bobtje, I am happy that we still find time to hang around and meet up somewhere in the Netherlands and hope we can continue this in the future!

These four years would not have been so enjoyable without all the fun colleagues and friends around at the office! Laurens, shoeimaster, I am going to miss your positive Rotterdam attitude. I am glad we could share an office for a few more months! Koen, pikkie, I loved synthesizing balls with you. We had some great discussions, some were even science related! Maarten, thanks for being my roommate at NCCC! I very much enjoyed your down-to-earth and simple view at things! Remco, I have never met anyone more random than you. Keep up spreading the great jokes! Joren, ballenmeneer 2.0, good luck with the continuation of the project! I am sure you will do great! Nikos, I very much enjoyed the trip to NY! Christia, we had a great time at Schiermonnikoog! You always brought a smile to my face when you were hating on the world (YIIII). Sophie, we were "in hetzelfde schuitje". It was always nice to discuss how things went and share our experiences. We went out with a bang in NY! Sofie and Jelle K it was a pleasure to share an office with you two! It made the quiet VMC building so much more enjoyable. Charlie, let me know when you are back in NL again! Silvia, always enjoyed the chats we had! Lastly, I want to thank the rest of the Lunchgroup, Francesco, Giorgio, Laura, Roozbeh and Savvie, for all the fun times we had at UMC and outside of the office!

I want to thank the (former) colleagues of ICC and MCC that I did not mention yet (and I hope that I did not forget anyone): Adriaan, Jim, Joelle, Michael, Suzan, Luc, Nienke, Florian Z, Jochem, Caroline, Erik, Frederique, Ina, Iris, Johan, Joris K, Laura dK, Oscar, Romy, Sebastian H, Sebastian R, Thimo, Yannick, Shuang, Yadolah, Xinwei, Kristian, Rafael, Hongyu, Bettina, Nina, Max, Ward, Florian M, Ellen, Robin, Bram, Daan, Joyce, Laura Z, Mirjam, Nicolette, Chunning, Donglong, Luke, Miguel, Katinka, Anne-Eva, Loreta, Mariangela, En, Adrian, Angela, Jochem, Kordula, Sibylle, Fieke, Tom, Xiang, Hans, Valerio, Bea, Egor, Robin G, Oscar D, Marianna, thank you for the great time!

Then, I want to thank my paranymphs. Guuuus! We first met when I had my interview at ICC. I don't know if is a good thing or a bad thing that you did not remember me when I started at ICC (?). With the opening of the VMB, we were the only two at the office for a long time and thus dependent on each other. We experienced highs (birth of the manatee after weeks of following the news) and lows (Guusje crying behind the AFM, which is apparently a rare thing). I am glad you joined to go to NY as our tour guide and show us all the best food stops! You left ICC but we are still in touch and I hope we can continue drinking wine together and keep bother each other with dog movies. I wish you all the best in the future, together with Matteo and Phoebe!

Huygen, Mr. synthesis, at first I thought you did not want to be my paranymph as it took you a bit to respond. Later, you surprised me by giving me a bottle of beer with a true "prins carnaval" photoshopped on the bottle. One thing is sure, when Huygen is around, unexpected things are going to happen. I don't think we have to go over the details here but getting stopped by the police deserves an honourable mention. I always enjoyed your stories during lunch and I am very thankful that you introduced me to Huzur. All the best finishing your PhD and if the scientific career does not work out, you can always open a broodje bufkes!

Vrienden en familie, heel erg bedankt voor de onvoorwaardelijke steun en de nodige ontspanning in de afgelopen jaren! De vraag: "wat doe je nou eigenlijk precies" is me heel vaak gesteld in de afgelopen jaren.

Stijn en Maarten, toen ik begon aan mijn PhD kwam ik bij jullie in huis wonen. Het heeft niet lang geduurd om te wennen want het was altijd gezellig. Onze avonden werden gevuld met domme YouTube filmpjes, een plaatje draaien of gamen. We hebben zoveel lol gehad op de Hermannus, daar kijk ik echt met een nostalgisch gevoel op terug! Af en toe was ons huisdier Tijmen er ook die voor de nodige reuring zorgde. Ik ken niemand die gemorste cola met zijn sok afveegt en daarna zijn voet weer in zijn schoen stopt. Het resultaat na die twee jaar op de hermannus is dat we hele goede vrienden zijn geworden en ik hoop dat dat nog een tijdje zo gaat blijven (Fab en Anne, jullie horen daar natuurlijk ook bij)! Eva en Pieter, jullie hebben me flink uitgedaagd om mijn deadlines te halen door er een fles champagne op te zetten. Ik moet zeggen dat dat een hele grote drijfveer was om er flink tegenaan te gaan! Ik geniet altijd heel erg van alle activiteiten die we ondernemen en hoop dat we dat in de toekomst voort zullen zetten!

Patrick, het is toch vrij ironisch dat ik niet bij jou verdediging kon zijn en jij niet bij die van mij. Ik denk dat het maar goed is omdat het anders te emotioneel was geworden tijdens de verdedigingen haha! Na die jaren samengewoond te hebben in Eindhoven kennen we elkaar zo goed dat het eigenlijk niet uit maakt hoe vaak we elkaar wel of niet spreken. In die jaren in Eindhoven is zeker de basis gelegd voor deze thesis. We hebben wat uurtjes gestudeerd samen! Bart, wat in Eindhoven ooit begonnen is als een vriendschap die alleen maar ging over sporten en kip eten, is de laatste jaren toch wel wat veranderd. Ik denk dat onze vriendschap zeker een stuk volwassener is geworden doordat we nu vooral flauwe grappen maken en elkaar proberen te stangen. Denk je dat Gerald trots is? Even serieus, af en toe zit er nog wel eens een goed gesprek bij met goed advies. Bedankt dat ik af en toe even bij je kon ventileren! Ali, ik denk nog steeds met heel veel plezier terug aan ons bezoekje in Zurich!

Beren uit landgraaf, Koen, Joey, Maikel, Dylan, Jacco, Tony, Bjorn en Patrick, bedankt voor de interesse die jullie in de afgelopen Jaren in mijn PhD hebben getoond. We kennen elkaar al sinds de middelbare school en hebben al aardig wat met elkaar mee gemaakt. Waar gaat de volgende mannenweekend naartoe? We houden contact he!

Ik ben dit dankwoord begonnen met de zin "save the best for last" en deze zin is hier ook

7

van toepassing. Ik wil de hele familie bedanken voor alle steun de afgelopen jaren en de interesse die jullie in mij hebben getoond, vanaf kleins af aan tot nu! Rick, bedankt voor het mooie ontwerp van mijn kaft (en natuurlijk je gezelligheid als neef)! Oma, bedankt voor alle kopjes soep en plakjes cake! Je hebt heel vaak verteld dat papa chemicus is geworden doordat de schoorsteen van het dak af hebt geblazen toen je zwanger was van papa. Schijnbaar was die knal zo groot dat het nog een generatie is doorgegeven! Opa, je hebt het laatste deel van mijn promotie helaas niet meer kunnen meemaken maar ik weet zeker dat je het allemaal prachtig had gevonden!

Maarten en Yvonne, bedankt voor alle interesse die jullie hebben getoond de afgelopen jaren. Het was iets waar jullie totaal niks vanaf wisten, maar jullie hebben altijd je best gedaan om te begrijpen hoe het in elkaar zat en wat er speelde in mijn leven.

Koenie, misschien was je je naam al aan het zoeken maar doordat Lisanne en Geert zijn getrouwd sta je tussen de familie! We kennen elkaar nu al zo lang en zo goed dat dat eigenlijk ook wel terecht is. Ik vond het heel fijn om de afgelopen jaren het PhD traject en toekomstplannen met je te bespreken! Wanneer gaan we de "oomdag" invoeren?

Lisanne, ik ben mijn middelbare schooltijd doorgekomen door jouw goede samenvattingen van eigenlijk elk vak. Daarom denk ik dat jij ook echt een aanzienlijke bijdrage hebt geleverd aan dit boekje. Je kleine broertje heeft voor de verandering op pagina 150 een samenvatting voor jou gemaakt, ik hoop dat jij er dit keer wat aan hebt! In de afgelopen jaren heb je je ook over mij ontfermd als grote zus en dat voelde altijd heel vertrouwd. Ik vond het fijn dat ik mijn verhaal bij je kwijt kon, ook omdat je weet hoe ik in elkaar steek! Geert, helaas is de baanbrekende ontdekking nog niet gedaan. Zodra ik iets heb zal ik je het laten weten om een bedrijfsplan uit te werken! Je hebt altijd veel interesse getoond in wat ik deed en dat waardeer ik heel erg! Ties, we hebben nog niet heel veel goede gesprekken gevoerd, maar het is altijd een feestje om je te zien. Opa en ome Bassie zullen ervoor zorgen dat je ook gewoon scheikunde gaat studeren in plaats van dat medische geneuzel wat je mee krijgt van je ouders. Even zonder gekheid, ik mag heel blij zijn met een zussie, schoonbroer en kleine neefje als jullie!

Mama, ik vind het lastig om je voor specifieke momenten of dingen te bedanken omdat je er eigenlijk altijd voor me was. In de afgelopen jaren heb je altijd een luisterend oor geboden en heb je altijd met me mee gedacht. Jij zei altijd als je iets wilt bereiken dan zul je ervoor moeten werken, met dit boekje als resultaat! Papa, het was onbedoeld, maar ik ben toch helemaal in jouw voetsporen getreden. Na dezelfde studie gedaan te hebben, heb ik nu ook mijn promotie afgerond. Iets met bloed kruipt waar het niet gaan kan? Het was heel fijn dat ik met jou ook inhoudelijk over het onderzoek en promotie kon hebben aangezien je weet hoe het is. Met al die medische mensen thuis konden wij het gelukkig af en toe ook over scheikunde hebben! Lieve Pap en mam, ik weet zeker dat jullie allebei trots zijn en ik ben trots op jullie als mijn ouders!

Chris, liefie, het is niet uit te drukken hoeveel jij mij hebt gesteund in de afgelopen jaren. Het was af en toe zwaar voor mij, maar het was zeker ook niet makkelijk voor jou. In het

begin van het project heb ik je nog wel eens proberen uit te leggen wat ik inhoudelijk aan het doen was. Eigenlijk altijd was je binnen 3 woorden afgeleid en begon je te gapen. Wat ik precies deed was niet belangrijk voor je. Het enige wat je interesseerde was hoe het met mij ging, waar ik tegen aan liep en of ik het leuk vond. Je hebt me tijd gegeven als ik een drukke periode had, op de rem getrapt als ik niet meer kon afschakelen en me af en toe een schop onder mijn kont gegeven. Dit boekje had er heel anders uit gezien zonder jouw steun (presentaties oefenen, mezelf meer laten zien, successen vieren, leren plannen, advies geven etc.)! Nu dit hoofdstuk is afgesloten, gaan we eerst maar eens even ontspannen voordat we aan het volgende hoofdstuk gaan beginnen (en die gaat er zeker komen!). Ik hou van je!

7

APPENDIX E: CURRICULUM VITAE

Bas Johan Pieter Terlingen was born in Hengelo (the Netherlands) on August 14 1994. He obtained a BSc. degree in chemical engineering from Eindhoven University of Technology (TU/e; The Netherlands) in 2015. During his Bachelor thesis, he studied the formation and growth of cobalt hydroxide carbonate (nano) particles during precipitation deposition process at ambient temperature under the supervision of prof. dr. Nico Sommerdijk. Subsequently, he went to obtain his MSc. degree in chemical engineering with a specialization in molecular systems and material chemistry from TU/e. He wrote his Master thesis entitled "Bimetallic Nickel Manganese Catalysts for Hydrogenation Reactions" under the supervision of prof. dr. Evgeny Pidko and prof. dr. ir. Emiel Hensen at the Inorganic Materials and Chemistry (IMC) group of TU/e. This is where he gained interest and affinity for the field of heterogeneous catalysis. Afterwards, he went to the A*STAR's Institute of Chemical and Engineering Sciences (ICES, Singapore) for three months to complete his internship where he unravelled the effect of iron in Ir-Fe bimetallic catalysts for ethanol steam reforming in the group of prof. dr. ir. Armando Borgna. In 2018, he began his PhD project under the supervision of dr. Eline Hutter and prof. dr. ir. Bert Weckhuysen in the Inorganic Chemistry and Catalysis (ICC) group of Utrecht University (UU, The Netherlands). This work was conducted in close collaboration with the industrial partner Nobian within the Advanced Research Center – Chemical Building Block Consortium (ARC-CBBC). The results of this research are described in this PhD thesis.

7